

ADVERTIMENT. La consulta d'aquesta tesi queda condicionada a l'acceptació de les següents condicions d'ús: La difusió d'aquesta tesi per mitjà del servei TDX (www.tesisenxarxa.net) ha estat autoritzada pels titulars dels drets de propietat intel·lectual únicament per a usos privats emmarcats en activitats d'investigació i docència. No s'autoritza la seva reproducció amb finalitats de lucre ni la seva difusió i posada a disposició des d'un lloc aliè al servei TDX. No s'autoritza la presentació del seu contingut en una finestra o marc aliè a TDX (framing). Aquesta reserva de drets afecta tant al resum de presentació de la tesi com als seus continguts. En la utilització o cita de parts de la tesi és obligat indicar el nom de la persona autora.

ADVERTENCIA. La consulta de esta tesis queda condicionada a la aceptación de las siguientes condiciones de uso: La difusión de esta tesis por medio del servicio TDR (www.tesisenred.net) ha sido autorizada por los titulares de los derechos de propiedad intelectual únicamente para usos privados enmarcados en actividades de investigación y docencia. No se autoriza su reproducción con finalidades de lucro ni su difusión y puesta a disposición desde un sitio ajeno al servicio TDR. No se autoriza la presentación de su contenido en una ventana o marco ajeno a TDR (framing). Esta reserva de derechos afecta tanto al resumen de presentación de la tesis como a sus contenidos. En la utilización o cita de partes de la tesis es obligado indicar el nombre de la persona autora.

WARNING. On having consulted this thesis you're accepting the following use conditions: Spreading this thesis by the TDX (www.tesisenxarxa.net) service has been authorized by the titular of the intellectual property rights only for private uses placed in investigation and teaching activities. Reproduction with lucrative aims is not authorized neither its spreading and availability from a site foreign to the TDX service. Introducing its content in a window or frame foreign to the TDX service is not authorized (framing). This rights affect to the presentation summary of the thesis as well as to its contents. In the using or citation of parts of the thesis it's obliged to indicate the name of the author

UNIVERSITAT POLITÈCNICA DE CATALUNYA

DEPARTAMENT D'ENGINYERIA ELÈCTRICA



Departament d'Enginyeria Elèctrica



UNIVERSITAT POLITÈCNICA DE CATALUNYA



CITCEA

PhD Thesis

Operation and control of transmission systems for offshore wind power plants

Author: Mònica Aragüés Peñalba

Advisor: Oriol Gomis Bellmunt

Barcelona, February 2016

Universitat Politècnica de Catalunya
Departament d'Enginyeria Elèctrica
Centre d'Innovació Tecnològica en Convertidors Estàtics i Accionaments
Av. Diagonal, 647. Pl. 2
08028 Barcelona

Copyright © Mònica Aragüés Peñalba, 2016

Imprès a Barcelona
Primera impressió, Febrer 2016



Acta de qualificació de tesi doctoral

Curs acadèmic: 2015-2016

Nom i cognoms

Mònica Aragüés Peñalba

Programa de doctorat

Doctorat en Enginyeria Elèctrica

Unitat estructural responsable del programa

Resolució del Tribunal

Reunit el Tribunal designat a l'efecte, el doctorand / la doctoranda exposa el tema de la seva tesi doctoral titulada Operation and control of transmission systems for offshore wind power plants.

Acabada la lectura i després de donar resposta a les qüestions formulades pels membres titulars del tribunal, aquest atorga la qualificació:

NO APTÉ

APROVAT

NOTABLE

EXCEL·LENT

(Nom, cognoms i signatura)	(Nom, cognoms i signatura)	
President/a	Secretari/ària	
(Nom, cognoms i signatura)	(Nom, cognoms i signatura)	(Nom, cognoms i signatura)
Vocal	Vocal	Vocal

_____, ____ d'/de _____ de _____

El resultat de l'escrutini dels vots emesos pels membres titulars del tribunal, efectuat per l'Escola de Doctorat, a instància de la Comissió de Doctorat de la UPC, atorga la MENCIÓ CUM LAUDE:

SÍ

NO

(Nom, cognoms i signatura)	(Nom, cognoms i signatura)
President de la Comissió Permanent de l'Escola de Doctorat	Secretari de la Comissió Permanent de l'Escola de Doctorat

Barcelona, _____ d'/de _____ de _____

Diligència “Internacional del títol de doctor o doctora”

- Com a secretari/ària del tribunal faig constar que la tesi s'ha defensat en part, i com a mínim pel que fa al resum i les conclusions, en una de les llengües habituals per a la comunicació científica en el seu camp de coneixement i diferent de les que són oficials a Espanya. Aquesta norma no s'aplica si l'estada, els informes i els experts provenen d'un país de parla hispana.

(Nom, cognoms i signatura)

Secretari/ària del Tribunal

Le véritable voyage de découverte ne consiste pas à chercher de nouveaux paysages, mais à avoir de nouveaux yeux.

The voyage of discovery lies not in seeking new horizons, but in seeing with new eyes.

Marcel Proust

Acknowledgements

I would like to express my acknowledgement to all those who encouraged and gave me support during my PhD.

To my parents, Javier and Enriqueta, two unconditional pillars since I was born and, specially during my academic career. I don't know the material they are made of, but I admire their unbreakable fortitude. Also to Robert, for boosting my wishes and brightening all these years.

This thesis would not have been possible without the advise and vision of my supervisor, Oriol Gomis. Thanks to him I have also been working in a very powerful team inside UPC: CITCEA. Here I need to mention the valuable advice from Samuel Galceran, Andreas Sumper and Toni Sudrià. And, of course, Agustí Egea, Edu Prieto, Joan Sau, Adrià Junyent, Rodrigo Teixeira, Edu Bullich, Ricard Ferrer, Íngrid Munné, Carlos Collados, Guillem Viñals, Muhammad Raza, Pau Lloret, Francesc Girbau, Afsaneh Soljhoushah, Ana Cabrera, Pol Olivella, Gerard Clariana and Joan Marc Rodriguez for the enjoyable moments shared while working/learning. I would also like to thank Dirk Van Hertem for allowing my stay in ESAT, KU Leuven and for his guidance. Thanks to him I could work with the Belgian Transmission System Operator (Elia), collaborating successfully with Johan Rimez in the secure and optimal operation of transmission systems.

In this sense, I would also like to thank KIC Innoenergy PhD School for financing my stay.

Finally, it is worth mentioning some of the projects that have lead to the majority of the present studies: Vendaval 1 and Vendaval 2 (with Alstom Wind and IREC), Offwindtech, Smartpower (from EIT KIC Innoenergy)

and projects ENE2012-33043 and ENE2013-47296, financed by the Ministerio de Ciencia e Innovación. These projects are listed below chronologically:

- 2012, Vendaval - Alstom Wind. Modeling, control and simulation of offshore wind farms with HVDC and HVAC transmission using DIgSILENT Power Factory.
- 2013, Vendaval 2 - Alstom Wind- DC wind turbine concepts analysis for future DC wind power plants.
- 2013, KIC Smart Grids from power producers to consumers (Smart-power) Development of optimal power flows for large transmission systems, combining HVDC and HVAC.
- 2013, KIC Offshore Wind Enabling Technologies (Offwindtech) Project management and elaboration of reports related to Offshore Wind Technologies
- 2013, Microgrids. Desgin of primary and secondary control in DC microgrids.
- 2014, Photovoltaic plants control. Design of active and reactive power controls at PV plant level to accomplish with the strongest grid code requirements.
- 2014-2016 Offshore wind power integration in the spanish power system by multiterminal HVDC links Modeling, control and simulation of offshore wind power plants HVDC connected.

Abstract

This thesis deals with grid integration of offshore wind power plants through HVDC (High Voltage Direct Current) or HVAC (High Voltage Alternating Current) transmission. The behaviour of wind farms and their transmission systems in normal operation and under faults is analyzed.

On the field of HVDC transmission, a control scheme based on an optimum voltage algorithm is proposed and compared to voltage droop control. The differences between the proposed scheme and droop control in terms of losses are analyzed, in steady state as well as dynamically. This new control scheme is enhanced, being able to perform secondary and tertiary control strategies simultaneously for DC grids.

Concerning HVAC transmission, the operation of AC connected wind power plants equipped with full power converter wind turbines is analyzed under deep voltage sags on the main AC grid. Standard control schemes, based on the strict application of grid codes, can lead to instability problems when this kind of severe disturbances occurs. A coordinated control scheme is proposed to operate the system, ensuring fault ride through capability. An index alerts of instability proximity and allows to activate active power and reactive power regulation to guarantee safe operation during faults.

For enabling the optimal operation of transmission systems, an optimal power flow tool is described for hybrid HVDC-HVAC systems, for different objective functions. This tool is tested in a scaled platform. Finally, the secure and optimal operation of these systems is analysed for a scenario with high penetration of offshore wind, proposing a methodology to evaluate the cost of operation and wind energy curtailed.

Resum

La present tesi tracta la integració a xarxa de plantes eòliques marines a través de transmissió en HVDC (Alta Tensió en Corrent Continu) o HVAC (Alta Tensió en Corrent Altern). S'analitza el comportament dels parcs eòlics i del seus sistemes de transmissió en condicions normal i en situacions de perturbacions elèctriques.

En el camp de l'HVDC, es descriu un esquema de control basat en un algoritme de tensions òptimes i es compara amb el control de tensió *droop*. Les diferències entre l'esquema de control proposat i el *droop* s'analitzen, des del punt de vista de pèrdues, en estat estacionari i dinàmicament. L'esquema de control proposat es millora, oferint la possibilitat de realizar estratègies de control secundari i terciari en xarxes DC.

Dins de la transmissió en l'HVAC, s'analitza l'operació de parcs eòlics equipats amb convertidors de plena potència quan s'esdevenen sots profunds a la xarxa AC. Els esquemes de control estàndards, basats en l'aplicació estricta dels requisits de connexió, poden comportar problemes d'estabilitat transitòria quan s'esdevenen perturbacions severes. Es proposa un esquema de control coordinat per operar el sistema, assegurant el *fault ride through*. Un índex alerta de la proximitat d'una inestabilitat i permet activar la regulació de potència activa i reactiva per assegurar l'operació segura durant la falta.

Tenint en compte que l'expansió del sistema de transmissió presenta tant enllaços HVDC com HVAC, es desenvolupa una eina per determinar fluxos de potència òptims en xarxes híbrides HVDC-HVAC, per diferents funcions objectiu. Es realitzen proves experimentals en una plataforma de baixa tensió per comprovar el funcionament d'aquesta eina. Finalment, s'estudia l'operació òptima i segura d'aquests sistemes, per un escenari amb gran penetració d'energia eòlica, proposant una metodologia per evaluar el cost d'operació i la reducció d'energia eòlica produïda.

Contents

List of Figures	xiii
List of Tables	xix
Outline	xxi
Nomenclature	xxii
1 Introduction	1
1.1 Context	1
1.2 Objectives and scope	3
2 Background	7
2.1 Wind power scenario	7
2.1.1 Offshore	7
2.1.2 Repowering	9
2.2 Grid integration of offshore wind power plants	12
2.2.1 Introduction	12
2.2.2 Transmission options	12
2.2.3 HVDC transmission	17
2.3 Operation and control of offshore wind power plants	23
2.3.1 Introduction	23
2.3.2 Control and protection functions required	24
2.3.3 Control and protection integration	30
2.3.4 Wind power plant control	32
2.3.5 Conclusions	47
3 Loss minimization in HVDC multi-terminal transmission systems	49
3.1 Power control in multi-terminal HVDC grids	49

Contents

3.2	Optimum voltage control for loss minimization in HVDC multi-terminal transmission systems	51
3.2.1	Introduction	51
3.2.2	Multi-terminal HVDC transmission systems for offshore wind farms	52
3.2.3	Control Schemes	52
3.2.4	Case Studies	57
3.2.5	Dynamic simulation	66
3.2.6	Conclusions	72
3.3	Droop control for loss minimization in HVDC multi-terminal transmission systems	74
3.3.1	Introduction	74
3.3.2	Proposed control scheme	75
3.3.3	Steady state case studies	78
3.3.4	Dynamic case studies	82
3.3.5	Conclusions	93
4	Coordinated Control for an Offshore Wind Power Plant to Provide Fault Ride Through Capability	95
4.1	Introduction	95
4.2	Current limit and stability analysis for AC connected offshore wind power plants	101
4.3	Conventional operation for voltage sags	106
4.4	Coordinated control proposal	108
4.4.1	Angular Difference Index: ADI	108
4.4.2	Computation of ADI	109
4.4.3	System actions to avoid instability	111
4.5	Simulations	112
4.6	Conclusions	121
5	Optimal power flow for hybrid HVDC/HVAC transmission systems for grid integration of offshore wind	123
5.1	Introduction	123
5.2	Optimization problem	126
5.2.1	Notation	127

Contents

5.2.2	Inputs	129
5.2.3	Outputs	129
5.2.4	Mathematical formulation	129
5.2.5	Converter model	131
5.2.6	Objective functions	132
5.3	Case study 1	133
5.3.1	Minimum losses	133
5.3.2	Minimum deviation from a voltage profile	133
5.3.3	Sensitivity analysis	136
5.4	Case study 2	139
5.4.1	Minimum losses	140
5.4.2	Sensitivity to wind speed changes	144
5.5	Case study 3	146
5.5.1	HVDC scaled platform description	147
5.5.2	Signal exchanges with the central controller	149
5.5.3	Simulations	150
5.6	Conclusions	167
6	SCOPF in hybrid DC/AC power systems with large penetration of offshore wind taking into account spinning reserves	169
6.1	Introduction	169
6.2	Optimal operation of hybrid AC/DC systems including spinning reserves	171
6.2.1	SCOPF tool	171
6.2.2	Contingencies and security constraints	172
6.2.3	Generation and demand modelling	173
6.2.4	Spinning reserves modelling	174
6.3	Methodology for determining the cost of operation over one year	177
6.4	Study case	180
6.4.1	System description	180
6.4.2	Results	181
6.4.3	Scenarios identification	185
6.5	Conclusions	191

Contents

7 Conclusions	193
7.1 Contributions	193
7.2 Future work	195
Bibliography	197
8 Publications	211
8.1 Journal articles	211
8.2 Patents	212
8.3 Book chapters	212
8.4 Conference papers	212
8.5 Other publications	213
8.5.1 Other journals	213
8.5.2 Other conference papers	214
8.5.3 Magazines	215
8.5.4 Colloquiums	215
9 Appendix	217

List of Figures

2.1	Wind turbine's size and power evolution from 1980 until nowadays	8
2.2	Offshore wind farm connected through Medium Voltage AC transmission (MVAC)	13
2.3	Offshore wind farm connected through High Voltage AC transmission (HVAC)	14
2.4	Offshore wind farm connected through Low Voltage AC transmission (LVAC)	15
2.5	Offshore wind farm connected through High Voltage DC transmission (HVDC)	15
2.6	Offshore wind farms connected through Multiterminal High Voltage DC transmission (HVDC)	16
2.7	Converter station scheme and components for a VSC-HVDC system	17
2.8	HVDC systems topologies	18
2.9	Converter stations connection	20
2.10	VSC-HVDC offshore wind power plant	24
2.11	Normal operation	26
2.12	Restricted operation	27
2.13	Fault in the main AC grid	27
2.14	Reduced power operation	28
2.15	Frequency response: direct communication from the grid-side VSC-HVDC to the WPP	29
2.16	Frequency response: direct communication from the grid-side VSC-HVDC to the wind farm VSC-HVDC rectifier	29
2.17	Fault in the WPP grid	30
2.18	Integrated control scheme	31

List of Figures

2.19	Scheme of a PMSG wind turbine equipped with full power converter	34
2.20	Main components of a wind turbine	35
2.21	Main operating regions of a variable speed wind turbine	38
2.22	Control of a wind turbine equipped with full power converter	39
2.23	Active Power Plant Control	41
2.24	Reactive Power Plant Control	42
2.25	Layout of a 90 MW WPP represented in DIgSILENT Power Factory	43
2.26	HVDC transmission load flow in DIgSILENT Power Factory	43
2.27	Wind turbine load flow in DIgSILENT Power Factory	44
2.28	Active power reference sent by the TSO, ramp limited and active power measurement of the wind power plant output	45
2.29	Signal sent from the power plant control to each wind turbine	45
2.30	Active power output of a wind turbine inverter	46
2.31	Active power measured at the offshore and onshore substations	46
3.1	General scheme of the hierarchical power control for HVDC grids [58]	50
3.2	VSC control scheme	53
3.3	Voltage droop control in HVDC system	55
3.4	Optimum voltage algorithm in HVDC system	56
3.5	4-terminal HVDC test system	58
3.6	Voltages in the different multi-terminal HVDC system nodes	61
3.7	Loss reduction (%) using optimum voltage algorithm vs. droop voltage control	62
3.8	7-terminal HVDC test system	63
3.9	System efficiency distribution for random injected powers using voltage droop control	64
3.10	System efficiency distribution for random injected powers using optimum voltage algorithm	65
3.11	System efficiency distribution for random injected powers when using the two control schemes	67
3.12	Loss reduction using optimum voltage algorithm vs voltage droop control	67

List of Figures

3.13 Wind speed changes	69
3.14 Active and reactive power in wind farms	70
3.15 Voltages in wind farm and grid side VSCs	70
3.16 Detailed transient of voltages in grid-side VSCs	71
3.17 Multi-terminal HVDC branches currents	71
3.18 Voltages in wind farm and grid side VSCs	72
3.19 Optimization algorithm applied to a VSC-HVDC multi-terminal system	76
3.20 6-terminal HVDC system [73]	79
3.21 OPF for HVDC loss minimisation	80
3.22 OPF for VSC loss minimisation	81
3.23 Pareto front and total losses	82
3.24 Pareto fronts for different grid resistances	83
3.25 4 terminal HVDC system with central controller computing an OPF	85
3.26 Wind speed changes	86
3.27 Voltages in wind farm and grid side VSCs	87
3.28 Currents in the DC grid	87
3.29 Losses in the HVDC grid	88
3.30 Losses in each VSC	88
3.31 Efficiency	89
3.32 Wind speed changes	90
3.33 Voltages in wind farm and grid side VSCs	90
3.34 Currents in the DC grid	91
3.35 Losses in the HVDC grid	91
3.36 Losses in each VSC	92
3.37 Efficiency	92
4.1 Circuit representation	97
4.2 Transmission line diagram as a linear quadrupole	99
4.3 Offshore wind power plant connected through AC transmission to the terrestrial grid	102
4.4 Offshore Wind Power Plant (WPP) connected through AC submarine cable, represented through its π equivalent, to the grid	102

List of Figures

4.5	Example of current capability curve	104
4.6	Angle θ_w evolution when increasing WPP current for different power factors	105
4.7	Limit curves for the voltage/time pattern at the grid connection for Type 2 generating plants in the event of a fault in the grid [82]	107
4.8	Reactive power control in normal operation and under faulty conditions	108
4.9	Control action scheme for an offshore wind power plant with HVAC transmission	110
4.10	Electrical scheme of the AC cable and measures for estimation of the voltage phasor at the onshore platform	111
4.11	Voltage angles at the sending end (δ_1) and receiving end (δ_2) of the transmission and ADI before the fault	113
4.12	Voltage angles at the sending end (δ_1) and receiving end (δ_2) of the transmission and ADI during the fault	114
4.13	DC bus voltage of the wind turbine converter and AC voltage at the low voltage windings of the wind turbine transformer .	115
4.14	Active and reactive power at the sending end (i) and receiving end (j) of the transmission	116
4.15	Active and reactive powers in the wind turbine inverter and rectifier	117
4.16	Voltage and current at the AC grid	118
4.17	Voltage angles at the sending end (δ_1) and receiving end (δ_2) of the transmission and ADI during the fault without communications offshore-onshore	119
4.18	DC bus voltage of the back-to-back and AC voltage at the low voltage windings of the wind turbine transformer without communications offshore-onshore	120
4.19	Active and reactive power at the sending end (i) and receiving end (j) of the transmission without communications offshore-onshore	120
4.20	Active and reactive powers in the wind turbine inverter and rectifier without communications offshore-onshore	121

List of Figures

5.1	Hybrid HVDC-HVAC system for integrating offshore wind power	127
5.2	π equivalent of the AC branch between nodes k and l	131
5.3	3 DC bus system	134
5.4	5 AC bus system	134
5.5	Power flows in the 3 DC bus system for loss minimisation	135
5.6	Power flows in the 5 AC bus system for loss minimisation	136
5.7	Power flows in the 3 DC bus system for minimum deviation from a preset voltage	137
5.8	Power flows in the 5 AC bus system for for minimum deviation from a preset voltage	138
5.9	Effect of DC resistance, AC resistance and converter loss pa- rameters in power system loss	139
5.10	Power system analysed	141
5.11	Power flows for loss minimisation	143
5.12	Effect of wind power variation on the objective function	145
5.13	4 DC bus 6 AC bus power system analysed	146
5.14	4 DC scaled platform [100]	147
5.15	System monitoring and signals exchange	149
5.16	Power injection from wind farms	151
5.17	DC branch currents	152
5.18	DC bus voltages	153
5.19	Reactive power at the grid side VSCs	154
5.20	HVDC grid losses	155
5.21	VSC losses	156
5.22	Power injection from wind farms	157
5.23	DC branch currents	158
5.24	DC bus voltages	159
5.25	Reactive power at the grid side VSCs	160
5.26	HVDC grid losses	161
5.27	VSC losses	162
5.28	Power injection from wind farms	163
5.29	DC branch currents	164
5.30	DC bus voltages	165

List of Figures

5.31 HVDC grid losses	166
5.32 VSC losses	167
6.1 Hybrid HVDC-HVAC system for integrating offshore wind power	172
6.2 Flowchart of the methodology	179
6.3 HVDC-HVAC system based on [73]	180
6.4 Event tree for the system analysed	183
6.5 Possible power system scenarios for each hour analysed	184
6.6 Scenarios classification according to wind available and demand	185
6.7 Scenarios identification according to available wind energy and demand	186
6.8 Correlation in wind energy and in demand for 4 months	187
6.9 Correlation between wind energy and energy demand	188
6.10 Available wind energy and curtailment under different operation scenarios	188
6.11 Cost of operation under different operation scenarios	189
6.12 Cost of operation as a function of the monthly wind energy available and demand	190

List of Tables

3.1	Efficiency statistics obtained with both control schemes	66
3.2	Objective functions	77
5.1	Converter loss parameters in p.u. [89]	131
5.2	Bus voltages for loss minimisation	135
5.3	Bus voltages for minimum deviation from a voltage profile . .	137
5.4	Electrical parameters of the AC and DC branches	140
5.5	Active and reactive power demand in the AC nodes	140
5.6	Bus voltages for loss minimisation in MATLAB	142
5.7	Bus voltages for loss minimisation in GAMS	142
5.8	Execution time of GAMS for different power system sizes . .	144
5.9	VSC characteristics [100]	148
5.10	Electrical generators characteristics [100]	148
5.11	DC grid resistances [100] on Figure 5.15	148
6.1	Failure rates of the system lines and cables [114]	182
6.2	Failure rates of the system VSCs [114]	182
6.3	Failure rates of the system generators [116]	182
6.4	Total cost of operation during one year	189
6.5	Total wind power curtailed during one year	190

Thesis outline

This PhD presents the studies developed on the operation and control of transmission systems for grid integration of offshore wind. The energetic scenario and the scope of this research are detailed in **Chapter 1**. The tendencies in the wind power sector and the control of wind power plants and wind turbines are explained in **Chapter 2**. At the end of this chapter, the transmission options for wind power plants integration are described. The core of the research focuses on the operation and control of multi-terminal HVDC transmission (Chapters 3.2 and 3.3), HVAC transmission (Chapter 4) and hybrid HVDC/HVAC systems (Chapters 5 and 6).

Chapter 3 presents a voltage control scheme for operating multi-terminal VSC-HVDC systems that ensures minimum transmission losses. It is compared with droop control in steady state and through dynamic simulations, to show their transient behaviour when the wind power injected into the DC grid varies and when a communication fault occurs. Then, an enhanced voltage control for multi-terminal VSC-HVDC systems is proposed, taking advantage of the loss minimisation ensured by the control scheme explained at the beginning of the chapter and of the robustness of droop control.

Chapter 4 identifies stability problems in HVAC connected wind farms based on full power converters wind turbines when deep voltage sags occur on AC grid they are connected to. A coordinated control scheme is proposed to operate the system, ensuring fault ride through capability.

Chapter 5 explains a tool developed to perform optimal power flows in hybrid HVDC/HVAC systems for different objective functions.

Chapter 6 describes a methodology to analyse the secure and optimal operation of hybrid HVDC/HVAC grid with large penetration of offshore wind, taking into account the system spinning reserves.

Finally, **Chapter 7** summarizes the conclusions of the thesis.

Nomenclature

AC	Alternating Current
CAPEX	Capital Expenditures
DC	Direct Current
DFIG	Doubly Fed Induction Generator
EWEA	European Wind Energy Association
FRT	Fault Ride Through
FPC	Full Power Converter
HVDC	High Voltage Direct Current
HVAC	High Voltage Alternating Current
IGBT	Isolated Gate Bipolar Transistor
LCC	Line Commutated Converter
LFAC	Low Frequency AC Transmission
LVRT	Low Voltage Ride Through
MMC	Modular Multilevel Converter
MVAC	Medium Voltage AC Transmission
OPF	Optimal Power Flow
OWPP	Offshore Wind Power Plant
PCC	Point of Common Coupling
PMSG	Permanent Magnet Synchronous Generator
PLL	Phase Locked Loop
PWM	Pulse Width Modulation
SCOPF	Security Constrained Optimal Power Flow
WPP	Wind Power Plant
SCADA	Supervisory Control And Data Acquisition
TSO	Transmission System Operator
VSC	Voltage Source Converter

List of Tables

Chapter 1

Introduction

1.1 Context

According to the policies established by the EU for 2020, known as 20-20-20, the energetic scenario being built has to ensure that, in 2020, 20 % of the energy consumption will come from renewable energy, CO_2 emissions will be cut by 20% of and energetic efficiency will be improved a 20% [1]. These guidelines are encouraging the bulk integration of renewable sources through the installation of large scale plants (mainly wind or photovoltaic installations) which can range from a few MW to hundreds of MW [2,3]. In this context, wind power development has a key role for the achievement of European energy targets to be accomplished in the near future. But, it must be taken into account that the growth of wind power installations during the last decades has saturated the best terrestrial locations. Being an alternative to the onshore sites, offshore locations are acquiring interest for wind power generation. They also represent one of the solutions to ensure an increasing participation of wind power in the energetic mix.

This increasing wind power penetration tendency (both onshore and offshore) has led to multiple challenges at technical, economical and environmental levels. Focusing on the technical, one of them is the impact of the wind farms on the whole electrical system. The term wind power plants is replacing the designation of wind farms because they are supposed not only to deliver electrical power to the grid, but also to help the grid when it is working far from normal operating conditions (for instance, as a consequence of some disturbance, like short circuits). In other words, wind farms are ex-

Chapter 1 Introduction

pected to behave as other generating plants do, contributing to voltage and frequency control. To do so, wind power plants must follow grid connection requirements stated by the Transmission System Operator (TSO) of the grid they are connected to, the so called Grid Codes or Grid Code Requirements. One of the strongest requisites is that wind turbines must remain connected to the grid even during voltage sags.

Different transmission system schemes have been proposed for integrating wind power into the grid. AC transmission can be developed in medium or high voltage depending on the power rating and distance. HVDC (High Voltage Direct Current) [4, 5] becomes economically optimal for long cable distances around 100 km. The massive growth of offshore wind power plants distant from the shore, together with the new smart grid concepts [6] has enabled HVDC transmission systems [7, 8] to become a key technology for the integration of large quantities of renewable energy to the grid.

Offshore wind power plants can be based in different wind farm schemes, ranging from multiple generators connected to a single power converter [9–11] to solutions including a full power converter for each wind turbine in a DC wind farm [12]. In each case, a VSC (Voltage Source Converter) based HVDC seems to be an appropriate solution for interfacing offshore wind power plants with the terrestrial AC grid.

A multi-terminal VSC-HVDC [13–15] is particularly interesting when a number of wind power plants are to be connected to a number of grid substations, as in the so-called European supergrid [16]. Many projects are studying the feasibility of meshed HVDC grids for the future European transmission system and the possibility of building a DC Supergrid [17]. Specifically, HVDC multi-terminal systems based on VSC are being considered for the connection between renewable power generation remotely distanced from consumption, ensuring a flexible and independent active and reactive power control [18]. These VSC-HVDC multi-terminal grids are posing several challenges [19]. For instance, the availability of DC breakers [20], network restoration issues [21], the revision of existing Grid Codes or the control strategies that shall apply so as to ensure the power flow control inside the

1.2 Objectives and scope

network [22, 23].

Trying to address some of the challenges this energetic scenario has risen, the main aim of this thesis is to enhance the behaviour of wind power plants HVDC and HVAC connected in normal operation and under disturbances, taking into account the operating requirements fixed by Grid Codes.

In this direction, the studies developed can be classified in the next three fields:

- Operation and control of HVDC transmission systems for offshore wind
- Operation and control of HVAC connected wind power plants
- Operation of hybrid HVDC/HVAC transmission systems

1.2 Objectives and scope

The analysis performed on the operation and control of transmission systems for offshore wind power plants, respond to the following objectives (each of them, presented in different chapters).

- **Analyse droop based voltage control in VSC-HVDC multi-terminal systems and compare it with a proposed a control that can ensure an optimal transmission of the power produced in the wind power plants to the grid guaranteeing minimal losses**

An optimal power flow based control scheme is proposed in order to minimize the losses in multi-terminal HVDC systems for large offshore wind power plants. The scheme optimizes system power flows whilst delivering the generated wind power to the terrestrial AC grid (or grids). The proposed scheme is compared to droop control schemes in two case studies in order to illustrate the power loss reduction achieved. Dynamic simulations have been provided in order to show the dynamic behaviour of both the controller and the robust operation for wind speed changes and when a communication fault occurs.

Chapter 1 Introduction

- **Improve droop control to ensure minimal losses in VSC-HVDC multi-terminal systems**

A control scheme is proposed in order to minimize the losses in multi-terminal HVDC systems for large offshore wind power plants. This approach is based on two cascaded control schemes. A low level droop control regulates appropriately the DC current depending on the DC voltage with the purpose of ensuring a stable voltage in DC system. Another higher hierarchy controller guarantees that power flow is optimal by sending an appropriate voltage reference to the droop control of each grid side inverter. The proposed scheme takes profit of the advantages of each individual control scheme: the robustness of droop control and the minimisation of losses ensured by the Optimal Power Flow (OPF) algorithm. Total losses include transmission losses and converter station losses. A steady state analysis is provided to show the power flows that minimise several objective functions and dynamic simulations are performed to illustrate the dynamic behaviour of the control scheme under wind speed changes and communication faults.

- **Analyse the operation of AC connected wind power plants equipped with full power converter wind turbines under deep voltage sags on the main AC grid**

It is identified that standard control schemes, based on the strict application of grid codes, can lead to instability problems when this kind of severe disturbances occur. A coordinated control scheme is proposed to operate the system, ensuring fault ride through capability. An index alerts of instability proximity and allows to activate active power and reactive power regulation to guarantee safe operation during faults. The study describes the proposed control approach and demonstrates its performance by means of dynamic simulations with DIgSILENT Power Factory.

- **Develop a tool for solving the Optimal Power Flow (OPF) problem in mixed Direct Current (DC) and Alternating Current (AC) systems**

The aim is to provide a tool to analyse the optimal operation of multiple independent systems, DC connected and linked to the AC system,

1.2 Objectives and scope

from a steady state point of view and for several objective functions. The tool is benchmarked with another tool and sensitivity analysis is performed to assess the influence of DC and AC grid parameters on the operation of the system. The converter topology implemented is Voltage Source Converter (VSC), allowing an independent control of active and reactive power. The active power on the AC side and DC side of the converter differ on losses. So, the AC power can be defined as a function of the DC power and converter losses, modelled according to a second order polynomial of the AC converter current. DC cables are modelled through their resistances, AC cables are represented according to their equivalent and transformers are modelled as an equivalent impedance with inductive and resistive part. This tool is tested in a scaled platform.

- **Analyse the secure and optimal operation of hybrid DC/AC systems with high penetration of offshore wind**

This study presents a methodology to analyse the secure and optimal of a hybrid DC/AC power system with high penetration of offshore wind, taking into account the system spinning reserves. While AC systems are usually operated N-1, it is not clear which should be the criteria for operating DC grids. The expected cost of operation and wind power curtailment over one year operation are determined, taking into account the probability of failure of the different power system components. A study case, based on the CIGRÉ HVDC Test System, is presented. Generic wind profiles and representative AC generation parks are used to model the system behaviour over a complete year.

Chapter 2

Background

2.1 Wind power scenario

The wind power statistics corroborate the increase of wind installations during the last decades. According to the European Wind Energy Association (EWEA), in 2014 there were 128.8 GW of installed wind power capacity in the EU (approximately 120.6 GW onshore and over 8 GW offshore). The annual wind power installations have actually grown from 3.2 GW in 2000 to 11.8 GW in 2014 [24]. All these data point to an encouraging future for the wind industry, but, onshore locations with the best wind profiles are finite and most of them occupied by finished projects or under development.

To face this problem, there are basically two solutions allowing to continue increasing the wind power contribution in the energy mix despite the saturation of the best terrestrial sites. One promotes to install wind farms in the sea (offshore); the other, promotes the reuse of wind turbines that occupy the best locations replacing them by other wind turbines of larger power and with more advanced technologies. The old wind turbines can be then allocated in less developed countries, facilitating and expanding the use of renewable energy.

2.1.1 Offshore

The first solution is to locate wind turbines offshore (known as offshore wind power and deep offshore when it comes to deep waters). They do not only represent an alternative to terrestrial plants (also called onshore), but also offer more favourable wind profiles (more constant and less minor turbulent),

Chapter 2 Background

often have often lower social opposition due to its lower visual impact and allow the installation of larger wind turbines (and, thus, with larger rated power). The evolution of the wind turbines size and power is depicted in Figure 2.1 [24, 25].

This trend towards offshore wind farms can be seen in the evolution of the

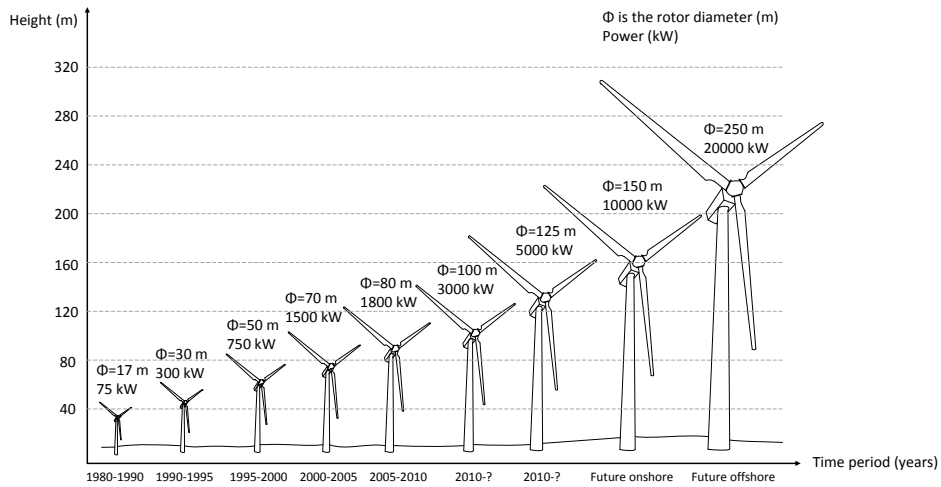


Figure 2.1: Wind turbine's size and power evolution from 1980 until nowadays

annual wind power installed in the last ten years in Europe. In Europe, on 2001, 4377 MW had been installed onshore and 4 MW offshore, while on 2011, 8750 MW were installed onshore and 866 MW offshore [26]. So, it can be observed that the annual wind power installed has doubled onshore and has been multiplied by a factor of 200 offshore (in 10 years).

With the installation of offshore wind farms, wind turbines design has evolved to achieve the production of major powers with the minimum maintenance of the generating units. Taking into account that one of the components with the highest rate of failure in wind turbines was transmission mechanical and multiplier (which allows to adapt the speed of the turbine at the speed of the generator) the latest designs of wind turbines have abolished this element through the use of multi-polar synchronous generators. Full power converters, connected to this type of electrical machines guarantee a

2.1 Wind power scenario

greater control of the wind turbine (see Figure 2.22). Technology associated with converters, is also in full swing, with tendencies toward converters of various levels, modular converters integrated multiphase generators and intended also as interface for storage systems. Due to the great variability of wind resources, it might be, in the future, allowing the installation of devices such as flywheels, supercapacitors, or batteries store power in excess when the generation exceeds demand and deliver the energy needed when the generation is less than the demand.

The advanced control techniques are thereby helping to maximize the energy captured from the wind, to minimize the mechanical loads, stabilize the control of floating structures, improve the control of the converters and generators, as well as the control for disruption of the network. Will also reduce the weight of the paddles and will increase your radio, thanks to the implementation of the finite element analysis and manufacturing techniques and advanced materials (such as carbon fibre).

So far, the majority of the large wind turbines are developed and orients itself on a horizontal axis. The structures to be placed on offshore sites can be classified into monopile, tripile and jacket. In the future floating structures will be developed, such as the so-called Ballast stabilized, Mooring lines and buoyancy, which allow you to install wind turbines in deeper waters. Therefore, technological developments planned for the next decade in the wind energy sector include new concepts of wind turbines, advanced control techniques for regulation, new designs of paddles, new topologies of park improvements and integration at the network. It should be emphasized that it was thanks to the possibility of installing wind turbines at marine sites that has been invested in R&D to adapt the existing wind turbines to a new environment and improve their design, operation, control and reliability.

2.1.2 Repowering

The second solution to expand the wind generation despite the exploitation of the best locations onshore, is inspired by the rule of 3R, proposal on the habits of responsible consumption popularized by the international environmental organization Greenpeace: reduce, reuse and recycle. In particular,

Chapter 2 Background

is based on the second R: reuse the wind turbines currently occupy the sites with best profiles of wind and that can be replaced by other higher powers and with more advanced technology. This replacement allows, on the one hand, extend the power installed in this location, and, on the other hand, take advantage of the wind turbines that have been replaced, install them onto developing countries, to encourage the use of renewable energy, to a more accessible price. This process is known as repowering.

According to Grontmij [27], the replacement of wind turbines may be based on five procedures. The first, to replace 1 old lonely windmill by 1 new. The second is to replace 2 older wind turbines by new larger 1. The third encourages grouping isolated wind turbines in a wind farm with a limited location (for example 20 solitary wind turbines could be replaced by a cluster of 6 or 10 new wind turbines). The fourth procedure be based on replacing 1 old wind turbine by 1 new similar power, but with newer machine. The fifth alternative calls for a substitution of 1 old wind farm new 1. Each option presents certain advantages over the others, but which has a minor impact on the landscape is clearly the third one: Reuse wind turbines which currently occupy the sites with best profiles of wind and that can be substituted for other major powers and with more advanced technology. This substitution allows, on the one hand, extend the power installed at that location and, on the other hand, take advantage of the wind turbines that have been replaced, installing them in developing countries, to encourage the use of renewable energy, at a more affordable price. This process is known as repowering.

The installation of new wind turbines not only allows to generate more wind power without using any more area, but also with a less number of wind turbines, since on having had major rotor diameter, the area included by the spades is also major and, consequently, the potency extracted from the wind and, therefore, the generated one, also it it is. Since a less number of wind turbines can produce the same one or even more potency than it was installed, the visual impact turns out to be limited (although the height of the new wind turbines will be major). The cost of production of the electric power originated from these new wind parks also will be low, since

2.1 Wind power scenario

the efficiency of the energy conversion turns out to be increased. Also, it is necessary to bear in mind that the licenses securing to construct wind parks offers less difficulties if it is a question of an already existing place, instead of a new one.

All of the above applies to the countries selling wind turbines which have become obsolete. What brings the repowering to purchasers of the wind turbines that are substituted? On the one hand, a lower investment (CAPEX) for the construction of the park and a shorter duration of the project, which reduces the financial risk. On the other hand, easy to transport and maintenance of wind turbines, by be smaller than the most current and sophisticated.

One of the disadvantages of the repowering is an adaptation to the codes of connection to specific network of the new location. All wind farm that is connected to mains power of a country must meet a series of technical requirements specified by the transmission system operator, which describe how you should behave the park and each of their generating units both in normal operating conditions as in the case of disturbances such as short circuits. They are what in English is known as Grid Code Requirements. In the event that there should be the repowering of a wind park english and decide locate their wind turbines in Spain, you need to adapt these units to meet the criteria of a network connection fixed by REE, instead of the required under National Grid (TSO of the United Kingdom) .

In conclusion, against the problems linked to the saturation of the best terrestrial sites to install wind turbines, the offshore location is becoming not only a solution, but also an alternative that allows for a greater contribution of wind energy in the energy mix. On the other hand, the repowering, hitherto raised at ground level, is allowing an expansion of wind power, thanks to the participation of new countries for which access to renewable energies had an unacceptable cost. All indications are that both strategies will be joined by also allowing the offshore repowering.

2.2 Grid integration of offshore wind power plants

2.2.1 Introduction

The progress in power electronics, as well as the improvement of cables performance have favoured and still stimulate the development of DC technology, in parallel with AC. The choice of a technology or the other one will depend, to begin with, on the technical feasibility of each one for the specific link to be constructed. Two examples of this large dependence on the technical requirements can be advanced. On the one hand, if the connection to be constructed links two systems working at different frequency (asynchronous systems), HVDC must be used. With HVDC the power transmitted is practically independent of distance, whereas, in HVAC the power capability transmission decreases with distance. But the final decision of constructing a link through DC or AC, will depend not only of technical criteria, but also economic and environmental.

2.2.2 Transmission options

The present section introduces different transmission system options for delivering the power generated in offshore wind farms to the main AC grid.

Medium Voltage AC transmission

For wind farms that are not high power rated and close to the shore (usually less than 15 km), their connection to the onshore grid can be done through Medium Voltage AC transmission (MVAC), according to Figure 2.2. As the voltage at the collection grid is the same that on the onshore side, no transformer platform is required. An example offshore wind farm connected through MVAC is the dutch wind farm Egmond aan Zee (108 MW, since 2006, around 10 km offshore) the wind turbines are directly connected to the shore by three 33 kV cables.

High Voltage AC transmission

For offshore wind power plants that are far from the onshore grid, HVAC transmission might be a solution for transmitting their power (see Figure

2.2 Grid integration of offshore wind power plants

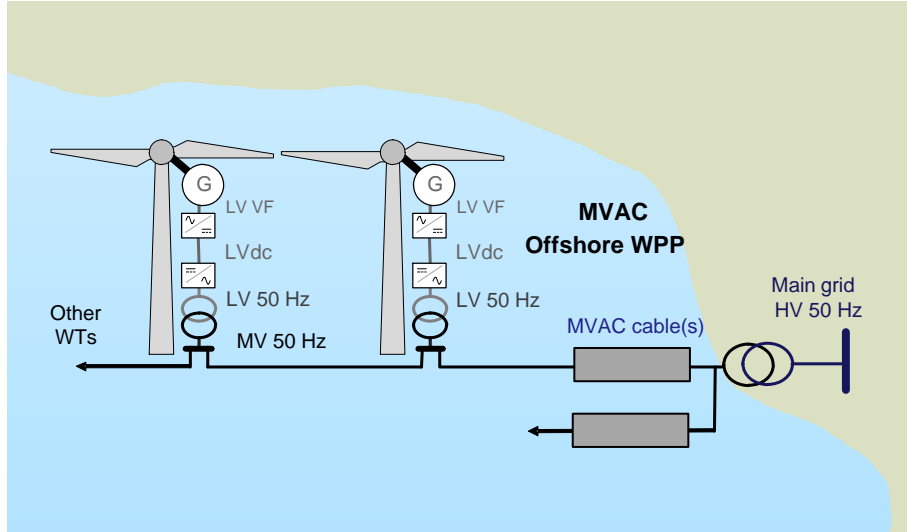


Figure 2.2: Offshore wind farm connected through Medium Voltage AC transmission (MVAC)

2.3). An offshore transformer increases the collection grid voltage (around 33 kV) to a higher transmission voltage (132 kV to 220 kV). The design of the protection system and the voltage level changes using transformers are not an obstacle. However, the capacitive effect of submarine power cables can limit the distance of the transmission. Although reactive power compensation equipment could be installed at the ends of the cable or in an intermediate point, this enlarges significantly the investment costs and is not always feasible. Consequently, HVAC can be an appropriate transmission system for relatively short distances (less than 60 km). An example of an HVAC connected offshore wind farm is Horns Rev (160 MW, since 2002), where the power is collected on an offshore substation and transmitted to the shore by a 15 km three-core AC cable with a rated voltage of 150 kV.

Low frequency AC transmission

In Low Frequency AC systems (LFAC) [28, 29], an intermediate frequency level of 16.67 or 20 Hz is used, which is created by using a cycloconverter, that lowers the grid frequency, normally to one-third its value. The main

Chapter 2 Background

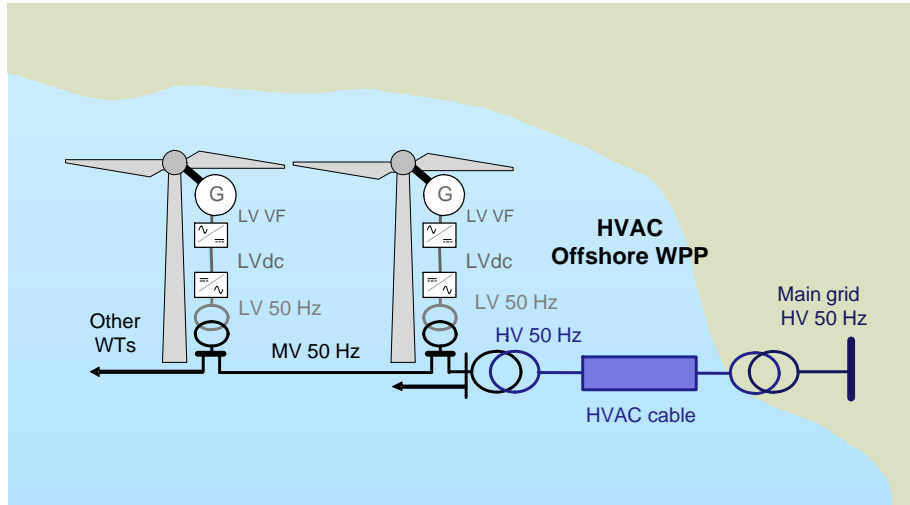


Figure 2.3: Offshore wind farm connected through High Voltage AC transmission (HVAC)

advantage of the LFAC technology is the higher power capacity and transmission distance compared to the standard frequencies (50 Hz or 60 Hz) used in HVAC. Derived from this, there are significant cost savings due to the reduction in cabling requirements and compensating devices. However, low frequency transformers increase in size and costs compared to a standard 50 Hz transformers. The scheme of a LFAC connected wind farm is depicted in Figure 2.4).

High Voltage DC transmission

HVAC is not feasible for transmitting large amounts of power over distances greater than 50 km. The alternative is High Voltage Direct Current (HVDC) transmission (Figure 2.5). The simplest HVDC connection for linking an offshore wind power plant to the onshore grid is an HVDC point to point. It consists of two converter stations and DC cables linking them. The first HVDC link to connect an offshore wind farm with an AC grid is the BorWin1 project, that connects the BARD Offshore 1 wind farm in the North Sea to German's mainland AC grid.

2.2 Grid integration of offshore wind power plants

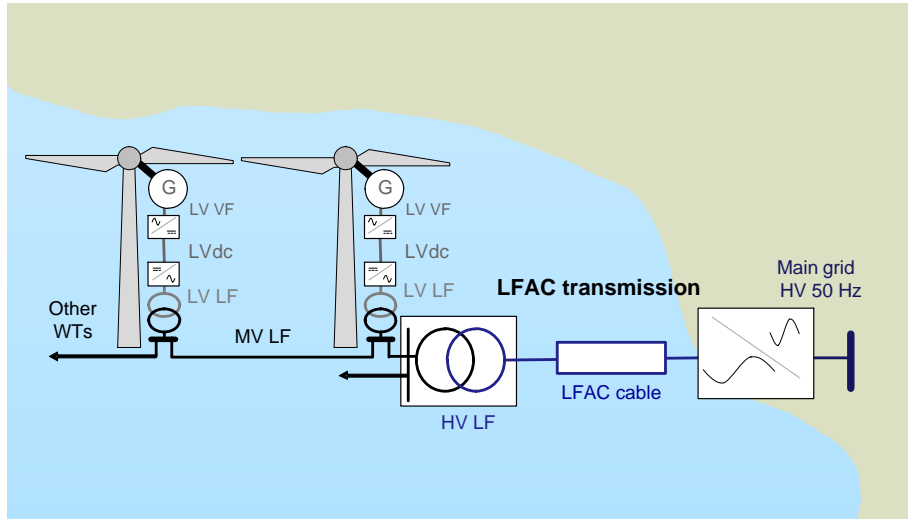


Figure 2.4: Offshore wind farm connected through Low Voltage AC transmission (LVAC)

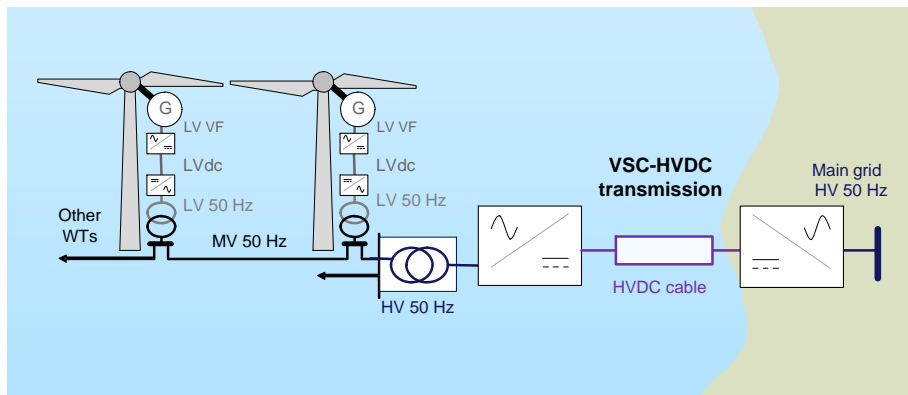


Figure 2.5: Offshore wind farm connected through High Voltage DC transmission (HVDC)

Multiterminal High Voltage DC transmission

When several offshore wind power plants need to be connected to the AC system, multiterminal HVDC configurations can be the solution, as represented in Figure 2.6. Instead of building several HVDC point to point connections, a multiterminal system can be constructed, adding redundancy to the whole system. The first multiterminal existing project is the Chinese three terminal HVDC system, for Southern Power Grid. The so called Nan'ao multi-terminal has a capacity of 200 MW and DC voltage level of ± 160 kV.

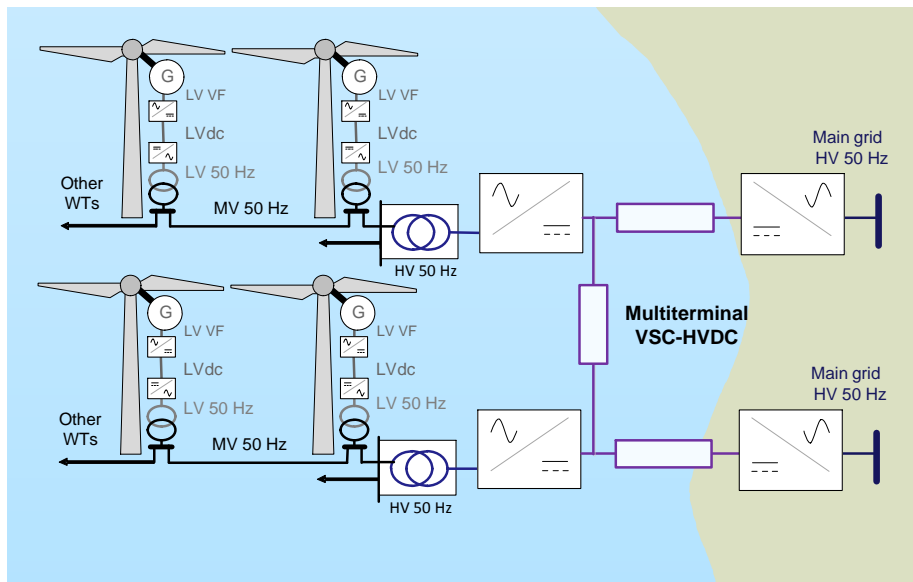


Figure 2.6: Offshore wind farms connected through Multiterminal High Voltage DC transmission (HVDC)

2.2 Grid integration of offshore wind power plants

2.2.3 HVDC transmission

HVDC components

The HVDC simplest system consists in two converter stations and a transmission line that links them.

- **Converter station**

The conversion from AC to DC and vice versa is performed in the converter stations. The elements that guarantee its correct operation are [30]:

- AC and DC filters (due to the large amount of harmonics generated).
- Transformers to adequate the voltage levels to the required by the converter.
- Converter (working as a rectifier or as an inverter).

These components are represented in Figure 2.7.

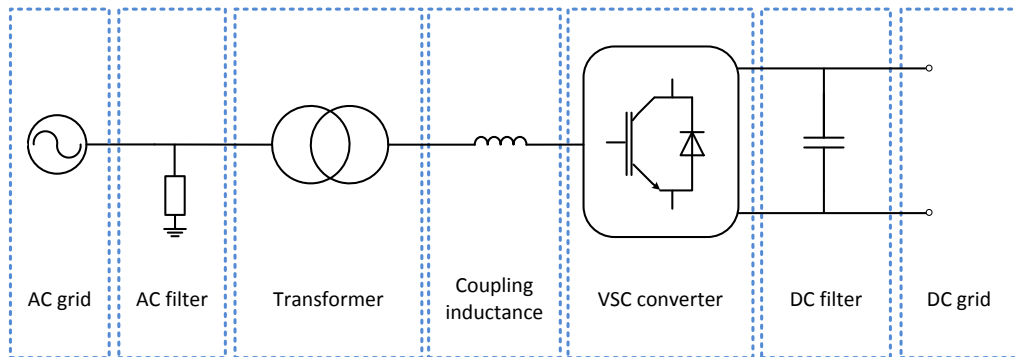


Figure 2.7: Converter station scheme and components for a VSC-HVDC system

- **Transmission line**

For submarine transmission, HVDC cables are used. For systems with back-to-back configuration, DC cables are not required, nor overhead lines.

Chapter 2 Background

HVDC configurations

The type of connections existing among the converters of HVDC systems permits to classify these systems in back-to-back, point to point and multi-terminal [30] (see Figure 2.8).

- **Back-to-back**

In this type of configuration, rectifier and inverter are located in the same converter station, allowing an asynchronous connection between two AC systems through a DC link, but without the need of a transmission line.

- **Point to point**

Most of HVDC systems present this type of configuration, based on the connection between two converter stations by means of a DC transmission line.

- **Multi-terminal**

HVDC systems with multi-terminal configuration have, at least, three converter stations, geographically separated and linked by means of DC transmission lines. The main advantages of this connection are the benefits in redundancy and losses and this connection can be made in series or in parallel.

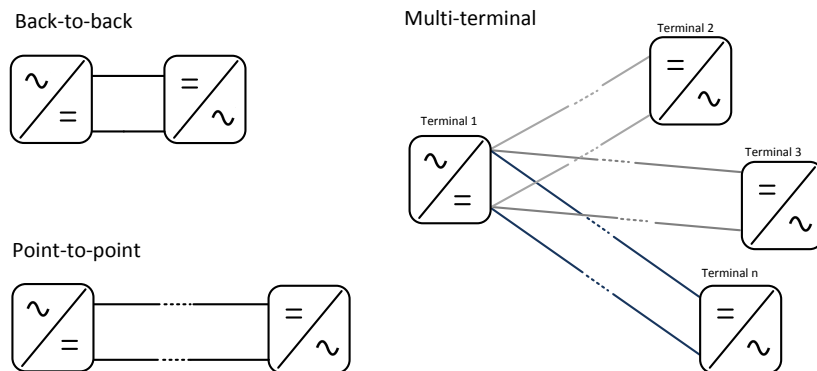


Figure 2.8: HVDC systems topologies

2.2 Grid integration of offshore wind power plants

HVDC topologies

The way the transmission lines of HVDC systems are connected to the converter station permits to classify the topologies as monopolar, bipolar and homopolar [30] (see Figure 2.9). For each of them, the return can be through ground or metallic.

- **Monopolar**

Both converter stations are linked by a single conductor, isolated, and the return is done by means of the electrodes of the stations, connected to ground.

- **Bipolar**

This type of connection is the most used. Both converter stations are linked through two conductors, one with positive polarity and the other one with negative polarity, which transmit simultaneously the same power. In normal operation mode, the return current is null (the current coming from the line with positive polarity is cancelled with the current coming from the line with negative polarity). In case of failure of one line, the system can operate with the other one and with ground return (like a monopolar connection).

- **Homopolar**

Both converter stations are connected with two or more conductors with the same polarity. The return is done through ground or through a metallic conductor. The drawback of this connection is the high returning current. This explains its less extended use.

HVDC technologies

Based on the converter technology used, HVDC can be classified in LCC-HVDC and VSC-HVDC, where LCC refers to Line Commutated Converters and VSC refers to Voltage Source Converters [30].

- **Line Commutated Converter (LCC)**

LCC employs thyristors as switching devices and this technology is more mature than VSC. Thyristors are triggered with a pulse at its

Chapter 2 Background

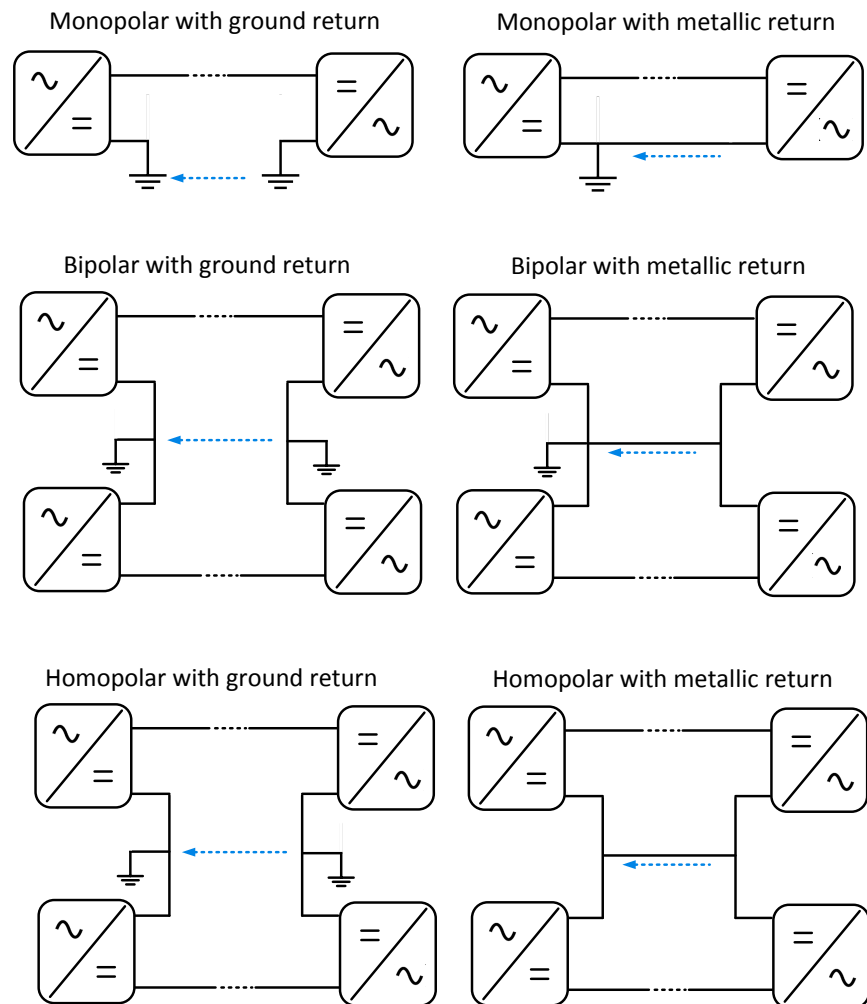


Figure 2.9: Converter stations connection

2.2 Grid integration of offshore wind power plants

gate, once every half cycle (next zero crossing blocks the device), so this limits its controllability [31], reflects its dependence on AC grid voltage and explains its lack of black start capability.

Thanks to the small number of switchings, switching losses are low. Furthermore, thyristors present very high current and blocking voltage and allow the transmission at higher voltage ratings and of higher power than VSC. LCC can reach 7200 MW power transmission at ± 800 kV voltage level, whilst VSC can transmit up to 1000 MW at ± 320 kV [32].

But, a minimum short-circuit capacity of the AC grid to which the LCC converter is connected is needed to ensure its stable operation. This is due to the fact that active power changes imply reactive power changes, leading to voltage fluctuations. Furthermore, if AC voltage falls, larger reactive power consumption is required (this could also cause voltage instability). This is why LCC are said to need a minimum short-circuit ratio, defined as the ratio between the AC system short-circuit power and the rating of the converter (approximately 2) [31].

- **Voltage Source Converter (VSC)**

The switching devices in VSC are Isolated Gated Bipolar Transistors (IGBTs), which do not commutate with the grid. As they do not need an AC grid to operate, the risk of commutation failures is low.

On the other hand, IGBT's present turn on and turn off capability, so VSC is characterized by a larger controllability, compared to LCC: VSC can control active and reactive power independently. PWM (Pulse Width Modulation) is the extended technique for switching the IGBTs. It allows a simultaneous adjustment of the amplitude and phase angle of the converter AC output voltage with constant DC voltage for two level converters [33]. Another advantage inherent to VSC is its black start capability [21, 34]. Moreover, as this technology presents a larger number of switchings, harmonics are reduced (and consequently, also the size of the needed filters diminishes). However, and also as consequence of the high switching frequencies, switching losses are higher.

Until a few years ago, the only VSC topology in use for HVDC was

Chapter 2 Background

two or three-level configurations making use of PWM. But in 2003, an alternative design was proposed by Prof. Rainer Marquardt in Germany [35, 36]. It is based on the series-connection of several submodules normally containing two semiconductor switches and a capacitor. Nowadays, this topology is more commonly known as modular multilevel converter (MMC). Compared to the two-level and three-level topologies, a significant feature of the MMC topology is the absence of a common capacitor connected at the DC side. Instead, the DC capacitors are distributed into each module, while the converter is built up by cascaded-connected modules. Owing to this scalability, MMC concept has attracted a lot of interest for high-voltage, high-power applications.

Furthermore, MMC takes advantage of the fact that large voltage steps associated with PWM operation can be reduced by generating the AC voltage from a large number of smaller voltage steps. The higher the number of voltage steps, the smaller is the proportion of harmonics generated by the switching process. In addition, due to lower switching frequency per IGBT [37], MMC presents significant converter loss reduction, compared to the PWM VSC-HVDC systems. Last, but not least, as its harmonic content only very small filters are needed, if necessary [38].

The world's first VSC HVDC Project with MMC is the so called Trans Bay Cable, in USA. It became operational on November 2014, to link Pittsburg, California to Potrero Hill in the San Francisco bay area. The 88 km transmission line is operated at 200 kV and connects two converter stations equipped with 400 MW MMC converters, from Siemens.

2.3 Operation and control of offshore wind power plants

One of the main triggers for the development of offshore grids is the need for transmission systems for the increasing number of offshore wind power plants (WPP). When connected to HVDC transmission systems, offshore wind power plants are not synchronous with the main terrestrial grid and therefore the operation and control requirement differ from those of AC connected WPP. The offshore grid must be established and maintained by means of the VSC-HVDC rectifier in close coordination with the wind turbines. Furthermore, the WPP are expected to provide support both to the HVDC transmission system and the terrestrial grid or grids according to the relevant grid codes [39–43]. The present chapter introduces the main functional requirements for HVDC connected WPP and describes some application examples.

2.3.1 Introduction

The operation of offshore wind power plants addresses the coordination and integration of WPP- and VSC-HVDC converters. The coordination of controllers and protections is a fundamental issue for VSC HVDC connected offshore wind power plants. An appropriate integration will often deal with different manufacturer technologies, and therefore it is extremely important to clearly specify how this integration can be conducted in a given installation [44].

The present section considers point to point VSC-HVDC connections integrated with wind power plants based both on doubly fed induction generators (DFIG) and full power converter (FPC). The considered scenarios include normal and fault operation. As far as the requirements are concerned, they include the start-up and the normal operation of the WPP, the eventual active power curtailment, the fault ride through capability and the onshore grid support. The onshore grid support will be mainly implemented in the grid side VSC-HVDC converter but it will require actions from the WPP.

The required control and protection strategies are also discussed looking

Chapter 2 Background

both at the obtained system performance and the required communication systems. The system under study is sketched in Figure 2.10.

The analyzed system considers a VSC-HVDC converter which is installed

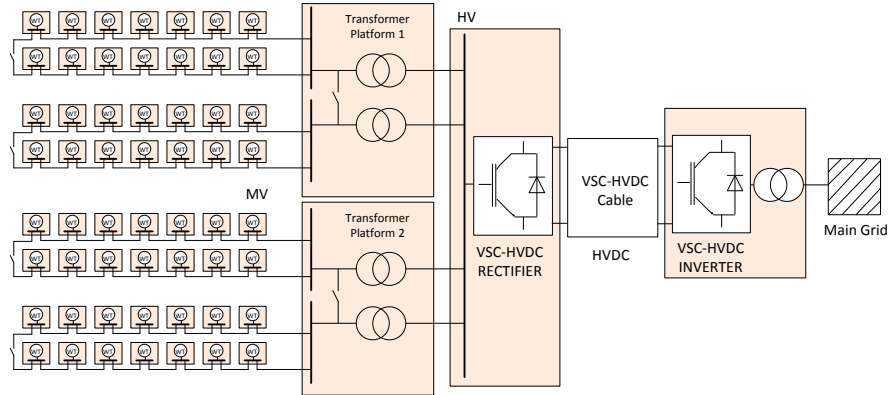


Figure 2.10: VSC-HVDC offshore wind power plant

in a platform and connected to two transformers located in two platforms where they collect the power from several strings of wind turbines. Each transformer collects the corresponding nominal power in normal operation, however the transformers will be typically overrated to allow to operate the WPP at partial load in certain circumstances with only one transformer. Reactive power compensation equipment may be considered depending on the configuration. Reactive power is also provided by the VSC-HVDC converter and the wind turbines. DC choppers will be considered in all the wind turbine converters and the VSC-HVDC.

2.3.2 Control and protection functions required

Functions required

The control and protection integration of the WPP and the VSC-HVDC will be required to provide the following functions:

2.3 Operation and control of offshore wind power plants

- Reactive power management. The management of reactive power is strongly linked to the voltage control both in the wind turbines and the VSC-HVDC. The WPP dispatches reactive power references to the wind turbines. The offshore grid voltage must be maintained in appropriate levels in all the wind turbines and in the VSC-HVDC converter.
- The offshore grid frequency must be controlled at the desired value. This task is performed by the VSC-HVDC rectifier which imposes the offshore grid frequency.
- An appropriate start or stop sequence must be applied considering issues such as the transformers inrush current and the possible voltage transients. Auxiliary power and communication system are needed for the start-up and shut/down sequences.
- Active power management. Active power will be managed in order to extract the maximum possible power for low wind conditions, extract the nominal power in high wind conditions and reduce power when needed or required by the grid operator.
- Fault ride-through capability.
- Main grid support. VSC-HVDC connections are expected to provide support to the grid where they are connected:
 - Voltage support will depend mainly on the grid side VSC-HVDC inverter.
 - Frequency support requires coordinating the VSC-HVDC inverter, VSC-HVDC rectifier and the WPP. The WPP VSC-HVDC rectifier will be demanded to reduce or increase power for onshore grid frequency support. In this case, one possibility is to change via communications the active power command or to mimic the onshore frequency on the offshore grid in order to obtain the same response from the WPP as it would perform in an onshore system. In any case, communications are needed.
- Power system stabilizer capability?

Chapter 2 Background

- Operation under communication failure?
- Provide auxiliary power to the WPP (1-2%) when there is no wind.
To illustrate the different situations, the following colour code is used:
 - Green is used for systems operating in normal conditions
 - Yellow is used for systems operated in restricted conditions
 - Red is used for systems which are faulted or are the problem origin

Considered situations

In order to be able to specify the control and protection functions required, the following situations are considered:

- Normal operation: The WPP is operated without any electrical restriction. In this case all the generated power should flow through the WPP grid and be injected in the VSC-HVDC cable. This situation is shown in the Figure below, where the green lines show the power flow.

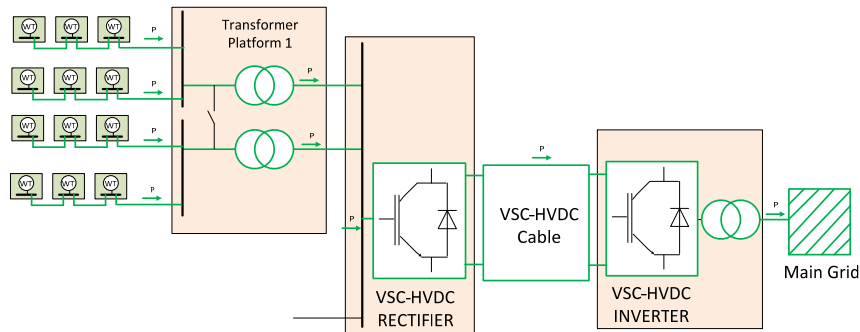


Figure 2.11: Normal operation

- Restricted operation: Due to eventual problems or maintenance operation, part of the electrical system might not be available. For example,

2.3 Operation and control of offshore wind power plants

one of the two transformers of the platform is unavailable. Coordinated control will be required to limit the generated wind power. As it is shown in the Figure below, the generated power will have to be reduced, but the operation of the system is possible.

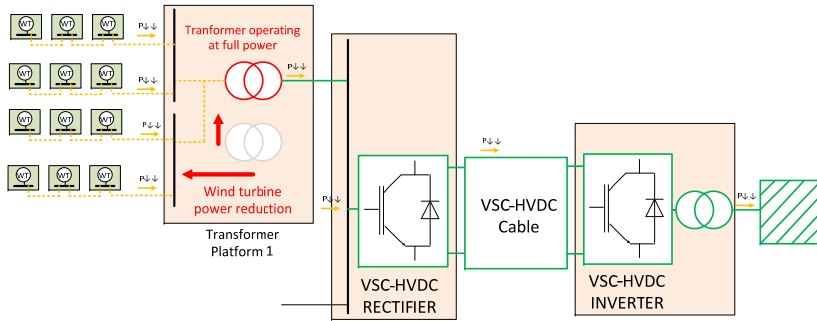


Figure 2.12: Restricted operation

- Main AC grid fault: A fault in the main AC grid reduces drastically the AC voltage in the VSC-HVDC inverter and therefore reduces the power extraction capability. These faults can be addressed providing fault ride-through capability by an appropriate use of a DC chopper in the grid-side VSC converter as shown in the Figure below.

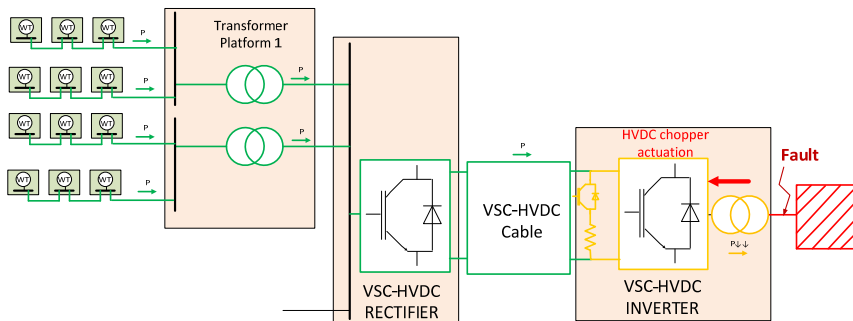


Figure 2.13: Fault in the main AC grid

Chapter 2 Background

- Reduced power operation. The grid operator may send power references to the WPP in order to reduce power, mainly due to congestion management issues. In this case a direct communication will be sent from the grid operator to the WPP which will dispatch reduced power references to the wind turbines.

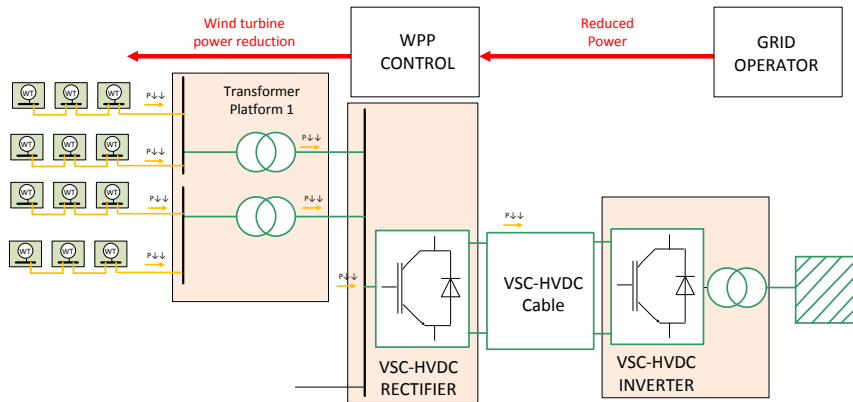


Figure 2.14: Reduced power operation

- Frequency response. In the case of frequency variations, the active power from the WPP may have to be changed according to the grid code requirements. In this case there are two possibilities (both assuming that the grid side VSC-HVDC is continuously measuring the onshore grid frequency):
 - A direct communication is sent from the grid-side VSC-HVDC to the WPP (containing the onshore grid frequency or the required WPP active power). The WPP control dispatches power references to the wind turbines.
 - A direct communication is sent from the grid-side VSC-HVDC to the wind farm VSC-HVDC rectifier which changes the offshore grid frequency to mimic the onshore grid frequency. The wind turbines react accordingly modifying the active power injected.
 - DC fault: A fault in the VSC-HVDC or one of the VSC-HVDC

2.3 Operation and control of offshore wind power plants

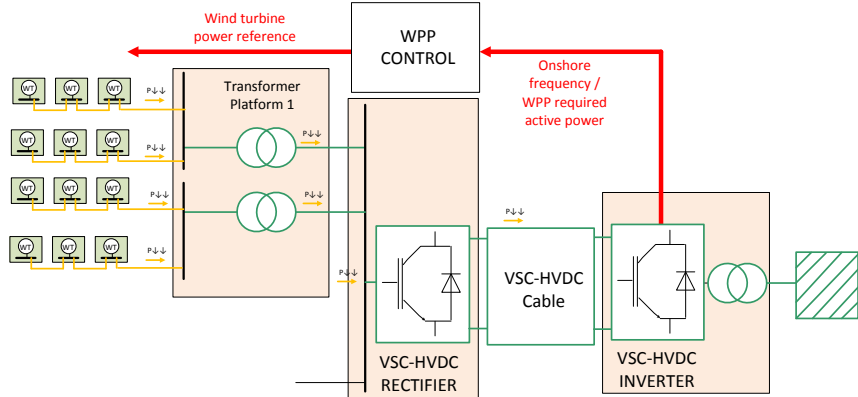


Figure 2.15: Frequency response: direct communication from the grid-side VSC-HVDC to the WPP

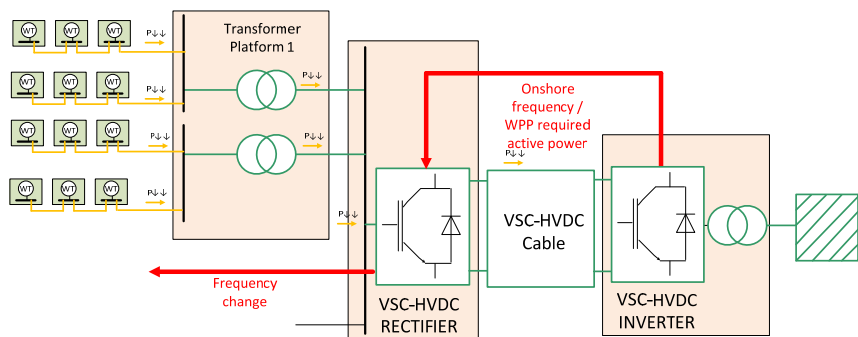


Figure 2.16: Frequency response: direct communication from the grid-side VSC-HVDC to the wind farm VSC-HVDC rectifier

Chapter 2 Background

converters will imply the whole system disconnection. It has to be ensured that the disconnection is performed safely.

- WPP grid fault: For faults in the WPP grid, part or all the WPP will be disconnected, the fault has to be located and isolated rapidly. The disconnected part will depend mainly on the number of circuit breakers available in the WPP grid and the available redundancy. Since the WPP grid is an only power electronics grid, the short circuit current will be provided by the several VSC converters. It must be ensured that the relay protections operate appropriately.

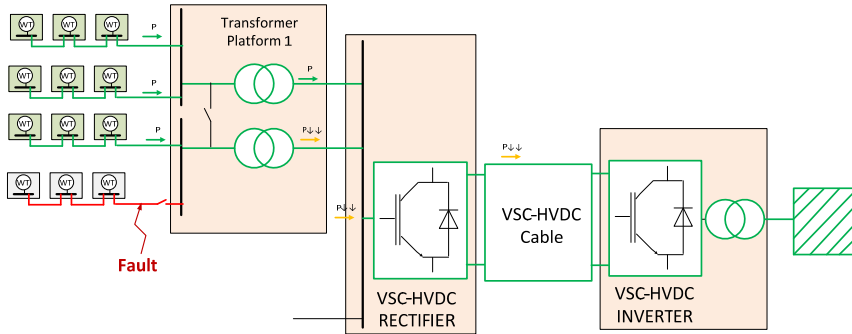


Figure 2.17: Fault in the WPP grid

- Wind turbine internal fault: Internal faults in the WT will imply the WT disconnection.

2.3.3 Control and protection integration

The available controllable variables are the active and reactive power of all the individual wind turbines and also the active and reactive power (or the equivalent frequency and voltage) of the VSC-HVDC. The control scheme will have to both ensure the active and reactive power balance, injecting all the wind power generated to the HVDC cable, while maintaining an appropriate voltage in the different buses and controlling the WPP frequency.

2.3 Operation and control of offshore wind power plants

Control integration

A typical control integration scheme is shown in Figure 2.18.

Electrical magnitudes as frequency can be used to modulate the informa-

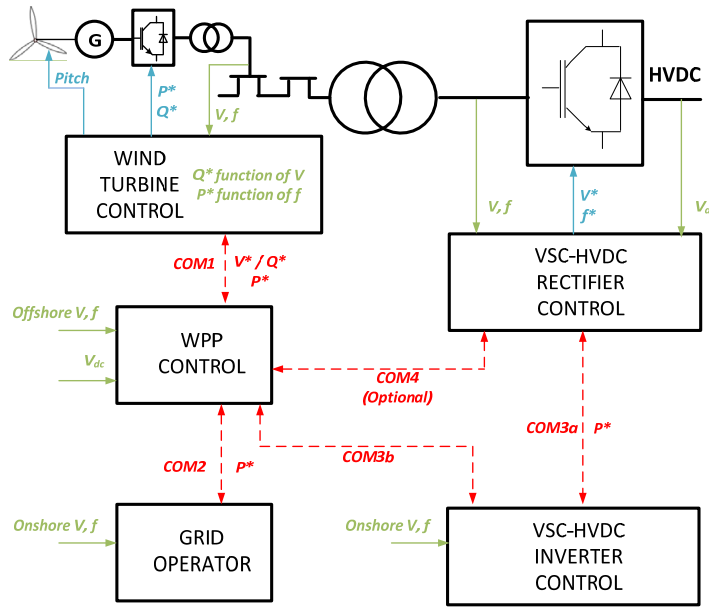


Figure 2.18: Integrated control scheme

tion needed for the coordination allowing devising a system without fast communications between VSC-HVDC and wind turbines. Whenever the active power reference of the wind turbines is to be modified it can be performed by means of communications from the central WPP controller or from the offshore VSC-HVDC converter by modifying appropriately the offshore grid frequency (or just mirroring the onshore grid frequency on the offshore grid). Wind turbine controls can be the same as for an onshore or HVAC connected wind turbine.

The considered communications systems include:

- COM 1: Communications between the WPP control system and the individual wind turbines, to allow power dispatching.

Chapter 2 Background

- COM 2: Communications between the grid operator and the WPP control system, to allow power reductions for congestion management.
- COM 3: One of the following communication schemes will be required:
 - COM 3a: Communications between the onshore VSC-HVDC converter and the offshore VSC-HVDC converter to allow active power regulation for frequency support.
 - COM 3b: Communications between the onshore VSC-HVDC converter and the offshore WPP control to allow active power regulation for frequency support.
- COM 4: Communications between the WPP control and the offshore VSC-HVDC converter. It is an optional communication link that it might be necessary.

Protections integration

The design of the protection scheme for the offshore WPP will take into account the low short-circuit current of the offshore grid, related to power electronics nature of such a grid. Protections will be designed and adjusted to avoid any damage to the equipment.

2.3.4 Wind power plant control

Offshore wind farms can be based on different wind farm schemes, ranging from multiple generators connected to a single power converter [9–11] to solutions including a full power converter for each wind turbine in a DC wind farm [12]. Although the variety of proposals, mainly generators equipped with Full Power Converters (FPC) and Doubly Fed Induction Generator (DFIG) wind turbines are being installed and connected to MV grid (rated to 33 kV, typically).

The typical control structure for a wind farm is hierarchical and can be divided in two levels: the control applied inside each wind turbine (local control or control at wind turbine level) and an outer control, applied to the whole wind farm (global control or control at wind farm level) [45]. The

2.3 Operation and control of offshore wind power plants

interaction between the wind farm control and each wind turbine control is possible thanks to SCADA systems [46]. As indicated by the capital letters of its acronym, the SCADA ensures the Supervision and Control of the wind power plant as well as the Acquisition of the Data of its different components. Their specific functions include the real time data caption, recording and management, data transmission among different devices and data display through HMI.

When the wind power plant control does not send any active/reactive power reference to the wind turbines, the wind turbine control ensures that for wind speeds under nominal wind speed, the active power generated is maximum and above it, the active power produced is kept to the rated value. In both cases the wind turbine control will guarantee the needed reactive power exchange with the grid so as to keep the AC voltage of the generator. If the wind power plant control sends an active/reactive power reference signal to the wind turbines, the wind turbine control will ensure that each wind turbine produces the needed active and reactive power to operate the wind farm as close as possible to the set-point specified by the wind farm control.

Next sections explain the control present in each generating unit of the wind farm (wind turbine control) and the coordinated control of all the wind turbines (wind farm control). Finally, their performance in a 90 MW wind farm are shown through simulations in DIgSILENT Power Factory.

- **Wind turbine**

Each wind power generating unit is constituted by a turbine, an electrical machine (PMSG, all along this chapter), a full power converter and a transformer, as shown in Figure 2.19. The turbine captures the kinetic energy of wind and transforms it into rotating mechanical energy, which, after the mechanical transmission, is the input power for the PMSG, which delivers it in form of electrical power. The transformer connected to the electrical machine permits to adapt the voltage of the output power to the voltage of the cable transmission until the wind farm platform. According to the conversion energy processes inside a

Chapter 2 Background

wind turbine, its main components can be classified in aerodynamic, mechanic and electric. They are listed below and their location in the wind turbine are presented in Figure 2.20.

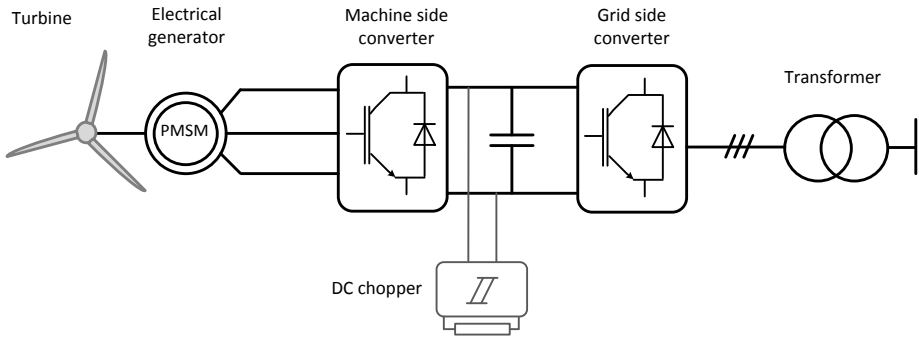


Figure 2.19: Scheme of a PMSG wind turbine equipped with full power converter

- **Blades.** They allow the wind energy caption and are usually made of composite materials so as to bring stiffness and light weight.
- **Hub.** Part where the blades are fixed to the turbine rotor.
- **Rotor and axis.** The rotor is connected to the mechanical transmission, usually constituted by an axis system and, occasionally, a gearbox, so as to transmit the rotational mechanic energy to the generator.
- **Gearbox.** Adapts the turbine rotor rotating speed to the high rotating speeds of the generator rotor.
- **Generator.** Converts mechanical power into electrical power. Two of the technologies used nowadays are DFIG (Doubly Fed Induction Generator) and multipolar PMSG. The advantage of the latter is that it avoids the need of including a gearbox, as for being multipolar, presents lower rotational speeds, matching the rotational speed of the wind turbine rotor.

2.3 Operation and control of offshore wind power plants

- **Nacelle.** Located at the upper part of the tower, the nacelle contains the rotor, gearbox and wind turbine.
- **Tower.** As wind speed varies with the altitude, in order to maximize wind power caption, the blades and the nacelle are located on the tower.
- **Controls.** They allow to generate electrical power above a certain wind speed (cut-in speed) and to stop generating when the wind speed reaches the so called cut out speed. Wind power caption can also be regulated through systems like Pitch and Stall. Moreover, the nacelle can be oriented in the wind direction to maximize wind power caption, thanks to Yaw system. Other systems enable to monitor and control the quality of the power generated.

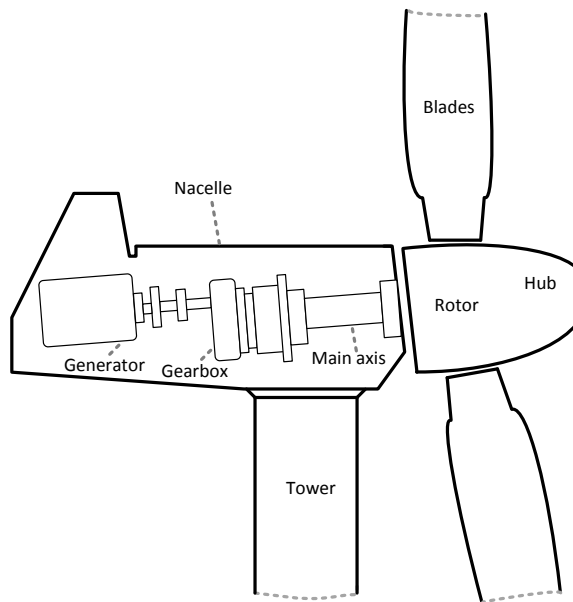


Figure 2.20: Main components of a wind turbine

- **Wind farm**

The wind farm layout can be designed according to different criteria, like maximizing energy production, minimising cost or ensuring the

Chapter 2 Background

highest reliability. The decision of where the wind turbines should be located can be based on wind speed direction so that maximum power is obtained. However, many criteria to connect the turbines exist [47]. The different possibilities of connecting wind turbines can be distinguished according to the following concepts: clustering, redundancy, voltage level and type of cable [47, 48].

- **Clustering** [48]. Defines the way wind turbines are grouped. In string/radial configurations the wind turbines are connected to a MV bus, since the transformer to increase the voltage (LV to MV) and protections are installed in the housing (nacelle and tower) of the wind turbine. In star configuration the wind turbines are connected via LV to platform, where the step-up transformer adapts the voltage to MV and the protections are located. This topology avoids the need of transformers and protections in every wind turbine, however the platform is expensive and the losses are also higher due to the use of LV lines. The cable rating and rated power of the turbines determine the number of clusters.
- **Redundancy** [47]. In order to obtain higher system reliability (keeping as many wind turbines as possible during a contingency) some redundancy may be introduced to wind farm. For instance, in a single-sided ring design, a redundant path is implemented through the end of a radial connection to the collector. The additional security comes with an extra cable at full rate capacity.
- **Voltage level** [47]. The electricity from the generator is adapted to the voltage level of the distribution system by a wind turbine transformer to minimize power collection and transmission losses. The wind turbines generate electricity at low voltage (LV), usually 690 V three-phase alternating current AC, and it's raised by a voltage transformer to a medium voltage (MV) range. So medium voltage (MV) level is usually chosen to be 33 kV because are commercially available 0.69/33 kV transformers with compact sizes and costs. Under normal conditions the voltage level in the collector system must be within certain levels defined by the grid code, usually $33 \text{ kV} \pm 10\%$.

2.3 Operation and control of offshore wind power plants

- **Type of cable** [49]. Cross-Linked Polyethylene (XLPE) and Ethylene Propylene Rubber (EPR) insulated cables have excellent properties that permit their application to submarine AC power transmission. Compared to oil-filled paper insulated submarine cables, they offer longer continuous delivery lengths and easier handling during transportation and laying, free maintenance (no oil supervision) and better electrical and mechanical characteristics (lower dielectric losses, higher insulation resistance and higher operation and short-circuit temperatures).

Next sections explain the control present in each generating unit of the wind power plant (wind turbine control) and the coordinated control of all the wind turbines (wind power plant control). Finally, an example in a 90 MW wind power plant is shown through simulations in DIgSILENT Power Factory.

Wind turbine control

When a variable speed wind turbine is connected to the grid, operation at partial load and full load operation can be distinguished. Between these two operating zones (indicated by *I* and *III*, respectively, in Figure 2.21), it exists a transition (indicated by *II*, in Figure 2.21). The main characteristics of each operating mode are:

- **Partial load (*I*)**. Electrical power is being produced below the rated power. The objective is to maximize the power generation by means of MPPT (Maximum Power Point Tracking) algorithms. The pitch angle is adjusted to an optimum value and the generator control adapts the rotating speed.
- **Transition between partial load and full load (*II*)**.
- **Full load (*III*)**. Power is being limited, through pitch control and at constant rotating speed. In this operating region, wind speed is above rated value and the generator is working at full load. The aerodynamic control (pitch control) and the generator control which controls the rotating speed ensure the tracking of rotating speed and power values,

Chapter 2 Background

set by the supervision system whilst limiting them to maximum values that could damage the wind turbine.

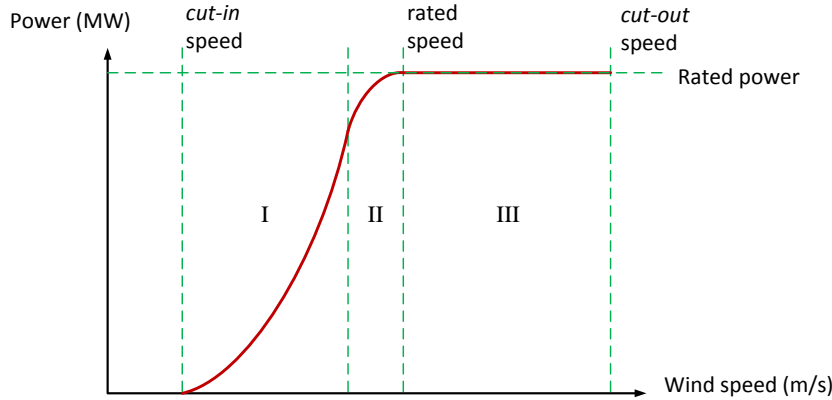


Figure 2.21: Main operating regions of a variable speed wind turbine

The wind turbine controls guarantee its correct performance along the before mentioned operating zones and they can be classified according to the hierarchy reflected in Figure 2.22. The high control level includes controls of the mechanical and aerodynamics quantities and a low level control deals with the power converter and generator control.

Mechanic control Mechanic (and aerodynamic) control optimizes the wind power caption through MPPT algorithms, reduces the overall wind turbine mechanical loading, orients the wind turbine nacelle in the wind speed direction using the yaw mechanism, and is in charge of reducing the power capture when necessary by means of pitch or stall systems. Thanks to the power control, the wind turbine generates electric power above the cut-in-speed (around 3 m/s) and stops generating when the wind speed is too high and can damage the stability of the wind turbine (cut-out speed, close to 25 m/s). The main outputs of the mechanic control are the generator reference torque which is sent to the low level control, and the pitch and yaw angles.

2.3 Operation and control of offshore wind power plants

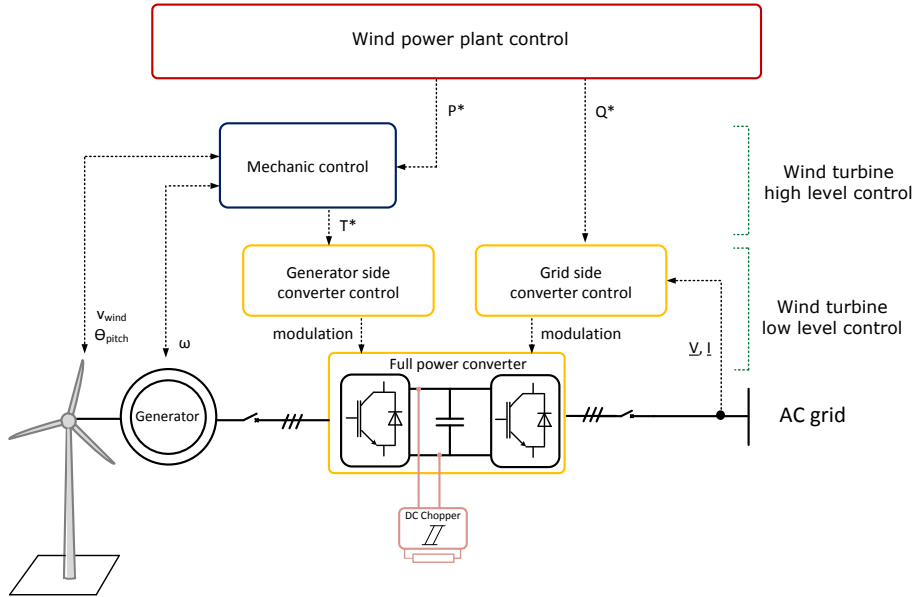


Figure 2.22: Control of a wind turbine equipped with full power converter

Converter control Converter control includes the generator side converter control and the grid side converter control. The machine side converter regulates the current through the generator in order to obtain the needed torque demanded by the mechanical control, as well as the reactive power exchanged with the generator. The grid side converter control regulates the DC bus voltage to a desired value and the reactive power to a defined set-point. To do so, each converter control applies the necessary voltages at the AC side by means of a proper modulation strategy [50].

Control at power plant level

Being at a higher hierarchy level than the wind turbine control, the control at wind power plant level presents slower dynamics. It permits the wind power plant integration to the main grid according to the TSO requirements, and, consequently, leads to the participation of the wind power plant on primary and secondary controls, approaching its behaviour to the conventional power plant. The main objectives of the wind power plant control are the control of

Chapter 2 Background

active power and reactive power at the PCC (Point of Common Coupling).

Active power control The balance between active power generation and demand in a system ensures that its electrical frequency is kept within certain limits. Conventional power plants contribute to frequency regulation through primary and secondary strategies by varying the power they produce. Taking into consideration the dimension that wind power plants are acquiring, they are also required to participate in frequency regulation [51–55]. When the WPP are connected to offshore grids, they also have to participate in the frequency control of the terrestrial system where they are connected. According to recent grid codes, wind power plants should also operate at a lower production so as to have a reserve to increase power output in case of under-frequency operation. Similarly to the behaviour of conventional power plants, the power variation in WPP generally is required to respond to a frequency droop function, which changes the power output according to the grid frequency. On the other hand, even if the grid frequency does not change, the operator can ask for a specific active power set-point in the point of connection. The evolution from the WPP operating point to new operator set-points is usually required to follow a ramp rate (imposed by the TSO) which defines the temporary increase or decrease of power (generally MW/min). Therefore, the active wind power plant control must ensure the active power regulation in wind power plants to accomplish power curtailment, ramp rates and frequency response. Further requirements related to active power include virtual (or synthetic) inertia emulation or power oscillation damping capability. Both requirements imply a fast response from the wind turbines and therefore require an appropriate control implementation in the wind turbine and wind power plant controllers.

An example of a possible interaction between the active power control, the AC grid and the wind turbines is reflected in Figure 2.23. The operator sends an active power reference (P_{TSO}) to the active power control, which also receives the value of active power being produced by the power plant (P). Additionally, the grid electrical frequency must be known ($f_{onshore}$). Based on this data, the active power control computes an active power reference signal (α) to be sent to the wind turbine control.

2.3 Operation and control of offshore wind power plants

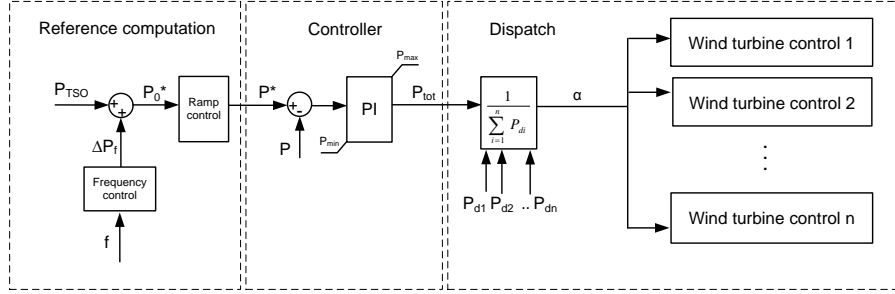


Figure 2.23: Active Power Plant Control

In order to implement this control, a communication system is needed between the power plant controller and each generating unit. In case communications are bidirectional, the power plant controller can receive information of the operating point of each wind turbine, P_{di} . This allows to know the total active power available at the power plant instantaneously (by adding the capabilities of all the wind turbines) and to adjust the reference sent to each wind turbine accordingly.

Reactive power control For HVDC connected wind power plants, the TSO reactive power requirements are ensured by the VSC-HVDC inverter/s. The reactive power plant control main goal is to maintain the voltage at the point of connection of the wind power plant and in all the wind turbines. A possible implementation of reactive power plant control is sketched in Figure 2.24, based on [56]. The control receives a reactive power reference or voltage reference to accomplish at the point of connection of the wind power plant and the reactive power being produced by the wind power plant (Q), measured at the wind power plant substation. The output of the PI controller is the new reactive power reference, Q_{tot} , needed to produce from the wind turbines, corrected in case reactive power compensations have been connected. This new reactive power reference is divided by the total available reactive power in the wind power plant, so as to obtain a percentage to be sent to each wind turbine control, β . Similarly to the strategy implemented for active power control, the signal sent to each wind turbine is the same and each wind turbine control adjusts this percentage to a reactive power

Chapter 2 Background

reference taking into consideration the available reactive power (Q_{di}).

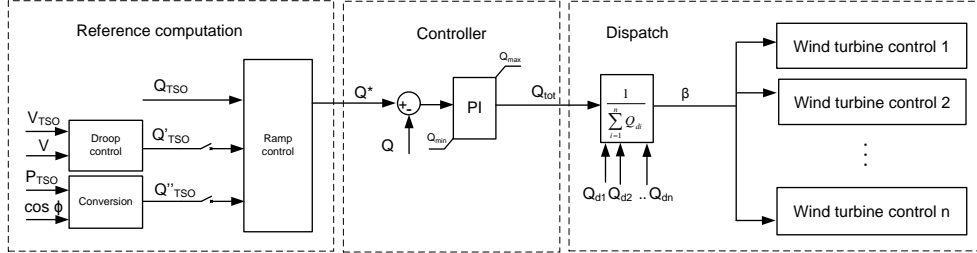


Figure 2.24: Reactive Power Plant Control

Dynamic simulation of a simplified example In order to show an example of active power control, a simplified system has been implemented in DIgSILENT Power Factory for a 90 MW wind power plant, based on 18 PMSG, rated to 5 MW each. The wind power plant grid voltage level is 33 kV and it is connected to the main grid through a point-to-point HVDC of ± 150 kV. The scenario simulated is reduced power operation. The wind farm is sketched in Figure 2.25 and the load flow for one of its wind turbines and the HVDC transmission system are shown in Figures 2.26 and 2.27, respectively.

As shown in Figure 2.28, the wind power plant is generating nominal power until time instant 10 s. At this moment, the TSO asks for a lower active power set-point at the PCC: 85.5 MW. The active power ramp has a slope of ± 10 MW/min. So, the active power plant controller finds the appropriate active power signal to be sent to the wind turbines to reach the new set-point (represented in Figure 2.29), following a decrease of 10 MW/min. At time instant 50 s the TSO sends an active power set-point of 90 MW. The active power plant controller recalculates the new power signal needed and sends it to the wind turbines, guaranteeing a ramp rate increase of 10 MW/min. In Figure 2.30 It can be noted how the wind turbine control reduces the active power output until the TSO reference is reached, keeping it constant until a new set-point is required. This is also reflected at transmission level, in Figure 2.31, where the active power measurement on the AC side of the wind power plant converter and grid side converter

2.3 Operation and control of offshore wind power plants

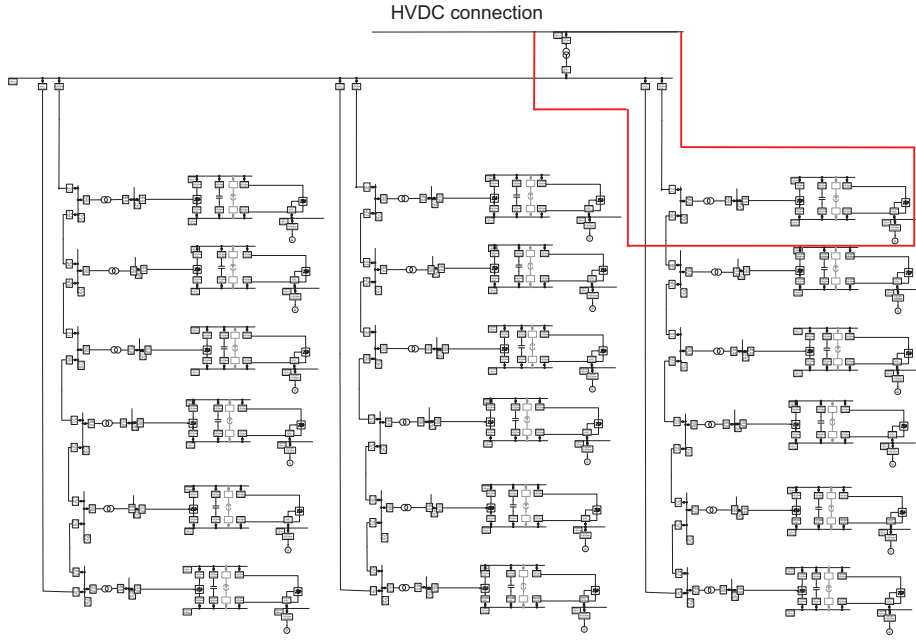


Figure 2.25: Layout of a 90 MW WPP represented in DIgSILENT Power Factory

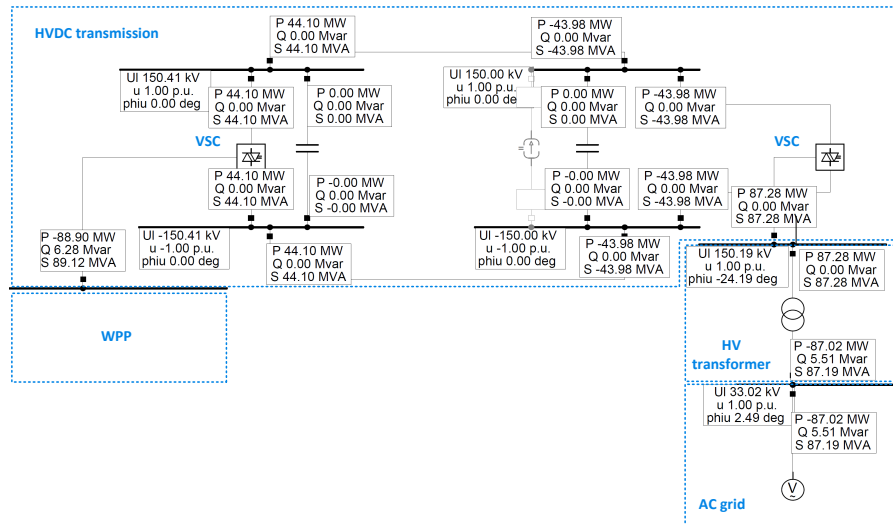


Figure 2.26: HVDC transmission load flow in DIgSILENT Power Factory

Chapter 2 Background

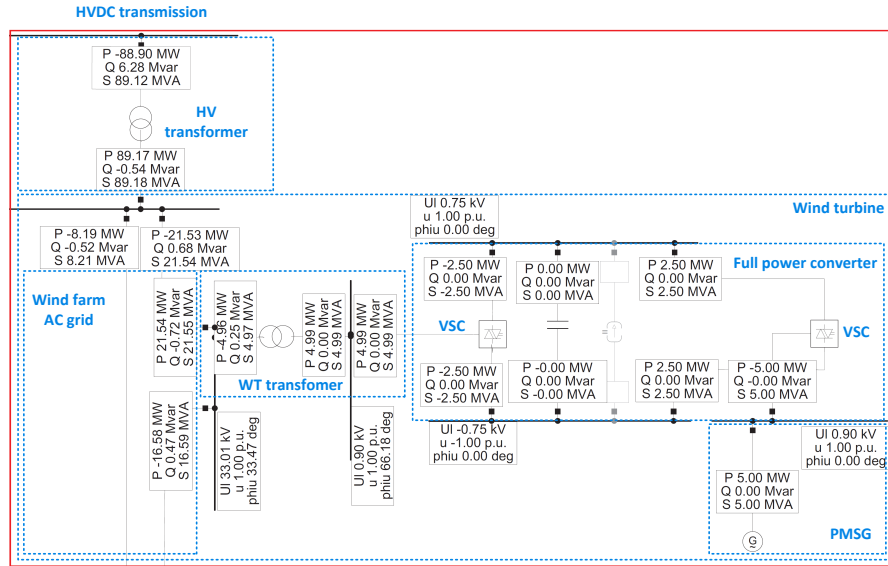


Figure 2.27: Wind turbine load flow in DIGSILENT Power Factory

evolves as the wind power plant power output does, ensuring the tracking of the TSO requests.

2.3 Operation and control of offshore wind power plants

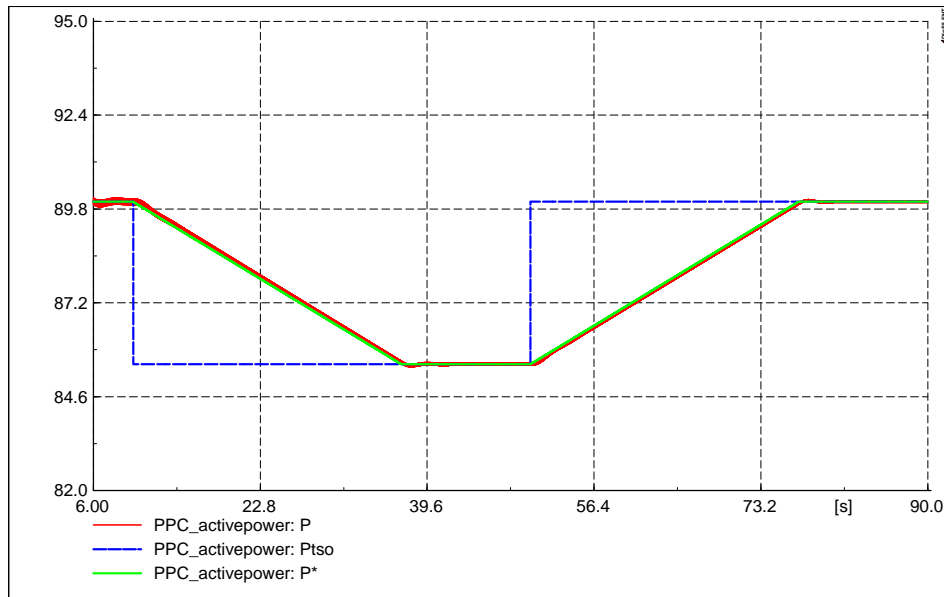


Figure 2.28: Active power reference sent by the TSO, ramp limited and active power measurement of the wind power plant output

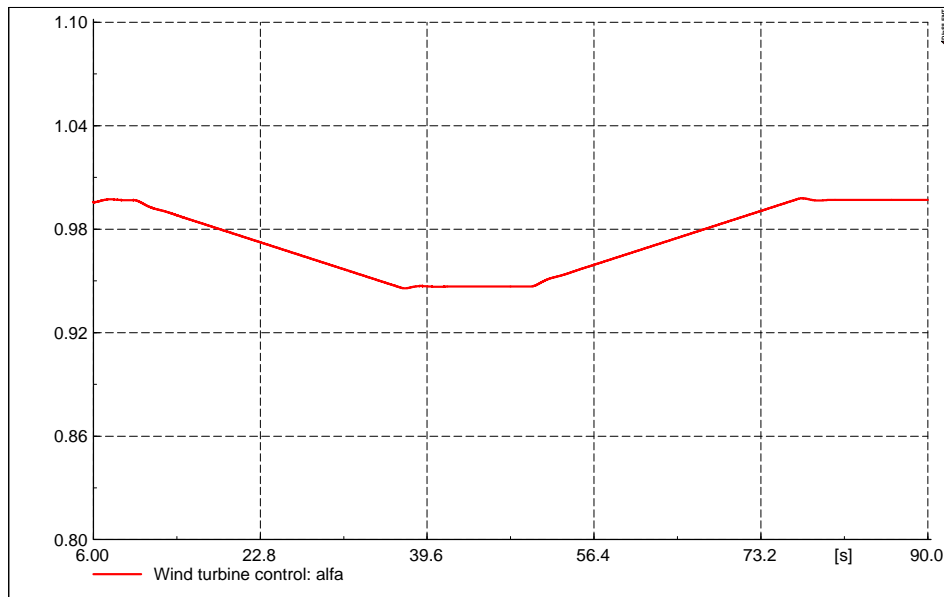


Figure 2.29: Signal sent from the power plant control to each wind turbine

Chapter 2 Background

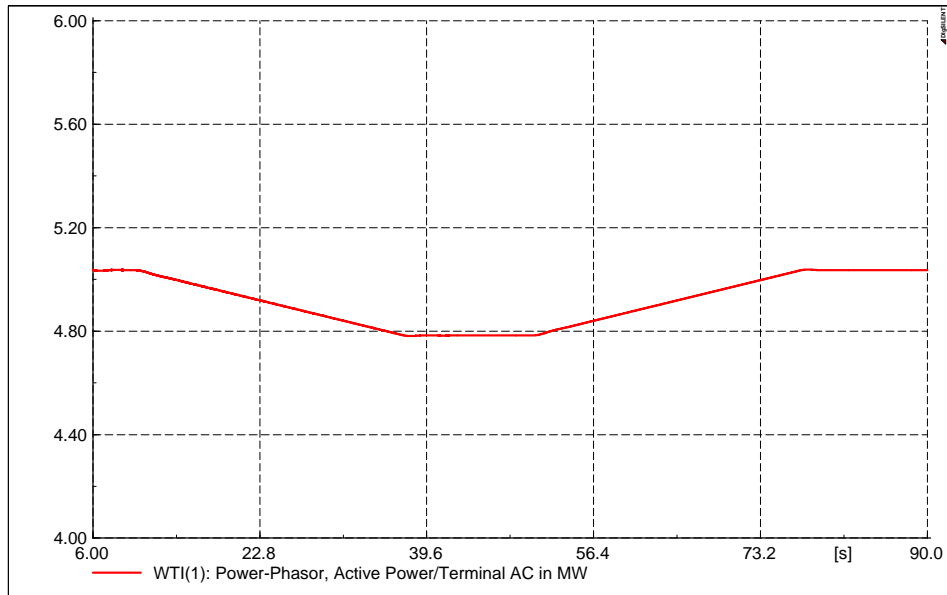
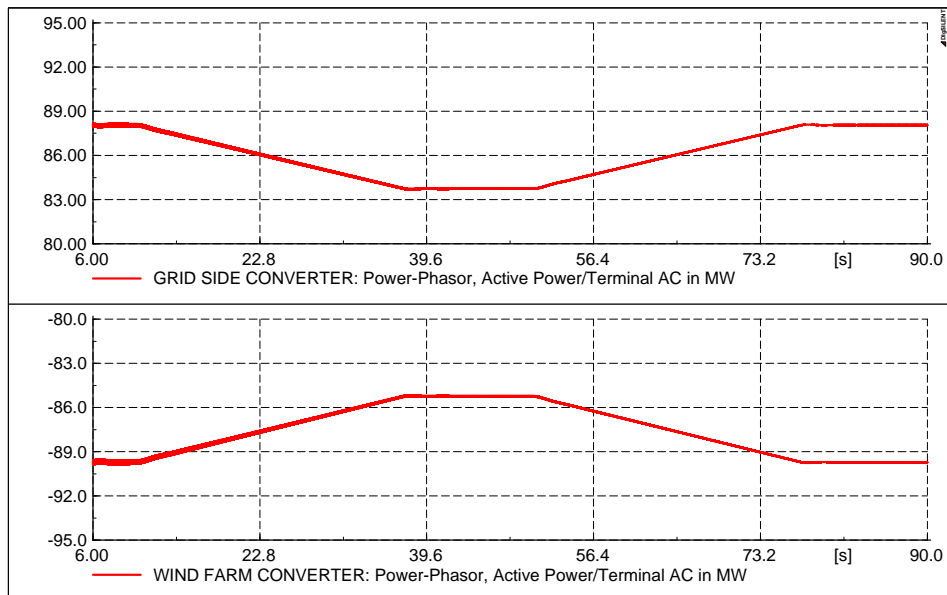


Figure 2.30: Active power output of a wind turbine inverter



2.3 Operation and control of offshore wind power plants

2.3.5 Conclusions

Offshore wind power plants connected to HVDC transmission systems are not synchronous with the main terrestrial grid. Therefore, such offshore wind power plants bring along novel and challenging requirements demanding strong coordination between the different power electronics converters of wind power plants: the VSC-HVDC rectifier and the wind turbine converters. The offshore grid is maintained by means of the VSC-HVDC rectifier which is in charge of controlling voltage and frequency with appropriate coordination with the wind turbine converters. The wind power plants also provides support to the HVDC transmission system and the terrestrial grid or grids according to the relevant grid codes. The present chapter has introduced the most relevant requirements also highlighting different operation conditions in normal and fault condition. A simplified example is also introduced to show how the coordination between the different systems can be performed.

Chapter 3

Loss minimization in HVDC multi-terminal transmission systems

3.1 Power control in multi-terminal HVDC grids

Many strategies have been proposed for enabling DC voltage control in DC grids. They have been classified and compared in [57], being voltage droop control one of most extended. Section 3.2 proposes an alternative control for ensuing minimum losses in HVDC grids and compares it with droop control. Section 3.3 combines this proposal with droop control, leading to a two level structure for the control of HVDC grids, where an OPF sends references to voltage droop control. This scheme has evolved to a more complex hierarchical structure.

The idea behind both is similar in the sense that a high level power control (based on optimization algorithms) sets the references for a low level control. In the proposal presented in Section 3.3 the OPF sends voltage references to voltage droop, while in [58] the OPF sends references to a power loop, that later sends voltage references to voltage droop. So, [58] includes a power loop to have a direct control of the power through the converters. The argument is that from the point of view of power flow control, droop control as such does not allow to fix the power injected by a converter due to constant variations in operation points. After an eventual converter outage, the powers change according to the droop characteristics would no longer reflect the pre-fault values. This three level hierarchy is depicted in Figure 3.1 and described next.

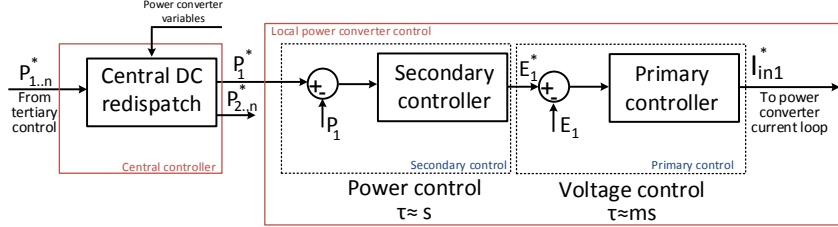


Figure 3.1: General scheme of the hierarchical power control for HVDC grids [58]

The lowest control level is based on voltage droop control, the second one is the power control and the third one calculates the optimal power references, according to different criteria. These three layers are defined as primary, secondary and tertiary control and keep a strong similarity with AC systems regulation. While in AC systems, power imbalances are reflected in frequency deviations, in DC systems, power imbalances are reflected in DC voltage variations. So, the voltage control in the multi-terminal HVDC scheme acts as the primary (frequency) control in AC systems. But, in AC systems where there is a substantial kinetic inertia from the rotating machines, while in DC systems the energy stored is limited and related to the charge and discharge of capacitors. This leads to fast changes of DC voltage. So, the controllers response should be also fast. That is why, the time constant for the primary control loop is in the order of a ten's of milliseconds and depends strongly on the DC grid characteristics.

The secondary control, which sends references to the primary control, works in the order of seconds. In case of VSC outage, the secondary control will allow to redistribute the power injections by modifying the voltage droop reference. The power reference received by the secondary control is determined by the highest level control (tertiary control), to ensure optimal operation, based on criteria including market, losses or security constraints.

3.2 Optimum voltage control for loss minimization in HVDC multi-terminal transmission systems

3.2.1 Introduction

Different possible multi-terminal HVDC circuit topologies were discussed in [4] analyzing the number of circuit breakers required to integrate large wind power plants into the terrestrial grid using multi-terminal HVDC. Different control schemes for multi-terminal HVDC systems were summarized in [4], classifying the control schemes in those requiring communications between different controllers and those being able to operate without communications. The control of the multi-terminal HVDC using droop controllers was discussed and simulated in [59–61]. Voltage-current characteristics for power converters involved in multi-terminal HVDC systems for offshore wind power were discussed in [5], also analyzing the steady-state operating point of the system when using droop control.

Droop controllers represent a robust control scheme for multi-terminal VSC-HVDC systems [5, 59–61] without the need for communication systems; but this control scheme does not guarantee the minimization of power losses in the HVDC grid. The present study proposes a control scheme based on communications between the different converters. The required communication systems would be already available as they are required for monitoring and protection. If a communication fault occurred, the control system would rapidly switch to droop control and the system could be safely operated without communications. The proposed scheme is based on solving an optimal power flow optimization problem for a multi-terminal HVDC system and provides appropriate references to the grid-side VSC, whilst allowing the wind farm VSC to inject all the available wind power to the HVDC grid.

The present study presents the optimal power flow problem to be solved by a centralized controller and analyzes in two different case studies the loss reduction that would be achieved in comparison with droop control schemes. Simulation results are also provided in order to show the dynamic behavior of the proposed scheme and the robust operation in the event of a commu-

nication fault.

3.2.2 Multi-terminal HVDC transmission systems for offshore wind farms

Multi-terminal HVDC transmission systems for offshore wind farms are based on a HVDC grid where different wind farms are connected by means of VSC rectifiers. The HVDC grid is interfaced with the main AC grid by means of grid side VSC inverters.

Wind farms rectifiers inject the wind power to the HVDC grid. In normal operational mode, the wind farm rectifier absorbs all the power produced and injects it into the DC grid and supplies the reactive power needed to maintain the AC wind farm voltage [30, 62]. If a fault occurs in the main AC grid, the grid side converters may not be able to inject all the power into the grid. In this case, the HVDC grid voltage increases and the wind farm rectifier is operated, reducing the generation of the wind farm.

The power in the DC network is injected to the AC grid by means of grid connected inverters which are in charge of HVDC grid voltage control. In normal operational mode, the control schemes described in subsection 3.2.3 calculate the appropriate power to be injected to the main AC grid. When a fault in the main AC grid occurs, inverters may enter the current limit mode, since their power extraction capability may be reduced. Grid side VSC also provide reactive power support to the grid where they are connected [19].

3.2.3 Control Schemes

The present work considers two possible different control schemes for the multi-terminal HVDC system: *Voltage Droop Control* and *Optimum Voltage Algorithm*. Both control schemes are high level control schemes that provide DC current references (equivalent to active power references) to the VSC control scheme, as shown in Figure 3.2.

It is worth mentioning that the operation of the HVDC grid in as part of the electric power market includes also restrictions related to the power injections per node in the terrestrial grid that have not been considered in this study. However, they could be included by adding new constraints in the optimization formulation, that would limit the power to be delivered

3.2 Optimum voltage control for loss minimization in HVDC multi-terminal transmission systems

in the grid side nodes. Too many constraints in the power to be injected in these nodes would probably leave less margin for loss minimization. As an alternative approach, a multiobjective optimization could be used, where the objective function takes into account not only transmission losses, but also power deviations at grid side nodes. Their respective weights could be determined by taking into account the the economics cost of losses and the cost penalization of having power deviations in the terrestrial nodes.

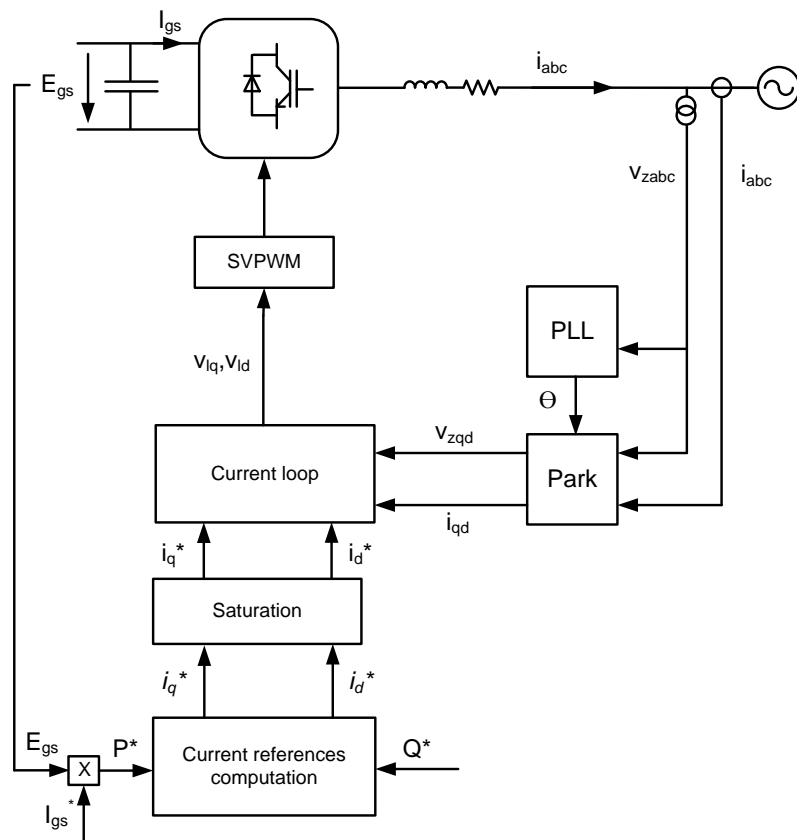


Figure 3.2: VSC control scheme

Voltage Droop Control In [57] a classification of methods for DC node voltage control for HVDC grids is proposed. Two basic control principles are compared: current based control and power based control. The main advantage of a voltage current control characteristic is that it reflects linear control behaviour: a voltage deviation results in an equivalent current deviation. Furthermore, current based control can be directly related to the DC grid dynamics: the charging of the capacitances in the DC network relies on a linear current voltage relation, which has the physical unit Ω . In this sense, current based control can be thought as intuitive from a physical perspective as it has the same physical units as the DC line impedance. Power based control could be considered more intuitive from a power system perspective, where the focus often is on transmitted power [57].

In this study, current based control is adopted and based on droop control. Droop control scheme has been extensively reported about in literature [4,5,61]. The main advantage is that it does not require communications between different converters. However, it does not ensure that the generated power is delivered to the main AC grid with minimum losses.

The droop control scheme is based on calculating the DC current injected by the inverters as:

$$I_{gs}^* = k_{droop} (E_{gs} - E_{gsL}) \quad (3.1)$$

where I_{gs}^* is the inverter DC current reference and E_{gs} is the measured DC inverter voltage. The proportional coefficient, k_{droop} , and the offset parameter, E_{gsL} , are the droop parameters and depend on the design of the control system [63].

This voltage droop control is sketched in Figure 3.3. As shown, the droop scheme is applied to every grid-side VSC inverter, while the wind farm converters inject all the available wind power to the HVDC grid.

The equilibrium points of a multi-terminal system operated with droop control in the grid side inverters can be found by solving the equation system

$$\mathbf{I} = \mathbf{GE} \quad (3.2)$$

$$P_i = E_i I_i \quad i \in (n+1, n+m) \quad (3.3)$$

$$I_i = k_{droop_i} (E_i - E_{gsLi}) \quad i \in (1, n) \quad (3.4)$$

3.2 Optimum voltage control for loss minimization in HVDC multi-terminal transmission systems

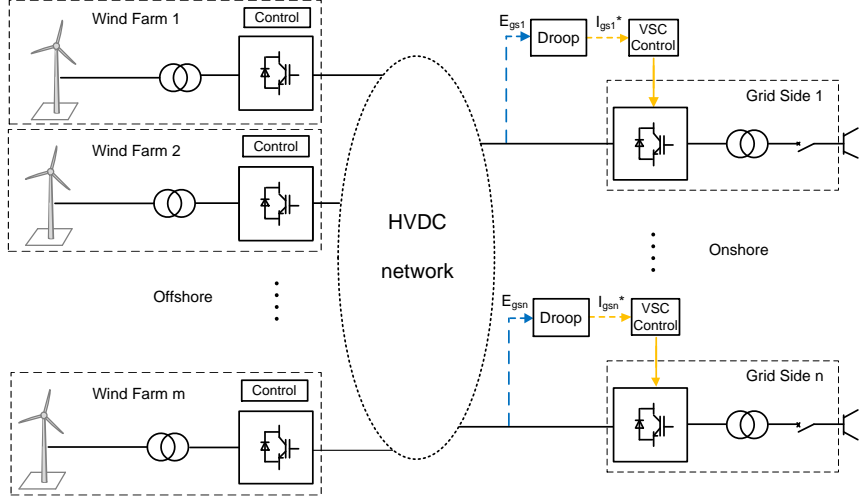


Figure 3.3: Voltage droop control in HVDC system

where $\mathbf{I} = (I_1 \cdots I_{n+m})^T$ and $\mathbf{E} = (E_1 \cdots E_{n+m})^T$ are the vectors of currents and voltages in all the nodes, \mathbf{G} is the conductance matrix, n is the number of grid-side VSC and m is the number of wind farm VSCs.

Optimum Voltage Algorithm When communications between the different nodes are available (in most applications, a communication system will be required for different purposes, including system monitoring, protection, etc...), it is possible to operate the grid side converters in order to not only maintain the HVDC voltage but to try to also minimize overall HVDC grid losses. It is clear that this will be achieved by maintaining the HVDC voltage as high as possible in the wind farm VSCs; but a power flow optimization approach is required when a number of wind farms are involved. Studying the droop characteristics, one can easily note that for high power, the droop can be designed in order to maintain a high voltage in the wind farm VSC, obtaining optimal losses. However, when the power is reduced, the droop function will lead to lower voltages and the system efficiency will not be optimal. In order to maintain the maximum possible efficiency in a wide range of powers, an optimal power flow can be used, at the cost of re-

quiring communications between the different nodes. If any communication fault occurs, the system could rapidly change to the droop control operation mode. The communication signals are appropriately filtered before sending the communication frames in order to reduce noise data.

The proposed optimal power flow algorithm is based on the knowledge of the available power in all wind farms and the subsequent computation of the grid side VSCs HVDC voltage references. Each grid side VSC can adjust the active power injection into the main AC grid in order to regulate the HVDC voltage to the reference value. The wind farm VSCs are operated as in the droop control scheme, injecting all the available power into the HVDC grid. The proposed control is shown in Figure 3.4.

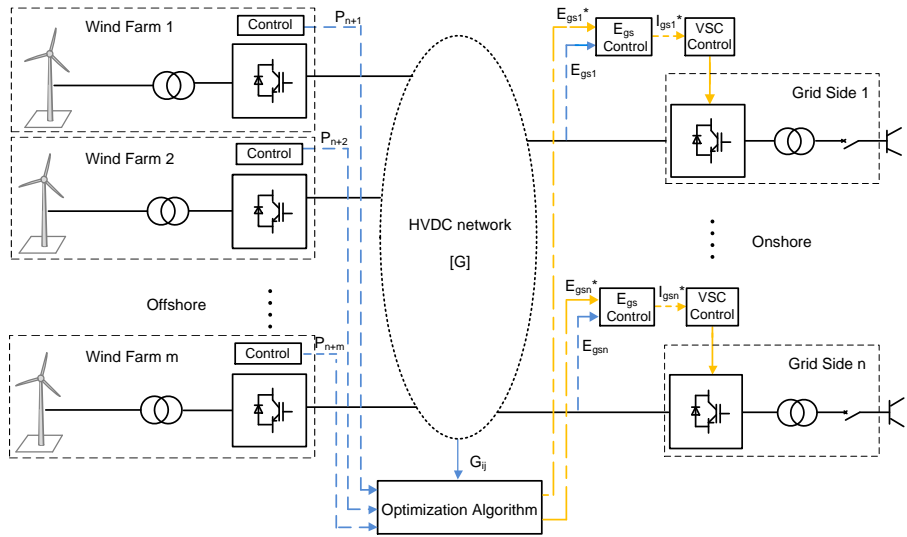


Figure 3.4: Optimum voltage algorithm in HVDC system

The optimal power flow problem, solved by the centralized controller, obtains the optimum voltages E_1, E_2, \dots, E_n of the grid side VSCs, in order to minimize the HVDC grid losses, which can be written as

$$[MIN] z = \frac{1}{2} \sum_{i=1}^{n+m} \sum_{j=1}^{n+m} G_{ij}(E_i - E_j)^2 \quad (3.5)$$

3.2 Optimum voltage control for loss minimization in HVDC multi-terminal transmission systems

subject to the electrical grid restrictions:

$$\mathbf{I} = \mathbf{GE} \quad (3.6)$$

$$P_i = E_i I_i, i \in (n+1, m+n) \quad (3.7)$$

where $\mathbf{I} = (I_1 \dots I_{n+m})^T$ and $\mathbf{E} = (E_1 \dots E_{n+m})^T$ are the vectors of currents and voltages in all the nodes and \mathbf{G} is the conductance matrix. The optimal power flow problem is also subject to the voltages and current limits restrictions

$$E_{min} \leq E_i \leq E_{max} \quad (3.8)$$

$$I_{min-node} \leq I_i \leq I_{max-node} \quad (3.9)$$

$$I_{min-branch} \leq G_{ij} (E_i - E_j) \leq I_{max-branch} \quad (3.10)$$

where $i, j \in (1, m+n)$, n is the number of grid side VSCs, m is the number of wind farm VSCs, and E_i and I_i are, respectively, the voltage and the current in node i .

The optimization problem can be solved using the Interior Point Algorithm with barrier function [64]. A brief description of this algorithm is included in Appendix 1.

3.2.4 Case Studies

The voltage droop control and optimum voltage algorithm are compared in two case studies in order to assess the loss reduction that can be achieved for different wind power generation situations. The case studies include a 4 node HVDC multi-terminal system and a 7 node HVDC multi-terminal system. In both cases, the cabling between system nodes is reflected in the conductance matrix \mathbf{G} . The values of the conductance matrix, G_{ij} , are determined by means of ABB cable data [65]. A 160 kV (± 80) bipolar cable with 300 mm² copper subsection has been used. Conductance can be expressed as $G_{ijreal} = A(\rho l_{ij})^{-1}$, where $\rho = 0.01786 \Omega \text{mm}^2 \text{m}^{-1}$ is the copper resistivity, $A = 300 \text{ mm}^2$ is the copper subsection and l_{ij} is the length of the cable that connects the nodes i and j . In order to express the conductance in pu, a base admittance is defined as $Y_b = S_b/U_b^2$ where $U_b = 160 \text{ kV}$ is the base voltage and $S_b = 100 \text{ MW}$ is the base power. All the magnitudes

are expressed in pu. The droop constants, k_{droop_i} , have been determined so as to ensure maximum power transmission in the HVDC grid (minimum losses) when the wind farms are operating at rated power.

Case study 1: Multi-terminal system with 4 nodes A multi-terminal system, consisting of two grid side terminals ($n=2$) and two wind farms ($m=2$) shown in Figure 3.5, is analyzed. It is assumed that the lengths between the nodes involved are $l_{13} = 85 \text{ km}$, $l_{34} = 55 \text{ km}$, $l_{42} = 75 \text{ km}$. E_1 , E_2 and I_1 , I_2 are the voltages and currents of the nodes corresponding with the grid side converters. E_3 , E_4 and I_3 , I_4 are the voltages and currents of the nodes corresponding with the wind farms.

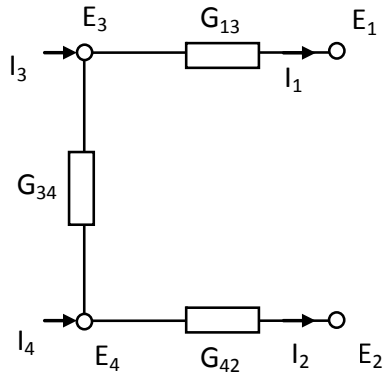


Figure 3.5: 4-terminal HVDC test system

Voltage droop control The voltage droop control expressions yield $I_1 = k_{droop_1} (E_1 - E_{gsL_1})$ and $I_2 = k_{droop_2} (E_2 - E_{gsL_2})$, with $k_{droop_1} = 24.69$, $k_{droop_2} = 25.52$, $E_{gsL_1} = 0.9904$ and $E_{gsL_2} = 0.9896$. Knowing the power P_3 and P_4 injected by the wind farms, voltages and currents can be determined

3.2 Optimum voltage control for loss minimization in HVDC multi-terminal transmission systems

by solving the system:

$$\begin{bmatrix} k_{droop_1} (E_1 - E_{gsL_1}) \\ k_{droop_2} (E_2 - E_{gsL_2}) \\ \frac{P_3}{E_3} \\ \frac{P_4}{E_4} \\ E_4 \end{bmatrix} = \mathbf{G} \begin{bmatrix} E_1 \\ E_2 \\ E_3 \\ E_4 \end{bmatrix} \quad (3.11)$$

Optimum voltage algorithm Knowing the powers injected by the wind farms, P_3 and P_4 , the algorithm finds the voltages in the grid terminals, E_1 and E_2 (control variables) that guarantee the minimum losses for the system. The objective function can be stated as:

$$[MIN] z = G_{13}(E_1 - E_3)^2 + G_{42}(E_2 - E_4)^2 + G_{34}(E_4 - E_3)^2 \quad (3.12)$$

subject to the restrictions:

$$G_{13}(E_3 - E_1) - I_1 = 0 \quad (3.13)$$

$$G_{42}(E_4 - E_2) - I_2 = 0 \quad (3.14)$$

$$-E_1 G_{13} + E_3 (G_{13} + G_{34}) - E_4 G_{34} = \frac{P_3}{E_3} \quad (3.15)$$

$$-E_2 G_{42} + E_4 (G_{42} + G_{34}) - E_3 G_{34} = \frac{P_4}{E_4} \quad (3.16)$$

$$0.90 \leq E_i \leq 1.10 \quad (3.17)$$

$$-1.25 \leq I_i \leq 1.25 \quad (3.18)$$

$$-1.25 \leq G_{ij}(E_i - E_j) \leq 1.25 \quad (3.19)$$

with $i, j \in (1 \dots 4)$. The upper and lower bounds are established allowing voltages of all nodes to increase or decrease 10 % of the nominal value. Current limits are defined, allowing overloads to ensure that all power generated in the wind farms can be absorbed by the grid nodes.

It is known that a minimisation problem is convex if its objective function and the feasible domain are convex [66]. As the hessian of the objective function

$$He(f) = \begin{bmatrix} 2G_{13} & 0 & -2G_{13} & 0 \\ 0 & 2G_{42} & 0 & -2G_{42} \\ -2G_{13} & 0 & 2(G_{13} + G_{34}) & -2G_{34} \\ 0 & -2G_{42} & -2G_{34} & 2(G_{42} + G_{34}) \end{bmatrix} \quad (3.20)$$

is semi-definite positive, the objective function is convex [67]. Regarding the feasible domain, as P_3/E_3 and P_4/E_4 are approximately constant, the equality constraints can be considered linear and, consequently, the feasible domain is also convex. Thus, the problem defined by (5.2) - (3.19) is non linear and convex. The method chosen for solving it is the Interior Point Algorithm with barrier function, presented in [64]. For being the minimisation problem convex, then local minimum found will also be global [66].

Analysis of results The voltages obtained in grid-side terminals (E_1, E_2) and wind farm nodes (E_3, E_4) for each control scheme are shown in Figure 3.6 for different values of injected powers P_3 and P_4 . The surfaces with the highest voltage values correspond to the application optimum voltage algorithm in all the figures, whereas the planes with the lowest values correspond to the application of the voltage droop control.

3.2 Optimum voltage control for loss minimization in HVDC multi-terminal transmission systems

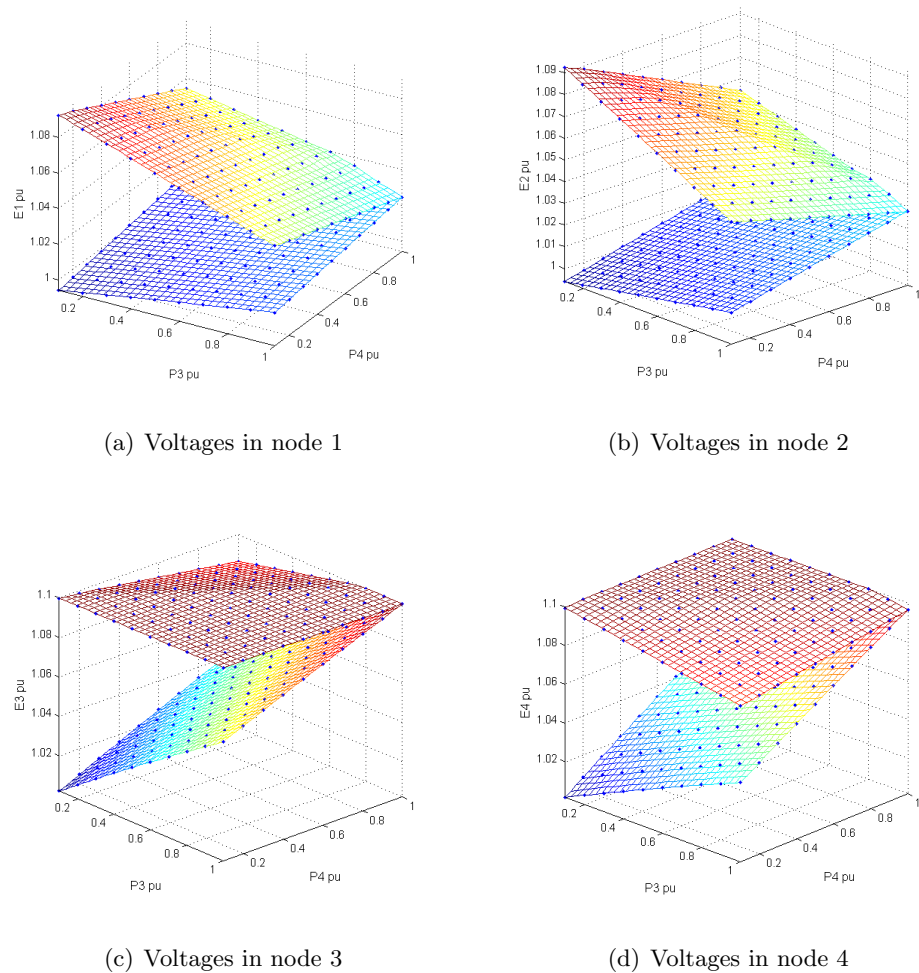


Figure 3.6: Voltages in the different multi-terminal HVDC system nodes

It can be observed that, whereas with the optimum voltage algorithm the voltage values in the grid-side grow as power decreases, for droop control, the voltages in grid side VSCs grow as the transmitted power increases. The reduction of losses (see equation (3.21)) achieved with optimum voltages control can reach relevant values (more than 16 %) when wind farms generate low power (see Figure 3.7). When both wind farms are at full power (situation for which the droop control has been designed), there is no loss difference.

$$r = \frac{\text{losses}_{\text{droop}} - \text{losses}_{\text{optimumvoltage}}}{\text{losses}_{\text{droop}}} \times 100 \quad (3.21)$$

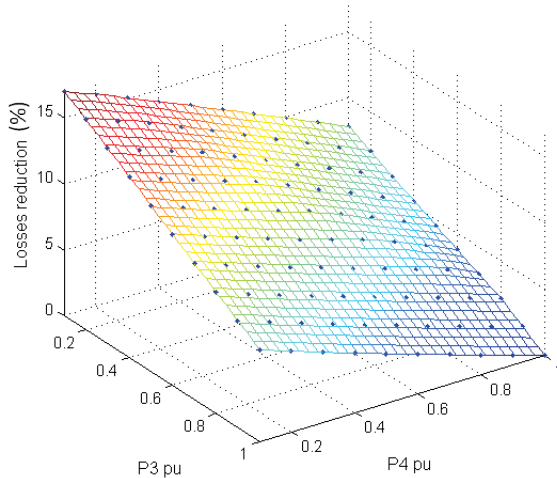


Figure 3.7: Loss reduction (%) using optimum voltage algorithm vs. droop voltage control

Case study 2: HVDC multi-terminal system of 7 nodes The second system analyzed consists of three grid-side terminals ($n=3$) and four wind farms ($m=4$), as shown in Figure 3.8. The lengths assumed between the nodes involved are $l_{14} = 90 \text{ km}$, $l_{45} = 110 \text{ km}$, $l_{25} = 50 \text{ km}$, $l_{56} = 50 \text{ km}$, $l_{36} = 110 \text{ km}$, $l_{67} = 50 \text{ km}$, $l_{47} = 70 \text{ km}$.

3.2 Optimum voltage control for loss minimization in HVDC multi-terminal transmission systems

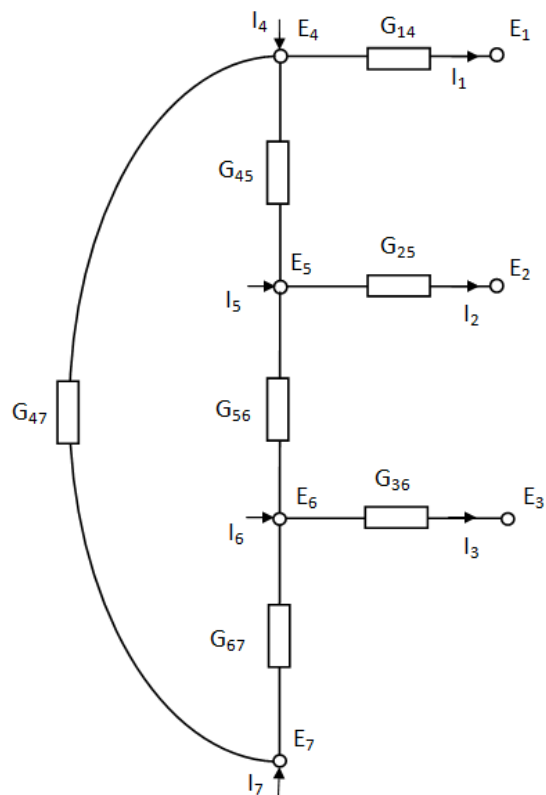


Figure 3.8: 7-terminal HVDC test system

Voltage droop control The voltage droop control expressions can be written as $I_1 = k_{droop} (E_1 - E_{gsL})$, $I_2 = k_{droop} (E_2 - E_{gsL})$, $I_3 = k_{droop} (E_3 - E_{gsL})$, with $k_{droop_1} = 23.11$, $k_{droop_2} = 25.32$, $k_{droop_3} = 19.70$, $E_{gsL_1} = 0.9858$, $E_{gsL_2} = 0.9840$, $E_{gsL_3} = 0.9859$.

Knowing the power injected by the wind farms, voltages and currents can be determined. In this case, 3D-plots are not suitable for representing the voltages obtained in the grid sides or the efficiency, because more than two wind farms inject power. Therefore the voltage in each grid terminal and the efficiency should be expressed as a function of four powers. In this case, a histogram (see Figure 3.9) shows the distribution of the system efficiency for multiple injected wind farm powers. These powers are pseudorandom values from the standard uniform distribution between 0 and 1. The created sample has a size of 1000, which means 1000 different states of power generation are considered. The efficiency values are between 0.9550 and 0.9950 and the distribution curve is centered in 0.9743 (mean value).

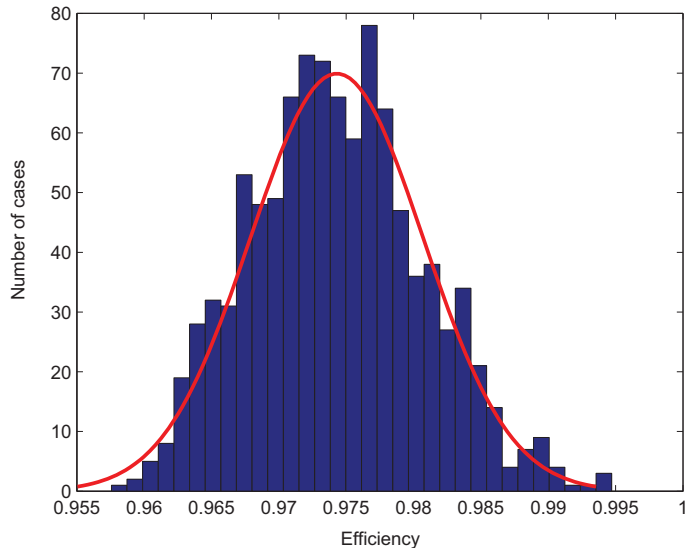


Figure 3.9: System efficiency distribution for random injected powers using voltage droop control

3.2 Optimum voltage control for loss minimization in HVDC multi-terminal transmission systems

Optimum voltage algorithm Knowing the powers that the wind farms inject, P_4 , P_5 , P_6 and P_7 , the algorithm finds the voltages in the grid terminals, E_1 , E_2 and E_3 (control variables) that guarantee the minimum losses for the system. The bounds defined for the different variables appearing in the algorithm are $0.90 \leq E_i \leq 1.10$, $-1.50 \leq I_i \leq 1.50$, $-1.50 \leq G_{ij}(E_i - E_j) \leq 1.50$ with $i, j \in (1 \dots 7)$. The upper and lower bounds are established, allowing voltages of all nodes to increase or decrease 10 % of the nominal value. Current limits are defined, allowing overloads to ensure that all the power generated in the wind farms can be absorbed by the grid nodes.

The histogram (Figure 3.10) is used for the representation of the distribution of the system efficiency for pseudorandom injected powers (the same as in the droop control scheme). It can be observed that most of the efficiency values are between 0.9550 and 0.9950 and its distribution curve is centered in 0.9767 (mean value).

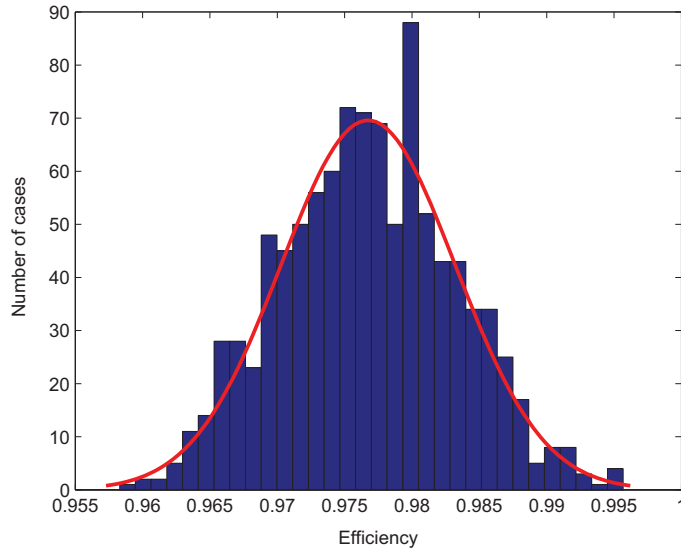


Figure 3.10: System efficiency distribution for random injected powers using optimum voltage algorithm

Table 3.1: Efficiency statistics obtained with both control schemes

Control scheme	mean	median	mode
Voltage droop control	0.9743	0.9740	0.9770
Optimum voltage algorithm	0.9767	0.9767	0.9800

Analysis of results In Figure 3.11, the histograms of the distributions using the two control schemes are represented together in order to enable an easy comparison. The efficiencies are very high in both cases, but better results are obtained with the application of the optimum voltage algorithm, as more values are accumulated near the highest efficiencies. Table 5.1 shows relevant statistic parameters of the efficiency distribution corresponding to each control scheme.

The histogram in Figure 3.12 shows the loss reduction obtained by the optimum voltage algorithm in front of the voltage droop control. For the before-mentioned sample, the loss reduction percentage (horizontal axis) attained, and the number of cases presenting this reduction (vertical axis) are shown. The most frequent case is a loss reduction of 10 %. As it happened in the system of 4 nodes, when less power is transmitted, loss reduction is higher, as the difference of efficiencies is also higher.

3.2.5 Dynamic simulation

Dynamic simulations, developed with Matlab Simulink using SimPowerSystems toolbox, are presented for a 4 node HVDC multi-terminal system with two wind farms and two grid-side converters with the parameters of the first steady-state case study. In the HVDC model developed the converters are represented through their average model [50], the wind farms are represented through an aggregated model [68], the AC electrical grids are simplified through the Thevenin equivalent and DC cables are represented using its π equivalent. More details on the HVDC system modeling can be found in [69].

The simulations include wind speed changes in order to see the dynamic evolution of voltages and currents. A communication loss and recovery is simulated in order to illustrate how the proposed scheme can be operated

3.2 Optimum voltage control for loss minimization in HVDC multi-terminal transmission systems

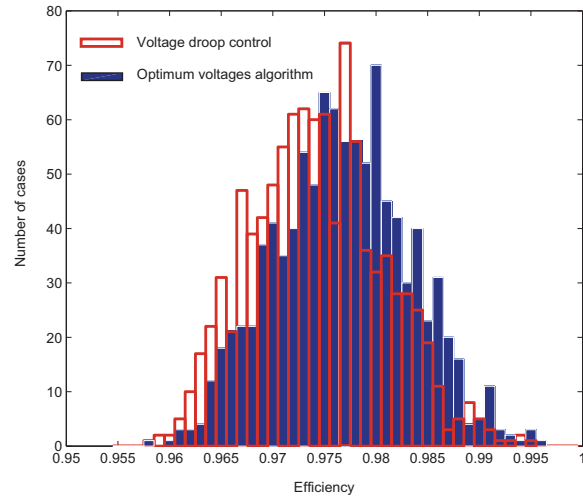


Figure 3.11: System efficiency distribution for random injected powers when using the two control schemes

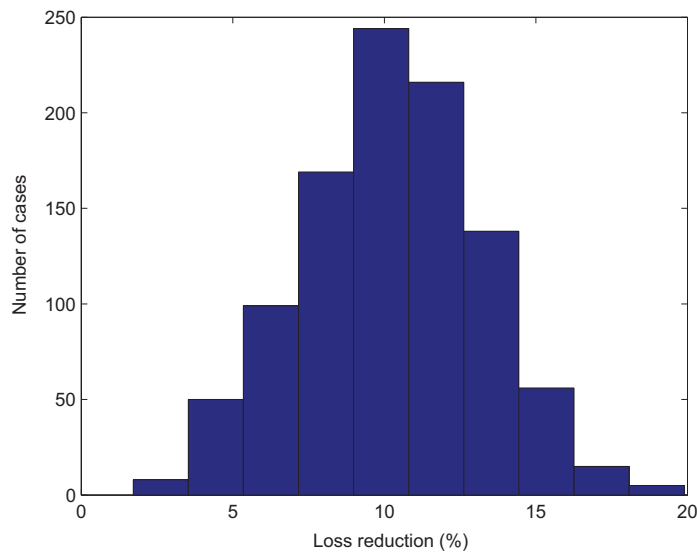


Figure 3.12: Loss reduction using optimum voltage algorithm vs voltage droop control

with droop control if communications are lost.

The wind farm has been simulated as an aggregated wind farm based on wind turbines equipped with full power converter. The aggregated wind farm is operated at unity power factor and is connected to the VSC-HVDC rectifier by means of a cable and a transformer.

For dynamic simulations, the inductance of the cables is $L=1$ mH/km and the total capacitance connected to each converter station is $C=250$ μ F. Wind farms are modelled as an aggregation of 50 wind turbines rated to 2 MW based on full power converters. Wind turbines are connected at the wind farm voltage 33 kV, a 1 km cable is considered between the wind farm aggregation and the transformer platform that elevates voltage to 90 kV. The transformer parameters are: rated power = 120 MVA; voltages transformation 33 kV/90 kV; short circuit voltage = 10%; ratio R/X = 0.04. The following wind turbine parameters are used: C_p values correspond to Heier constants from [70]; Wind turbine radius = 39 m; Air density = 1.225 kg/m³; Mass rotor inertia reduced to the wind turbine shaft = 3.6×10^6 kg m².

Wind speed changes The optimum voltage algorithm is applied with a sampling period of 1.5 s which includes the communication and execution time of the central controller. The wind speed of the two wind farms changes, as shown in Figure 3.13. In wind farm 1, the wind speed is initially 11 m/s and, at time 8 s it decreases to 8 m/s. In wind farm 2, wind speed is initially 10 m/s and, at time 3 s, it decreases to 7 m/s. Figure 3.14 shows that, after these wind speed reductions, lower active powers are obtained in the VSC-HVDC rectifier. In the presented example, reactive power is of inductive nature and is also reduced when the active power is reduced. For other electrical configurations reactive power could result of capacitive nature. Furthermore, the VSC-HVDC power factor could be modified by simple adjusting the reactive power provided by the wind turbines.

The evolution of the wind farm and grid side voltages is shown in Figure 3.27. It can be seen that, when wind speed decreases, as less power is generated, the optimum voltages algorithm tries to maintain low losses by increasing the grid-side VSC voltage. This would be the opposite action

3.2 Optimum voltage control for loss minimization in HVDC multi-terminal transmission systems

produced for a droop controller where the voltage increases when power increases. A detail of the transient in grid-side converters is illustrated in Figure 3.16. Every 1.5 s, the optimum voltages algorithm calculates the reference voltages for the grid side VSCs. The currents flowing through each branch are shown in Figure 3.28.

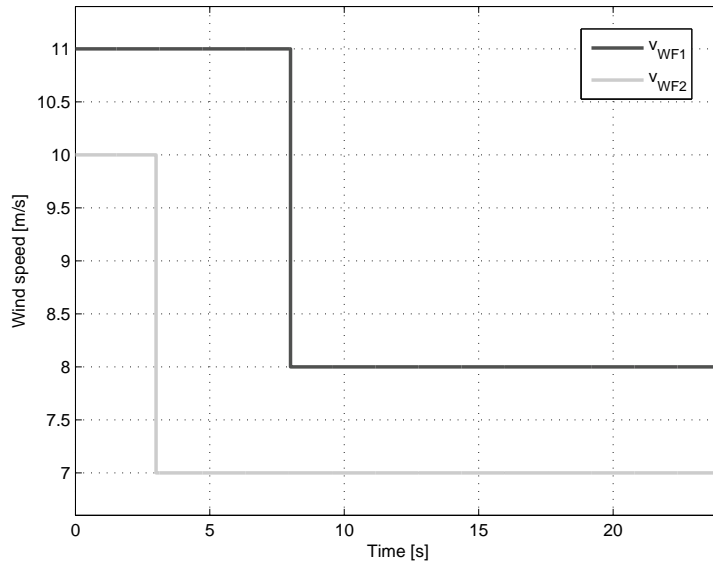


Figure 3.13: Wind speed changes

Communication loss For a wind speed of 7 m/s, a communication fault occurs at time 7 s. and is recovered at 12 s. Before the fault, the wind farm voltages are kept at the maximum available value ($160 \text{ kV} + 10\%$) in order to minimize losses. When the VSC controllers detect the communication fault, the voltage droop control is activated and, consequently, all the voltages decrease (droop control only provides maximum voltage for maximum power), until the communications are recovered (at time = 13 s) and the optimum voltage algorithm is operated again. The evolution of the wind farm and grid side voltages is shown in Figure 3.18.

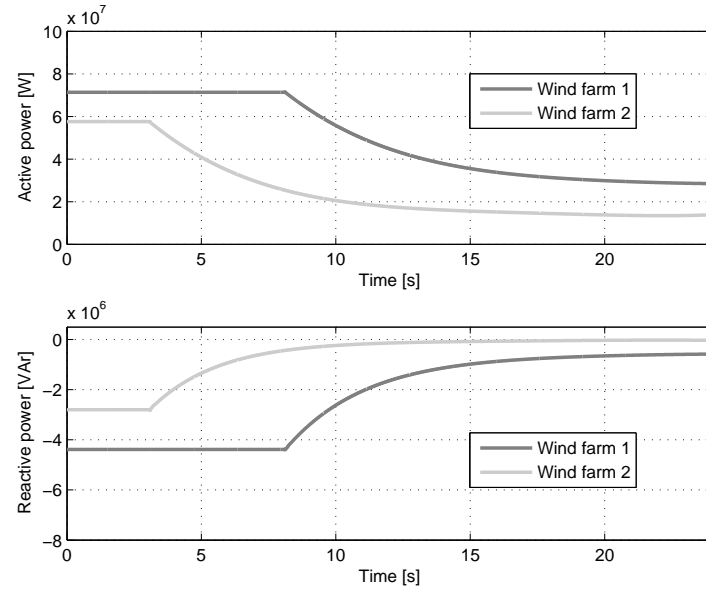


Figure 3.14: Active and reactive power in wind farms

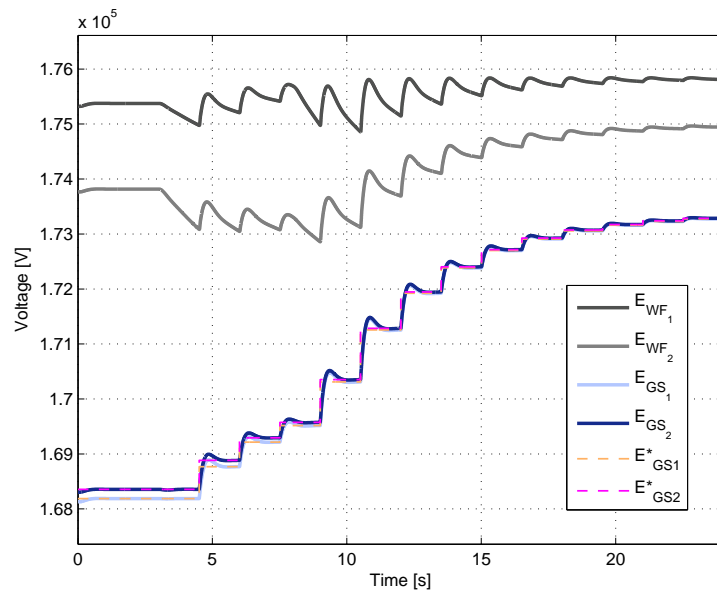


Figure 3.15: Voltages in wind farm and grid side VSCs

3.2 Optimum voltage control for loss minimization in HVDC multi-terminal transmission systems

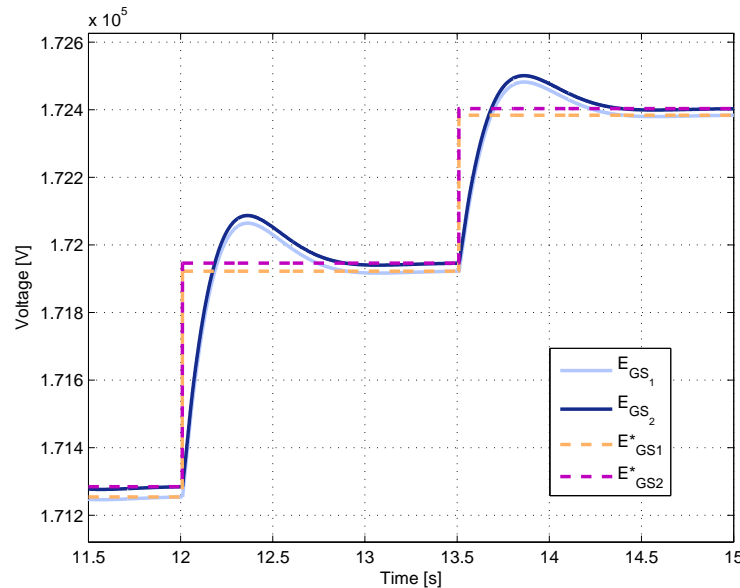


Figure 3.16: Detailed transient of voltages in grid-side VSCs

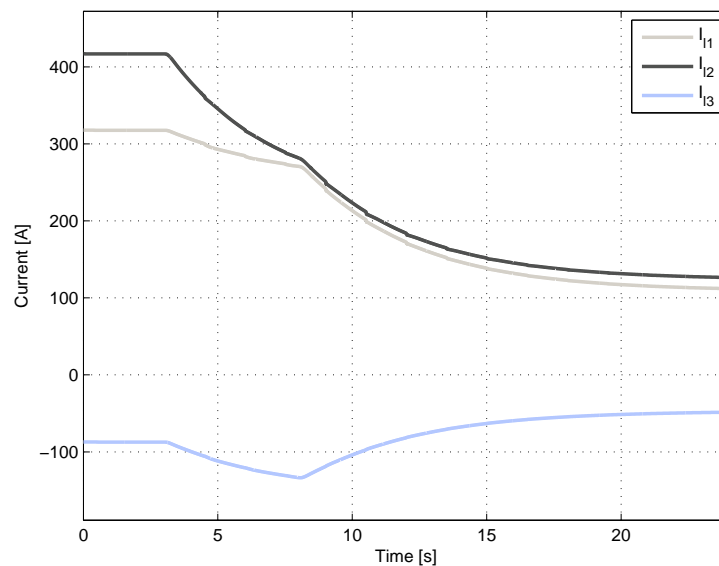


Figure 3.17: Multi-terminal HVDC branches currents

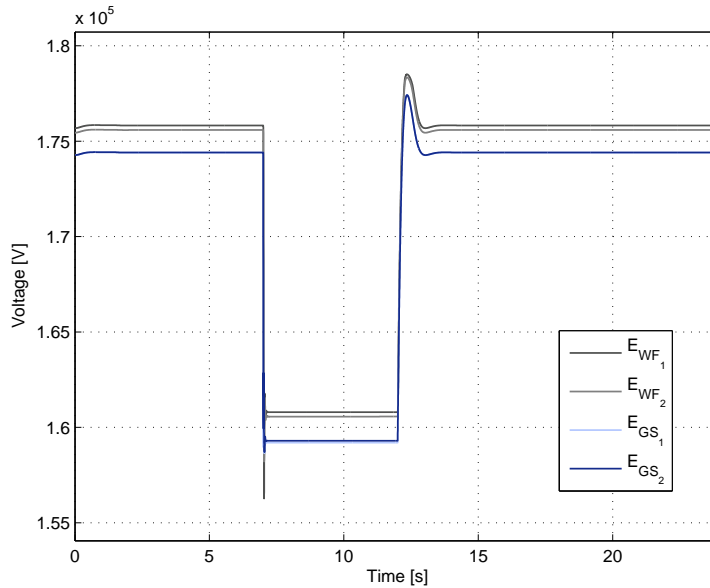


Figure 3.18: Voltages in wind farm and grid side VSCs

3.2.6 Conclusions

This study presents an optimal power flow approach to operate a multi-terminal HVDC system with large offshore wind farms. The optimal power flow computes optimal voltages and communicates them to the grid-side VSC in order to ensure minimum losses in the power transmission to the terrestrial AC grid. The proposed scheme requires communications, but in most applications, they will be already available for protection or monitoring purposes. When a communication fault occurs, the grid-side VSC control switches to droop control in order to guarantee a safe operation.

The differences between the proposed scheme and droop control in terms of losses have been analyzed, in two case studies with four and seven terminals, in steady state for multiple wind speeds. Results show that the proposed scheme can significantly reduce the system losses without further important investments (if communications are already available).

Dynamic simulations have been performed with a four terminal system in order to illustrate the transient behavior of the proposed scheme for wind

3.2 Optimum voltage control for loss minimization in HVDC multi-terminal transmission systems

speed changes and communication faults. Simulations show a good transient performance of the proposed scheme.

3.3 Droop control for loss minimization in HVDC multi-terminal transmission systems

3.3.1 Introduction

This study focuses on the challenge of optimizing power flows inside the VSC HVDC multi-terminal grid. The control of the multi-terminal HVDC using droop controllers was discussed and simulated in [59–61]. In [71], a hierarchical 3-level control structure, similar to the applying for AC networks was proposed for VSC-HVDC multi-terminal systems. It was shown in Section 3.2 that, although its robustness and the advantage of not needing communications, droop control could not guarantee optimal operation in the sense of ensuring minimum transmission joule losses for any power injection into the HVDC grid.

The approach presented in this study reaches optimal operating points for loss minimisation and when communications are lost, the system remains stable. The control scheme proposed is based on cascading an optimization algorithm and droop control. Converter losses are also taken into account, in addition to transmission losses. A communication system is assumed to be available between different converters (which would be already available as they are required for monitoring and protection).

This proposal assumes a simple control for VSC HVDC multi-terminal systems based on a two level hierarchy, instead of a three level one. The latter is the classical applying for AC networks (primary, secondary and tertiary controls) and adapted for HVDC multi-terminal systems in [71]). In this study the higher level control computes the voltage references to be sent to each grid side converter based on an optimization algorithm that ensures minimum losses in the system. These voltage references are sent to a lower level control, which is the voltage control of each grid side converter, that receives them and computes the needed current reference based on the droop control law.

3.3.2 Proposed control scheme

VSC-HVDC multi-terminal system description The control scheme proposed for operating VSC-HVDC multi-terminal grids is based on solving periodically an OPF algorithm, as depicted in Figure 3.19. The system under study is constituted by m wind farm VSCs, operating as rectifiers and n grid side VSC, operating as inverters, linked between each other through the HVDC grid. The wind farm VSCs inject the power produced from the wind farm into the DC grid and supply the reactive power needed to maintain the AC wind farm voltage [30, 62]. The grid side VSCs inject the power available in the DC grid into the main AC grid, while providing reactive power support [19]. Reference [5] analyses in detail the operating modes of the VSCs constituting a HVDC multi-terminal system, as well as its voltage current characteristics and equilibrium points.

By controlling the active power delivered from the HVDC grid to the AC main grid, the DC bus voltage is controlled. One of the extended solutions to do so is droop control [5, 59–61]. The DC current of the grid side VSC is controlled according to a voltage droop function, as shown in Equation (3.22).

$$I_{gs}^* = k_{droop} (E_{gs} - E_{gsL}) \quad (3.22)$$

where I_{gs}^* is the inverter DC current reference and E_{gs} is the measured DC inverter voltage. The proportional coefficient, k_{droop} , and the offset parameter, E_{gsL} , are the droop parameters and depend on the design of the control system [63].

Analysing droop characteristics, in Section 3.2, it was noted that droop can be designed in order to maintain a high voltage in the wind farm VSC, obtaining optimal losses for the designed point, but when the power reduces, the droop function leads to lower voltages and transmission losses are not minimum. The control scheme proposed shows that grid side converters can be operated, not only to keep the HVDC voltage but also ensuring the minimisation of the overall HVDC grid losses: transmission losses and converter station losses.

It is assumed that the power being produced on the wind farms and injected into the DC grid, denoted by P_i , is known, as well as the electrical parameters of the HVDC grid. As represented in Figure 3.19, the central

controller in charge of executing the OPF, receives the signals P_i , executes the algorithm that determines the voltages that ensure minimum losses and sends the output of the algorithm to each VSC as voltage references of the droop control ($E_{gsL1}, E_{gsL2}, \dots, E_{gsLn}$). The rate of change of the voltage references sent by the central controller is limited in order to avoid voltage peaks.

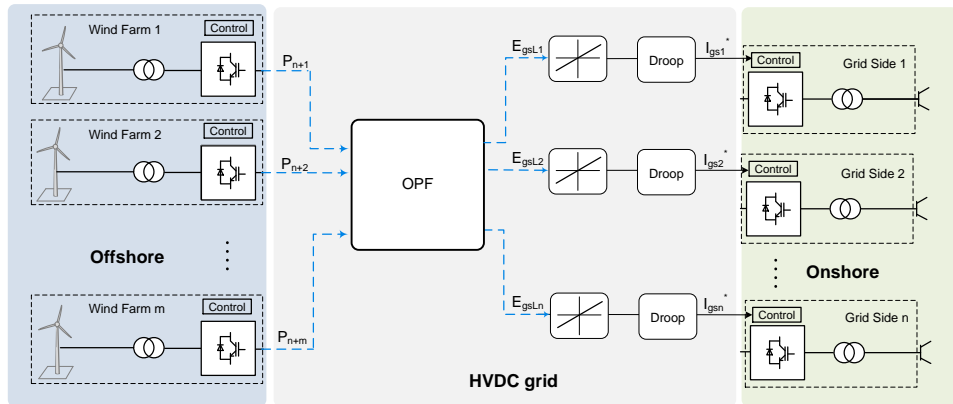


Figure 3.19: Optimization algorithm applied to a VSC-HVDC multi-terminal system

OPF formulation The notation used for the OPF problem formulation is detailed next: $\mathbf{I} = (I_1 \cdots I_{n+m})^T$ and $\mathbf{E} = (E_1 \cdots E_{n+m})^T$ are the vectors of currents and voltages in all the nodes and \mathbf{G} is the conductance matrix of the whole system.

E_i and I_i are, respectively, the voltage and the current in node i and E_{gsLi} are the voltage droop references in node i . n is the number of grid side VSCs, m is the number of wind farm VSCs and $i, j \in (1, m + n)$,

The objective function of the optimization problem can be chosen from Table 5.1. The optimization problem is detailed below choosing as objective function z_3 : the minimisation of the total power losses inside the HVDC system expressed as the sum of the losses inside the HVDC grid, $P_{lossDCgrid}$

Table 3.2: Objective functions

Objective function	Mathematical formulation
Minimum losses in DC grid	[MIN] $z_1 = \frac{1}{2} \sum_{i=1}^{n+m} \sum_{j=1}^{n+m} G_{ij}(E_i - E_j)^2$
Minimum losses in VSCs	[MIN] $z_2 = \sum_{i=1}^n P_{lossVSC_i}$
Minimum total losses	[MIN] $z_3 = \alpha z_1 + \beta z_2$

(z_1) and of the losses in all converter stations, $P_{lossVSC}$, (z_2) as shown in Equation (5.2). In (5.2), the two components of the objective function have been weighted with factors α and β ,

$$[MIN] z_3 = \alpha z_1 + \beta z_2 \quad (3.23)$$

where

$$z_1 = P_{lossDCgrid} = \frac{1}{2} \sum_{i=1}^{n+m} \sum_{j=1}^{n+m} G_{ij}(E_i - E_j)^2 \quad (3.24)$$

$$z_2 = \sum_{i=1}^n P_{lossVSC_i} = \sum_{i=1}^n R_a + R_b I_{ac} + R_c I_{ac}^2 \quad (3.25)$$

R_a models the no load losses, R_b models linearly dependent losses and R_c models quadratically dependent losses, according to [72]. I_{ac} represents the current flowing on the AC side of the converter and is computed according to Equation (3.26), based on the real power flow balance (including losses) between the AC side and DC side of the converter.

$$I_{ac} = \frac{E_i I_i}{\sqrt{3} V_{ac} \cos \theta} \quad (3.26)$$

V_{ac} corresponds to the phase-to-phase voltage of the converter.

The objective function (5.2) is subjected to the electrical grid restrictions (equality restrictions) and to voltages and current limits restrictions (inequality restrictions).

$$\mathbf{I} = \mathbf{GE} \quad (3.27)$$

$$P_i = E_i I_i, i \in (n+1, m+n) \quad (3.28)$$

$$I_i^* = k_{droop_i} (E_i - E_{gsLi}), i \in (1, n) \quad (3.29)$$

$$E_{min} \leq E_i \leq E_{max} \quad (3.30)$$

$$E_{min} \leq E_{gsLi} \leq E_{max} \quad (3.31)$$

$$I_{min-node} \leq I_i \leq I_{max-node} \quad (3.32)$$

$$I_{min-branch} \leq G_{ij} (E_i - E_j) \leq I_{max-branch} \quad (3.33)$$

The optimization problem can be solved applying the Interior Point Algorithm with barrier function [64]. MATLAB Optimization Toolbox has been used, specifically function *fmincon* (thought for nonlinear constrained optimization).

Despite requiring a communication system, the control can ensure reliable operation even if communications are lost. The last voltage reference signal is kept on converters until communications are recovered and a soft transition to the new references is ensured once communications are again available to avoid peaks in electrical quantities due to different operating conditions at the instant when communications are lost and recovered.

3.3.3 Steady state case studies

This subsection shows the results reached by the optimization problem in steady state for several objective functions when applied to a 6-terminal HVDC system. This system is inspired in the benchmark system defined by CIGRÉ in [73] and is represented in Figure 3.20, consisting of two offshore wind power plant nodes and four grid side nodes, from which 3 include a grid side converter with droop voltage function. The distance between nodes is expressed in km in Figure 3.20. The resistance value is 0.0095 ohm/km

for the ± 400 kV cables and 0.0114 ohm/km for the ± 400 kV overhead lines. The wind power plants are rated 500 MW each, and the DC power entering the HVDC grid is a known for the optimization problem. The base value for admittances is defined as follows: $Y_b = S_b/U_b^2$ where $U_b = 800$ kV is the base voltage and $S_b = 500$ MW is the base power.

In all the steady state cases analysed, it is assumed that the power coming from both wind power plants and entering the DC grid is 0.8 p.u.

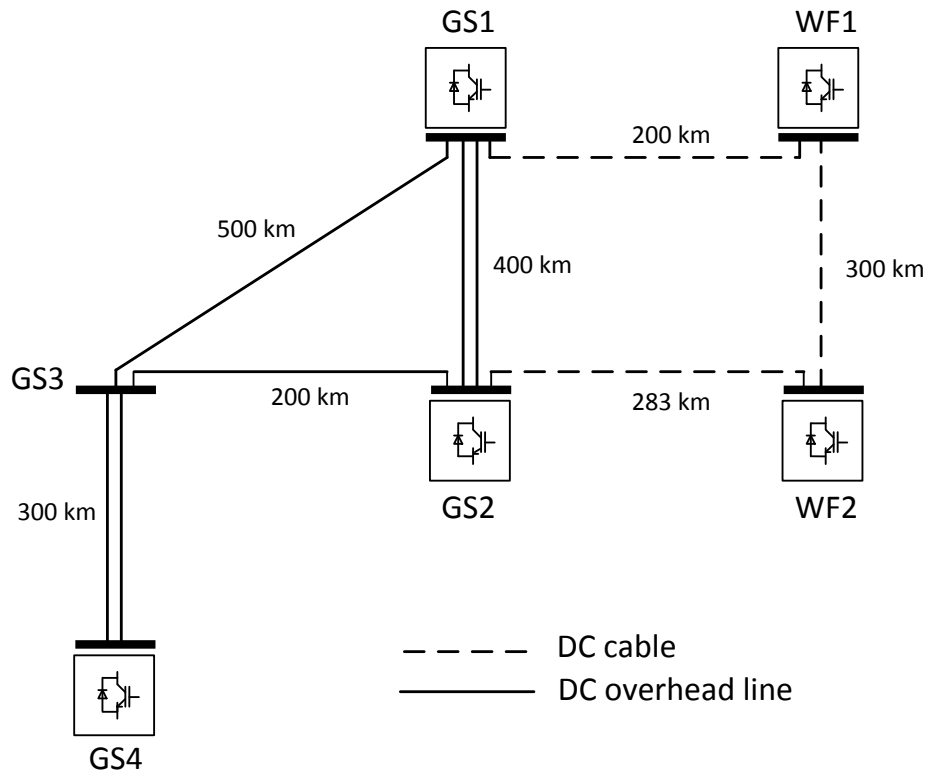


Figure 3.20: 6-terminal HVDC system [73]

Minimum HVDC grid losses In this case the objective function is the total losses in lines and cables of the HVDC grid:

$$z_1 = P_{lossDCgrid} = \frac{1}{2} \sum_{i=1}^6 \sum_{j=1}^6 G_{ij}(E_i - E_j)^2 \quad (3.34)$$

The power flow that leads to minimum HVDC grid losses (0.00207 p.u.) is shown in Figure 3.21.

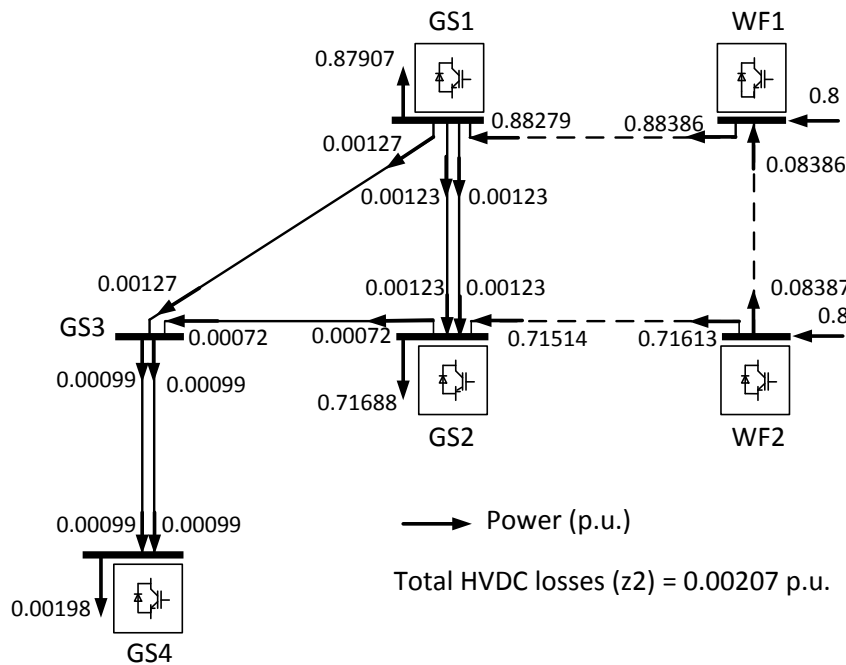


Figure 3.21: OPF for HVDC loss minimisation

Minimum VSCs losses In this case the objective function corresponds to the sum of the losses in the three converters:

$$z_2 = \sum_{i=1}^3 P_{lossVSC_i} \quad (3.35)$$

where $P_{lossVSC_i}$ is determined using expressions (3.25) and (3.26). The power flow that leads to minimum converter losses (0.03818 p.u.) is shown in Figure 3.22.

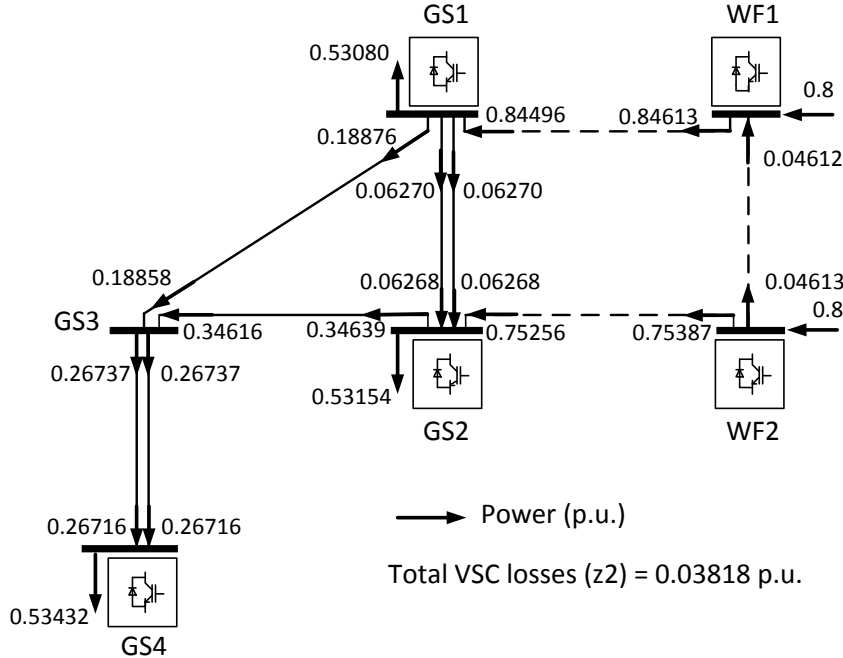


Figure 3.22: OPF for VSC loss minimisation

Minimum total losses The same wind farm power injections that in the before analysed cases (0.8 p.u.) are considered. The objective function selected is total losses. Choosing as weighting factors α varying from 0 to 1 in steps of 0.02 and $\beta = 1 - \alpha$, the Pareto front obtained is shown in Figure 3.23(a). The imaginary line resulting from joining all the plotted points represents the barrier of the region of feasible points, for which all constraints are satisfied, and the region of infeasible points.

$$[MIN] z_3 = \alpha z_1 + \beta z_2 \quad (3.36)$$

$$z_3 = \alpha \frac{1}{2} \sum_{i=1}^6 \sum_{j=1}^6 G_{ij} (E_i - E_j)^2 + \beta \sum_{i=1}^3 P_{lossVSC_i} \quad (3.37)$$

The values of the objective function, for the different values of α are represented in Figure 3.23(b).

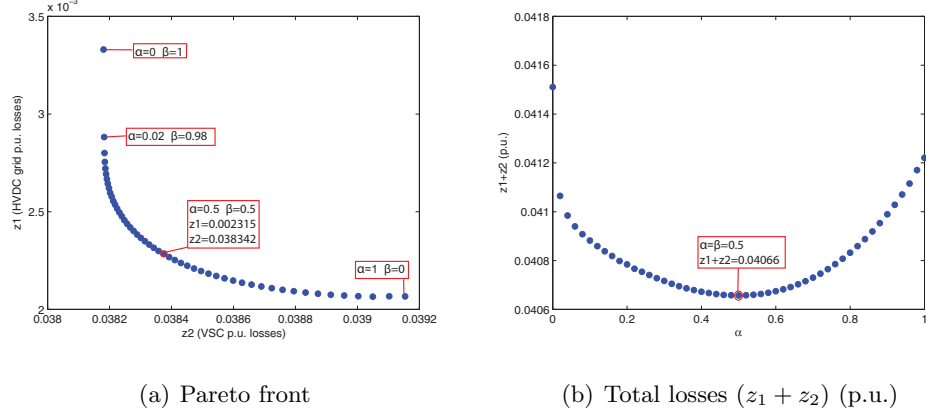


Figure 3.23: Pareto front and total losses

Sensitivity analysis to resistance changes In order to analyse the effect of a change on grid resistance values on losses, a 10% variation on the CIGRÉ resistance data for overhead lines and cables has been applied. Keeping the model and parameters for VSC losses, the Pareto front obtained is shown in Figure 3.24.

3.3.4 Dynamic case studies

The proposed control scheme is applied to a 4-terminal system, consisting in two wind farm VSCs and two grid side VSCs sketched in Figure 3.25, modelled according to the parameters detailed next. For more details on the 4-terminal system modelling, see Section 3.2.5.

The values of the conductance matrix, G_{ij} , are determined by means of ABB cable data [65]. A 160 kV (± 80) bipolar cable with 300 mm^2 copper subsection has been used. Conductance can be expressed as $G_{ijreal} = A(\rho l_{ij})^{-1}$, where $\rho = 0.01786 \Omega \text{mm}^2 \text{m}^{-1}$ is the copper resistivity, $A = 300 \text{ mm}^2$ is the

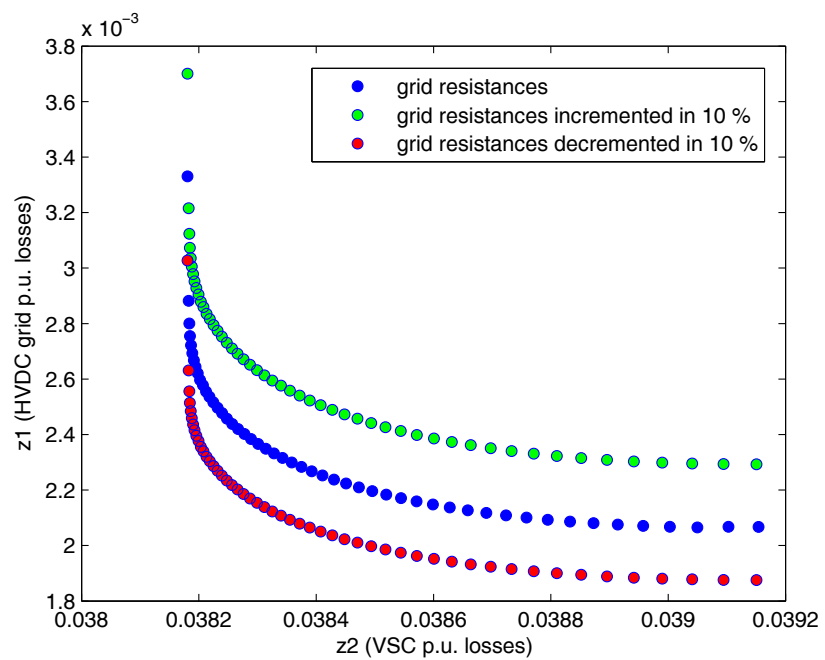


Figure 3.24: Pareto fronts for different grid resistances

copper subsection and l_{ij} is the length of the cable that connects the nodes i and j . In order to express the conductance in pu, a base admittance is defined as $Y_b = S_b/U_b^2$ where $U_b = 160$ kV is the base voltage and $S_b = 100$ MW is the base power. For dynamic simulations, the inductance of the cables is $L = 1 \text{ mH/km}$ and the total capacitance connected to each converter station is $C = 250 \mu\text{F}$. Wind farms are modelled as an aggregation of 50 wind turbines rated to 2 MW based on full power converters. Wind turbines are connected at the wind farm voltage 33 kV, a 1 km cable is considered between the wind farm aggregation and the transformer platform that elevates voltage to 90 kV.

The transformer parameters are: rated power = 120 MVA; voltages transformation 33 kV/90 kV; short circuit voltage = 10 %; ratio R/X = 0.04.

The following wind turbine parameters are used: C_p values correspond to Heier constants from [70]; Wind turbine radius = 39 m; Air density = 1.225 kg/m^3 ; Mass rotor inertia reduced to the wind turbine shaft = $3.6 \times 10^6 \text{ kgm}^2$.

The simulations have been performed using MATLAB Simulink, with a variable step solver: Ode-45 Dormand-Prince. The OPF presents a sampling period of 1.5 s which includes the communication and execution time of the central controller. The wind speed of each wind farm changes according to different wind series in the first study case and following different step changes in the second study case. Unity power factor operation is assumed for the AC grids to which grid side converters are connected, thus $\cos \theta = 1$. The objective function set defines the total losses in the HVDC system, according to (5.2), with weighing factors $\alpha = 1$ and $\beta = 1$.

Case study 1: Wind series This case study analyses normal operation of the HVDC system, assuming communications are available and showing the performance of the control scheme proposed when wind is blowing according to the wind series represented in Figure 3.26. The voltages evolution in wind farm and grid-side converters is illustrated in Figure 3.27. It is represented how every 1.5 s, the optimal power flow recalculates the reference voltages for the grid side VSCs. The currents flowing through each branch are shown in Figure 3.28. The higher is the wind speed, higher is the power produced

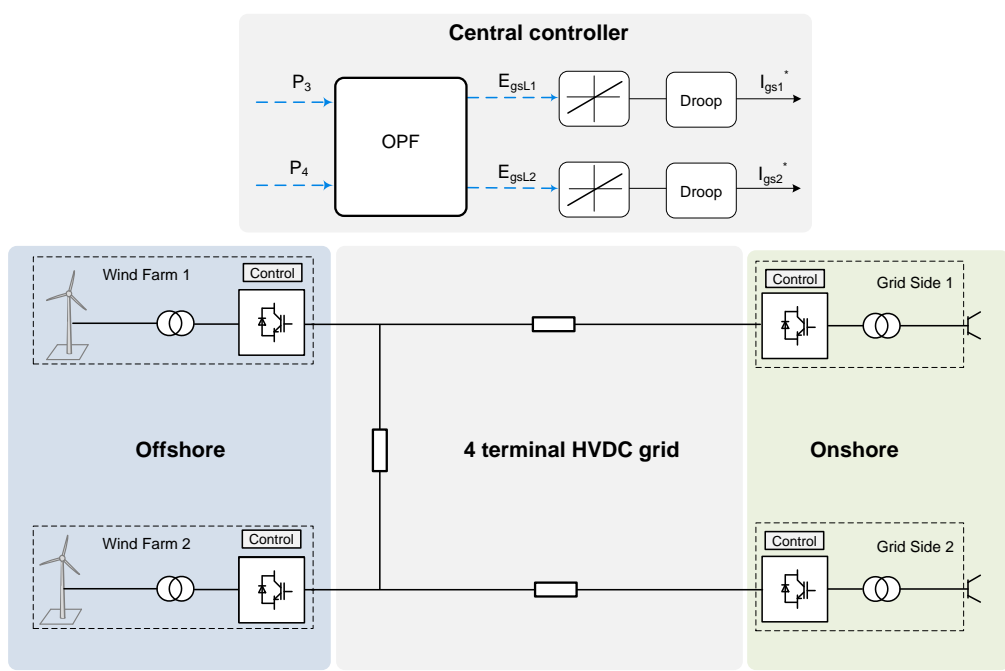


Figure 3.25: 4 terminal HVDC system with central controller computing an OPF

by the wind farms and injected into the DC grid and the OPF leads to higher DC voltages and less transmission losses. The transmission losses inside the HVDC grid, as well as the VSC losses in grid side converters and wind farm converters are represented in Figure 3.29 and Figure 3.30, respectively. The efficiency of the HVDC grid is shown in Figure 3.31.

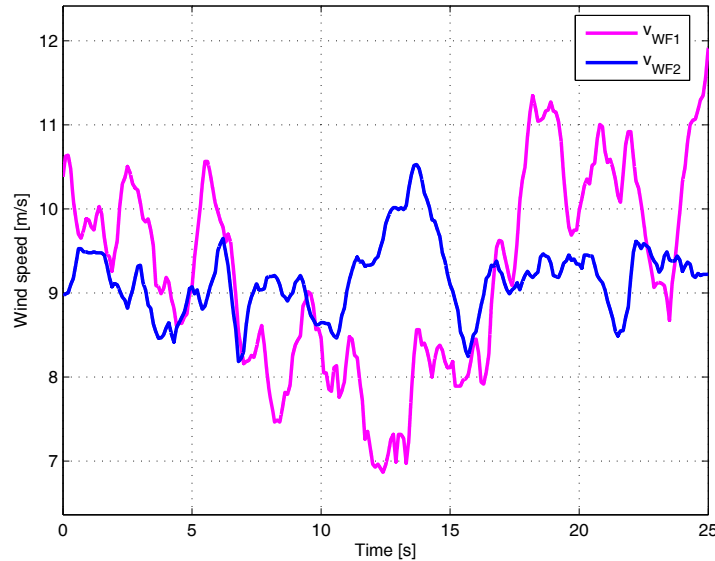


Figure 3.26: Wind speed changes

Case study 2: Loss of communications while wind speed changes This case study analyses the operation of the HVDC system, assuming communications are available, but eventually lost during 30 seconds. During the time period where communication signals are not available, wind speed changes in both wind farms as represented in Figure 3.32. For all the graphs depicted in this subsection a dotted vertical line indicates a change on communications availability -loss and recover-. The communication loss occurs at time 25 s and is recovered at 55 s.

In Figure 3.32 the time instants with a significant change in the simula-

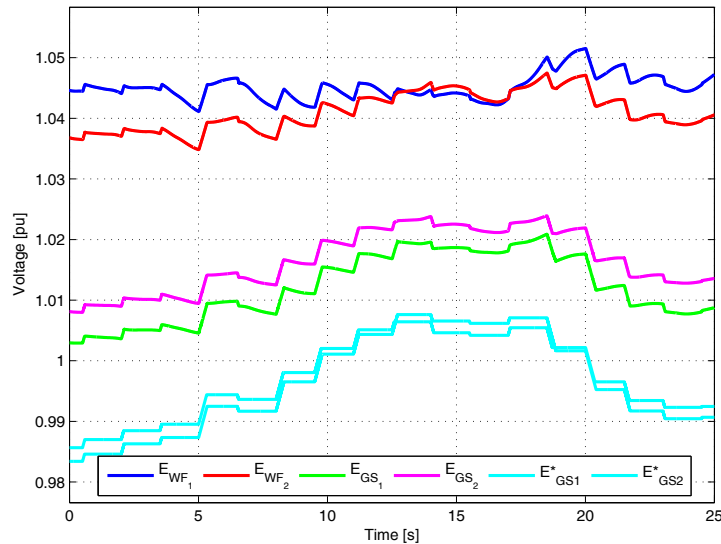


Figure 3.27: Voltages in wind farm and grid side VSCs

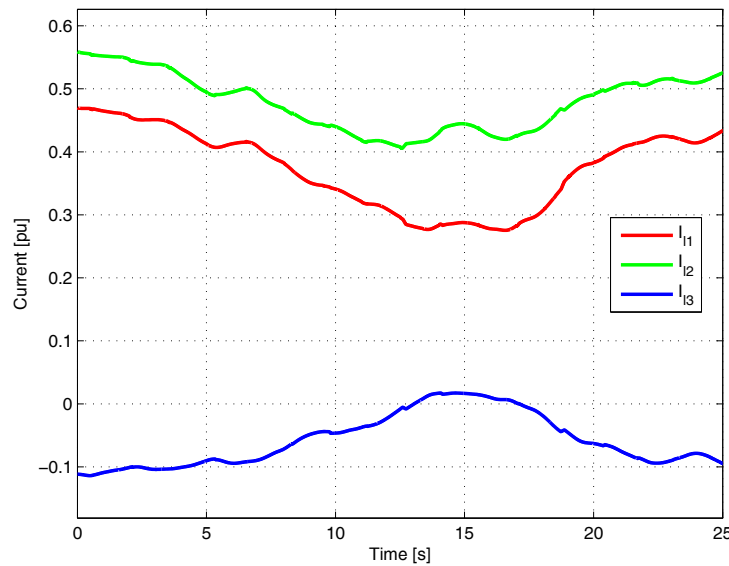


Figure 3.28: Currents in the DC grid

Chapter 3 Droop control for loss minimization in m -HVDC

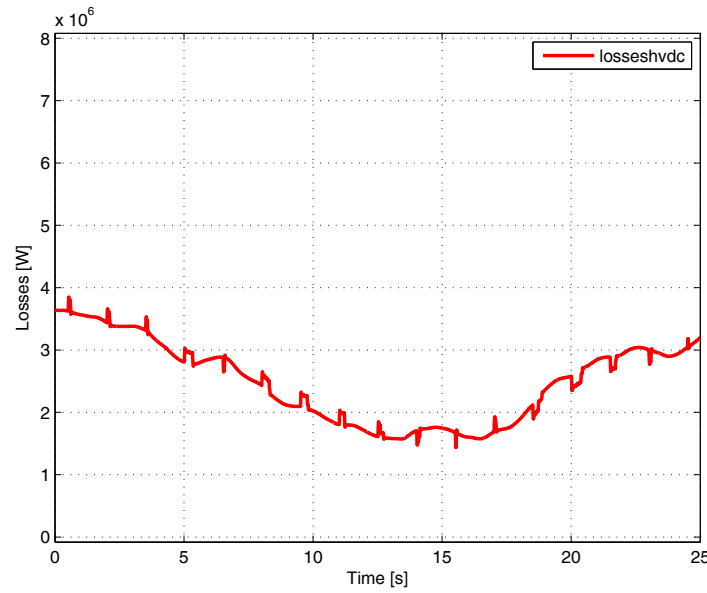


Figure 3.29: Losses in the HVDC grid

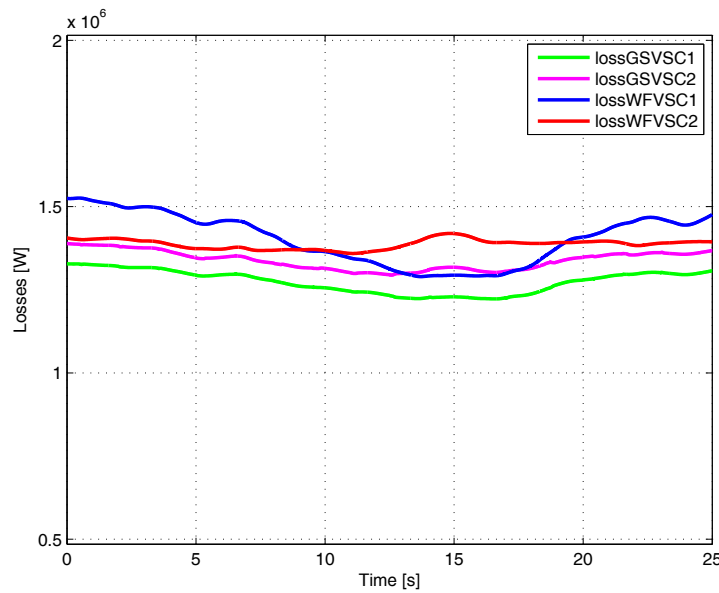


Figure 3.30: Losses in each VSC

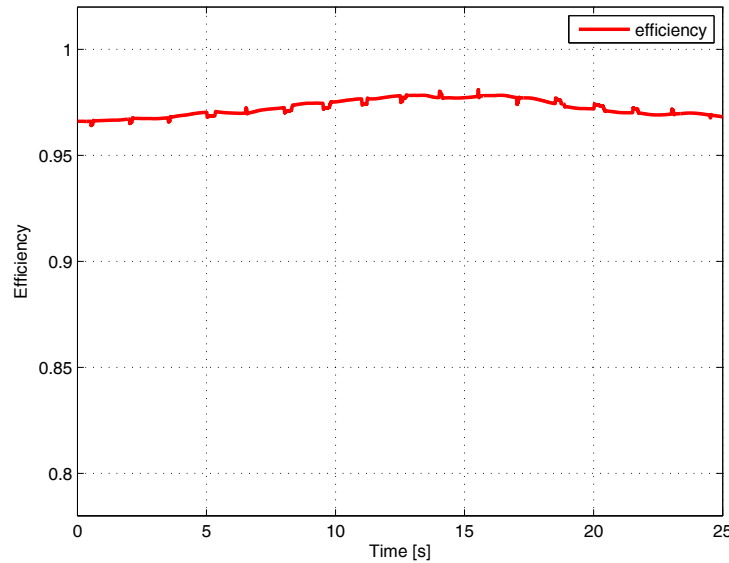


Figure 3.31: Efficiency

tion have been marked with a capital letter. In time intervals AB and DE wind speed changes in both wind farms. At time instant C , communications are lost and at time instant F they are recovered. A detail of the transient in grid-side converters is illustrated in Figure 3.27.

Before the communication loss (on C), two intervals can be analysed. From the origin until point A wind speed is kept constant in both wind farms. After point B , while wind speed increases in both wind farms, the OPF drops the DC voltages of the grid so as to keep the maximum power injection: voltages are stable and losses are minimum.

When communications are lost (on C), the OPF references are kept and, as wind speed has not varied, losses are kept minimum (CD). At times indicated by D and E , wind speed decreases in both wind farms, but, as no communications are available, the grid side VSCs do not perceive this variation and can not react to compensate it. Although the grid side voltage references are kept constant, the grid side voltages fall as a consequence of

Chapter 3 Droop control for loss minimization in m -HVDC

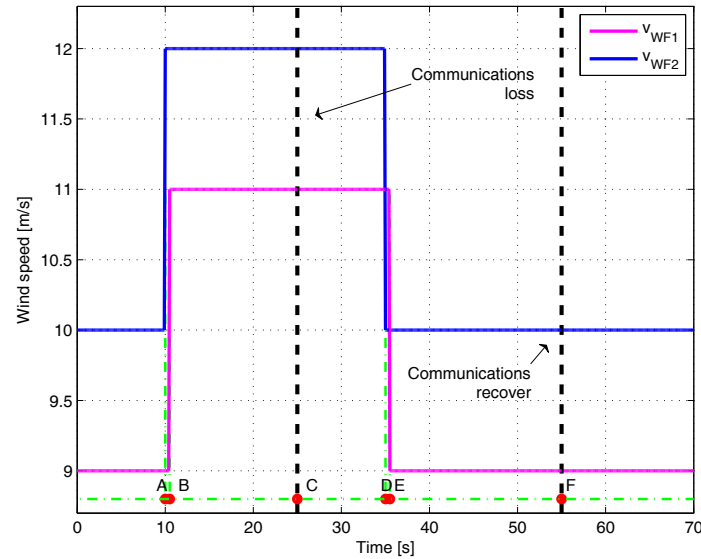


Figure 3.32: Wind speed changes

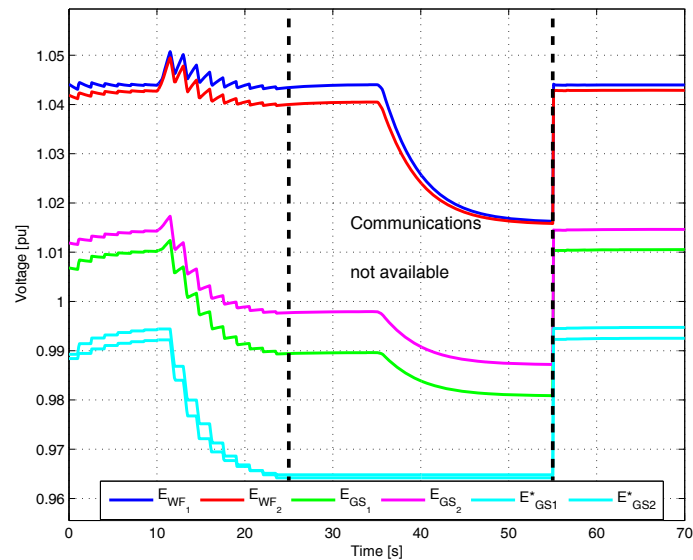


Figure 3.33: Voltages in wind farm and grid side VSCs

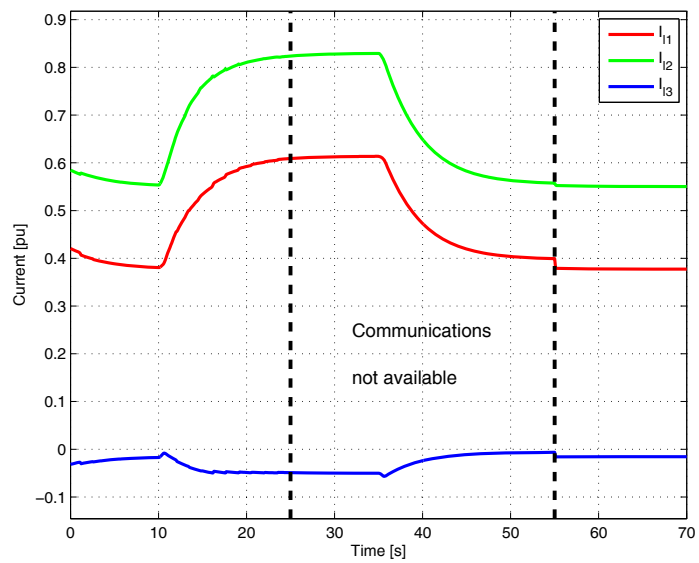


Figure 3.34: Currents in the DC grid

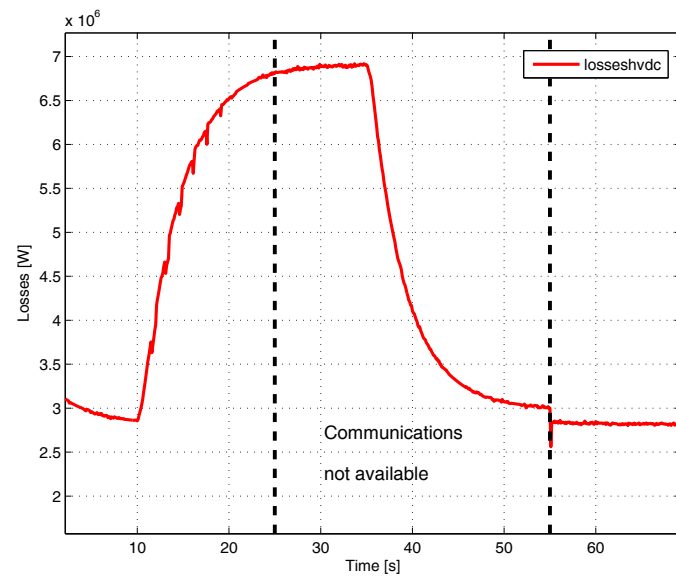


Figure 3.35: Losses in the HVDC grid

Chapter 3 Droop control for loss minimization in m -HVDC

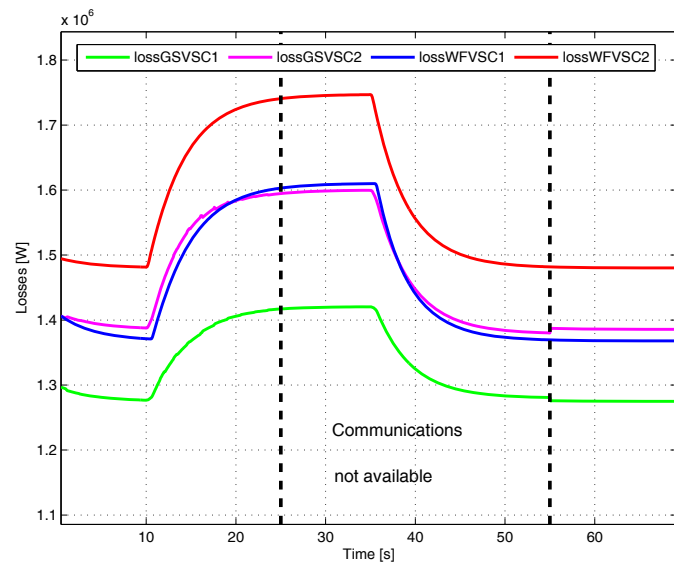


Figure 3.36: Losses in each VSC

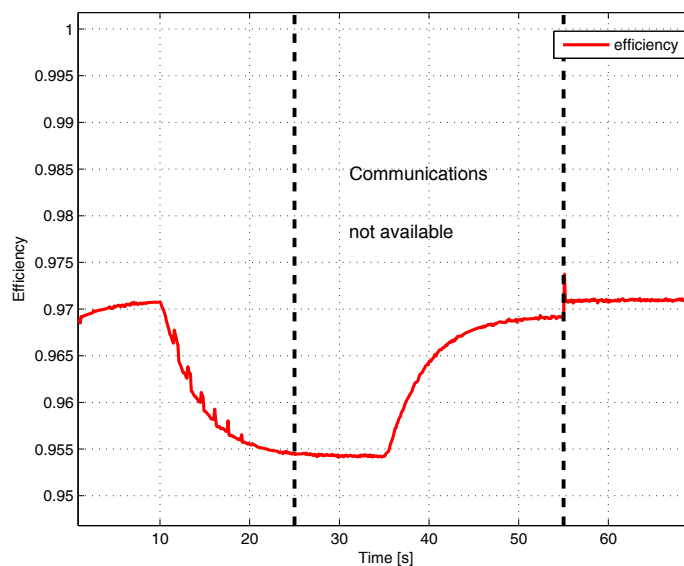


Figure 3.37: Efficiency

the wind speed decrease, leading to lower DC voltage profiles. So, from D to F the DC grid voltages are stable, but losses are not optimal.

At instant F , communications are recovered. As the operating conditions are different when communications are recovered in comparison to when they were lost, the new references computed by the OPF when communications are again available are not applied directly. Instead, the rate of change is limited until the difference between this rate limitation and the actual DC voltage is less than a certain threshold. This action avoids peaks in voltage and current and, therefore, in powers. After F , the OPF applies the computed references again each 1.5 s, leading to the same operating point that at the origin, because the power injection from the wind farms is the same that in A . The transmission losses inside the HVDC grid, as well as the VSC losses in grid side converters and wind farm converters are represented in Figure 5.20 and Figure 3.36, respectively. The efficiency of the HVDC grid is shown in Figure 3.37.

3.3.5 Conclusions

This study presents an OPF to operate a multi-terminal HVDC system with large offshore wind farms based on an optimization algorithm combined with droop control. The optimal power flow computes the appropriate voltages references for droop control and communicates them to the grid-side VSC in order to ensure minimum losses in the power transmission to the terrestrial AC grid. Although the proposed scheme requires communications, they will be already available for protection or monitoring purposes. When a communication fault occurs, the grid-side VSC control keeps the last reference received until communications are recovered in order to guarantee a safe operation while keeping the optimal operation of the DC grid. Through steady state analysis, the transmission losses and converter losses (separately and together) have been minimised for a 6-terminal HVDC system. Dynamic simulations have been performed with a 4-terminal HVDC system in order to illustrate the transient behavior of the proposed scheme for wind speed changes and communication faults. Simulations show a good transient performance of the proposed scheme and the improved response in comparison to the proposal presented in Section 3.2.

Chapter 4

Coordinated Control for an Offshore Wind Power Plant to Provide Fault Ride Through Capability

4.1 Introduction

During the last decades, the penetration of offshore wind power generation into the grid has experienced a large increase. This massive growth of offshore wind generation has lead to a revision and modification of the existing grid codes so as to improve the wind turbine behaviour, reduce the amount of wind power lost after disturbances and provide the wind power plants with operational characteristics similar to those of conventional power plants [39]. Nowadays, transmission system operators demand, through grid codes specifications, that large wind power plants withstand a voltage dip down to a certain percentage of the nominal voltage for a specific time caused by eventual short circuits affecting the transmission system. These Low Voltage Ride Through (LVRT) requirements are accompanied by the needed active and reactive power control strategies to be carried out.

Although there have been some advances and research on HVDC transmission systems for offshore wind including multi-terminal VSC-HVDC [63, 74], most of the current offshore wind power plants are connected in AC (MVAC and HVAC) and therefore the stability issues related to AC transmission technology are important. In [75, 76], it was detected that some active and reactive power control strategies applied during voltage sags can lead to in-

stability problems. Some authors have proposed improvements of fault ride through strategies. In [75], the E.ON grid code is implemented and its influence on stability of the nearby grid during disturbances is shown. The overrating of the converter of a wind turbine is used to improve the voltage profile and stability by slightly modifying the used example grid code. In [77], an optimised fault ride through strategy is proposed on the basis that active power should instantaneously be as low as possible and that reactive power should instantaneously be as high as possible whenever a fault occurs.

This study, based on [78] from the same authors, analyses how the HVAC transmission system that connects an offshore wind power plant (constituted by PMSM equipped with full power converter) with the main grid behaves when a three-phase symmetrical short circuit occurs at the onshore substation, causing a deep voltage sag. Using the conventional operation procedure fixed by the Grid Code Requirements of Tennet (Transmission System Operator of the Netherlands, South Holland and part of Germany), fault ride through capability cannot be ensured for some faults. To avoid this, a Coordinated Control is proposed in order to ensure fault ride through capability. The proposed scheme is demonstrated by means of dynamic simulations with DIgSILENT Power Factory. It is worth mentioning that the control scheme proposed can also be applied to onshore wind power plants, but in this study its application is focused on offshore wind power plants.

Introduction to voltage stability

Voltage stability is the ability of a power system to maintain steady acceptable voltages at all buses in the system under normal operating conditions and after being subjected to a disturbance. A system enters a state of voltage instability when a disturbance, increase in load demand, or change in system condition, causes a progressive and uncontrollable drop in voltage. The main factor causing instability is the inability of the power system to meet the demand for reactive power. The heart of the problem is usually the voltage drop that occurs when the active and reactive power flow through inductive reactances associated with the transmission network [79].

Active and reactive power transmission limits

Voltage instability results from the attempt of loads to draw more power than can be delivered by the transmission generation system. In this section, the maximum power obtained at a receiving end of a simple system is determined [80]. The studied system is sketched in Figure 4.1. It consists in an infinite bus (represented by an ideal voltage source E) that feeds a load through a transmission line (represented through its resistance R and reactance X). The transmission impedance is $Z = R + jX$. By definition, the voltage magnitude and frequency are constant at the infinite bus. It is assumed that the 3-phase operating conditions are balanced, so that the per phase representation is sufficient. Steady-state sinusoidal operating conditions are also considered.

Alternatively, E and Z may be thought as the Thévenin equivalent of a power system seen from one bus. In fact, because power generators are not pure voltage sources, the Thévenin emf varies as a larger power is drawn from the system. This variation will be now neglected, considering a constant emf E as before mentioned.

For the sake of simplicity, the transmission resistance R is neglected. The ideal voltage source is selected as the phase reference, by setting $\underline{E} = E\angle 0$. The load voltage magnitude and phase are denoted by V and θ respectively.

From 4.1, it is deduced:

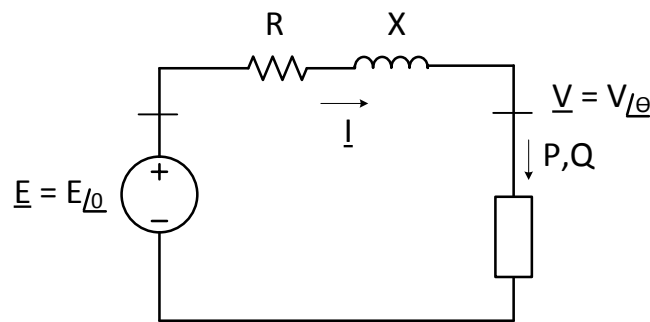


Figure 4.1: Circuit representation

$$\underline{V} = \underline{E} - jX\underline{I} \quad (4.1)$$

The complex power on the load is:

$$\underline{S} = P + jQ = \underline{V}\underline{I}^* = \underline{V} \frac{\underline{E}^* - \underline{V}^*}{-jX} \quad (4.2)$$

Knowing that \underline{E} and \underline{V} can also be expressed as

$$\underline{E} = Ee^{j0} = E \quad (4.3)$$

$$\underline{V} = Ve^{j\theta} \quad (4.4)$$

And replacing these expressions in equation (4.2):

$$\underline{S} = \frac{j}{X} (EV \cos \theta + jEV \sin \theta - V^2) \quad (4.5)$$

which decomposes into:

$$P = -\frac{EV}{X} \sin \theta \quad (4.6)$$

$$Q = -\frac{V^2}{X} + \frac{EV}{X} \cos \theta \quad (4.7)$$

Equation (4.6) and equation (4.7) are the *power flow* or *load flow* equations of a lossless system. For a given load (P, Q), they have to be solved with respect to V and θ , from which all other variables can be computed.

Angle θ represents the difference of the angle of the voltage phasors at the beginning and the end of the transmission line. This angle is limited, and, theoretically, when it reaches 90° the maximum active power is being transmitted. If this angle grows until 90° and this value is kept, this will lead to Voltage Instability.

Let us consider an offshore wind power plant connected to the terrestrial grid through HVAC transmission. The single phase diagram of the three-phase transmission can be represented by means a linear quadrupole, as shown in Figure 4.2. The equations that relate the input variables (voltage at the sending end, \underline{V}_s and sending current, \underline{I}_s) with the output variables (voltage at the receiving end, \underline{V}_r and receiving current, \underline{I}_r) are the transmission equations of the system. They can be expressed in matrix notation,

4.1 Introduction

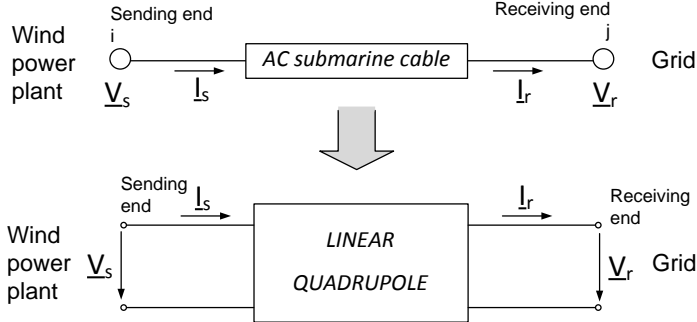


Figure 4.2: Transmission line diagram as a linear quadrupole

as follows:

$$\begin{bmatrix} \underline{V}_s \\ \underline{I}_s \end{bmatrix} = \begin{bmatrix} \underline{A} & \underline{B} \\ \underline{C} & \underline{D} \end{bmatrix} \begin{bmatrix} \underline{V}_r \\ \underline{I}_r \end{bmatrix} \quad (4.8)$$

where \underline{A} , \underline{B} , \underline{C} and \underline{D} are the transmission line constants. So, the phase current at the end of the line is [81]:

$$\underline{I}_r = \frac{\underline{V}_s - \underline{A} \underline{V}_r}{\underline{B}} \quad (4.9)$$

Using Equation (4.9), the receiving power of the line can be obtained as a function of the voltages of its endings:

$$\underline{S}_r = 3\underline{V}_r \underline{I}_r^* = 3 \left(\frac{\underline{V}_s^* \underline{V}_r}{\underline{B}^*} - \frac{\underline{A}^* |\underline{V}_r|^2}{\underline{B}^*} \right) \quad (4.10)$$

A similar expression results for the sending power when replacing Equation (4.9) in Equation (4.11)

$$\underline{I}_s = \underline{V}_r \underline{C} + \underline{I}_r \underline{D} \quad (4.11)$$

which leads to:

$$\underline{I}_s = \underline{V}_r \underline{C} + \frac{\underline{V}_s - \underline{A} \underline{V}_r}{\underline{B}} \underline{D} \quad (4.12)$$

As the quadripole is passive ($\underline{A} \cdot \underline{D} - \underline{B} \cdot \underline{C} = 1$), then Equation (4.12) can be rewritten as [81]:

$$\underline{I}_s = \frac{\underline{D}}{\underline{B}} \underline{V}_s - \frac{1}{\underline{B}} \underline{V}_r \quad (4.13)$$

And the sending power corresponds to:

$$\underline{S}_s = 3\underline{V}_s \underline{I}_s^* = 3 \left(\frac{\underline{D}^* |\underline{V}_r^2|}{\underline{B}^*} - \frac{\underline{V}_s^* \underline{V}_r}{\underline{B}^*} \right) \quad (4.14)$$

Let us consider the voltage at the receiving end as a reference: $\underline{V}_r = V_r \angle 0$ and the sending-end voltage: $\underline{V}_s = V_s \angle \delta$. The transmission line constants are such that: $\underline{A} = A \angle \alpha$, $\underline{B} = B \angle \beta$, $\underline{D} = D \angle \alpha$

The expressions of active and reactive power in each ending of the line can be easily deduced from Equations (4.10) and (4.14) -now considering line-to-line voltages instead of line-to-ground-. For the receiving end:

$$P_r = \frac{V_s V_r}{B} \cos(\beta - \delta) - \frac{AV_r^2}{B} \cos(\beta - \alpha) \quad (4.15)$$

$$Q_r = \frac{V_s V_r}{B} \sin(\beta - \delta) - \frac{AV_r^2}{B} \sin(\beta - \alpha) \quad (4.16)$$

For the sending end:

$$P_s = \frac{DV_s^2}{B} \cos(\beta - \alpha) - \frac{V_s V_r}{B} \cos(\beta + \delta) \quad (4.17)$$

$$Q_s = \frac{DV_s^2}{B} \sin(\beta - \alpha) - \frac{V_s V_r}{B} \sin(\beta + \delta) \quad (4.18)$$

Thus, the maximum power that can be achieved in the receiving end of a transmission line is reached when $\delta = \beta$ and its expression is:

$$P_{rmax} = \frac{V_s V_r}{B} - \frac{AV_r^2}{B} \cos(\beta - \alpha) \quad (4.19)$$

For systems that can be modelled by means its π equivalent, the transmission constant $B = Z_\pi = R + jX$, so the angle associated to the phasor of this coefficient is:

$$\beta = \arctan \left(\frac{X}{R} \right) \leq 90^\circ \quad (4.20)$$

and the maximum power for non lossless transmission is reached when

$$\delta = \beta < 90^\circ \quad (4.21)$$

For the particular case of a lossless line ($R=0$) and neglecting the effect of the line admittance, then $A=1$ and $B=jX$. So, using $\alpha = 0$ and $\beta = 90^\circ$ in Equation (4.15):

$$P_r = \frac{V_s V_r \sin(\delta)}{X} \quad (4.22)$$

4.2 Current limit and stability analysis for AC connected offshore wind power plants

In this case the maximum power is reached when $\delta = 90^\circ$ and its value is:

$$P_{rmax} = \frac{V_s V_r}{X} \quad (4.23)$$

The angle limitation concluded in Equation (4.21) will be considered for the dynamic study of the transmission system that connects an offshore wind power plant to the terrestrial grid, represented in Figure 4.3.

4.2 Current limit and stability analysis for AC connected offshore wind power plants

The present section addresses an analysis on the current and stability limits which have to be considered for offshore wind power plants [76]. The typical system sketched in Figure 4.3 is considered. Wind turbines are equipped with full power converter that can independently control active and reactive power. Similar conclusions would be drawn considering doubly fed induction generators. Reactors are located at both AC cable ends for reactive power compensation purposes.

The system can be simplified as shown in Figure 4.4, where the wind power plant includes the wind turbines, the WPP cables and transformers and the compensation reactors. An overall current \underline{I}_w is injected by the equivalent wind power plant into the cable which is modelled using a π -equivalent with parameters R_{cable} , $X_{L-cable}$ and $X_{C-cable}$.

The relationship between the WPP voltage \underline{U}_w and the main grid voltage are \underline{U}_g is given by

$$\underline{U}_w = \underline{U}_g + (R_{cable} + jX_{L-cable}) \underline{I}_c \quad (4.24)$$

Using $\underline{I}_c = \underline{I}_w - \underline{U}_w / (-jX_{C-cable})$, the WPP voltage can be expressed as

$$\underline{U}_w \gamma = \underline{U}_g + \underline{Z}_c \underline{I}_w \quad (4.25)$$

where $\underline{Z}_c = R_{cable} + jX_{L-cable}$ and

$$\underline{\gamma} = 1 + \frac{R_{cable} + jX_{L-cable}}{-jX_{C-cable}}.$$

Chapter 4 Coordinated Control for an OWPP to provide FRT Capability

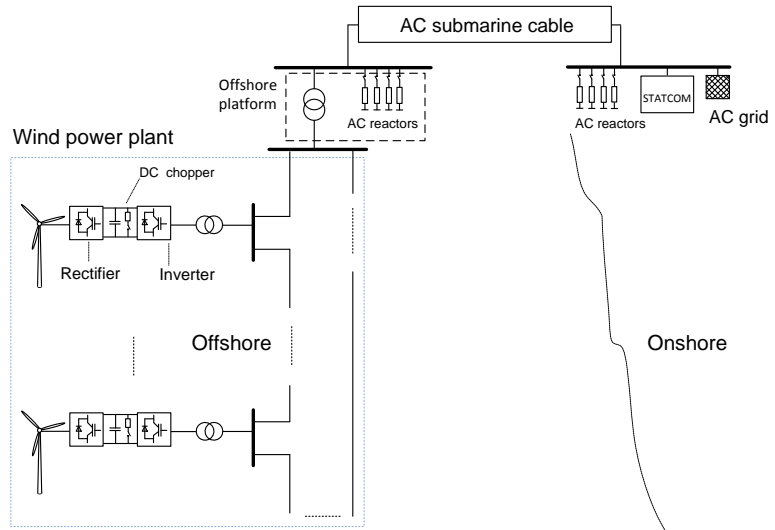


Figure 4.3: Offshore wind power plant connected through AC transmission to the terrestrial grid

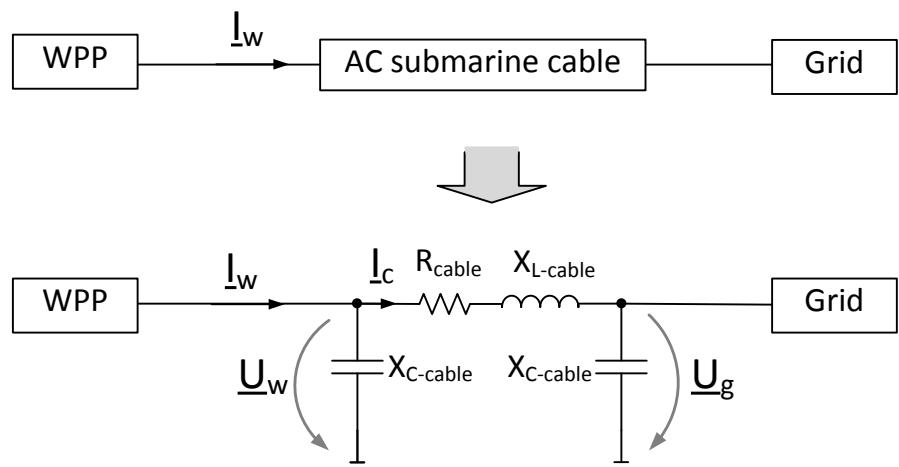


Figure 4.4: Offshore Wind Power Plant (WPP) connected through AC submarine cable, represented through its π equivalent, to the grid

4.2 Current limit and stability analysis for AC connected OWPP

In this simplified scheme, it can be assumed that the WPP can provide a maximum current (I_{max}) for any power factor, resulting in a circle centred in the origin in the current capability curve shown in Figure 4.5. The generating nature of the WPP will allow only operation in the right side region with positive active current. As far as stability is concerned, it is well known that the phase difference between voltages \underline{U}_w and \underline{U}_g should not exceed $\pi/2$.

Choosing the reference phasor $\underline{U}_g = U_g \angle 0$, the current drawn by the WPP can be expressed as

$$\underline{I}_w = \frac{\gamma \underline{U}_w - \underline{U}_g}{\underline{Z}_c} = -\frac{\underline{U}_g}{\underline{Z}_c} + U_w \angle \theta_w \frac{\gamma}{\underline{Z}_c} = \underline{I}_O + \underline{Y}_c U_w \angle \theta_w \quad (4.26)$$

where $\underline{Y}_c = \frac{\gamma}{\underline{Z}_c}$ and $\underline{I}_O = -\frac{\underline{U}_g}{\underline{Z}_c}$. It can be noted that \underline{I}_O is the current in the WPP when the WPP voltage is null. When the WPP voltage increases, for each angle θ_w , it can be seen in Figure 4.5, that straight lines with origin in \underline{I}_O describe the operating currents. The Figure 4.5 illustrates an example (close to the system which will be analyzed in Section 4.5) WPP current capability curve when the grid voltage is reduced to 2%. In normal voltage conditions, the point O (\underline{I}_O) will be far from the current limit circle.

The point A (intersection between null active current and maximum angle) can be found

$$\underline{I}_A = j \operatorname{Im}(\underline{I}_O) + j \frac{\operatorname{Re}(\underline{Y}_c) \operatorname{Re}(\underline{I}_O)}{\operatorname{Im}(\underline{Y}_c)} \quad (4.27)$$

where $\operatorname{Re}(\underline{Z})$ and $\operatorname{Im}(\underline{Z})$ denote the real and imaginary part of \underline{Z} , respectively. The points B1 and B2 (showing the intersection between maximum current and maximum angle) can be found solving the second order polynomial equation to find the WPP voltage $\underline{U}_w = 0 + jU_{wB}$ that match the conditions.

$$Y_c^2 U_{wB}^2 + 2 [\operatorname{Re}(j\underline{Y}_c) \operatorname{Re}(\underline{I}_O) + \operatorname{Im}(j\underline{Y}_c) \operatorname{Im}(\underline{I}_O)] U_{wB} + I_O^2 - I_{max}^2 = 0 \quad (4.28)$$

and substituting $\underline{U}_w = 0 + jU_{wB}$ in (4.26).

Using the same example, the evolution of the angle θ_w when increasing the WPP current for different power factors is illustrated in Figure 4.6. It can be noted that for certain WPP current angles, the instability is reached when the current is increased over a certain threshold.

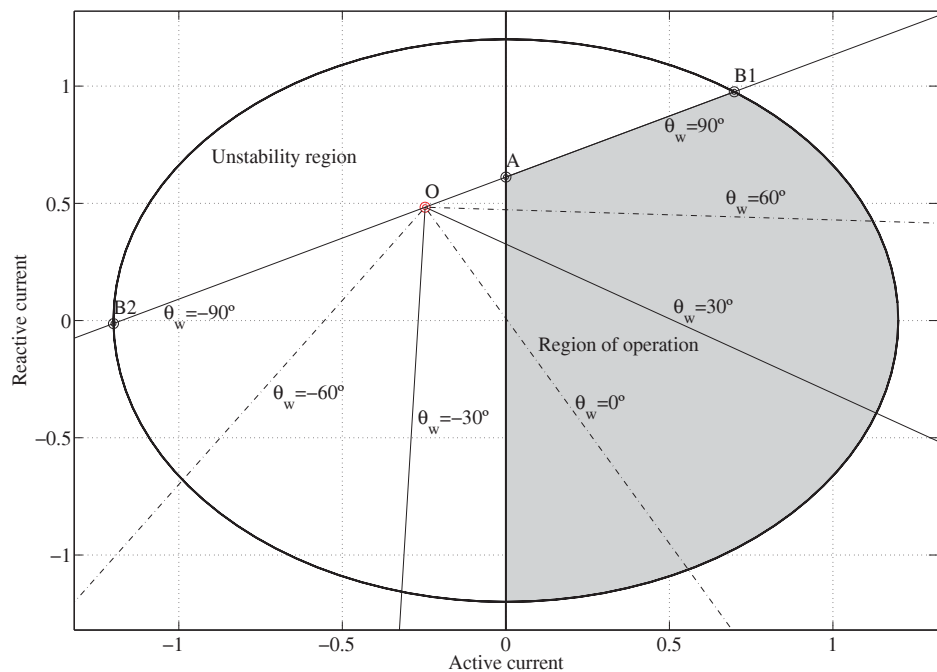


Figure 4.5: Example of current capability curve

4.2 Current limit and stability analysis for AC connected OWPP

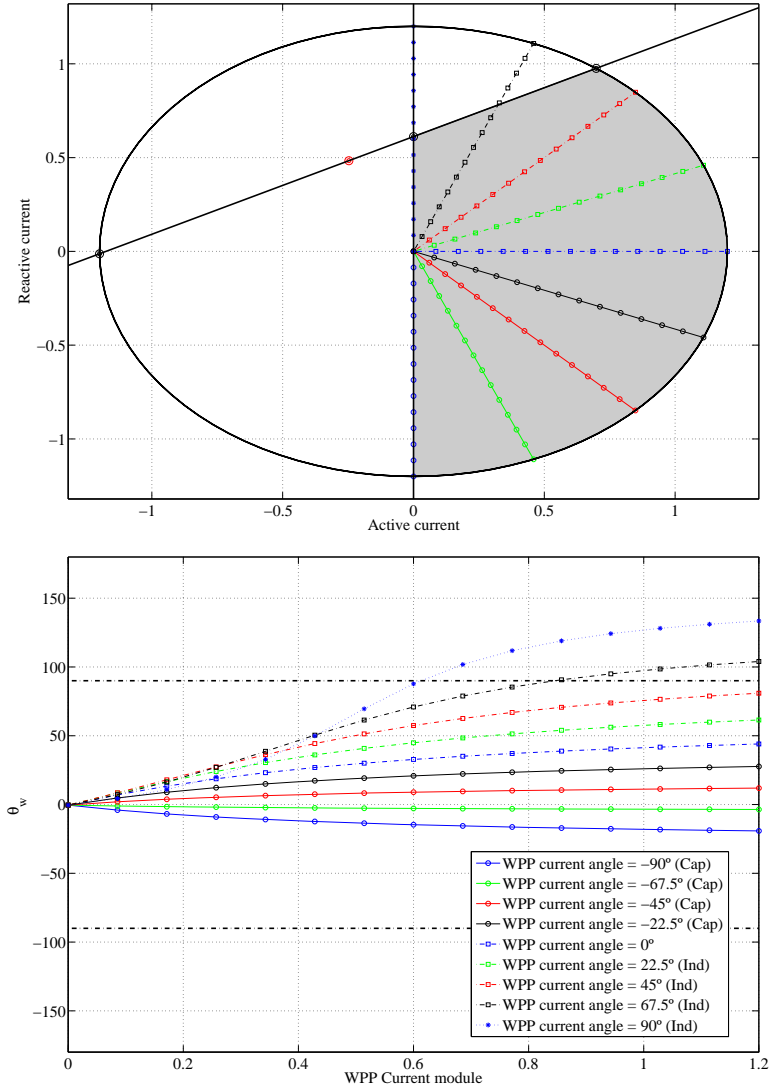


Figure 4.6: Angle θ_w evolution when increasing WPP current for different power factors

In order to ensure stability, the present work proposes to monitor the angle θ_w and readjust the WPP current when θ_w overcomes a certain threshold.

4.3 Conventional operation for voltage sags

According to the Tennet grid code [82,83] (one of the most restrictive grid codes), under three-phase short circuits or fault-related symmetrical voltage dips, the wind power plant must remain connected as long as the voltage at the grid connection point is above limit line 1 shown in Figure 4.7. Within the shaded area and above limit line 2, generating plants should experience the fault without disconnecting from the grid. If a generating plant can not accomplish it, the limit line can be shifted if agreed with Tennet TSO GmbH and accomplishing the requirements of the grid at the grid connection point. In case that, when experiencing the fault, a generator becomes unstable or its protection responds, a brief disconnection (less than 2 s) of the generating plant from the grid is permitted by agreement with Tennet TSO GmbH. A brief disconnection of the generating plant from the grid is always allowed below limit line 2 [82].

Reactive current support must be provided on the low voltage side of each wind turbine transformer. The voltage control must take place within 20 ms after fault recognition by providing reactive current amounting to at least 2% of the rated current for each percent of the voltage dip [82]. Active current is therefore limited by the converter rating and demanded reactive current. This means that if the voltage remains equal or below 50%, then 100% reactive current should be delivered. If the wind turbines are supposed to inject 100% reactive current under these circumstances, very low active power (or even null) is going to be produced.

In normal operation mode, the wind turbine inverter controls the DC bus voltage of the back-to-back and the reactive power (associated with d-component). The pulse-width modulation index vector is obtained as the output of a dq-current controller. The voltage angle is measured using a PLL and this gives the reference-system for the pulse width modulation vector [79].

Under fault conditions, assuming i_{lmax} is the maximum p.u. current deliver-

4.3 Conventional operation for voltage sags

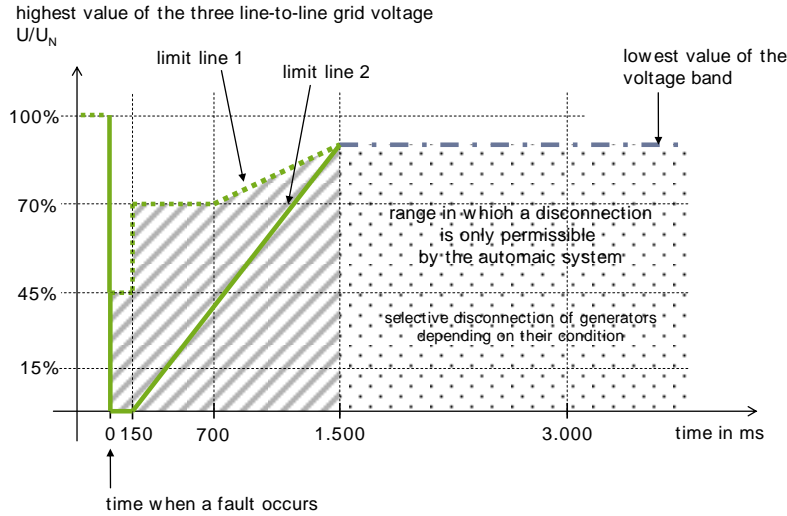


Figure 4.7: Limit curves for the voltage/time pattern at the grid connection for Type 2 generating plants in the event of a fault in the grid [82]

able by the wind turbine inverter, the active power reference accomplishes:

$$i_{qmax}^* = \sqrt{i_{lmax}^2 - i_d^{*2}} \quad (4.29)$$

In order to clarify the reactive power control implemented on the wind turbine with conventional operation, a graph is presented in Figure 4.8. It is shown how reactive current reference varies with the voltage of the bus connected to the LV side of wind turbine transformer.

While the wind turbine inverter controls the active and reactive power output as before described, the wind turbine rectifier should either adapt its output power, by changing to a lower torque reference or it can keep generating as in normal operation and the DC chopper will burn the excess power. According to usual industry practice, this second option is the one implemented in simulations. The current reference through the chopper resistance is calculated as:

$$I_{dc\ chopper}^* = k \frac{E_{dc} - E_{min}}{E_{max} - E_{min}} \quad (4.30)$$

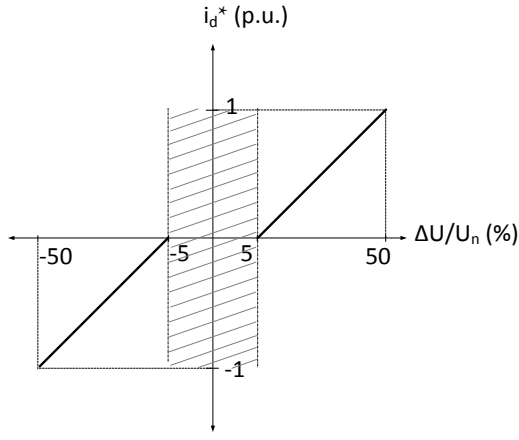


Figure 4.8: Reactive power control in normal operation and under faulty conditions

which is equivalent to:

$$I_{dc \text{ chopper}}^* = \frac{E_{dc}}{R_{chopper}^*} \quad (4.31)$$

4.4 Coordinated control proposal

This section presents a coordinated control strategy to operate HVAC connected wind farms while providing fault ride through capability, even when deep voltage sags occur on the main AC grid. The wind power plant needs information on the main grid voltage, which is obtained by means of fast communications or through an observer.

4.4.1 Angular Difference Index: ADI

The coordinated control proposed is based on the computation of an index which gives information of an instability proximity. This index is computed as the difference between the angles of the voltage phasors at the sending i and receiving j end of the transmission line:

$$ADI_{ij} = \frac{|\delta_i - \delta_j|}{\delta_{lim}} \quad (4.32)$$

4.4 Coordinated control proposal

where:

δ_i is the angle of the voltage phasor at bus i

δ_j is the angle of the voltage phasor at bus j

δ_{lim} is the angle that permits maximum active power transmission (90° , theoretically and for a lossless and short transmission line)

The value of ADI varies between 0 and 1 and it determines the proximity to voltage instability in line ij . When the difference $\delta = \delta_i - \delta_j$ reaches the limit set by the critical angular difference, $\delta_{critical}$, the line is approaching an unstable operating point. So, some countermeasures can be taken with anticipation. ADI is going to be calculated at different parts of the system, based on angles measured or estimated in the sending and receiving end of the transmission. ADI will be computed and/or communicated so that all the wind turbines, as well as the offshore and onshore platforms are aware of its value. A general scheme of the control action system is presented in Figure 4.9.

4.4.2 Computation of ADI

The computation of ADI requires the communication of the angle from one end of the transmission to the other, which can be achieved by means of optical fibre inside the cables. In case it was not available or communications failed, an observer of the angle can be used.

With communications

In this case the proposed coordinated control works assuming a communication system is available from the onshore to offshore substations. The angle is measured at each end of the transmission using a PLL and communicated to the other end through optical fibre inside the AC cable, with a sampling time of 20 ms.

Without communications

In this case, the coordinated control works without a communication system being available between onshore and offshore, but existing inside the wind power plant grid. The needed angles are estimated by means of measures at

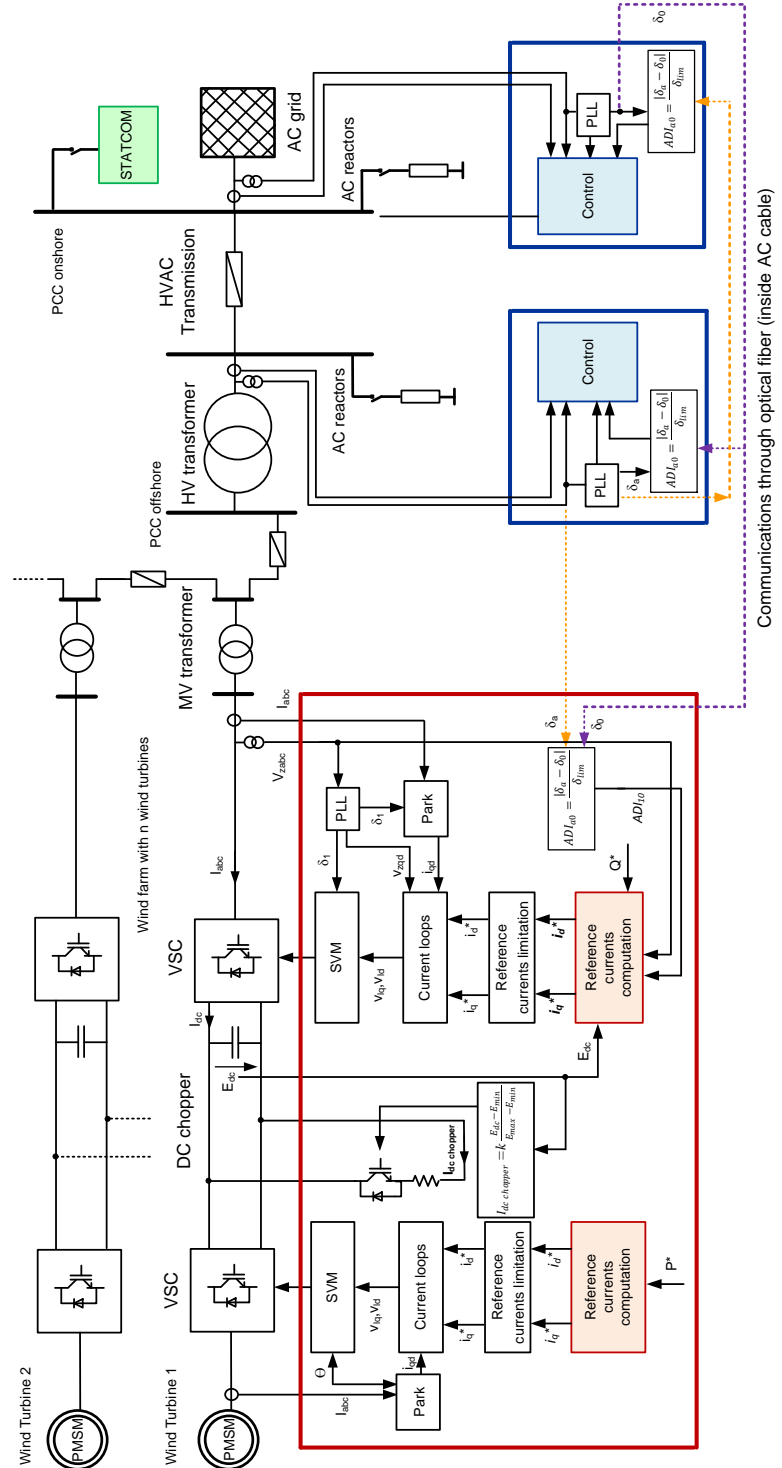


Figure 4.9: Control action scheme for an offshore wind power plant with HVAC transmission

4.4 Coordinated control proposal

the point where ADI information is needed, assuming the electrical parameters of the cable are known. So, two angles need to be estimated. One on the offshore platform (from where the ADI will be communicated to each wind turbine) and the other on the onshore platform. To calculate ADI in the offshore platform, the angle of the sending end will be measured by means a PLL and the angle of the receiving end will be estimated by means of current and voltage measures at the offshore platform and using electrical data of the cable. Similarly, to calculate ADI in the onshore platform, the angle of the receiving end will be measured by means a PLL and the angle of the sending end will be estimated by means of current and voltage measures at the onshore platform and using electrical data of the cable. If the cable is modelled according to the π model, with resistance R , inductive reactance X_l and capacitive reactance X_c , as shown in Figure 4.10, then, in steady state, the voltage phasor at the onshore platform, before the PCC, \underline{V}_a , can be estimated knowing the parameters of the cable and by means of the measures of the voltage and current at the HV side of the offshore transformer, \underline{V}_{HV} and \underline{I}_{HV} , respectively (see Equation (4.33)).

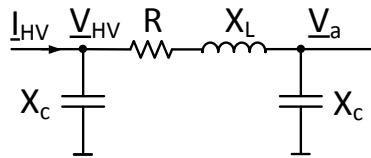


Figure 4.10: Electrical scheme of the AC cable and measures for estimation of the voltage phasor at the onshore platform

$$\underline{V}_a = V_a \angle \delta_a = \underline{V}_{HV} - \left(\underline{I}_{HV} - \frac{\underline{V}_{HV}}{jX_c} \right) (R + jX_l) \quad (4.33)$$

4.4.3 System actions to avoid instability

A fundamental action that needs to be taken once instability proximity is detected is the reduction of the active power delivered by the generating units and the adjustment of the reactive power injection. The wind turbine will keep on generating power during the disturbance, but by means of the DC chopper and thanks to the control implemented on each wind turbine

inverter, the active power and reactive power will be regulated. The active power reference, i_q^* and the reactive power reference, i_d^* are computed as explained in Section 4.3, but in case instability proximity is detected they are recomputed as a function of ADI, and the remaining voltage after the voltage sag of the bus bar to which the wind turbine is connected (V):

$$i_q^{*new} = \alpha_p i_q^* \quad (4.34)$$

being α_p , limited between 0 and 1:

$$\alpha_p = k_{1p}(1 - ADI) + k_{2p}(1 - V) \quad (4.35)$$

$$i_d^{*new} = \alpha_q i_d^* \quad (4.36)$$

being α_q , limited between 0 and 1:

$$\alpha_q = k_{1q}(1 - ADI) + k_{2q}(1 - V) \quad (4.37)$$

The other action in case instability proximity is detected is the disconnection of the reactive power compensations, based on the ADI value and the remaining voltage at the bus where compensations are connected.

4.5 Simulations

The offshore wind power plant simulated (see the diagram presented Figure 4.3) is constituted by 19 wind turbines, consisting in PMSM (5 MW each) equipped with full power converter (6.5 MVA). The power it generates is transmitted through a 150 kV three-core submarine cable [84] made of copper conductors (240 mm^2), with a current rating of 0.480 kA and 50 km long. The electrical parameters of this cable are: resistance: $R=0.0754 \Omega/\text{km}$, reactance: $X=0.1476 \Omega/\text{km}$ and capacitance: $C=0.13 \mu\text{F}/\text{km}$. Dynamic simulations are presented to show the system performance when a three-phase short circuit of 500 ms occurs at time=2 s in the terrestrial grid, with a remaining voltage of 0.08 p.u.

According to [81], for non lossless transmissions (like the cable of this study case, which presents a certain resistance), theoretically, the maximum power is achieved at the receiving end when the transmission angle $\delta=\beta=\arctan(X/R)$. Particularising this expression for the cable used,

4.5 Simulations

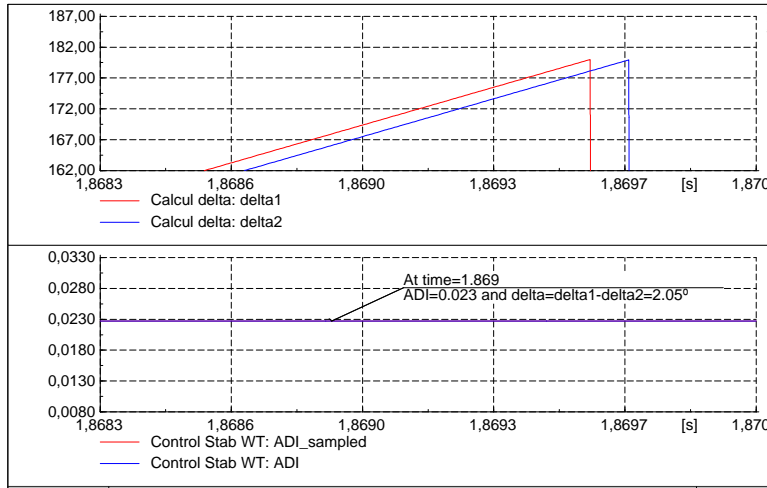


Figure 4.11: Voltage angles at the sending end (δ_{delta1}) and receiving end (δ_{delta2}) of the transmission and ADI before the fault

$\delta = \beta \approx 62.8^\circ$. In fact, during the disturbance, the values of reactance and resistance can change (for example, resistance can increase due to a rise in temperature). So, the maximum transmission angle could even be lower than 62.8° . Furthermore, the DC voltage limits are supposed to be $E_{\min} = 1.01$ p.u. and $E_{\max} = 1.10$ p.u. These considerations must be taken into account when analysing the simulation results. The plots included in this section correspond to the results obtained for two case studies: on the one hand, when Conventional operation (explained in Section 4.3) applies and, on the other hand, when Coordinated control (developed in Section 4.4.2 and assuming $\delta_{\text{critical}} = 33^\circ$). The results for both study cases are shown in the same figures and with different labels. figures/ labelled with letter (a) correspond to the system response under Conventional operation, while figures labelled with letter (b) correspond to the system response when the Coordinated control applies with a communication system being available.

The voltage angles at both ends of the transmission and the ADI before the fault are represented in Figure 4.11. It can be observed that the angular difference in normal conditions is approximately 2° . If a deep three-phase short circuit occurs, the evolution of the system changes if Conventional op-

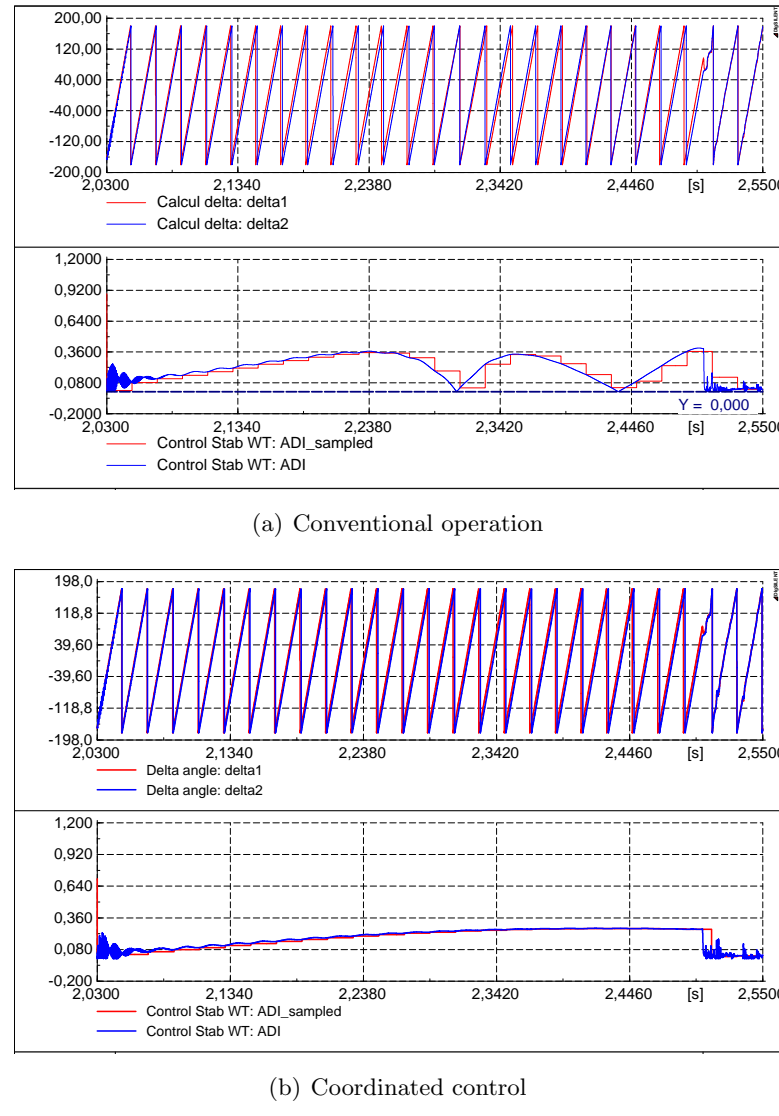


Figure 4.12: Voltage angles at the sending end (Δ 1) and receiving end (Δ 2) of the transmission and ADI during the fault

4.5 Simulations

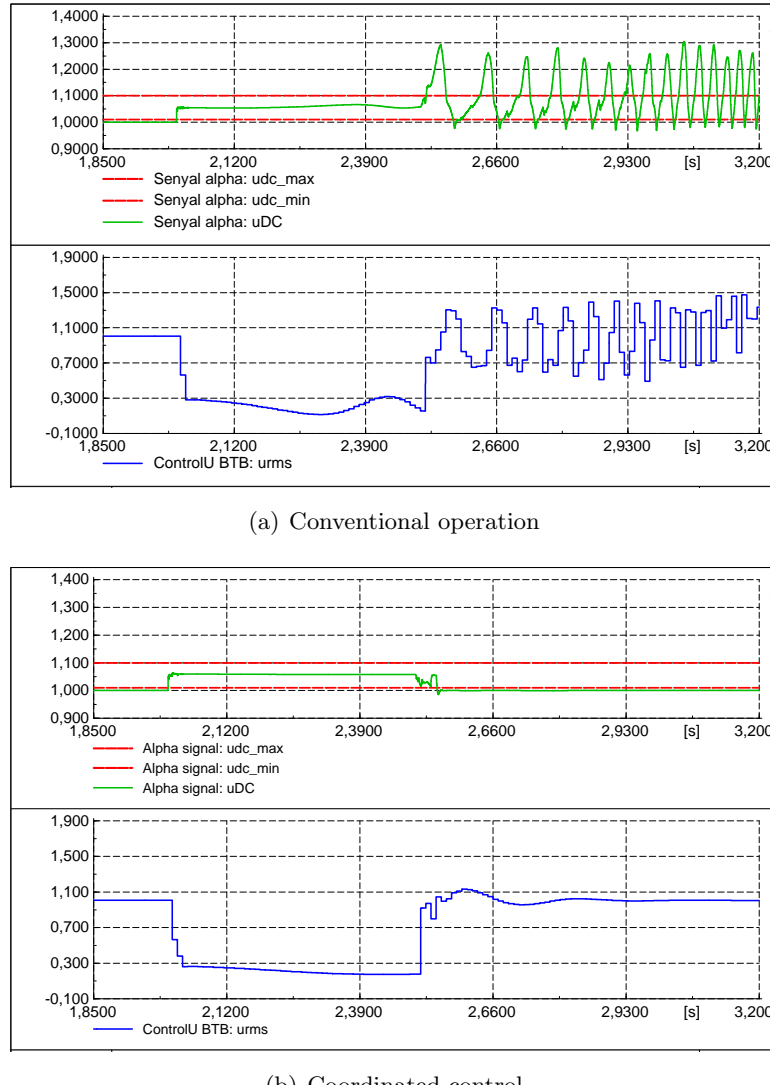


Figure 4.13: DC bus voltage of the wind turbine converter and AC voltage at the low voltage windings of the wind turbine transformer

Chapter 4 Coordinated Control for an OWPP to provide FRT Capability

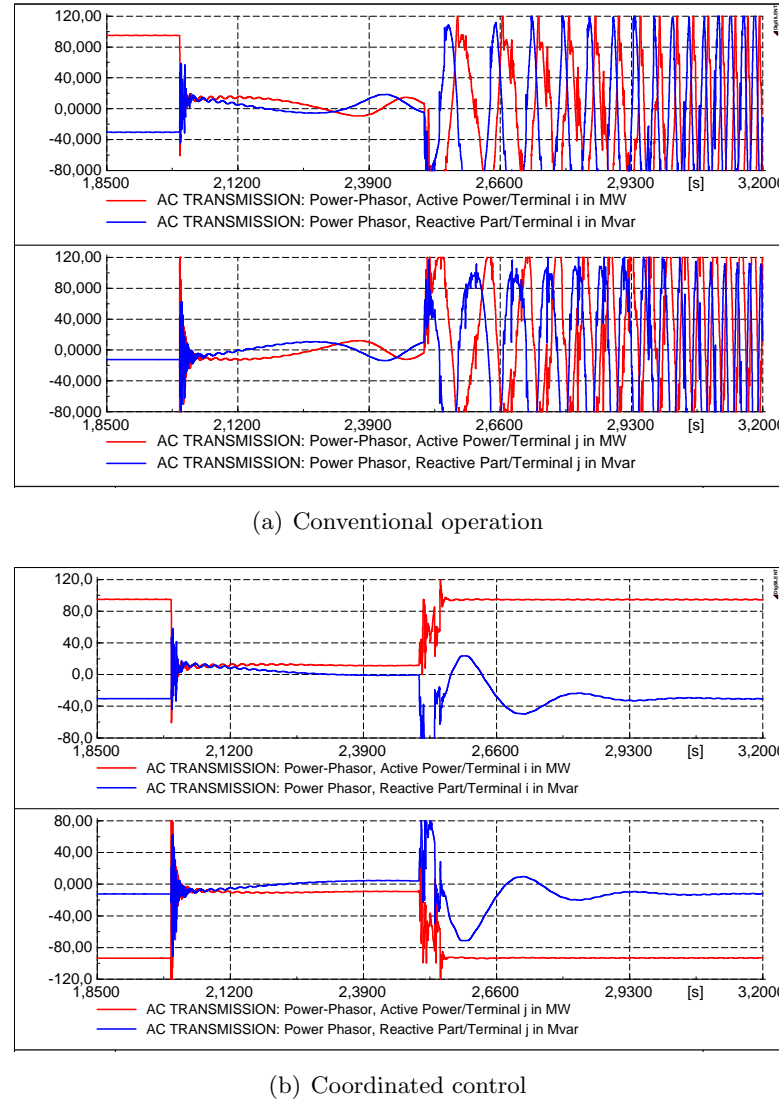


Figure 4.14: Active and reactive power at the sending end (i) and receiving end (j) of the transmission

4.5 Simulations

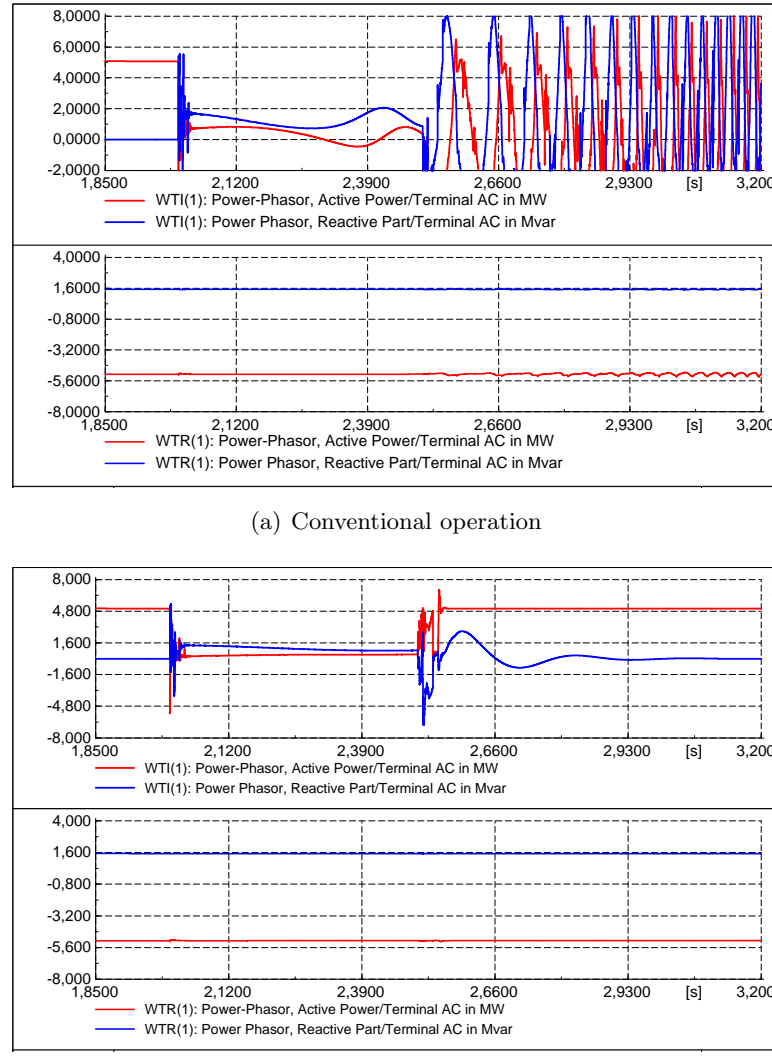


Figure 4.15: Active and reactive powers in the wind turbine inverter and rectifier

Chapter 4 Coordinated Control for an OWPP to provide FRT Capability

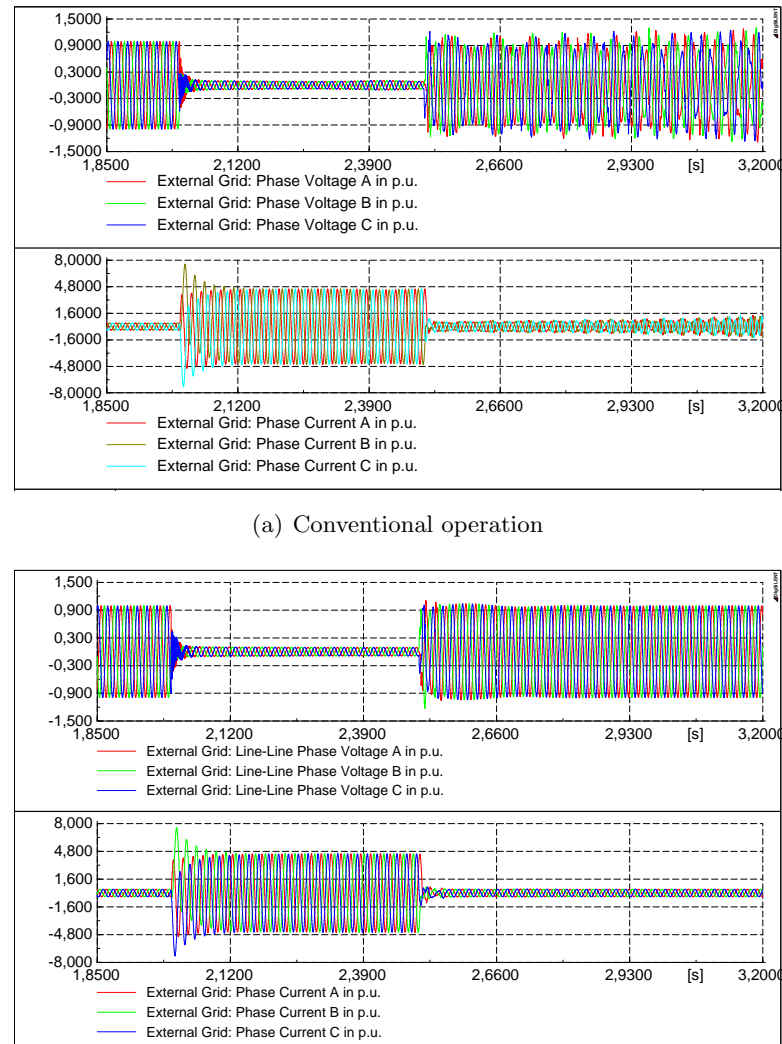


Figure 4.16: Voltage and current at the AC grid

4.5 Simulations

eration or the Coordinated control apply. The voltage angles at the transmission ends evolute as shown in Figure 4.12. The DC bus voltage of the back-to-back and AC voltage at the low voltage windings of the wind turbine transformer are shown in Figure 4.13. In Figure 4.12 and Figure 4.13 it can be observed that under Conventional operation the voltage angle difference exceeds 33.3° and suddenly decreases until 0° (which means no power is being transferred) and leads to an unstable voltage profile, whilst with Coordinated control the voltage angle difference is kept under critical values and leads to a stable voltage profile. Active and reactive power at both ends of the transmission are presented in Figure 4.14. Under Conventional operation, numerical oscillations are shown in active and reactive powers, corroborating the instability. Active and reactive powers at the wind turbine rectifier and inverter are plotted in Figure 4.15. So, the Conventional operation will lead to the wind power plant disconnection, while the Coordinated control ensures the fault ride through capability.

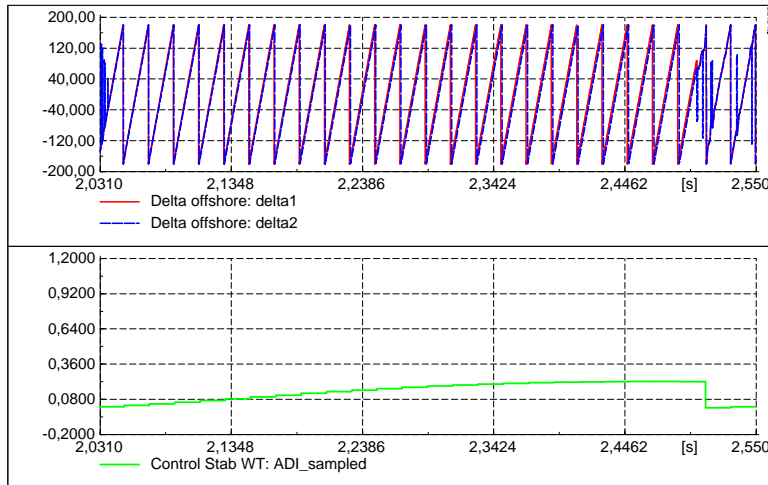


Figure 4.17: Voltage angles at the sending end (δ_{delta1}) and receiving end (δ_{delta2}) of the transmission and ADI during the fault without communications offshore-onshore

In case the communication system is not available between offshore and onshore or in case there is a loss of communications, the proposed control

Chapter 4 Coordinated Control for an OWPP to provide FRT Capability

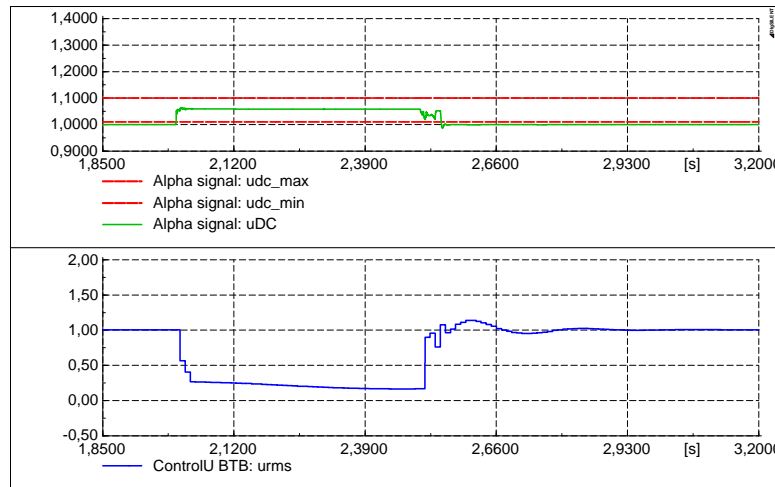


Figure 4.18: DC bus voltage of the back-to-back and AC voltage at the low voltage windings of the wind turbine transformer without communications offshore-onshore

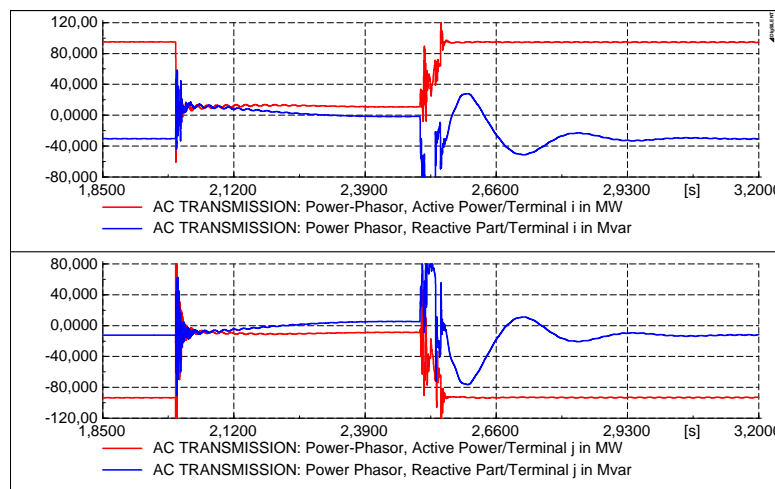


Figure 4.19: Active and reactive power at the sending end (i) and receiving end (j) of the transmission without communications offshore-onshore

4.6 Conclusions

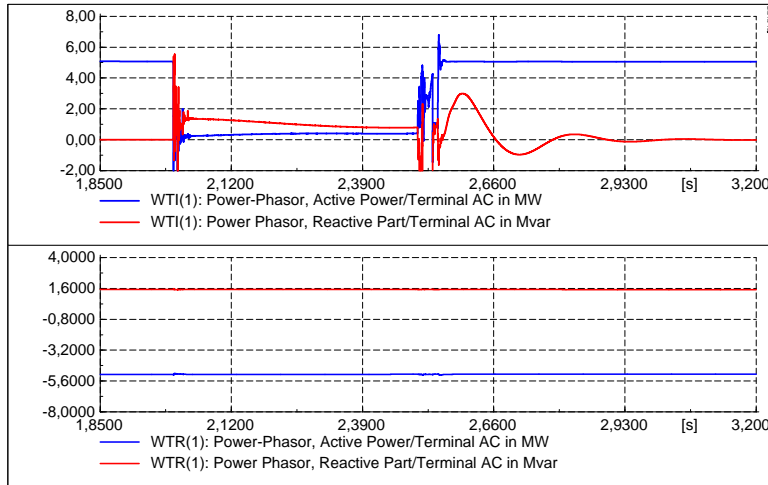


Figure 4.20: Active and reactive powers in the wind turbine inverter and rectifier without communications offshore-onshore

to avoid instability would apply through the estimation of the angles at the sending and receiving end of the transmission, as described in Section 4.4.2. The angles estimated are very close to its real value in steady state. When the communication system between offshore and onshore is not available, the error made due to the voltage angle estimation is noticeable during transients. Despite this, the proposed control shows good performance and ensures fault ride through capability. The voltage angles at the transmission ends evolve as shown in Figure 4.17. The DC bus voltage of the back-to-back and AC voltage at the low voltage windings of the wind turbine transformer are shown in Figure 4.18. Active and reactive power at both ends of the transmission are presented in Figure 4.19. Similarly, active and reactive powers at the wind turbine rectifier and inverter are plotted in Figure 4.20.

4.6 Conclusions

This study presents a coordinated control strategy to operate wind farms with HVAC transmission while providing fault ride through capability. The

Chapter 4 Coordinated Control for an OWPP to provide FRT Capability

proposed control can ensure safe operation when deep voltage sags occur on the main AC grid, but requires that the wind power plant has information on the main grid voltage. This information can be obtained by means of fast communication technology or using a model based observer. In some applications, communications will be already installed for protection or monitoring purposes. In case communications are not available or for an eventual communications fault, an observer is used and allows the correct operation of the proposed system. Several simulations have been conducted for the different control approaches under a severe onshore fault. Dynamic simulations show that, while conventional control schemes can lead to the wind power plant disconnection when a deep voltage sag occurs in the terrestrial grid, the proposed coordinated control scheme deals with those disturbances, ensuring the fault ride through capability of the system.

Chapter 5

Optimal power flow for hybrid HVDC/HVAC transmission systems for grid integration of offshore wind

5.1 Introduction

The progress in power electronics, as well as the improvement of cables performance have favoured and still stimulate the development of HVDC (High Voltage Direct Current) technology, in parallel with HVAC (High Voltage Alternating Current). The choice of a technology or the other one will depend, to begin with, on the technical feasibility of each one for the specific link to be constructed [30]. Two examples of this large dependence on the technical requirements can be advanced. If the electrical connection to be constructed links two systems working at different frequency (asynchronous systems), HVDC must be used. With HVDC the power transmitted is practically independent of the distance, whereas, in HVAC the power capability transmission decreases with distance. However, the larger expenses of HVDC installations for certain distances compared to the HVAC option (around 50-80 km for submarine or underground transmissions and around 600-800 km for overhead transmission) can favour the HVAC construction. Taking into consideration the before mentioned, a scenario for transmission networks based on interconnections between High Voltage Direct Current and High Voltage Alternating Current grids is feasible and seems probable [85]. Specifically, if HVDC technology is used for delivering the power produced in the wind power plants to the terrestrial grid. Thinking in remote wind power

plants to be connected to different AC grids, then the HVDC system could be multiterminal [4, 19, 63, 71, 86, 87].

An OPF for operating HVDC multiterminal grids was proposed and compared to droop control in [86]. The present study enlarges the OPF for mixed HVDC-HVAC systems. Although many studies exist focusing on the operation of AC grids and DC grids separately, only a few have been published analysing the operation of AC and DC grids combined. In [88], an algorithm for solving power flows in AC/DC networks is presented and implemented in MATPOWER, taking into account converter losses through a generalized converter loss model proposed in [89]. The optimal operation of hybrid AC/DC systems is addressed in the studies [90–94]. In the first study listed, [90], some power system elements are represented with limited accuracy: terminal VSC losses are neglected and only point-to-point connections are defined. Converter losses are included in [91–94]. [91] focuses on the mathematical formulation of the problem, which is non convex. The problem is reformulated for AC grids with embedded DC networks based on Second Order Cone Programming, which converts it into a convex problem. However, the optimal operation is only addressed in terms of loss minimization. Similarly, the authors of [92] only deal with transmission losses. But it is worth mentioning that [92] takes into consideration additional constraints to include grid code requirements, neglected in other studies.

In [93, 94] different optimization goals are addressed. They define and optimize, for different objective functions, DC and AC load flows simultaneously in a random AC-DC network, allowing the possibility of meshing the DC system. [93] was implemented through MATLAB Optimization Toolbox and [94] was implemented in MATPOWER, modifying the code and solver so as to add easily non linear constraints and define cost functions. Although combining DC and AC links, the effect of a scenario with large wind power penetration transmitted through the DC grids is not evaluated in none of them.

The here proposed tool has been applied to a scenario where the HVDC system would enable the transmission of a large amount of wind power, providing a sensitivity analysis of the effect of wind power variation in the objective function analyzed. It was implemented first in MATLAB Op-

5.1 Introduction

timization toolbox (function *fmincon*) and it was benchmarked with [94], leading to the same results for a particular study case and for two different objective functions, in [95], so it was validated. Secondly, it was implemented in GAMS, reducing the computation time significantly compared to the MATLAB implementation. The fact that it was implemented in an optimization dedicated software, allows the choice among multiple solvers and guarantees fast computations, which is essential for dealing with large networks. The OPF results enable a comparison of the losses in the different system components: DC and AC cables/lines, converters and transformers, for different wind power plant injections. The analysis of a particular study show show the results of the OPF can help in an operational perspective.

This study is organised as follows. The mathematical formulation of the tool is first presented in Section 5.2. Then, the tool is applied to different case studies. First, to a 3 DC 5 AC system, where it is benchmarked with another tool, leading to the same results for the two objective functions analysed: loss minimization and minimum deviation from a preset voltage profile (Section 5.3). Then, the tool is applied to a 6 DC 8 AC bus network for loss minimization, in Section 5.4, so as to apply it in a scenario with large penetration of offshore wind and so as to compare its implementation in two different softwares (MATLAB and GAMS). Finally, in Section 5.5, the tool is tested in a scaled platform. Therefore, the tool has been validated, offering a flexible methodology for analysing hybrid AC/DC grids optimal operation.

Comments The framework of operation of the HVDC and HVAC grid taking into consideration the specific interactions with the electrical market is out of scope of the present study, but next lines point at their effect and how they are could be taken into account. In some nodes, a day ahead profile must be fulfilled or followed with the minimum deviation. This is reflected in the optimization formulation specifying power constraints in some AC nodes. Alternatively, the objective function can be defined to ensure the minimum deviation from a pre-set power profile in specific nodes.

A recent publication examines the market integration scheme of a multi-

terminal HVDC Grid in the North Seas [96] proposing a droop-controlled scheme combining OPF dispatch and imbalance volume management. This study considers a scenario governed by the trade arrangement denoted as Virtual Case Study 1 by the North Seas Countries' Offshore Grid Initiative (NSGOCI) consortium [97]. It is assumed that each offshore wind farm participates in only one market. The proposed market integration approach is based on the existence of a multi-terminal HVDC operator as an independent entity that participates into the onshore imbalance settlements.

5.2 Optimization problem

The optimization problem involves DC and AC power systems and can be thus, considered as a non-linear constrained optimization type. Mainly two strategies can be used to solve DC and AC power flows: sequential and unified. The sequential approach ([89, 98]) separates the problem in two parts corresponding each one to DC and AC power flow equations, respectively. Unified approach, [91] solves all the equations together. The optimal power flow tool here presented is based on a unified strategy. Several objective functions can be defined for the optimization tool. An interesting one that will be shown through a case study is the overall Joule losses in the HVDC-HVAC network.

The layout of a general HVDC-HVAC system to which the tool is applied is shown in Figure 6.1. The converter topology is Voltage Source Converter (VSC), allowing an independent control of active and reactive power. The VSC (Voltage Source Converter) connected to the wind farms (wind farm rectifiers) inject the wind power to the HVDC grid. In normal operational mode, the wind farm rectifiers absorb all the power produced and inject it into the DC grid while supplying the reactive power needed to maintain the AC wind farm voltage. The power in the DC network is injected to the AC grid through grid connected VSC, responsible for the HVDC grid voltage control and which provide reactive power support to the AC grid when needed. The AC grid is constituted by AC links (overhead lines or underground cables), forming a mesh, that allow the electrical power to be transmitted to the consumption nodes.

5.2 Optimization problem

The active power on the AC side and DC side of the converter differ on losses. So, the AC power can be defined as a function of the DC power and converter losses, modelled according to a second order polynomial of the AC converter current. DC cables are modelled through their resistances, AC cables are represented according to their π equivalent and transformers are modelled as an equivalent impedance with inductive and resistive part.

The active and reactive power demands in the AC nodes and the injections from the wind power plants are an input for the tool. The electrical characteristics of the DC and AC grids, as well as of lines and cables and the converter loss parameters are also known data. The tool determines the active and reactive power injections (or absorptions) from generators and converters and the power flowing through each branch that minimize a specified objective function while accomplishing the electrical system constraints.

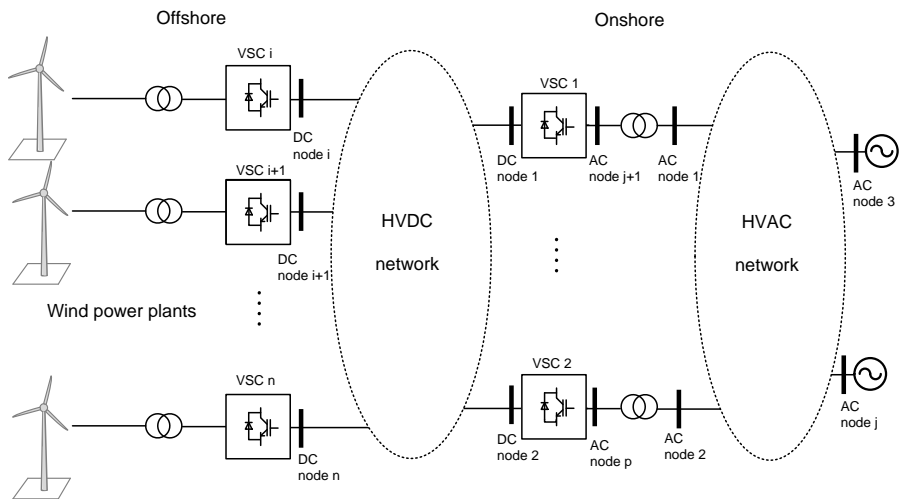


Figure 5.1: Hybrid HVDC-HVAC system for integrating offshore wind power

5.2.1 Notation

All the variables and parameters required for the mathematical formulation of the problem are listed below.

- G_{DC} conductance matrix of the DC grid

- G_{AC} conductance matrix of the AC grid
- B_{AC} susceptance matrix of the AC grid
- $i \in (1, n)$, n is the number of VSC converters
- $j \in (1, p)$, p is the number of AC nodes
- $\mathbf{I} = [I_1 \cdots I_n]^T$ vector of DC currents
- $\mathbf{E} = [E_1 \cdots E_n]^T$ vector of DC voltages
- $\mathbf{V} = [V_1 \cdots V_p]^T$ vector of AC voltage magnitude
- $\delta = [\delta_1 \cdots \delta_p]^T$ vector of AC voltage angles
- E_i and I_i are, respectively, the DC voltage and the current in node i .
- V_j and δ_j are, respectively, the AC voltage magnitude and angle of voltage phasor in node j .
- $\mathbf{P}_{DC} = [P_{DC_1} \cdots P_{DC_n}]^T$ is the power entering the DC system through the converters
- $\mathbf{P}_g = [P_{g_1} \cdots P_{g_p}]^T$ is the active power generated in each AC node
- $\mathbf{P}_d = [P_{d_1} \cdots P_{d_p}]^T$ is the active power demanded in each AC node
- $\mathbf{Q}_{vsc} = [Q_1 \cdots Q_n]^T$ is the reactive power injection/absorption by each converter
- $\mathbf{Q}_g = [Q_{g_1} \cdots Q_{g_p}]^T$ is the reactive power generated in each AC node
- $\mathbf{Q}_d = [Q_{d_1} \cdots Q_{d_p}]^T$ is the reactive power demanded in each AC node
- $\mathbf{S}_{vsc} = [S_1 \cdots S_n]^T$ is the power rating of each converter

5.2 Optimization problem

5.2.2 Inputs

The input data for the optimization problem is listed below:

- Conductance matrix of the DC grid: G_{DC}
- Conductance and susceptance matrix of the AC grid: G_{AC} and B_{AC}
- Active and reactive power demand in the AC grid nodes: P_d and Q_d
- Converter loss parameters

5.2.3 Outputs

The optimization algorithm determines the voltages in all the nodes and the power flowing in the different branches of the system that minimize a user defined objective function and guarantee all the equality and inequality constraints. Therefore, the output vector of the algorithm, x , contains the following information:

$$x = \begin{bmatrix} E \\ I \\ V \\ \delta \\ P \\ Q \end{bmatrix} \quad (5.1)$$

5.2.4 Mathematical formulation

The problem is here formulated taking a general objective function, $f(x)$, which is dependent on the variables defined in (5.1).

$$[MIN]z = f(x) \quad (5.2)$$

subject to the following constraints:

$$\mathbf{I} = \mathbf{G}_{DC}\mathbf{E} \quad (5.3)$$

$$P_{DCi} = E_i I_i \quad (5.4)$$

$$P_{DC_i} - P_{lossvsc_i} = P_j + P_{g_j} - P_{d_j} \quad (5.5)$$

$$Q_j = Q_{vsc_j} + Q_{g_j} - Q_{d_j} \quad (5.6)$$

$$E_i^{min} \leq E_i \leq E_i^{max} \quad (5.7)$$

$$I_i^{min} \leq I_i \leq I_i^{max} \quad (5.8)$$

$$P_{kl}^{min} \leq G_{kl} (E_k - E_l) E_k \leq P_{kl}^{max} \quad (5.9)$$

$$V_j^{min} \leq V_j \leq V_j^{max} \quad (5.10)$$

$$P_j^{min} \leq P_j \leq P_j^{max} \quad (5.11)$$

$$Q_j^{min} \leq Q_j \leq Q_j^{max} \quad (5.12)$$

$$S_{kl}^{min} \leq S_{kl} \leq S_{kl}^{max} \quad (5.13)$$

$$\delta_j^{min} \leq \delta_j \leq \delta_j^{max} \quad (5.14)$$

$$S_{vsc_i}^{min} \leq S_{vsc} \leq S_{vsc_i}^{max} \quad (5.15)$$

being

$$P_j = V_j \sum_{k=1}^p V_k (G_{ACjk} \cos \delta_{jk} + B_{ACjk} \sin \delta_{jk}) \quad (5.16)$$

$$Q_j = V_j \sum_{k=1}^p V_k (G_{ACjk} \sin \delta_{jk} - B_{ACjk} \cos \delta_{jk}) \quad (5.17)$$

The AC links are modelled according to the π equivalent diagram, as sketched in Figure 5.2.

5.2 Optimization problem

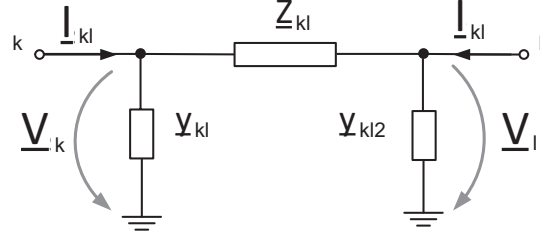


Figure 5.2: π equivalent of the AC branch between nodes k and l

5.2.5 Converter model

The converter topology chosen for this study is VSC, allowing and independent control of active and reactive power. The active power exchange on the AC and DC side of the converter differ on losses. So, the AC power can be defined as a function of the DC power and converter losses, modelled according to a second order polynomial, as in [89]:

$$P_{lossvsc_i} = a + bI_{vsc_i} + cI_{vsc_i}^2 \quad (5.18)$$

where a , b and c are p.u. parameters given by Table 5.1 and I_{vsc_i} represents the p.u. current flowing through the converter i :

$$I_{vsc_i}^* = \frac{\sqrt{P_{vsc_i}^2 + Q_{vsc_i}^2}}{\sqrt{3}V_i} \quad (5.19)$$

As reflected in Table 5.1, two operating modes are distinguished for VSCs: rectifier and inverter.

VSC	a	b	c
Rectifier	11.033×10^{-3}	3.464×10^{-3}	5.40×10^{-3}
Inverter	11.033×10^{-3}	3.464×10^{-3}	7.67×10^{-3}

Table 5.1: Converter loss parameters in p.u. [89]

5.2.6 Objective functions

The objective function presented in (5.2) can be chosen among several functions which are of interest in terms of operation or planning of the system. Some of them, are listed below:

Minimum power losses (to be applied in systems or subsystems where the total transmission losses want to be minimized):

$$[MIN]z = \sum_{j=1}^p (P_{g_j} - P_{d_j}) \quad (5.20)$$

Minimum generation costs (to be applied when the cost function of generation of the different generating units is known and depends on the power delivered; the production of units with minimum generating cost will be prioritized):

$$[MIN]z = \sum_{j=1}^{ng} C_j(P_{g_j}) \quad (5.21)$$

where ng represents the number of generators

Maximum reactive power margin (to be applied when some generators have to deliver maximum reactive power support):

$$[MAX]z = \sum_{j=1}^{ng} Q_{g_j} \quad (5.22)$$

where ng represents the number of generators

Bus voltages closest to a profile (to be applied when certain buses need to keep their voltage at a specific value or the closest possible to it):

$$[MIN]z = \sum_{j=1}^p (V_j - V_{set})^2 \quad (5.23)$$

Minimum deviation from another state (to be applied when a specific magnitude wants to be kept at a specific value or the closest possible to it):

$$[MIN]z = \sum_{j=1}^p (x_j - x_{set})^2 \quad (5.24)$$

5.3 Case study 1

The aim of this study is to benchmark the proposed tool with the tool developed by [94]. The system used for this study is a 3 DC bus and 5 AC bus network, from [88, 94] sketched in Fig. 5.3 and Fig. 5.4. The DC and AC systems are linked through three VSC converters. The power in the DC network is injected into the AC grid through the connected inverters, responsible for the DC grid voltage control and which provide reactive power support to the AC grid when needed. The AC grid has two generators, one in bus 1 and another in bus 2. Loads are connected to buses 2, 3, 4 and 5. The DC grid is connected in AC buses 2, 3, and 5. The user needs to specify the control variables of the system (for example the generators injections, voltages setpoints)

The active and reactive power demand (loads) is defined by vectors P_d and Q_d in MW, and MVar, respectively. As restrictions, the DC power flows are limited to 10 MW and the power converters rating is 20 MVA.

$$P_d = [0, 20, 45, 40, 60] \quad (5.25)$$

$$Q_d = [0, 10, 15, 5, 10] \quad (5.26)$$

5.3.1 Minimum losses

This section shows the results of the optimization problem obtained when minimizing losses in the hybrid DC/AC system sketched in Fig. 5.3 and 5.4. The minimum losses of the whole system, computed as the difference between total active generation and total demand Equation (5.20)), are 5.52 MW. The active and reactive power flows are shown in Fig. 5.5 and 5.6. The DC and AC voltages on the different buses are reflected in Table 5.6.

5.3.2 Minimum deviation from a voltage profile

This section shows the results of the optimization problem obtained when minimizing the deviation of AC voltages from a preset voltage profile in the hybrid DC/AC system sketched in Fig. 5.3 and 5.4. The objective function

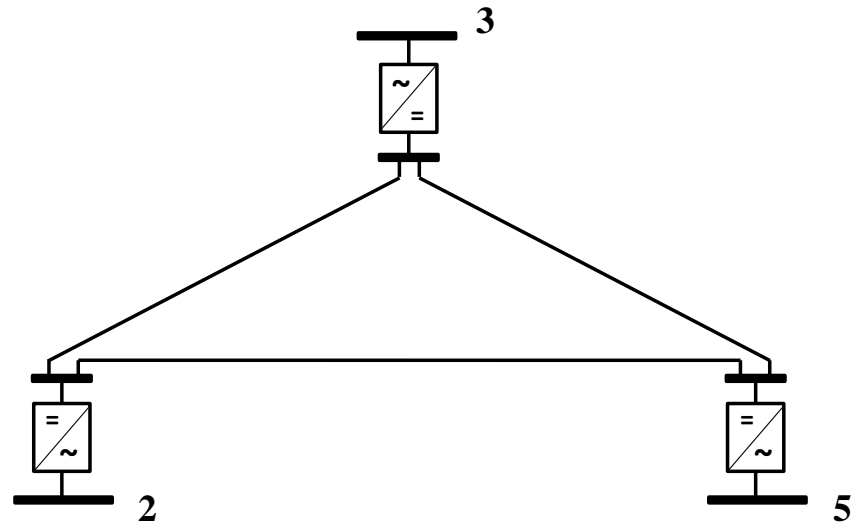


Figure 5.3: 3 DC bus system

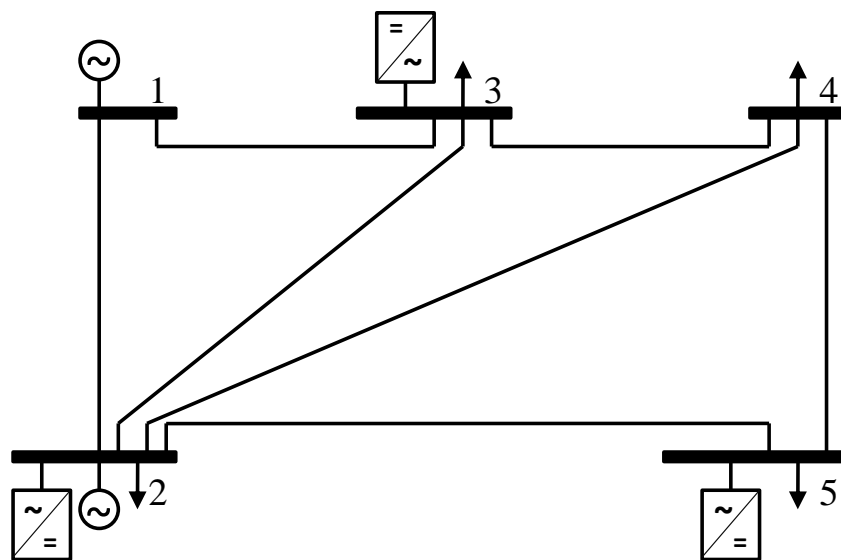


Figure 5.4: 5 AC bus system

5.3 Case study 1

Bus	AC voltage magnitude (p.u)	AC voltage angle(rad)	DC voltage of VSC
1	1.1000	0	-
2	1.1000	0	1.003
3	1.0809	-0.0430	1.000
4	1.0807	-0.0458	-
5	1.0811	-0.0468	0.999

Table 5.2: Bus voltages for loss minimisation

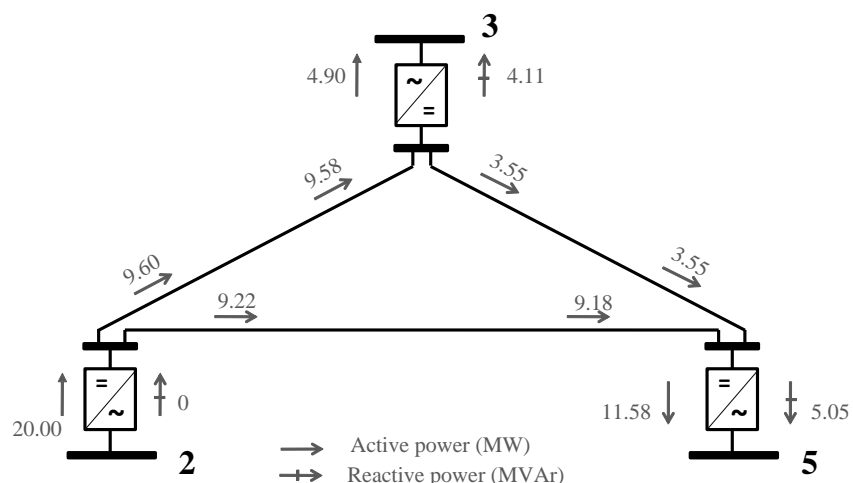


Figure 5.5: Power flows in the 3 DC bus system for loss minimisation

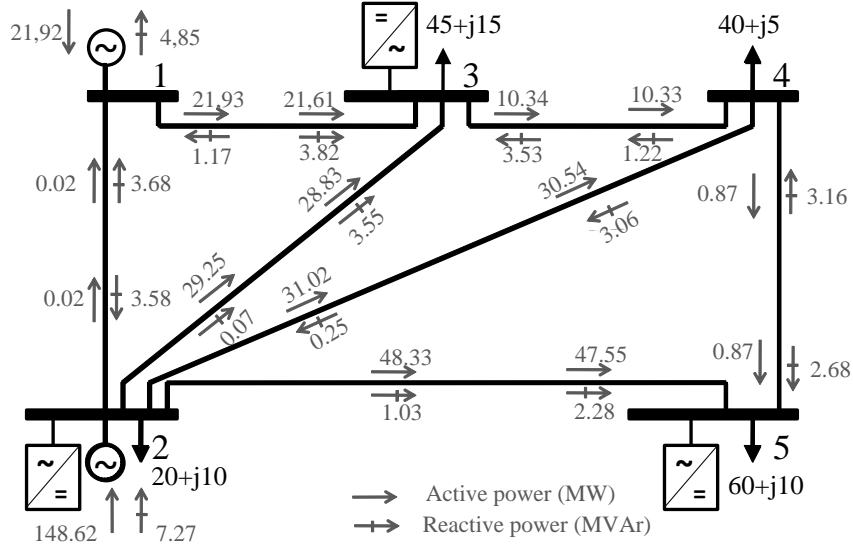


Figure 5.6: Power flows in the 5 AC bus system for loss minimisation

(see (5.24)) is set so as to ensure that the system reaches the AC voltages specified by vector V_{set} , where

$$V_{set} = [1.08, 1.08, 1.05, 1.05, 1.05] \quad (5.27)$$

The objective function value resulting is 5.82×10^{-7} . The active and reactive power flows are shown in Fig. 5.7 and 5.8. The DC and AC voltages on the different buses are reflected in Table 5.7.

5.3.3 Sensitivity analysis

In this section, the effect of cable parameters and converter efficiency on loss minimization is analysed. For this purpose, the cable resistances (both DC and AC), as well as converter loss parameters values are varied $\pm 10\%$. As shown in Figure 5.9, each parameter being analysed is multiplied by a correction factor to change its value between 90 and 110 %. The parameter values are represented on the x-axis and the corresponding objective function result is represented on the y-axis. It is worth mentioning that the effect of

5.3 Case study 1

Bus	AC voltage magnitude (p.u)	AC voltage angle(rad)	DC voltage of VSC
1	1.0800	0	-
2	1.0799	-0.0223	0.9989
3	1.0496	-0.0663	1.0000
4	1.0506	-0.0709	-
5	1.0499	-0.0866	1.0006

Table 5.3: Bus voltages for minimum deviation from a voltage profile

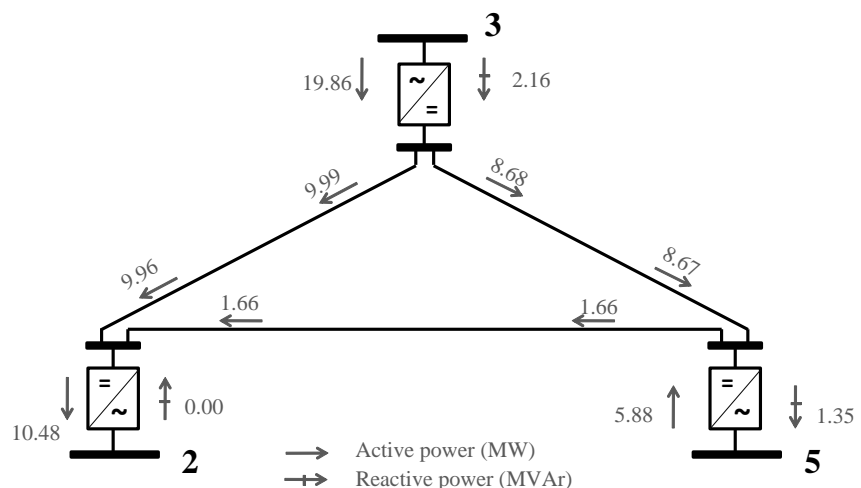
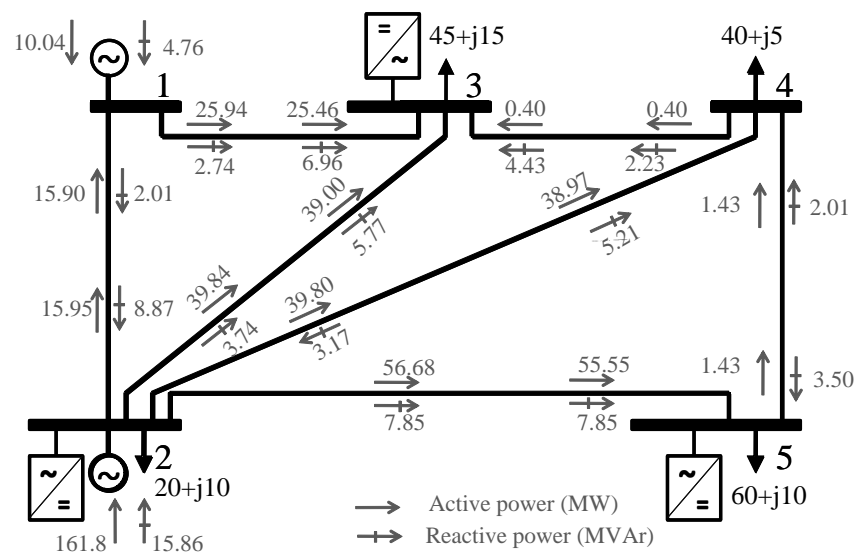


Figure 5.7: Power flows in the 3 DC bus system for minimum deviation from a preset voltage



5.4 Case study 2

the parameters is very dependent on the system configuration.

In this case, the parameter showing the largest effect on total system losses is the AC cables resistance. The lower is the AC cable resistance, less power is flowing into the DC grid and more power is pushed to the AC grid. The DC resistance variation on $\pm 10\%$, which has practically no effect on the objective function, does not change neither the power flows on the system. When VSC losses increase, the power is injected from the DC grid to the AC grid decreases. As expected, for any change on the grid parameters, the power flows are adapted so that current follows the path that leads to the lowest losses.

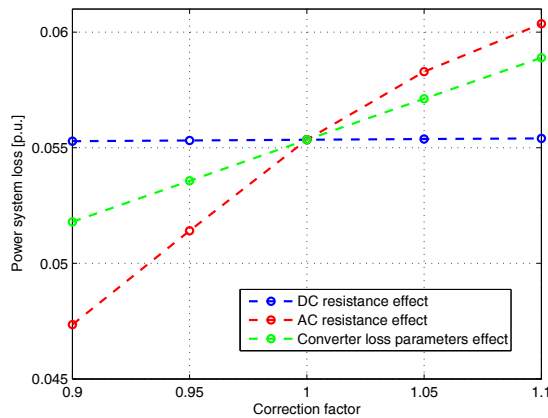


Figure 5.9: Effect of DC resistance, AC resistance and converter loss parameters in power system loss

5.4 Case study 2

The aim of this case study is to apply the tool to a scenario with large penetration of offshore wind and compare its implementation in two softwares: (MATLAB and GAMS. The system used for this study is a 6 DC bus and 8 AC bus network, based on the test system defined by CIGRÉ in [73] and sketched in Fig. 5.10. Basically two DC systems, consisting of 3 buses each, allow to export and distribute the power generated by two wind

power plants. Their internal AC grid and step up transformer are modelled through an equivalent impedance. The power produced is then transmitted to a 6 bus AC system to reach the loads. The DC and AC systems are linked through six VSC converters. The AC system, where all the branches are overhead lines (OHL), is rated to 380 kV and the DC system voltage, where all the branches are cables, has a voltage level of +/-400 kV. Their electrical parameters are specified in Table 6.2.4. The wind farm VSCs are rated to 1000 MVA. The user needs to specify the control variables of the system (for example the generators injections, voltages setpoints).

Branch type	Resistance Ω/km	Inductance mH/km	Capacitance $\mu\text{F}/\text{km}$
DC cable +/-400 kV	0.0095	2.1120	0.1906
AC OHL 380 kV	0.0200	0.8532	0.0135

Table 5.4: Electrical parameters of the AC and DC branches

The active and reactive power demand (loads) is defined by vectors P_d and Q_d in MW, and MVar, respectively. Their values for the 8 AC nodes of this study case are represented in Table 5.5.

Demand	1	2	3	4	5	6	7	8
P_d (MW)	400	600	800	400	0	0	0	0
Q_d (MVar)	50	50	50	20	0	0	0	0

Table 5.5: Active and reactive power demand in the AC nodes

5.4.1 Minimum losses

This section shows the results of the optimization problem obtained when minimizing losses in the the hybrid DC/AC system sketched in Fig. 5.10. The minimum losses of the whole system, computed as the difference between total active generation and total demand Equation (5.20)), are 12.705 MW in MATLAB and 12.712 MW in GAMS. The DC and AC voltages on the different buses are reflected in Table 5.6 and Table 5.7. Although there

5.4 Case study 2

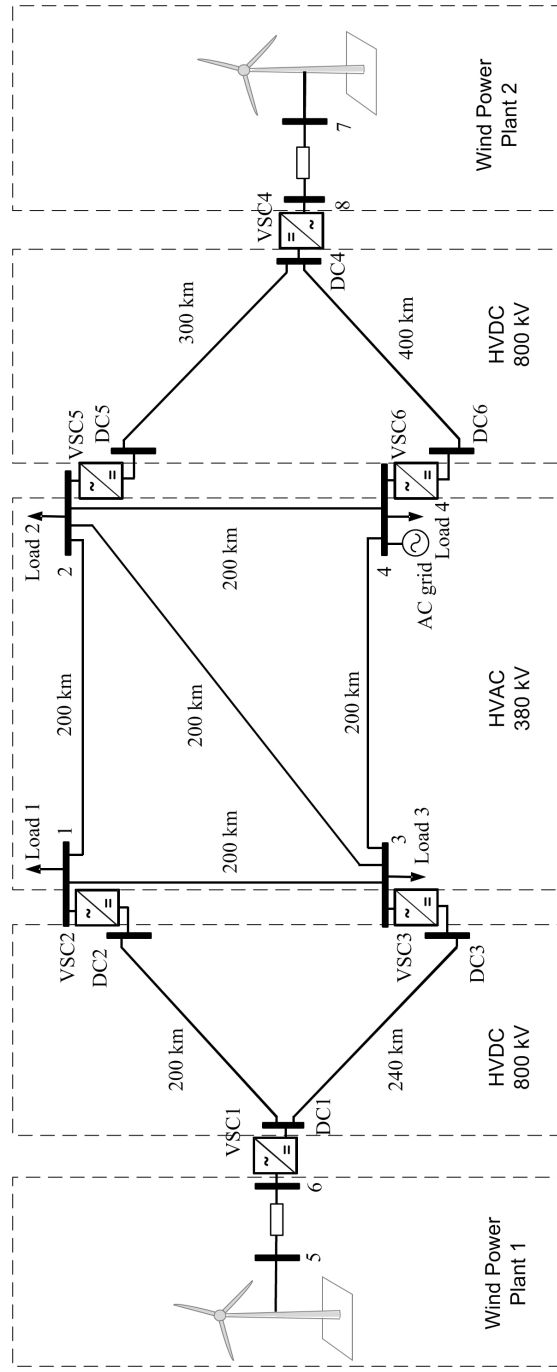


Figure 5.10: Power system analysed

is some difference after the third decimal, it can be concluded that both softwares lead to the same operating point. The active and reactive power flows are shown in Fig. 5.11.

Bus	AC voltage magnitude (p.u)	AC voltage angle(rad)	DC voltage of VSC
1	0.998	-0.059	1.099
2	1.000	-0.019	1.098
3	0.997	-0.064	1.097
4	1.000	0	1.099
5	1.099	0.006	-
6	1.098	-0.006	1.098
7	1.099	0.006	-
8	1.098	-0.006	1.099

Table 5.6: Bus voltages for loss minimisation in MATLAB

Bus	AC voltage magnitude (p.u)	AC voltage angle(rad)	DC voltage of VSC
1	0.998	-0.059	1.099
2	1.000	-0.018	1.098
3	0.997	-0.064	1.099
4	1.000	0	1.099
5	1.100	0	-
6	1.099	-0.012	1.100
7	1.100	0	-
8	1.099	-0.012	1.100

Table 5.7: Bus voltages for loss minimisation in GAMS

It is worth mentioning that the computation time of GAMS for the presented study case is 0.087 s using solver CONOPT and 0.069 s using solver IPOPT, while it takes 8 s in MATLAB *fmincon* with Interior Point Algorithm using a barrier function [64] as solver. Table 5.8 shows that GAMS keeps low computation time values for larger grids. In MATLAB *fmincon*

5.4 Case study 2

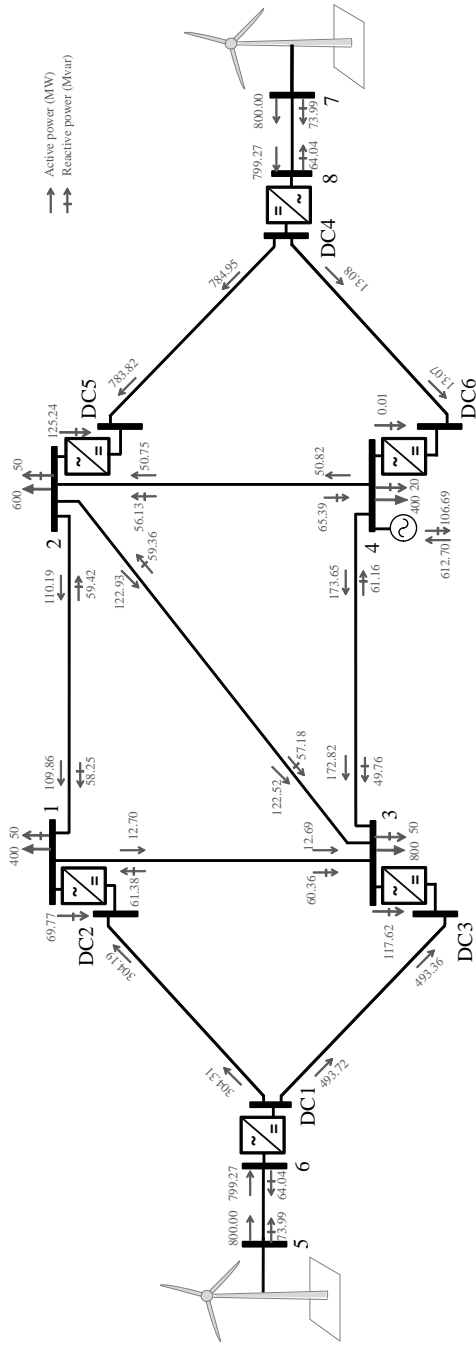


Figure 5.11: Power flows for loss minimisation

the execution time rises faster with the number of buses (and thus,variables). So, GAMS not only allows fast computation times, but is also prepared to deal with larger problems.

The first solver used in GAMS is CONOPT. CONOPT is designed for large

Solver	8 AC 6 DC	12 AC 6 DC	20 AC 6 DC	70 AC 6 DC
CONOPT (s)	0.087	0.121	0.150	0.228
IPOPT (s)	0.069	0.070	0.126	0.288

Table 5.8: Execution time of GAMS for different power system sizes

and sparse models and it removes from the model recursive equations and variables. It has a fast method for finding a first feasible solution, especially interesting for models with few degrees of freedom. It is very appropriate for models with approximately the same number of constraints as variables. It is thought for models with smooth functions, but it can also be applied to models that do not have differentiable functions [99]. To see the effectiveness of other solvers available in GAMS for non linear programming (and to check that the low computation time is not only a matter of the solver but also thanks to the mathematical pre-treatment of this software) another solver has been tried: IPOPT. If the number of variables is much larger than the number of constraints CONOPT and IPOPT will use second derivatives, but their methodology is different and it is not easy to predict which solver will be more appropriate.

5.4.2 Sensitivity to wind speed changes

The variation of wind speed in any of the two wind power plants changes the power flows distribution and affects the objective function value. A variation of the wind power injected from each wind power plant has been evaluated keeping the other wind power plant generation, as depicted in Figure 5.12. The active and reactive power demands are assumed to be the same that in Section 5.4.1. So, while in the before mentioned study case both wind power plants were producing 800 MW, if the one connected to bus 5 (wind power plant 1) increases its production in 10 %, the total transmission losses turn to be 11.92 MW (lower). In case this wind power plant decreases its

5.4 Case study 2

production in 10 %, the transmission losses are 14.54 MW (higher). So, if the wind power generation increases in wind power plant 1, the total transmission losses decrease.

However, the effect of wind power variation of the wind power plant connected to bus 7 (wind power plant 2) on the objective function is in the opposite sense: if the generation increases, the transmission losses also increase. The main explanation is that the DC grid to which wind power plant 2 is connected presents longer distance and therefore losses, compared to the DC grid to which wind power plant 1 is connected.

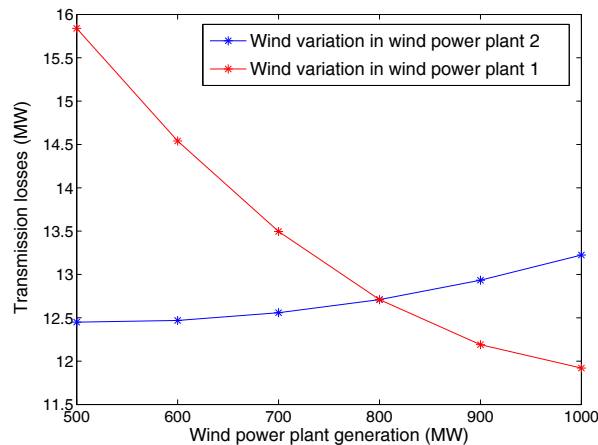


Figure 5.12: Effect of wind power variation on the objective function

5.5 Case study 3

The aim of this study case is to test experimentally the hybrid DC/AC optimal power tool proposed. Furthermore, the concept is integrated with the optimum droop control (proposed in Chapter 3.3) applied to each grid side converter. Therefore, this section provides a double validation. On the one hand, the feasibility of the optimal power flow tool for hybrid DC AC grids, and, on the other hand, the applicability of the optimum droop control for loss minimization.

The topology of the system has been chosen so as to verify it in a 4 terminal DC system platform available at the laboratory, emulating a 4 terminal system where two converters inject the power produced by two wind farms into the DC grid and two converters transmit this power to the AC grid. The AC grid used is the same that in the previous study case, but scaling its parameters at low voltage. The AC grid is not physically built in the laboratory. The system topology used for this study is a 4 DC bus and 6 AC bus network, based on the test system defined by CIGRÉ in [73] and sketched in Fig. 5.13.

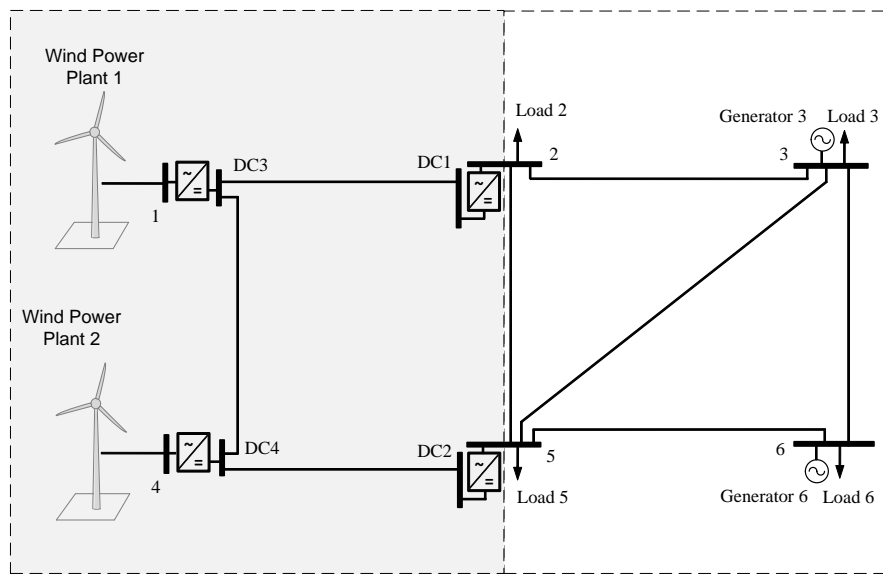


Figure 5.13: 4 DC bus 6 AC bus power system analysed

5.5.1 HVDC scaled platform description

The scaled platform available at the laboratory is depicted in Figure 5.14. Its design, operation and control are discussed in [100]. Each wind power plant injection is emulated through a squirrel cage induction motor mechanically coupled to a squirrel cage induction generator connected to a VSC. The aerodynamics behaviour of the wind turbines is emulated via a PC, connected to the platform through a LABVIEW SCADA system in charge of supervising the status of the different variables and allowing the sending of wind power references by means of a DAQ (Data Acquisition).

The VSC converters used are two-level converters based on IGBTs. They

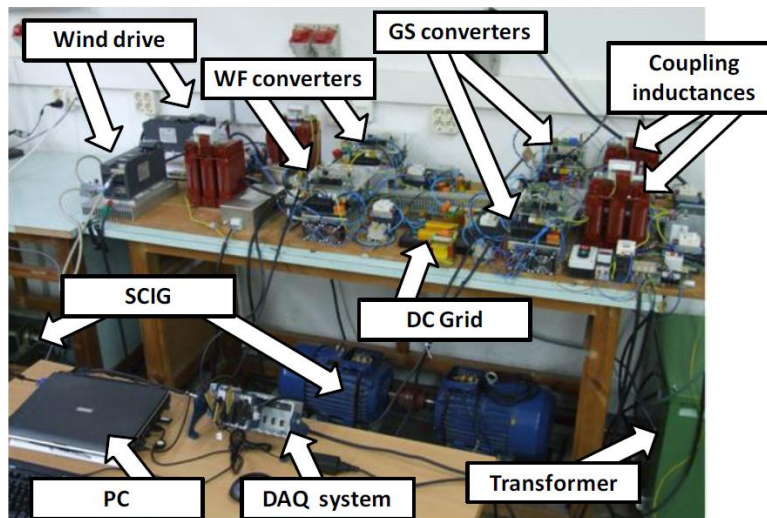


Figure 5.14: 4 DC scaled platform [100]

consist of three boards: the power board, the drivers board and the control board (based on a Texas instrument Digital Signal Processor (DSP) TMS320F2808). This DSP interacts with the IGBTs by means of a driver board that provides the necessary gate-excitation signals. The electrical characteristics of the converters, generators and cables of the DC system of the platform are depicted in Table 5.9, Table 5.10 and Table 5.11, respectively.

Parameter	Value
DC rated voltage	800 V
AC rated current	15 A
Maximum switching frequency	20 kHz
Coupling inductance	4.6 mH

Table 5.9: VSC characteristics [100]

Parameter	Wind Farm 1	Wind Farm 2
Rated power	2200 W	7500 W
Rated speed	1470 min ⁻¹	1465 min ⁻¹

Table 5.10: Electrical generators characteristics [100]

Cable	Resistance
Cable 1 (from VSC1 to VSC3)	0.22 Ω
Cable 2 (from VSC3 to VSC4)	0.10 Ω
Cable 3 (from VSC2 to VSC4)	0.44 Ω

Table 5.11: DC grid resistances [100] on Figure 5.15

5.5.2 Signal exchanges with the central controller

An OPF algorithm is solved periodically (every 5 s) in a PC to ensure minimum losses in the system. The OPF is solved using GAMS. To do so, the admittance matrices for the DC and AC grids are known (G_{DC} and Y_{AC}), as well as the DC power injected by wind farms into the DC grid (they are measured and sent to the PC through CAN communication).

The demands of all the nodes are also input data. The outputs of the OPF

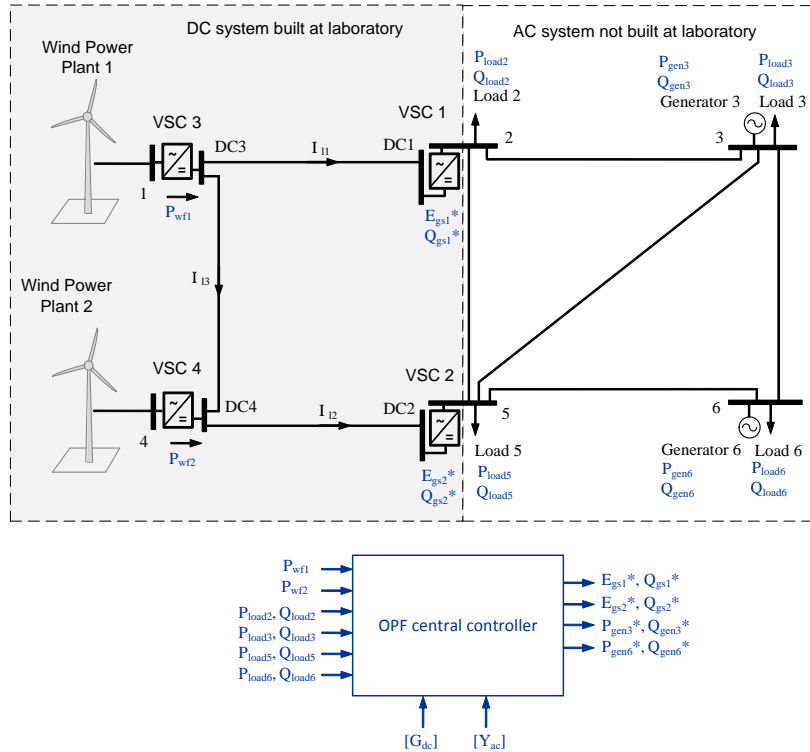


Figure 5.15: System monitoring and signals exchange

algorithm are the voltage references for the droop controls implemented in each grid side converter and their reactive power reference, and the active and reactive power setpoints for the AC generators (see Figure 5.15). These signals are sent from the PC to the DSPs of the grid side converters through CAN communications. Between the output USB port of the PC and the CAN there is a USBtoCAN device. Matlab has special toolboxes to communicate

with CAN (*Vehicle Network Toolbox* and *CAN Communication* were used). That's the reason why GAMS is called from Matlab to execute the OPF. Matlab is here used as interface between the platform measures and the OPF algorithm executed periodically.

5.5.3 Simulations

In next sections the experimental results are compared to the results obtained in simulation. (for MATLAB model details see 3.2.5).

For enabling an easier comparison between experimental and simulation results, all the figures include two subfigures: one with label (a) to indicate simulation results and one with label (b) to indicate experimental results. The operation scenarios analysed are:

- Wind speed variation
- Loss of communications
- Change in the AC demand

For all these scenarios the reactive power demand in each node is considered to be 10% of the active power demand. For the two first scenarios the demand is supposed to be constant. For the next sections, when plotting the experimental measures of power injection from wind farms into the DC grid, DC voltages and reactive powers, the original signals (plotted in transparent grey) have been filtered using calculating their mean value each 1 s, so as to remove the signals noise.

Wind speed change

The first operation scenario corresponds to wind speed step changes in both wind farms. The demand in the AC nodes is set null in all the nodes except in nodes 3 and 6 (see Figure 5.15), where it is 0.1 p.u. (1000 W) for active power and 0.01 p.u (100 VAr) for reactive power. This variation causes changes in the power injected into the DC grid.

As depicted in Figure 5.16 at time 17 s, Wind Power Plant 2 (see Figure 5.15) increases the power produced from 1000 W to 1850 W. Then, at time 47 s, it decreases the generation to 700 W, and finally it increases again to

5.5 Case study 3

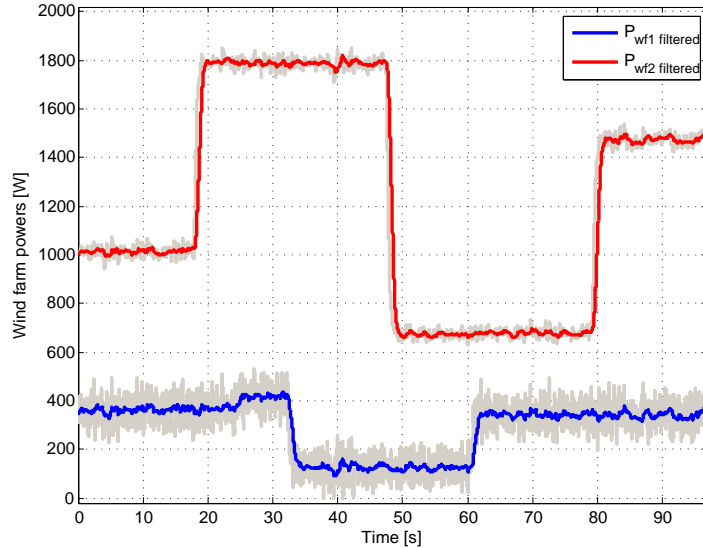
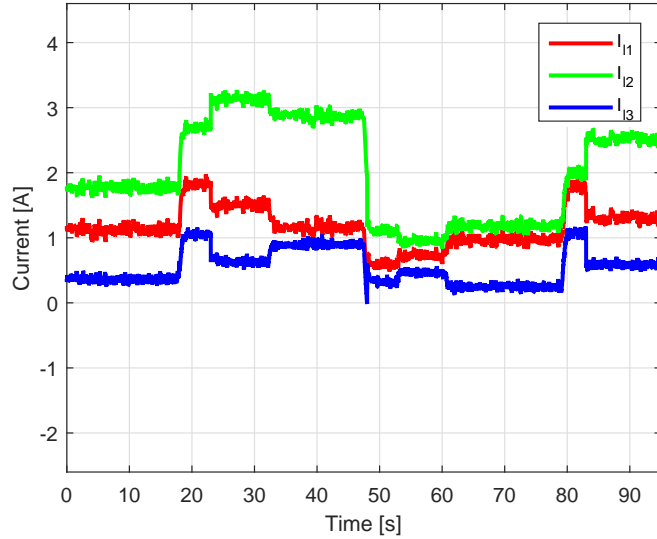
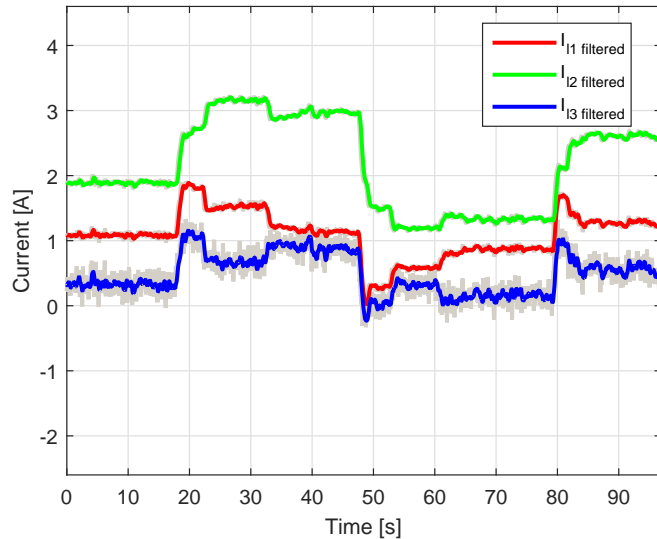


Figure 5.16: Power injection from wind farms

1550 W at time 80 s. On the other hand, Wind Power Plant 1, decreases its power injection from 380 W until 150 W at time 32 s and then recovers the 380 W at time 60 s. The power variation from wind farms leads to voltage changes (see Figure 5.18) and therefore, to a current branches redistribution (see Figure 5.17). As the power injected into the DC grid increases, the OPF drops the DC voltages of the grid so as to keep the maximum power injection: voltages are stable and losses in both DC and AC systems are minimum. Comparing simulation and experimental results, the voltages of the DC grid present present a similar time evolution. The peaks on voltages appear probably due to the fact that there is a change in the power injected from the wind power plants but the central controller has not yet seen this variation. Figure 5.20 and Figure 5.21 show the losses evolution for the DC grid and converters. As a consequence of the different operating points on the DC grid as time evolves, the AC grid power flows will also be affected. This is reflected in the fact that the grid side VSCs change the reactive power references and, therefore, the reactive power measured varies (see Figure 5.19).



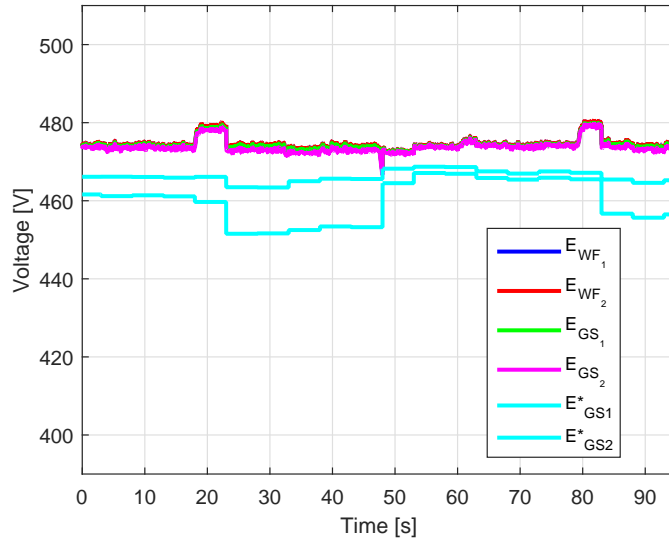
(a) Simulation results



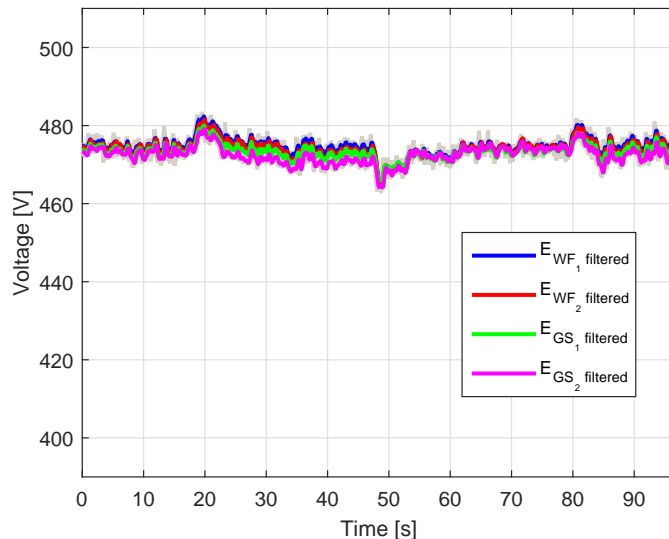
(b) Experimental results

Figure 5.17: DC branch currents

5.5 Case study 3

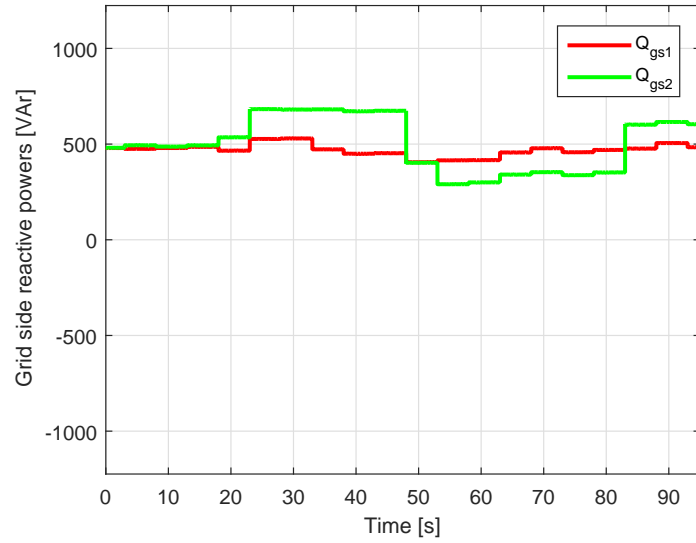


(a) Simulation results

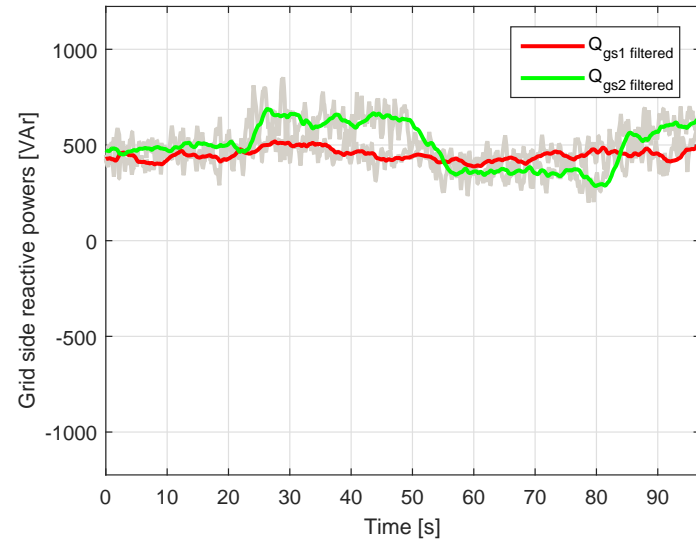


(b) Experimental results

Figure 5.18: DC bus voltages



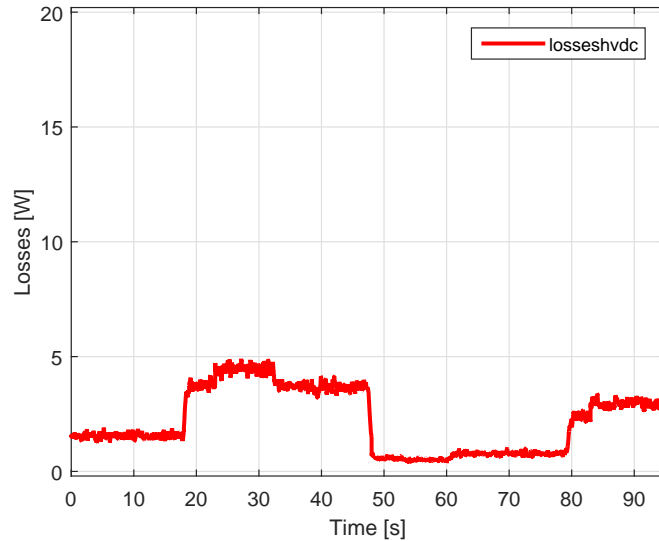
(a) Simulation results



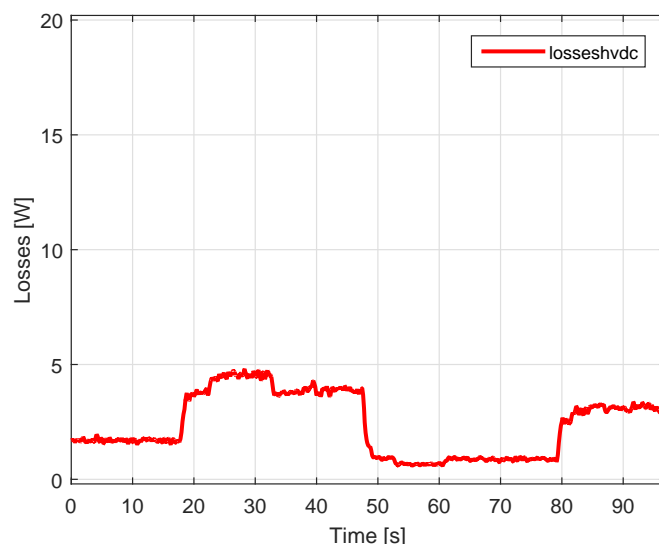
(b) Experimental results

Figure 5.19: Reactive power at the grid side VSCs

5.5 Case study 3



(a) Simulation results



(b) Experimental results

Figure 5.20: HVDC grid losses

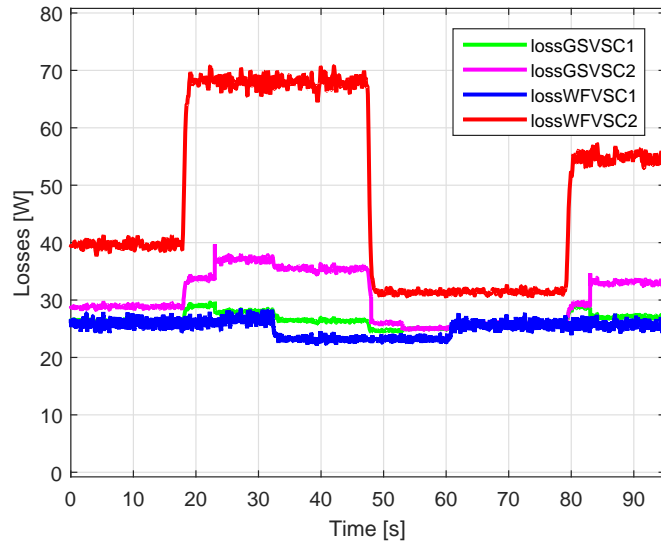


Figure 5.21: VSC losses

Communication loss

The second operation scenario corresponds to a loss in the communication system: from time 10 s until time 87 s (a rose band clarifies the time range when communications are not available). The demand in the AC nodes is set null in all the nodes except in nodes 3 and 6 (see Figure 5.15), where it is 0.1 p.u. (950 W) for active power and 0.01 p.u (100 VAr) for reactive power. In this case, as depicted in Figure 5.22 the power injection from wind farms changes at time 8 s for Wind Power Plant 2, increasing from 400 W to 950 W and decreasing again to 400 W at time 68 s. Wind Power Plant 1 increases its generation at time 28 s from 350 to 450 W and reduces it from 450 until 250 W at time 59 s. However, the OPF algorithm is not able to adapt the voltage references according to all these wind power changes, because communications are lost at time 10 s. In Figure 5.24 it can be seen that the voltage reference for droop control is kept since communications are lost until they are recovered. Comparing simulation and experimental results, the voltages of the DC grid present a few V difference, but their time evolution very close. In this situation minimum losses can

5.5 Case study 3

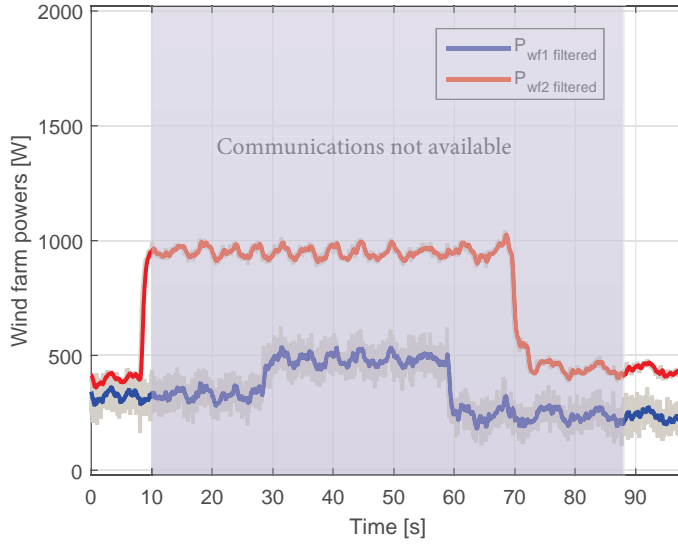
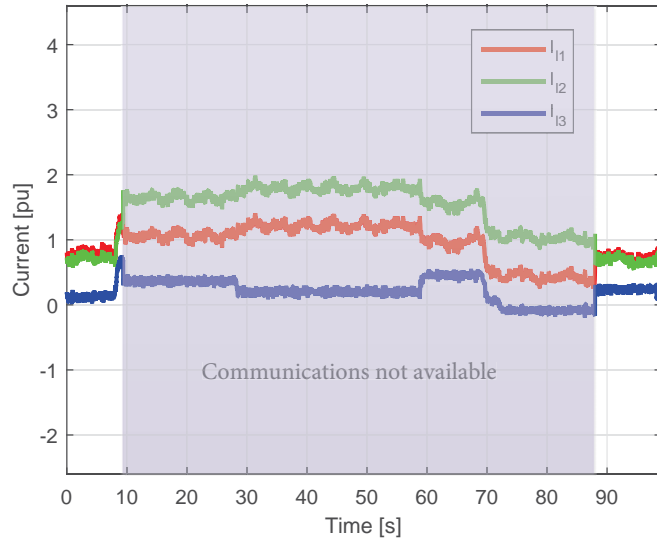
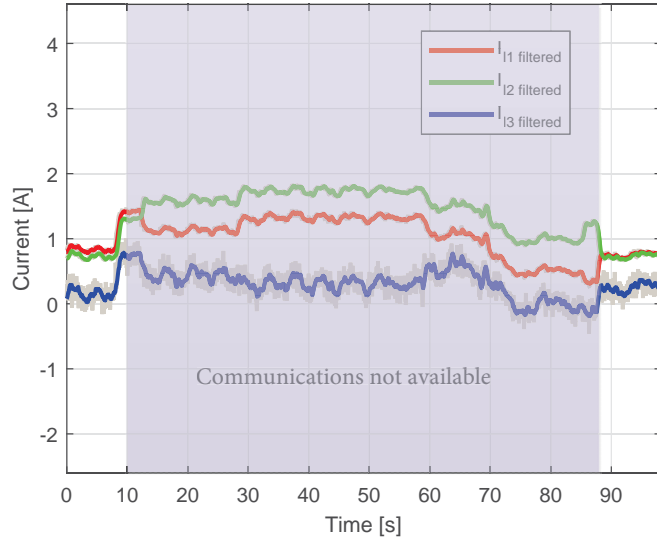


Figure 5.22: Power injection from wind farms

not be ensured, but stable operation is guaranteed. The evolution of the DC branches currents is depicted in Figure 5.23. Figure 5.26 and Figure 5.27 show the losses evolution for the DC grid and converters. The reactive power at the grid side converters is represented in Figure 5.25. It can be noted that the communication loss in the experimental results is a few seconds shifted when affecting reactive powers. The reason is that in the scaled platform, the loss of communications in signals affecting DC voltage references and reactive powers references could not be done at the same time instant (as two different parameters had to be changed manually) while it was in operation.



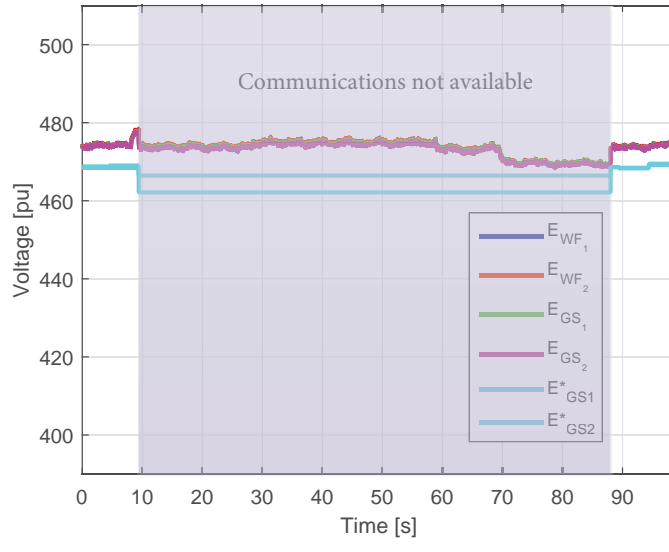
(a) Simulation results



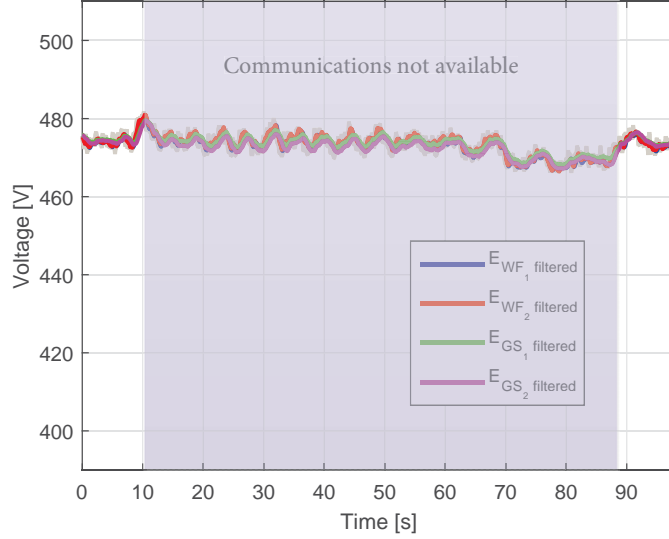
(b) Experimental results

Figure 5.23: DC branch currents

5.5 Case study 3

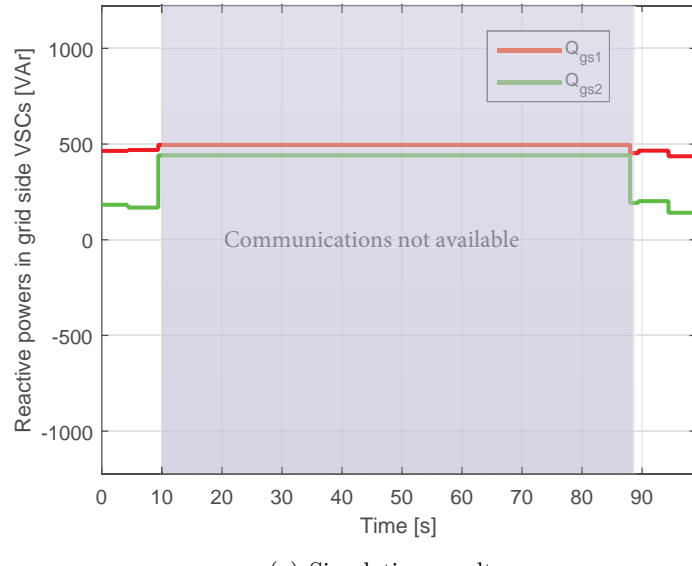


(a) Simulation results



(b) Experimental results

Figure 5.24: DC bus voltages



(a) Simulation results

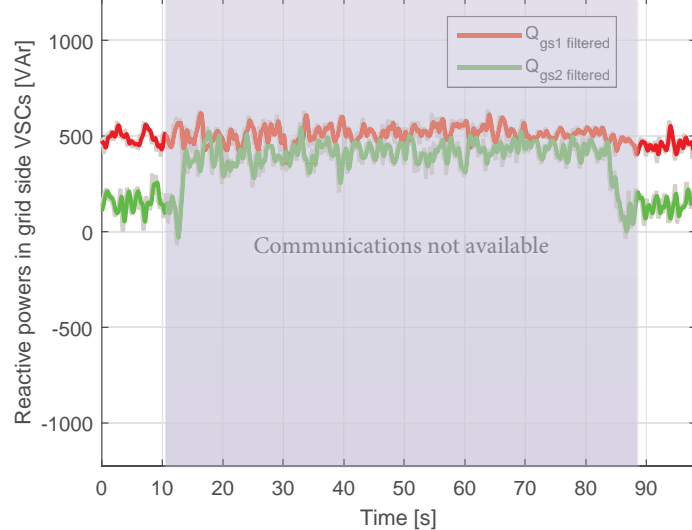
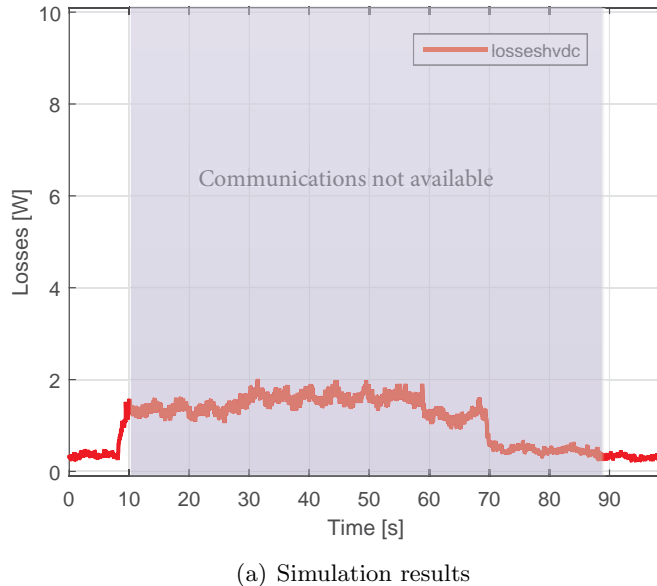
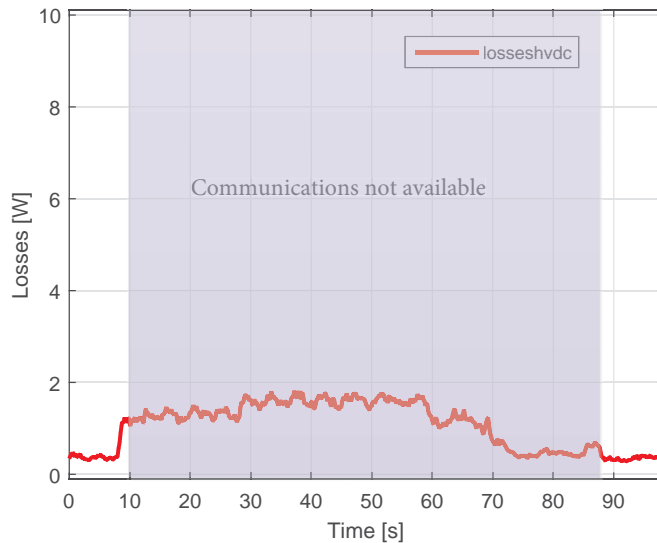


Figure 5.25: Reactive power at the grid side VSCs

5.5 Case study 3



(a) Simulation results



(b) Experimental results

Figure 5.26: HVDC grid losses

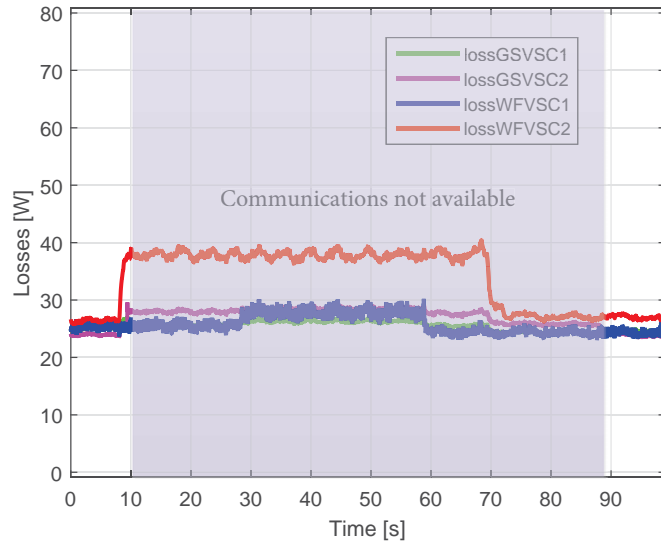


Figure 5.27: VSC losses

Demand variation

The third operation scenario corresponds to a demand change on the AC system. The demand in the AC nodes is set null in all the nodes except in node 6 (see Figure 5.15), where it is 0.5 p.u. (500 W) for active power and 0.005 p.u. (50 VAr) for reactive power. At time 27 s the demand in this node decreases to 0.1 p.u. (100 W) for active power and 0.001 p.u. (10 VAr) for reactive power. As depicted in Figure 5.28, the wind power in both wind power plants remains constant: it is kept at 250 W for Wind Power Plant 1 and at 1000 W for Wind Power Plant 2.

As a consequence of the load decrease, although the power injection from wind farms does not change but the AC demand does, the DC power flows will change to ensure minimum losses for the new operating point. This is due to the fact that the OPF solves the system using a unified approach and not sequential. If a sequential strategy was used, this means solving the AC system and DC system separately and using the outputs of one as inputs for the other, the DC power flows would not have probably changed. So, in this case, the OPF changes the droop references to ensure minimum

5.5 Case study 3

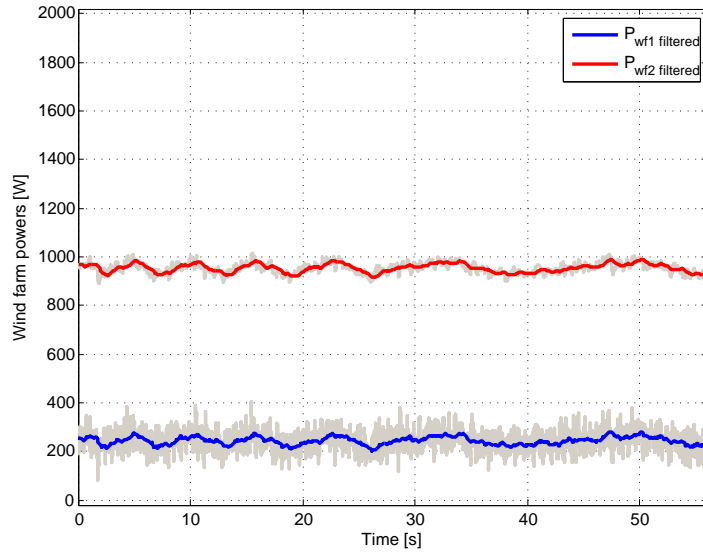
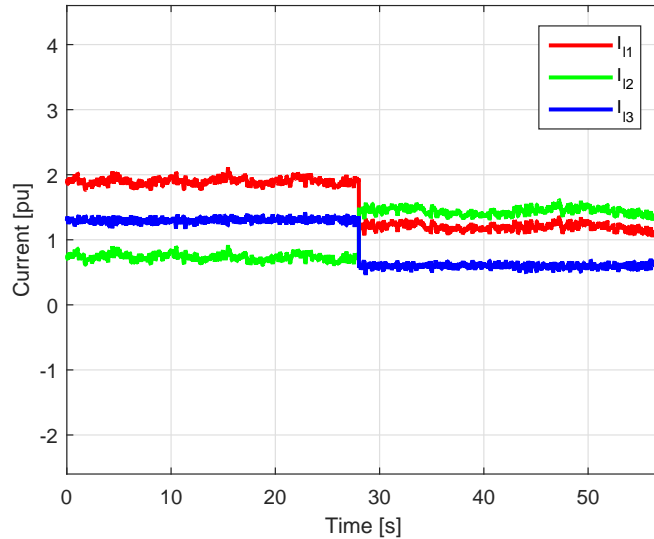
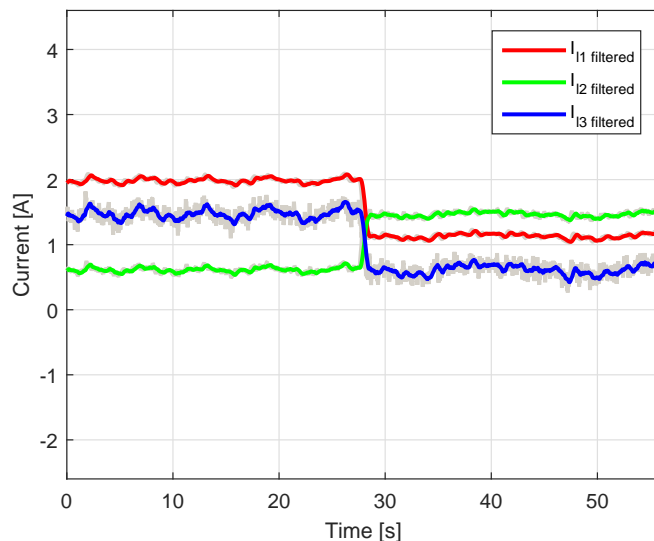


Figure 5.28: Power injection from wind farms

losses, as depicted in Figure 5.30. Comparing simulation and experimental results, the voltages of the DC grid present a few V difference, but their time evolution coincides. The current branches redistribution is presented in Figure 5.29. Figure 5.31 and Figure 5.32 show the losses evolution for the DC grid and converters. The DC grid losses do not practically change, while the converter losses do, as well as the losses in the AC grid.



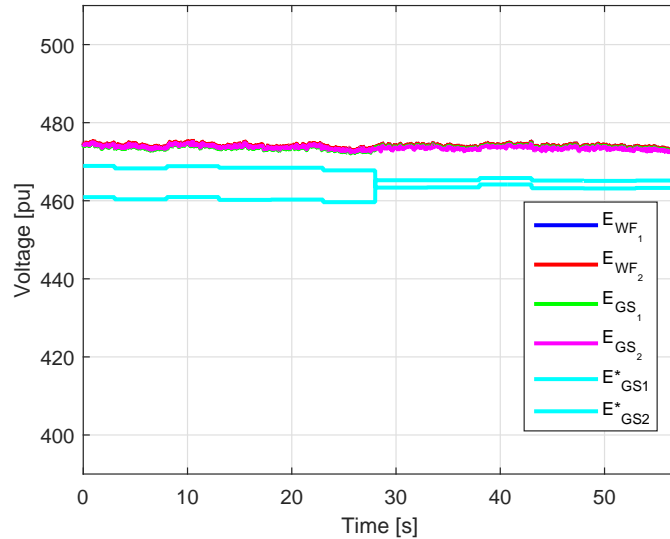
(a) Simulation results



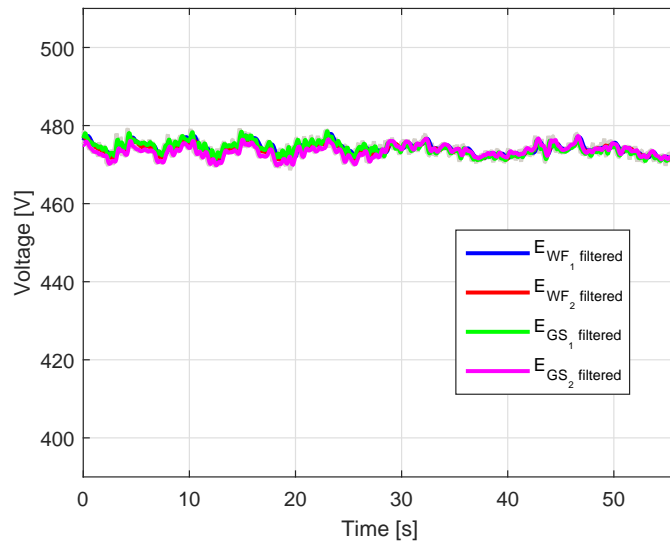
(b) Experimental results

Figure 5.29: DC branch currents

5.5 Case study 3

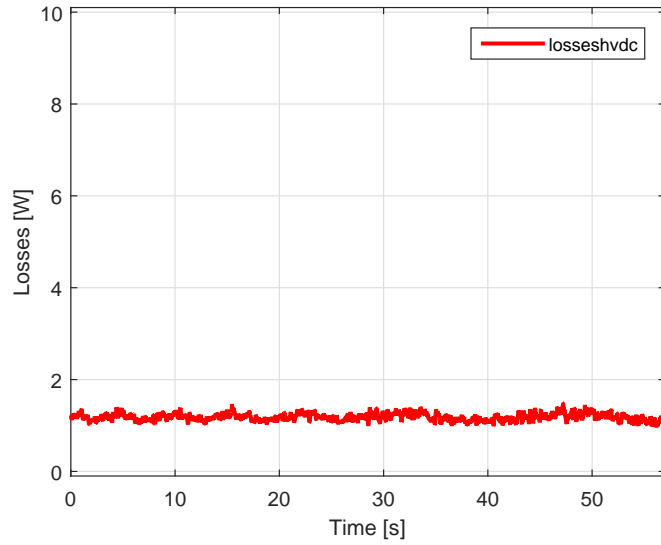


(a) Simulation results

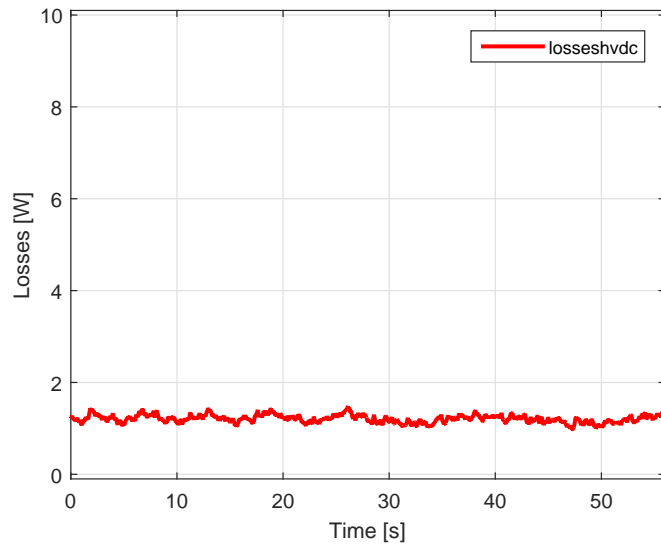


(b) Experimental results

Figure 5.30: DC bus voltages



(a) Simulation results



(b) Experimental results

Figure 5.31: HVDC grid losses

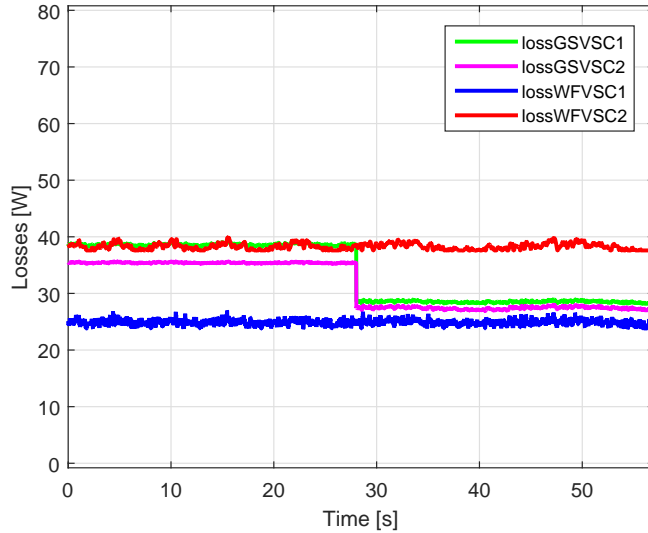


Figure 5.32: VSC losses

5.6 Conclusions

An optimal power flow strategy to operate hybrid DC/AC systems with large penetration of offshore wind has been presented. This methodology, has been benchmarked with [94], obtaining the same results for two objective functions analyzed in [95]. The tool has been applied to a particular study case consisting in a two DC systems connected to an AC system. Two softwares have been used for its implementation (MATLAB and GAMS) leading to the same results for the study case of loss minimisation presented. However, GAMS, for being an optimization dedicated software, has been proved to be far more efficient than MATLAB *fmincon*. Finally, the tool has been tested in a scaled platform, showing stable operation. So, the tool represents a fast, flexible and validated methodology for analysing the optimal operation of hybrid AC/DC grids with large wind power integration for several objective functions. Finally, the experimental tests show an appropriate dynamic response of the proposed strategy combined with droop control for the operation of hybrid AC/DC systems.

Chapter 6

SCOPF in hybrid DC/AC power systems with large penetration of offshore wind taking into account spinning reserves

6.1 Introduction

The security of a power system represents the degree of risk in its ability to overcome disturbances (contingencies) without interruption of customer services [79]. Contingencies refer to outages such as sudden and not scheduled loss of service of one or more of the main power system components [79]. Normally, power systems are operated according to the deterministic N-1 criterion, so the permanent loss of one power system component may not affect the stable operation of the rest of the system. However, recent changes in power systems are influencing the way they are planned, operated and controlled.

As detailed in [101], power systems have to deal with an evolving demand and generation, with not always an appropriate adaptation of generation and transmission, leading to more stressed operating conditions. Furthermore, the larger penetration of renewable energy generation implies larger uncertainty in systems operation. For instance, in a system with large penetration of offshore wind, the uncertainty and fluctuating behaviour inherent to this power source can compromise its secure operation, as the wind power is not always available when needed to react to an outage, or can worsen

the situation in case the wind power cannot be absorbed or when the grid is not able to accommodate the power flows. On the other hand, a system designed for high wind penetration is often highly loaded due to the low capacity factor. Due to these aspects, the security of power systems is being compromised. In addition, new devices such as HVDC or FACTS, are being installed, enabling renewable power integration through added flexibility in the grid operations at the expense of adding complexity to the power system control.

The European transmission system is being extended by combining both AC and DC technologies. With the projected advent of HVDC grids, contingencies such as converter outages cause a quasi-instantaneous power redistribution by means of a voltage droop control [102], in a way that shows similarities with the frequency droop control in the AC system. However, these power redistributions might result in line overloads when not taken into account properly. Fast HVDC controls allow to shift power flows to the most optimal value nearly instantaneously. All this adds to the complexity of the study of the reliability of such systems, as it is not yet clear to which level of reliability hybrid HVAC-HVDC systems should be operated.

Some authors have analysed the optimal operation of AC grids and DC grids [91–94]. The tool developed in [94] is here applied in the present study to a scenario with large penetration of offshore wind.

Some studies regarding SCOPF (Security Constrained Optimal Power Flow) that take into account wind power integration exist: [103–106]. The authors from [103] propose a SCOPF to allow the post-contingency control of a VSC-HVDC system through corrective actions based on the current injection method. But the only contingency analysed is the outage of DC lines. In [104] a probabilistic robust generation dispatch to guarantee N-1 secure operation under wind uncertainty, is proposed, but it is assumed that enough reserves are available to balance the generation-load mismatch, so no reserve scheduling is considered. This analysis is extended to multi-area systems involving different levels of data exchange in [106]. In [105], the authors from [104, 106] design a N-1 secure day-ahead dispatch, while determining the minimum cost reserves for power systems with high wind

6.2 Optimal operation of hybrid AC/DC systems including spinning reserves

penetration. Additional constraints ensure that the scheduled generation dispatch plus the reserve contribution are inside the generation capacity limits. Here, ramping up and down reserves are considered. Although the studies from [104, 106] are detailed, they only focus on the AC system. A scenario with HVDC links is not contemplated.

This study analyses the secure and optimal operation of hybrid HVAC-HVDC connected systems with large penetration of offshore wind, taking into consideration the system spinning reserves. The operation and economic consequences are investigated. Using the SCOPF tool for hybrid AC/DC power systems from [94], it is possible to optimize a specified objective function while guaranteeing all the equality and inequality constraints limiting the electrical variables. This tool has first been modified so as to enable modelling DC systems connected with wind farm generation and to include the system spinning reserves (ramping up and down capability). Then, the tool has been applied to a system with high penetration of offshore wind and a methodology has been developed to analyse the cost of operation of the whole system during one year taking into consideration corrective actions to ensure security. So, the ultimate goal is to determine the OPEX (Operational Expenditures) of the system. Maintenance and repair costs are not included.

6.2 Optimal operation of hybrid AC/DC systems including spinning reserves

6.2.1 SCOPF tool

The optimal operation of hybrid AC/DC systems is studied through the tool presented in [94], developed in Matlab as an extension of MATPOWER and based on extending an standard AC OPF with the constraints expressing the DC grid equations. For involving DC and AC power systems, the problem can be classified as non-linear constrained optimization. It is solved using an Interior Point Algorithm with barrier function [64].

The tool is applied to hybrid HVDC-HVAC systems integrating offshore wind power, whose general layout is sketched in Figure 6.1. The power pro-

duced by the wind power plants is injected in the DC grid through VSCs operating as rectifiers and it is transmitted to the AC grid through VSCs operating as inverters. The HVDC links enable the power transmission to the consumption nodes.

The available wind power in all the wind power plants, the active and reactive power demand, the electrical characteristics of the DC and AC grids, as well as the distances of lines and cables and the converter loss parameters are known data. The tool determines the active and reactive power injections from all the generating units and VSC converters, the power flowing through each branch. The basic constraints are that demand is met with minimum power generation costs while ensuring the secure operation of the system.

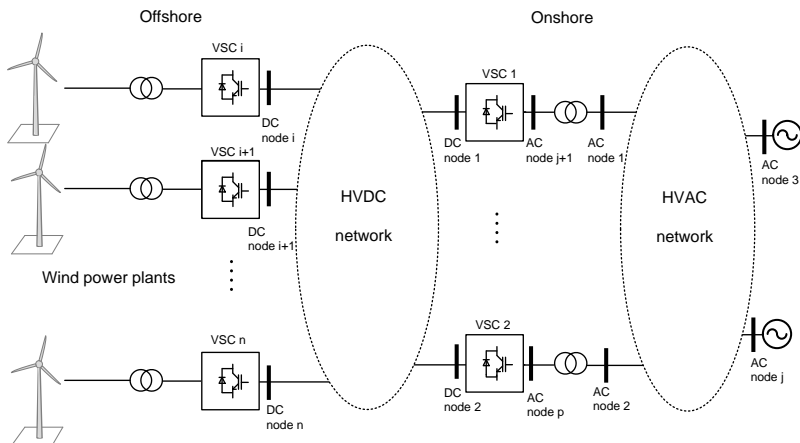


Figure 6.1: Hybrid HVDC-HVAC system for integrating offshore wind power

6.2.2 Contingencies and security constraints

The contingencies considered in this study are the outage of any power system component: AC branch, AC generator, DC branch or VSC. The control possibilities of the TSO to face a disturbance depend on the nature of the contingency and on the time available to ensure that the system returns to

6.2 Optimal operation of hybrid AC/DC systems including spinning reserves

a secure state. Preventive actions or measures are taken before the contingency occurs and they are based on the fact that the TSO relies on redundancy in the topology of the grid and on the appropriate selection of the generator and converter set-points to achieve a healthy state after a credible contingency occurs. Corrective or curative actions are taken immediately after an incident happens and it is assumed that the action can happen sufficiently quick to ensure the system recovers to a healthy state, relying on the fact that the system has a temporary overload capability.

The possibility to use corrective actions depends on the actual state of the system, with varying degree of renewable generation. The existing operational reserves on the power system do also influence the capability of reaching a secure state. For this reason, the system spinning reserves have been included in the formulation, as described in Section 6.2.4. In the present study, the goal is to minimize the cost of operation for all the credible system states, accounting that in case an outage occurs the TSO can make the following corrective measures:

- Generating units setpoints change
- VSCs setpoints change
- Wind power curtailment

The mathematical formulation of the security constraints is detailed in [94].

6.2.3 Generation and demand modelling

The generation units in this study are modelled as either wind power plants or traditional generating units. In both cases, they are aggregated in bigger units. As weather conditions vary, the wind speed changes over time, leading to wind power fluctuations. As such, wind power variability must be taken into account when modelling this resource. Another characteristic of wind power is uncertainty, which limits its predictability. In this study, forecasting errors are not considered. In order to include a realistic wind power generation profile, real data from the Belgian TSO, Elia, representing the Belgian aggregated wind farms production, have been used and scaled.

The wind farms are modelled as AC generating units whose maximum output power is the available wind power of the wind power plant and they are characterized by a lower marginal generating costs than the other generating units, so their injection is prioritised. The other generating units are aggregate per node, as well as the demand. Also, for the load values representing the demand, data from the Belgian system has also been used and scaled. The generation costs are modelled according to a second order polynomial and the wind power generation cost is assumed to be proportional to the power produced [107]. The objective function tries to minimize the cost of generation, so it is expressed as the sum of the cost of running all the generating units.

6.2.4 Spinning reserves modelling

The term spinning reserves is defined in literature in various ways. According to NREL (National Renewable Energy Laboratory), spinning reserve is formed by the generation and responsive load that is on-line, that can begin responding immediately, and is fully responsive within 10 minutes. According to NERC (North American Electric Reliability Council), spinning reserves is the unloaded generation that is synchronized and ready to serve additional demand. Many other definitions can be found in literature [108, 109] and, as identified in [110], some of them do not agree on who provides spinning reserve (in the sense that it is limited to generators or the demand can also participate), the time frame to respond to a request or how is this reserve activated (it happens automatically or it is only done at the request of the TSO). Thus, [110] proposes a general definition, assumed for this study: spinning reserve refers to the unused capacity which can be activated on decision of the system operator and which is provided by devices that are synchronized to the network and are able to affect the active power. Power system reserves are designed to handle unpredictable power deficits that could threaten the stability of the system. Mainly two approaches exist for modelling spinning reserves. The first is deterministic and the second probabilistic [111]. However, some authors, like [112], propose a hybrid methodology. The main difference between the deterministic and probabilistic approach is that the latter includes the stochastic behaviour of system

6.2 Optimal operation of hybrid AC/DC systems including spinning reserves

components by taking into account the load forecasting deviation, equipment failure and repair rates. For the sake of simplicity and for avoiding large computational times, the deterministic approach is adopted in this study. It is based on determining the spinning reserves for minimizing the operating cost up to a particular level of risk in the system throughout the operating period. The criteria for the total reserve estimation varies in each country. It can be one or a combination of fixed capacity margin, fixed percentage of system load, fixed percentage of on-line capacity or to fix it to be greater than the capacity of the largest on-line generating unit. For this study, the existing quantity of spinning reserves of the Belgian system have been scaled [111]. In the Belgian system the spinning reserves requirement criteria is currently at least 460 MW by generators [110].

In this analysis, it is also assumed that demand will not contribute to spinning reserves, while wind power plants and the existing generating units will. While conventional generating units will have both ramping up and down capabilities, the wind power plants only have ramping down capability. Wind power plants are able to provide spinning reserve with ramping up capability if they would include a storage system or when they are curtailed below the available power, which is not considered in this study. The costs for reserves are modelled as direct costs, proportional to the amount of reserves provided by the generating unit. The variables and parameters listed in Subsections 6.2.4 and 6.2.4 allow the mathematical formulation of spinning reserves constraints, in Section 6.2.4.

Variables

- i index of generating unit, $i=1..n_g$, where n_g is the number of generating units
- P_{gi} active power generation from generating unit i
- P_d corresponds to the total active power demand
- R_{gi}^{up} system spinning reserve up from generating unit i
- R_{gi}^{down} system spinning reserve down from generating unit i

Parameters

- P_{gi}^{min} minimum active power generation from generating unit i
- P_{gi}^{max} maximum active power generation from generating unit i
- RMP^{up} maximum ramp up rate of unit i
- RMP^{down} maximum ramp down rate of unit i
- τ^{up} is the time for ramping up. It corresponds to the time period considered (1h)
- τ^{down} is the time for ramping down. It corresponds to the time period considered (1h)
- R^{up} total system spinning reserve up, according to a deterministic criteria
- R^{down} total system spinning reserve down, according to a deterministic criteria

Constraints

Equation (6.1) expresses the balance between generation and demand and Equations (6.2)-(6.3) reflect that the total spinning reserve up and down must fit the system spinning reserves needs.

$$\sum_{i=1}^{n_g} P_{gi} = P_d \quad (6.1)$$

$$\sum_{i=1}^{n_g} R_{gi}^{up} \geq R^{up} \quad (6.2)$$

$$\sum_{i=1}^{n_g} R_{gi}^{down} \geq R^{down} \quad (6.3)$$

Active power generation in each unit is limited, as shown in Equation (6.4).

$$P_{gi}^{min} \leq P_{gi} \leq P_{gi}^{max} \quad (6.4)$$

6.3 Methodology for determining the cost of operation over one year

The spinning reserves delivered by each generating unit are limited, according to Equations (6.5)-(6.6), and must satisfy the ramp up and down rates defined in Equations (6.7)-(6.8).

$$R_{gi}^{up-min} \leq R_{gi}^{up} \leq R_{gi}^{up-max} \quad (6.5)$$

$$R_{gi}^{down-min} \leq R_{gi}^{down} \leq R_{gi}^{down-max} \quad (6.6)$$

$$R_{gi}^{up-max} = RMP_{gi}^{up} \times \tau^{up} \quad (6.7)$$

$$R_{gi}^{down-max} = RMP_{gi}^{down} \times \tau^{down} \quad (6.8)$$

The active power delivered by each generating unit and its ramping up and down reserves are limited by the maximum and minimum power available in this unit, as shown in Equations (6.9)-(6.10) respectively.

$$P_{gi} + R_{gi}^{up} \leq P_{gi}^{max} \quad (6.9)$$

$$P_{gi} - R_{gi}^{down} \geq P_{gi}^{min} \quad (6.10)$$

These constraints are added to the SCOPF formulation. So the tool output will include the spinning reserves from each generating unit (R_{gi}^{up} and R_{gi}^{down}) needed to satisfy the total spinning reserves of the system while ensuring the stable operation with minimum generation costs.

6.3 Methodology for determining the cost of operation over one year

The flowchart of the SCOPF tool process applied to determine the cost of operation of a power system over one year is shown in Figure 6.2. The blue text applies for the particular study case detailed in Section 6.4.1. First, the system under study needs to be defined, specifying the configuration and electrical characteristics. Then, the type of security analysis to be performed is detailed, defining all the possible states of the system based on the elements that can be unavailable and on the security level assumed for the power system. Next, an iterative computation process starts, taking into consideration the time horizon for computing the cost of operation. Assuming the cost needs to be determined for one year operation, with hourly

samples of generation and demand, the next steps will be run 8760 times. For a specific objective function, knowing the cost of operation of the generating units, the spinning reserves location, capacity and cost, as well as the ramping up/down capabilities of the generating units, several SCOPF are executed (one at the specified hour), taking into consideration the corrective actions of the TSO. For each SCOPF, the cost of operation of the system and the wind power curtailed are calculated and results are stored.

Once all the SCOPF calculations have been performed, the total cost of operating the hybrid HVAC-HVDC system over one year is computed considering the probability of occurrence of the different operating states. So as to compute the probability of each state, the failure rate of the different components and the downtime due to repair are considered. For the probabilistic analysis, the following criteria apply:

- Each power system component has two possible states: on-line and off-line
- The probability of component i of being off-line (or under failure) is u_i
- The probability of component i of being on-line (healthy) is $a_i = 1 - u_i$
- The probability of finding the system working in state s is equal to the product of the probabilities of the k available elements and the probabilities of the $N - k$ out-of-service elements, being N the total number of system components

So, the probability of the system of working under state s can be expressed as:

$$P_s = \prod_{j=1}^n a_j \times \prod_{i=1}^m u_i \quad (6.11)$$

$\forall j$ online $\forall i$ offline

6.3 Methodology for determining the cost of operation over one year

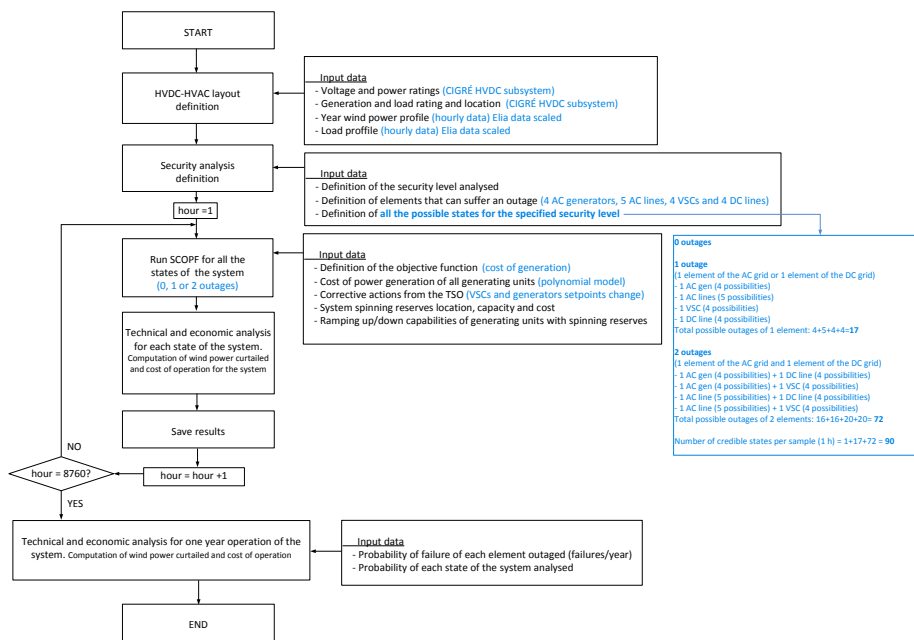


Figure 6.2: Flowchart of the methodology

6.4 Study case

6.4.1 System description

The steps detailed in Section 6.3 are applied to a hybrid HVDC/HVAC system, inspired in the Test System defined by CIGRÉ in [73] and represented in Figure 6.3. The bus letters in Figure 6.3 correspond to the designation used in [73]. The AC system voltage is 380 kV and the DC system voltage is +/-400 kV. The wind farm VSCs are rated 800 MVA, while the grid side VSCs are rated 1200 MVA. The aggregated wind generation in Belgium^[1] in 2013 (taken from Elia [113]) is scaled and now grouped in 2 wind farms. The two wind farms present different wind profiles (with correlated wind speeds). Similarly, the demand data for this country in 2013 (taken from Elia) is scaled and grouped in 2 loads, with a similar share (random values in the range of 40-60%). The generation that does not come from the wind resource is represented through two generating units connected to the same buses that the loads representing the demand.

¹ The probability of unavailability of the different power system components

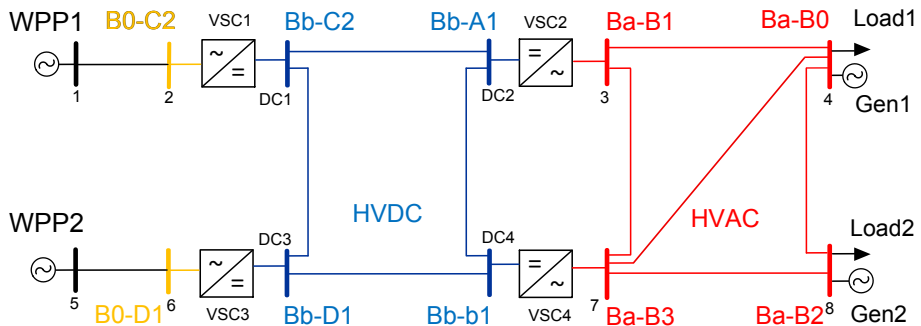


Figure 6.3: HVDC-HVAC system based on [73]

is computed taking into consideration its failure rate (failures/year) and its

¹Note that belgian data was simply used to represent a realistic time series and the results do not provide a quantitative insight in power system operations in Belgium.

6.4 Study case

downtime to repair (expressed in hours), from [114,115]. Their product gives the unavailability in hours/year, which can be turned into a probability by dividing it by the 8760 hours of a year. The failure rates of some power system elements can be found in the literature expressed as *number of failures/year* or *number of failures/(100 km·year)* for lines. The power system under study is constituted by 4 types of elements: AC branches, AC generators, DC branches and VSCs. Each element has a probability of failure. Furthermore, the probability of failure of lines depends on their length (so the probability of failure of the DC branches is different; but the same for all the AC branches because they have the same length), as reflected in Table 6.1. Based on the failure rates from [114], we set the failure rates per year to 0.006 failures/100 km for AC lines, 0.003 failures/100 km for DC bipolar lines and 1.4 failures/year for VSCs. Knowing the probability of failure for the different components and applying the probabilistic criteria described in Section 6.3, the probability of the system of working under normal operation is 0.7850, the probability of losing 1 element (AC or DC) is 0.2081 (0.0289 for a DC element and 0.1791 for a AC element) and the probability of losing 2 elements (1 AC element and 1 DC element) is 0.0051. The system operates normally, with 1 or 2 elements under outage 99.82 % of the time. The rest of the time corresponds to the sum of the probabilities of the scenarios not considered (outages of 2 elements of the same type and up to 18 elements) and which can be neglected due to the low probability of occurrence. A diagram reflecting all the possible events considered is depicted in Figure 6.4.

6.4.2 Results

The input data for the tool applied to the system described in Section 6.4.1 corresponds to the wind power available in WPP1 and WPP2 and to the active power demand of Load 1 and Load 2. Although the months should have data for all their days, some months present the loss of one day data due to the unavailability on the database consulted. The reactive power demand required by each load is assumed to be 10 % of the active power demand it consumes.

For each hourly sample, a SCOPF is executed. All the possible scenarios

Line or cable	Failures/year	Repair time (h)
AC 3-4 (200 km)	0.012	24
AC 3-7 (200 km)	0.012	24
AC 4-7 (200 km)	0.012	24
AC 4-8 (200 km)	0.012	24
AC 7-8 (200 km)	0.012	24
DC 1-3 (400 km)	0.012	1440
DC 3-4 (400 km)	0.012	1440
DC 2-4 (300 km)	0.009	1440
DC 1-2 (200 km)	0.006	1440

Table 6.1: Failure rates of the system lines and cables [114]

VSC	Failures/year
VSC1	1.4
VSC2	1.4
VSC3	1.4
VSC4	1.4

Table 6.2: Failure rates of the system VSCs [114]

Generator	Failures/year
Wind turbine	6
Others	0.02

Table 6.3: Failure rates of the system generators [116]

6.4 Study case

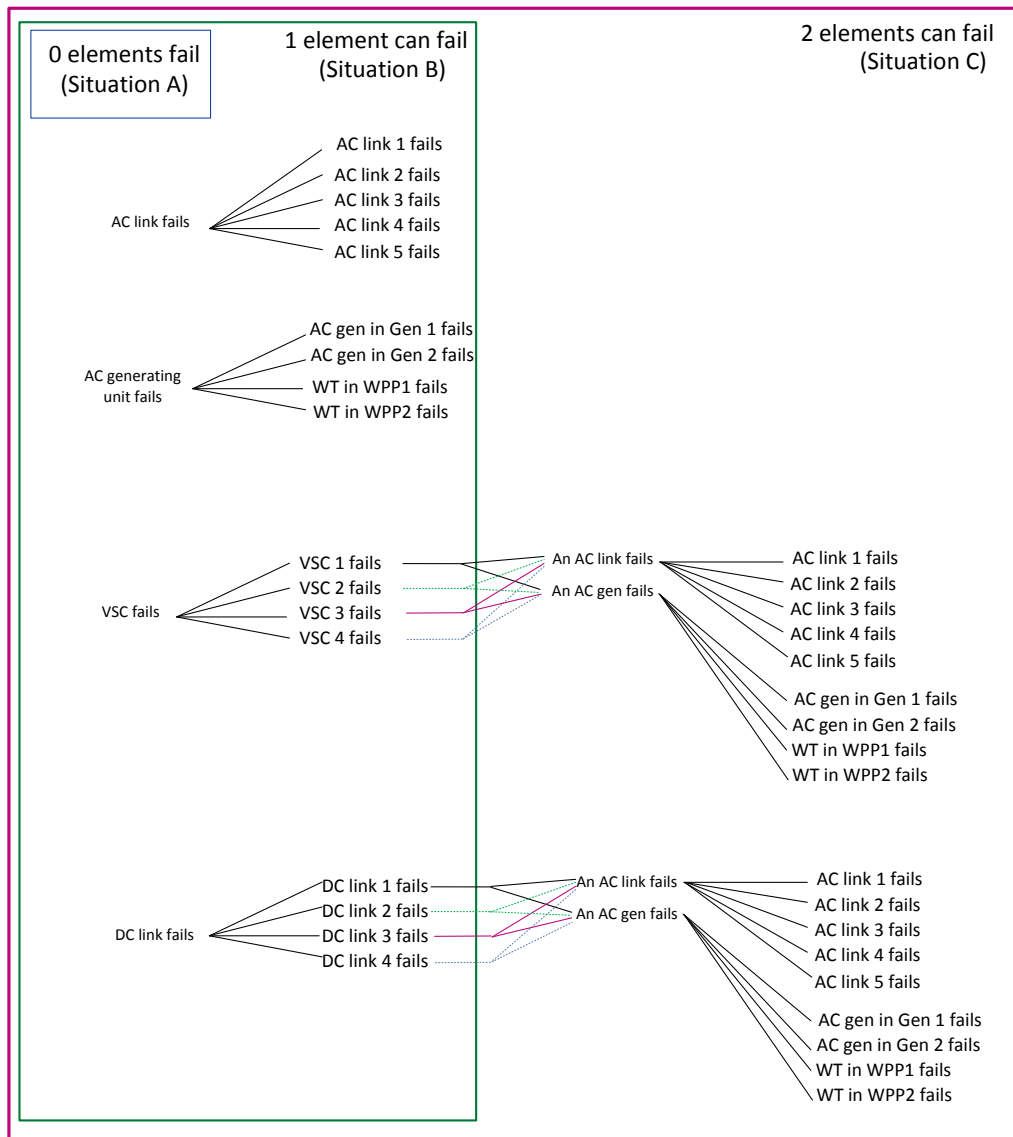


Figure 6.4: Event tree for the system analysed

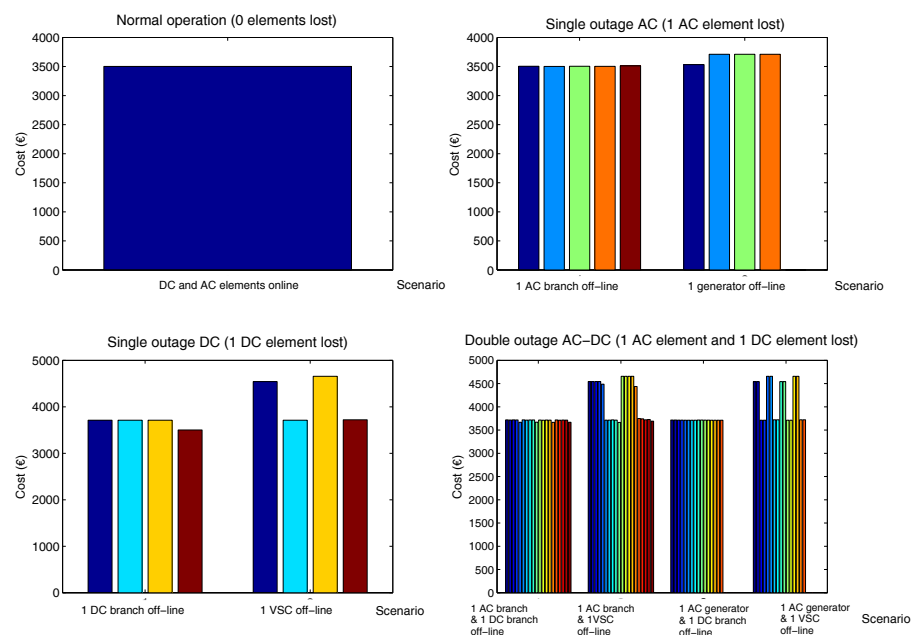


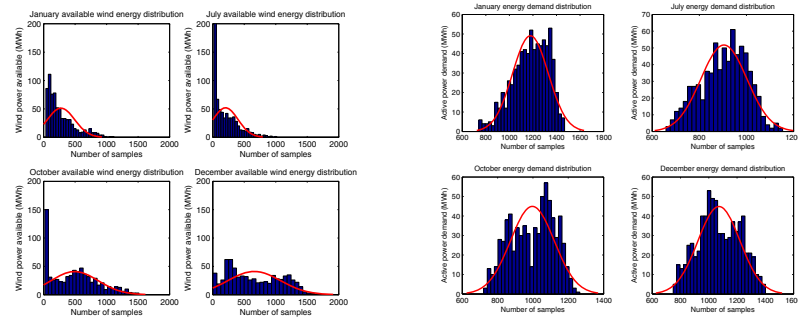
Figure 6.5: Possible power system scenarios for each hour analysed

6.4 Study case

considered for each hour are represented in Figure 6.5. They correspond to normal operation, the loss of 1 AC element, the loss of 1 DC element and the loss of 2 different elements (1 AC and 1 DC). The cost corresponds to one hour evaluation of one day of January (without weighting the probability of occurrence of each state). The most critical operation of the system appears when a VSC is lost or a VSC and a generator are lost.

6.4.3 Scenarios identification

In order to address a non time dependent analysis, and with the aim of classifying and understanding different operations scenarios according to the total wind power available and system demand, the samples corresponding to the total wind power available (merging the two WPP) and the total demand (merging the two loads) have been compared. Figure 6.6(a) shows the histograms of wind power available according to the samples of 4 months (January, July, October and December), which turn to be those presenting largest differences in the operating costs and wind power curtailed. Figure 6.6(b) represents histograms of the active power demand for the same 4 months.



(a) Wind power scenarios identification (b) Load power scenarios identification

Figure 6.6: Scenarios classification according to wind available and demand

Analysing both figures, it can be deduced that October and December are

Chapter 6 OPEX of hybrid DC/AC power system

the months with larger wind power available, while January and December are the months with the highest demand. If we aggregate all the wind energy and demand per month, we can obtain Figure 6.7. Based on this data, we can identify four different scenarios:

- High wind & Low load
- High wind & High load
- Low wind & Low load
- High wind & High load

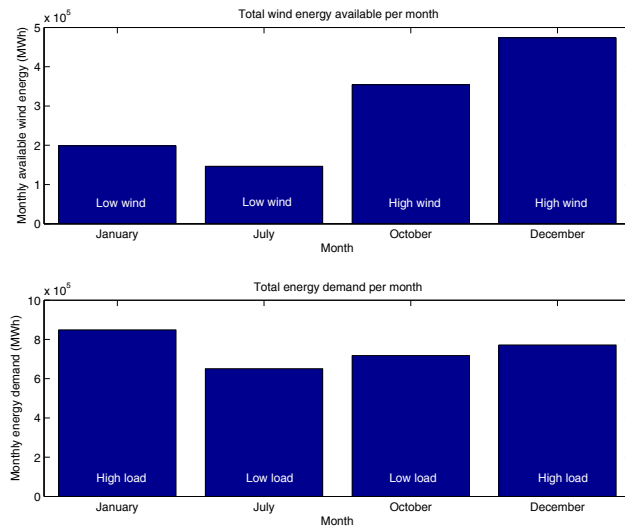


Figure 6.7: Scenarios identification according to available wind energy and demand

The correlation between the wind power power energy available in the two wind power plants for the aforementioned months is represented in Figure 6.8(a). The correlation for the energy demanded for these months is depicted in Figure 6.8(b) and the correlation for both the available wind energy and total demand in the system is shown in 6.9. The contribution to the year

6.4 Study case

operating cost of each of these scenarios, is represented in Figure 6.11. The wind power curtailed, for the same scenarios is depicted in Figure 6.10.

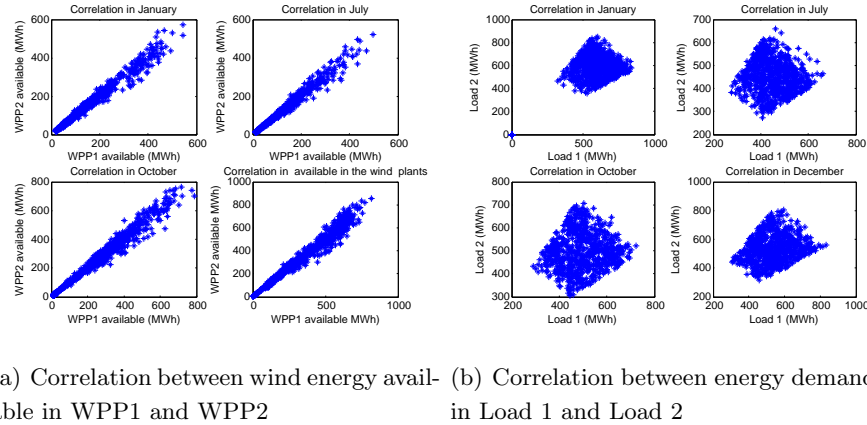


Figure 6.8: Correlation in wind energy and in demand for 4 months

It seems reasonable that with higher wind power availability, the curtailment increases if there is not sufficient demand to absorb it. On the other hand, the higher is the wind power availability, the lower is the cost of operating the system (the cost of generating the needed energy by means of conventional generation is comparatively higher during operational planning). Therefore, the scenarios presenting a high demand combined with low wind energy availability will lead to the highest cost of operation. And vice versa, the lowest cost of operation will appear in scenarios with low demand and high wind energy availability. This can be checked in Figure 6.12, depicting a three dimensional representation of the cost of operation of all the months as a function of the wind energy available and demand. The total cost of operation and wind power curtailed during are shown in Table 6.4 and Table 6.5 for different situations of operation.

- Situation A assumes all the elements of the system will be always ok.
- Situation B assumes the system operates in normal condition or with one AC element lost.
- Situation C assumes the system operates in normal operation or with

Chapter 6 OPEX of hybrid DC/AC power system

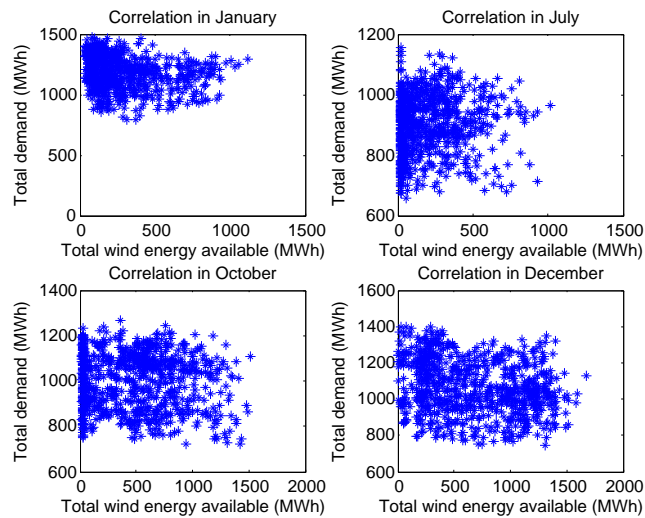


Figure 6.9: Correlation between wind energy and energy demand

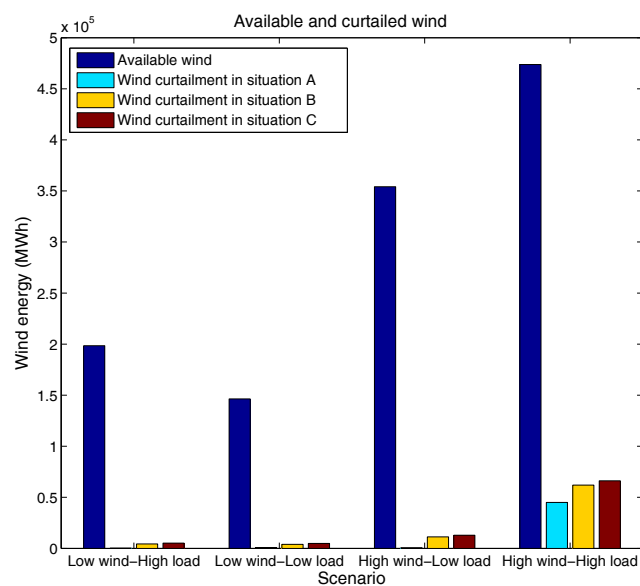


Figure 6.10: Available wind energy and curtailment under different operation scenarios

6.4 Study case

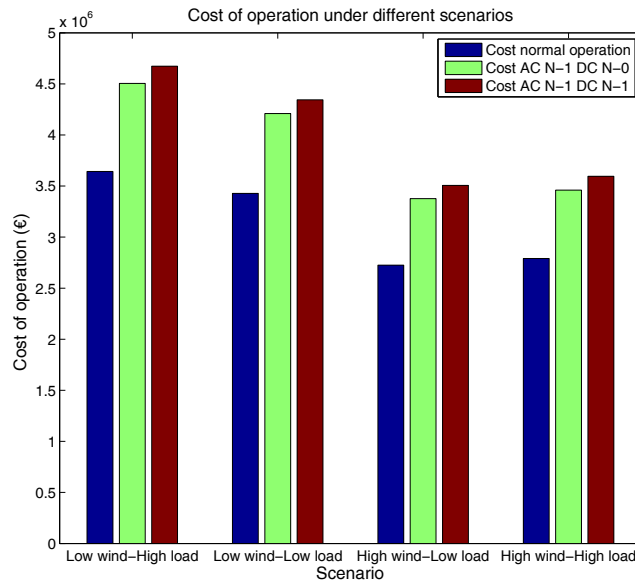


Figure 6.11: Cost of operation under different operation scenarios

one AC element or one DC element lost or an AC and a DC element lost.

The situation that is more realistic is situation C and leads to higher costs. The wind power needed to be curtailed also increases in this case as the power system becomes more constrained and can not absorb all the power injected as more elements are under outage and less power paths are available. The total cost of operation over one year is 46.62 M€/year and the wind power curtailed is 200.66 GWh/year.

Situation	Cost of operation (M€/year)
A	36.34
B	44.91
C	46.62

Table 6.4: Total cost of operation during one year

Situation	Wind curtailment (GWh/year)
A	99.33
B	180.15
C	200.66

Table 6.5: Total wind power curtailed during one year

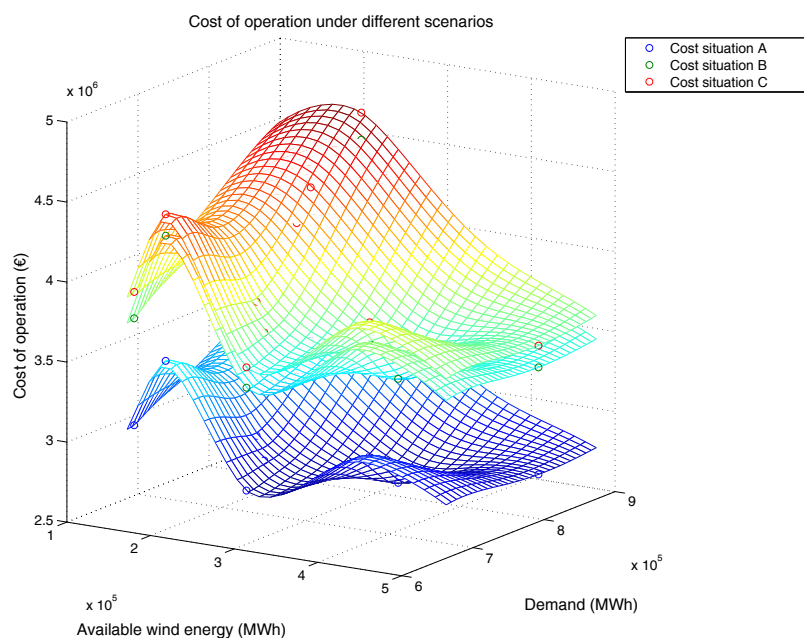


Figure 6.12: Cost of operation as a function of the monthly wind energy available and demand

6.5 Conclusions

This study has proposed a methodology for evaluating operating cost over a year of a hybrid AC/DC system with high penetration of offshore wind taking into account corrective actions. A SCOPF tool has been used, modeling the TSO corrective measures for facing disturbances. The system studied has been operated so as to maximise the social welfare. The wind power variability is taken into consideration using realistic wind profiles. The system spinning reserves are included as additional constraints and the probability of the different scenarios is taken into account for the total cost computation. The methodology here proposed is valid independently of the size of the power system analysed, however, the larger is the number of nodes means the power system has larger number of components, so also more possible states need to be considered and this is translated into bigger computation time. Future work could analyse the economic benefit of applying preventive measures vs corrective measures or the effect of different wind power correlations on the operation of the system.

Chapter 7

Conclusions

Several studies for improving the operation of transmission systems of off-shore wind power plants HVDC and HVAC connected have been presented in this thesis. This chapter details the main findings throughout the thesis and includes directions for future work.

7.1 Contributions

The contributions are detailed per chapter.

- In **Chapter 3.2** an algorithm based on an OPF is proposed to operate multi-terminal systems integrating offshore wind power plants while minimizing joule losses in the DC grid. The proposed scheme requires communications, but in most applications, they will be already available for protection or monitoring purposes. If a communication fault occurs, the grid-side VSC control switches to droop control in order to guarantee a safe operation. The differences between the proposed scheme and droop control in terms of losses have been analyzed in steady state and through dynamic simulations. It has been shown that the proposed scheme can significantly reduce the system losses without further important investments (if communications are already available).
- In **Chapter 3.3** a scheme has been proposed to enhance the strategy described in **Chapter 3.2**. It is based on optimizing the power flows for all powers being generated from wind farms while using droop control. The optimal power flow computes the appropriate voltages

Chapter 7 Conclusions

references for droop control and communicates them to the grid-side VSC in order to ensure minimum losses in the power transmission to the terrestrial AC grid (losses in this study include converter losses and DC grid losses).

- In **Chapter 4**, the connection of an offshore wind power plant to grid through a HVAC link has been analysed when deep voltage sags occur on the main AC grid. A coordinated control strategy to operate the system while providing fault ride through capability has been proposed, since it has been detected that conventional control schemes (based on strict grid code compliance) can lead to instabilities. The proposed control can ensure safe operation when deep voltage sags occur on the main AC grid, but requires that the wind power plant has information on the main grid voltage. In case communications are not available or for an eventual communications fault, an observer is used and allows the correct operation of the proposed system. It has been shown that while conventional control schemes can lead to the wind power plant disconnection when a deep voltage sag occurs in the terrestrial grid, the proposed coordinated control scheme deals with those disturbances, ensuring the fault ride through capability of the system.
- In **Chapter 5** an optimal power flow strategy to operate hybrid DC/AC systems with large penetration of offshore wind has been presented. The tool developed has been successfully benchmarked with another tool. It has also been applied to a particular study case with high penetration of offshore wind. GAMS, for being an optimization dedicated software, has been proved to be far more efficient than MATLAB *fmincon* when implementing this tool. Finally, the tool has been tested in a scaled platform, showing stable operation. So, it can be concluded that it represents a flexible and validated methodology for analysing the optimal operation of hybrid AC/DC grids with large wind power integration for several objective functions. The experimental tests have shown an appropriate dynamic response of the proposed strategy combined with the optimum droop control algorithm presented in **Chapter 3.3**.

7.2 Future work

- In **Chapter 6** a methodology for evaluating operating cost over a year of a hybrid AC/DC system with high penetration of offshore wind taking into account corrective actions is detailed. The system studied has been operated so as to maximise the social welfare. The wind power variability is taken into consideration using realistic wind profiles. The system spinning reserves are included as additional constraints and the probability of the different scenarios is taken into account for the total cost computation.

All the previous work can be summarized in the following contributions:

- Development of an optimum droop control algorithm for operating HVDC multi-terminal systems
- Development of a coordinated control to ensure FRT in HVAC connected wind farms under deep voltage sags
- Development of a tool for ensuring optimal operation in HVDC/HVAC transmission systems
- Evaluation of the cost of operation of hybrid DC AC systems with high penetration of offshore wind

7.2 Future work

HVDC technology has acquired a growing interest from research and industry during the last decades. However, most of our transmission systems use HVAC technology. The construction of future HVDC links needs to take into account their existence and possible interactions. In this sense, future work can be done in the following directions:

- Analysis of the three level hierarchical control for the operation of multi-terminal HVDC grids combined with market constraints and taking into account forecasting deviations
- Dynamic analysis of the the current references readjustment in the coordinated control scheme for ensuring FRT in HVAC connected wind farms

Chapter 7 Conclusions

- Analysis of frequency support of offshore wind farms connected through HVDC multi-terminal grids
- Comparison of preventive and corrective measures on the secure operation of hybrid DC/AC systems and analysis of their effect on the cost of operation
- Requirements for fault protection in HVDC grids
- Restoration procedures in hybrid DC/AC systems

Bibliography

- [1] European Commission. *Communication from the commission to the European Council and the European Parliament - An energy policy for Europe*. Commission of the European Communities, 2007. 1
- [2] Stan Kaplan. *Power Plants Characteristics and Costs*. Congressional Report Service, 2008. 1
- [3] IEA PVPS Task 8: *Project Proposals on Very Large Scale Photovoltaic Power Generation (VLS-PV) Systems in Deserts*, volume 2. May 2006. 1
- [4] Oriol Gomis-Bellmunt, Jun Liang, Janaka Ekanayake, Rose King, and Nicholas Jenkins. Topologies of multi-terminal hvdc-vsc transmission for large offshore wind farms. *Electric Power Systems Research*, 81(2):271–281, 2011. 2, 51, 54, 124
- [5] Oriol Gomis-Bellmunt, Jun Liang, Janaka Ekanayake, and Nicholas Jenkins. Voltage-current characteristics of multi-terminal hvdc-vsc for offshore wind farms. *Electric Power Systems Research*, 81(2):440–450, 2011. 2, 51, 54, 75
- [6] Fangxing Li, Wei Qiao, Hongbin Sun, Hui Wan, Jianhui Wang, Yan Xia, Zhao Xu, and Pei Zhang. Smart transmission grid: Vision and framework. *IEEE Transactions on Smart Grid*, 1(2):168–177, 2010. 2
- [7] J. Arrillaga. *High Voltage Direct Current Transmission*. Institution of Electrical Engineers, London, U.K., 2nd edition, 1998. 2
- [8] N.M. Kirby, L. Xu, M. Luckett, and W. Siepmann. HVDC transmission for large offshore wind farms. *Power Engineering Journal*, 16(3):135–141, 2002. 2

Bibliography

- [9] D. Jovcic. Offshore wind farm with a series multi-terminal CSI HVDC. *Electric Power Systems Research*, 78:747–755, 2008. 2, 32
- [10] O. Gomis-Bellmunt, A. Junyent-Ferre, A. Sumper, and J. Bergas-Jane. Control of a wind farm based on synchronous generators with a central hvdc-vsc converter. *Power Systems, IEEE Transactions on*, 26(3):1632 –1640, aug. 2011. 2, 32
- [11] Oriol Gomis-Bellmunt, Adria Junyent-Ferre, Andreas Sumper, and Samuel Galceran-Arellano. Maximum generation power evaluation of variable frequency offshore wind farms when connected to a single power converter. *Applied Energy*, 87:3103–3109, 2010. 2, 32
- [12] J. Robinson, D. Jovcic, and G. Joosi. Analysis and design of an offshore wind farm using a mv dc grid. *IEEE Transactions on Power Delivery*, 25(4):2164–2173, 2010. 2, 32
- [13] W. Lu and Boon-Teck Ooi. Dc overvoltage control during loss of converter in multi-terminal voltage-source converter-based hvdc (m-vsc-hvdc). *IEEE Transactions on Power Delivery*, 18(3):915–920, July 2003. 2
- [14] W. Lu and Boon Teck Ooi. Optimal acquisition and aggregation of offshore wind power by multi-terminal voltage source hvdc. *IEEE Transactions on Power Delivery*, 18(1):201–206, 2003. 2
- [15] W. Lu and Boon Teck Ooi. Premium quality power park based on multi-terminal hvdc. *IEEE Transactions on Power Delivery*, 20(2):978–983, April 2005. 2
- [16] Noman Ahmed, Staffan Norrga, H-P Nee, A. Haider, D. Van Hertem, Lidong Zhang, and Lennart Harnefors. HVDC supergrids with modular multilevel converters. the power transmission backbone of the future. In *9th International Multi-Conference on Systems, Signals and Devices, Chemnitz, Germany, 2012*, pages 1–7. 2
- [17] S. Cole, K. Karou, T. K. Vrana, O. B. Fosso, J.B. Curis, A.M. Denis, and Ch. Ch. Liu. A european supergrid: present state and future chal-

Bibliography

- lenges. In *17th Power Systems Computation Conference, Stockholm, Sweden*, 2011. 2
- [18] N. Flourentzou, V.G. Agelidis, and G.D. Demetriades. VSC-based HVDC power transmission systems: An overview. *IEEE Transactions on Power Electronics*, 24(3):592–602, March 2009. 2
- [19] Dirk Van Hertem and Mehrdad Ghandhari. Multi-terminal vsc hvdc for the european supergrid: Obstacles. *Renewable and Sustainable Energy Reviews*, 14(9):3156–3163, 2010. 2, 52, 75, 124
- [20] C.M. Franck. HVDC circuit breakers: A review identifying future research needs. *IEEE Transactions on Power Delivery*, 26(2):998–1007, 2011. 2
- [21] Mingxia Zhou, Sheng Li, Jianhua Zhang, Zongqi Liu, and Yinhui Li. A study on the black start capability of vsc-hvdc using soft-starting mode. In *Power Electronics and Motion Control Conference, 2009. IPEMC '09. IEEE 6th International*, pages 910–914, 2009. 2, 21
- [22] Jef Beerten and Ronnie Belmans. Modeling and control of multi-terminal VSC-HVDC systems. *Energy Procedia*, 24(0):123 – 130, 2012. 3
- [23] A. Egea-Alvarez, F. Bianchi, A. Junyent-Ferre, G. Gross, and O. Gomis-Bellmunt. Voltage control of multi-terminal VSC-HVDC transmission systems for offshore wind power plants: Design and implementation in a scaled platform. *IEEE Transactions on Industrial Electronics*, 60(6):2381–2391, 2013. 3
- [24] Jacopo Moccia Ivan Pineda, Sarah Azau and Justin Wilkes. *Wind in power. 2013 European statistics.* EWEA, European Wind Energy Association, 2014. 7, 8
- [25] EWEA. Deep water: The next step for offshore wind energy. *The European Wind Energy Association (EWEA)*, 2013. 8
- [26] P.E. Morthorst and S.Awerbuch. The economics of wind energy, a report by the european wind energy association. 8

Bibliography

- [27] Walter Hulshorst. Leonardo Energy report. In *REPOWERING AND USED WIND TURBINES*, 2008. 10
- [28] Wang X., C. Cao, and Z. Zhou. Experiment on fractional frequency transmission system. *Transactions on Power Systems, IEEE*, 21(1):372–377, 2006. 13
- [29] N. Qin, S. You, Z. Xu, and V. Akhmatov. Offshore wind farm connection with low frequency ac transmission technology. In *IEEE Power Energy Soc. Gen. Meeting, Calgary, AB, Canada*, 2009. 13
- [30] Michael P. Bahrman and Brian K. Johnson. The abcs of hvdc transmission technologies. *Power and Energy Magazine, IEEE*, 5(2):32–44, march-april 2007. 17, 18, 19, 52, 75, 123
- [31] X.-P.Zhang, C. Rehtanz, and B. Pal. *Flexible AC Transmission Systems*. Springer, Berlin, Germany, 2006. 21
- [32] Friends of the Supergrid. <http://www.friendsofthesupergrid.eu/>. 21
- [33] Michael P. Bahrman, Jan G. Johansson, and Bo A. Nilsson. Voltage source converter transmission technologies - the right fit for the application. *ABB*, 2012. 21
- [34] Stefan G Johansson, Gunnar Asplund, Erik Jansson, and Roberto Rudervall. Power system stability benefits with vsc dc-transmission systems. *CIGRÉ*, Session 2004. 21
- [35] A. Lesnicar and Marquardt R. An innovative modular multilevel converter topology suitable for a wide power range. In *Power Tech Conference Proceedings, IEEE Bologna*, 2003. 22
- [36] Glinka M. and Marquardt R. A new ac/ac multilevel converter family. *Transactions on Industrial Electronics, IEEE*, 52(3):662–669, 2005. 22
- [37] Working group B4.46. Voltage source converter (vsc) hvdc for power transmission. economic aspects and comparison with other ac and dc technologies. *CIGRÉ*, 2012. 22

Bibliography

- [38] J. Dorn, H. Gambach, and D. Retzmann. Hvdc transmission technology for sustainable power supply. In *9th International Multi-Conference on Systems, Signals and Devices (SSD)*, 2012. 22
- [39] M. Tsili and S. Papathanassiou. A review of grid code technical requirements for wind farms. *IET Renewable Power Generation*, 3(3):308–332, sept. 2009. 23, 95
- [40] C. Sourkounis and Tourou P. Grid code requirements for wind power integration in Europe. *Conference Papers in Energy*, 2013. 23
- [41] M. Tsili and S. Papathanassiou. A review of grid code technical requirements for wind farms. *IET Renewable Power Generation*, 3(3):308–332, 2009. 23
- [42] Tennet GmbH. Requirements for offshore grid connections in the grid of Tennet TSO GmbH. *Germany*, 2010. 23
- [43] I. Erlich and U. Bachmann. Grid code requirements concerning connection and operation of wind turbines in germany. In *IEEE Power Engineering Society General Meeting*, volume 2, pages 1253–1257, 2005. 23
- [44] Cigré. Cigré b4-55 report hvdc connection of offshore wind power plants. In *Technical report*, 2014. 23
- [45] E. Ela and al. Active power controls from wind power: Bridging the gaps. In *NREL*, 2014. 32
- [46] B. Badrzadeh. Wind power plant scada and controls. In *Power and Energy Society General Meeting, 2011 IEEE*, pages 1–7, July 2011. 33
- [47] G. Quinonez-Varela, G.W. Ault, O. Anaya-Lara, and J.R. McDonald. Electrical collector system options for large offshore wind farms. *Renewable Power Generation, IET*, 1:107 – 114, 2007. 36
- [48] J.T.G. Pierik, M.E.C. Damen, P. Bauer, and S.W.H. de Haan. Steady state electrical design, power performance and economic modeling of off-shore wind farms. *EPE Journal*, 16:44–49, 2006. 36

Bibliography

- [49] Thomas Worzyk. *Submarine Power Cables: Design, Installation, Repair, Environmental Aspects*. Springer, 2009. 37
- [50] Agustí Egea-Alvarez, Adrià Junyent-Ferré, and Oriol Gomis-Bellmunt. Active and reactive power control of grid connected distributed generation systems. In Lingfeng Wang, editor, *Modeling and Control of Sustainable Power Systems*, Green Energy and Technology, pages 47–81. Springer Berlin Heidelberg, 2012. 39, 66
- [51] Yunho Jeong, Kathryn Johnson, and Paul Fleming. Comparison and testing of power reserve control strategies for grid-connected wind turbines. *Wind Energy*, 17(3):343–358, 2014. 40
- [52] I. Erlich and M. Wilch. Primary frequency control by wind turbines. In *Power and Energy Society General Meeting, 2010 IEEE*, pages 1–8, July 2010. 40
- [53] H.T. Ma and B.H. Chowdhury. Working towards frequency regulation with wind plants: Combined control approaches. *Renewable Power Generation, IET*, 4(4):308–316, July 2010. 40
- [54] J. R. Kristoffersen and P. Christiansen. The Horns Rev wind farm and the operational experience with the wind farm main controller. *Wind Engineering*, 27(5):351–359. 40
- [55] Francisco Díaz-González, Melanie Hau, Andreas Sumper, and Oriol Gomis-Bellmunt. Participation of wind power plants in system frequency control: Review of grid code requirements and control methods. *Renewable and Sustainable Energy Reviews*, 34(0):551 – 564, 2014. 40
- [56] M Mata, J Carulla, and O Gomis. Reactive power regulation of a windpark. *Alstom Wind, Patent application WO2012016585*, 2012. 41
- [57] Til Kristian Vrana, Jef Beerten, Ronnie Belmans, and Olav Bjarte Fosso. A classification of DC node voltage control methods for HVDC grids. *Electric Power Systems Research*, 103:137 – 144, 2013. 49, 54

Bibliography

- [58] Agustí Egea-Alvarez, Jef Beerten, Dirk Van Hertem, and Oriol Gomis-Bellmunt. Hierarchical power control of multiterminal HVDC grids. *Electric Power Systems Research*, 121:207 – 215, 2015. xiv, 49, 50
- [59] Lie Xu, Liangzhong Yao, and Masoud Bazargan. Dc grid management of a multi-terminal hvdc transmission system for large offshore wind farms. *International Conference on Sustainable Power Generation and Supply, 2009. SUPERGEN '09*, pages 1 –7, 2009. 51, 74, 75
- [60] Lie Xu, B.W. Williams, and Liangzhong Yao. Multi-terminal dc transmission systems for connecting large offshore wind farms. *Power and Energy Society General Meeting - Conversion and Delivery of Electrical Energy in the 21st Century, 2008 IEEE*, pages 1 –7, jul. 2008. 51, 74, 75
- [61] J. Liang, O. Gomis-Bellmunt, J. Ekanayake, and N. Jenkins. Control of multi-terminal VSC-HVDC transmission for offshore wind power. In *EPE2009, 13th European conference on Power Electronics and Applications*, 2009. 51, 54, 74, 75
- [62] Lie Xu and Bjarne R. Andersen. Grid connection of large offshore wind farms using hvdc. *Wind Energy*, 9:371–382, 2006. 52, 75
- [63] E. Prieto-Araujo, F. D. Bianchi, A. Junyent-Ferre, and O. Gomis-Bellmunt. Methodology for droop control dynamic analysis of multi-terminal vsc-hvdc grids for offshore wind farms. *IEEE Transactions on Power Delivery*, 2011. 54, 75, 95, 124
- [64] Richard H. Byrd and Jean Charles Gilbert. A trust region method based on interior point techniques for nonlinear programming. *Mathematical Programming*, 89:149–185, 1996. 57, 60, 78, 142, 171
- [65] ABB. Technical description of hvdc light technology. pages section 4.2.1–80 kV modules, type M1. 57, 82
- [66] Reiner Horst and Tuy Hoang. *Global Optimization: deterministic approaches*. Springer, third edition, 1996. 60

Bibliography

- [67] Stephen P. Boyd and Lieven Vandenberghe. *Convex Optimization*. Cambridge University Press, first edition, 2004. 60
- [68] Aggregated dynamic model for wind farms with doubly fed induction generator wind turbines. *Renewable Energy*, 33(1):129 – 140, 2008. 66
- [69] Aragüés-Penalba. Optimització de sistemes multiterminal hvdc per grans parcs eòlics marins. 2010. 66
- [70] T.Ackermann. *Wind Power in Power Systems*. Wiley, 2005. 68, 84
- [71] A. Egea-Alvarez, J. Beerten, D. Van Hertem, and O. Gomis-Bellmunt. Primary and secondary power control of multi-terminal HVDC grids. pages 1–6, 2012. 74, 124
- [72] J. Beerten, S. Cole, and R. Belmans. A sequential AC/DC power flow algorithm for networks containing multi-terminal VSC-HVDC systems. In *Power and Energy Society General Meeting, IEEE, Minneapolis, MN., USA*, pages 1–7, 2010. 77
- [73] CIGRÉ Working Groups B4-58 (Devices for Load flow Control, Methodologies for Direct Voltage Control in a Meshed HVDC Grid), and B4-57 (Guide for the Development of Models for HVDC Converters in a HVDC Grid). The CIGRÉ B4 DC grid test system. *International Council for Large Electric Systems (CIGRÉ)*, 2013. xv, xviii, 78, 79, 139, 146, 180
- [74] O. Gomis-Bellmunt, A. Egea-Alvarez, A. Junyent-Ferre, Jun Liang, J. Ekanayake, and N. Jenkins. multi-terminal hvdc-vsc for offshore wind power integration. In *Power and Energy Society General Meeting, 2011 IEEE*, 2011. 95
- [75] N.R. Ullah, T. Thiringer, and D. Karlsson. Voltage and transient stability support by wind farms complying with the e.on netz grid code. *IEEE Transactions on Power Systems*, 2007. 95, 96
- [76] I. Erlich, F. Shewarega, S. Engelhardt, J. Kretschmann, J. Fortmann, and F. Koch. Effect of wind turbine output current during faults on grid voltage and the transient stability of wind parks. 2009. 95, 101

Bibliography

- [77] W. Christiansen D.T. Johnsen. Optimisation of the fault ride through strategy of a wind farm. Master's thesis, 2006. 96
- [78] Oriol Gomis Bellmunt and Mònica Aragüés Peñalba. Method for avoiding voltage instability in an electrical grid of an offshore wind park. *ALSTOM WIND Patent WO2013120976*, August 22, 2013. 96
- [79] P. Kundur. *Power System Stability and Control*. Mc.Graw Hill, Inc, 1993. 96, 106, 169
- [80] Thierry Van Cutsem and Vournas Costas. *Voltage Stability of Electric Power Systems*. Springer, 1998. 97
- [81] D.P. Kothari and I.J.Nagrath. *Modern Power System Analysis*. McGraw-Hill, 3rd edition, 2003. 99, 112
- [82] Tennet TSO GmbH. Grid code extra high voltage. *Germany*, October 2010. xvi, 106, 107
- [83] Tennet TSO GmbH. Requirements for offshore grid connections in the grid of tennet tso gmbh. *Germany*, October 2010. 106
- [84] ABB. Xlpe submarine cable systems. attachment to xlpe land cable systems user's guide. 112
- [85] CIGRÉ Working Group B-4.52. HVDC grid feasibility study. *International Council for Large Electric Systems (CIGRÉ), Technical Brochure 533*, 2013. 123
- [86] Mònica Aragüés Peñalba, Agustí Egea-Alvarez, Oriol Gomis-Bellmunt, and Andreas Sumper. Optimum voltage control for loss minimization in HVDC multi-terminal transmission systems for large offshore wind farms. *Electric Power Systems Research*, 89:54 – 63, 2012. 124
- [87] A. Egea-Alvarez, F. Daniel Bianchi, A. Junyent-Ferré, G. Gross, and O. Gomis-Bellmunt. Voltage control of multi-terminal VSC-HVDC transmission systems for offshore wind power plants: Design and implementation in a scaled platform. *IEEE Transactions on Industrial Electronics*, (6):2381–2391. 124

Bibliography

- [88] J. Beerten, S. Cole, and R. Belmans. A sequential AC/DC power flow algorithm for networks containing multi-terminal VSC HVDC systems. In *Power and Energy Society General Meeting, 2010 IEEE*, pages 1–7, 2010. 124, 133
- [89] J. Beerten, S. Cole, and R. Belmans. Generalized steady-state VSC MTDC model for sequential AC/DC power flow algorithms. *Power Systems, IEEE Transactions on*, 27(2):821–829, 2012. xix, 124, 126, 131
- [90] A Pizano-Martinez, C.R. Fuerte-Esquivel, H. Ambriz-Perez, and E. Acha. Modeling of vsc-based hvdc systems for a newton-raphson opf algorithm. *Power Systems, IEEE Transactions on*, 22(4):1794–1803, Nov 2007. 124
- [91] Mohamadreza Baradar. Modeling of multi terminal HVDC systems in power flow and optimal power flow formulations. *Licenciate thesis, KTH Royal Institute of Technology, Stockholm, Sweden*, 2013. 124, 126, 170
- [92] J. Cao, D. Wenjuan, H.F. Wang, and S.Q. Bu. Minimization of transmission loss in meshed ac/dc grids with vsc-mtdc networks. *Power Systems, IEEE Transactions on*, 28(3):3047–3055, Aug 2013. 124, 170
- [93] R. Wiget and G. Andersson. Optimal power flow for combined ac and multi-terminal hvdc grids based on vsc converters. In *Power and Energy Society General Meeting, 2012 IEEE*, pages 1–8, July 2012. 124, 170
- [94] J Rimez and R. Belmans. A combined AC/DC Optimal Power Flow Algorithm for meshed AC and DC Networks linked by VSC Converters. *International Transactions on Electrical Energy Systems, Wiley*, 2014. 124, 125, 133, 167, 170, 171, 173
- [95] M Aragüés-Peñaiba, J. Beerten, J. Rimez, D. Van Hertem, and O. Gomis-Bellmunt. Optimal power flow tool for hybrid dc/ac systems. In *IET AC DC*, 2015. 125, 167

Bibliography

- [96] Stamatos Chondrogiannis and Marta Poncela Blanco. Market integration scheme of a multi-terminal hvdc grid in the north seas. *Transactions on Power Systems, IEEE*, 2015. 126
- [97] The North Seas Countries Offshore Grid Initiative. Discussion paper: Possible market arrangements for integrated offshore network. 2013. 126
- [98] S. Messalti, S. Belkhiat, Saadate, and D. S.Flieller. A new approach for load flow analysis of integrated AC/DC power systems using sequential modified Gauss-Seidel methods. *Euro. Trans. Electr. Power*, 22:421–432, 2012. 126
- [99] *GAMS. The solver manuals.* GAMS Development Corporation, Washington, DC, USA, 2015. 144
- [100] A. Egea-Alvarez, F. Bianchi, A. Junyent-Ferre, G. Gross, and O. Gomis-Bellmunt. Voltage control of multiterminal vsc-hvdc transmission systems for offshore wind power plants: Design and implementation in a scaled platform. *Industrial Electronics, IEEE Transactions on*, 60(6):2381–2391, June 2013. xvii, xix, 147, 148
- [101] F. Capitanescu and al. State-of-the-art, challenges, and future trends in security constrained optimal power flow. *Electric Power Systems Research*, 81(8):1731 – 1741, 2011. 169
- [102] T.M. Haileselassie and K.Uhlen. Power system security in a meshed north sea hvdc grid. In *Proceedings of the IEEE*, pages 978–990, 2013. 170
- [103] Chatzivasileiadis S., Krause T., and Andersson G. Security-constrained optimal power flow including post-contingency control of vsc hvdc lines. In *12 SEPOPE, Rio de Janeiro*, pages 1–8, May 2012. 170
- [104] M. Vrakopoulou, K. Margellos, J. Lygeros, and G. Andersson. Probabilistic guarantees for the $n - 1$ security of systems with wind power generation. In *Proceedings of PMAPS, Istanbul*, June 2012. 170, 171

Bibliography

- [105] M. Vrakopoulou, K. Margellos, J. Lygeros, and G. Andersson. A probabilistic framework for security constrained reserve scheduling of networks with wind power generation. In *Energy Conference and Exhibition (ENERGYCON), 2012 IEEE International*, pages 452–457, Sept 2012. 170
- [106] M. Vrakopoulou, S. Chatzivasileiadis, E. Iggland, M. Imhof, T. Krause, O. Makela, J.L. Mathieu, L. Roald, R. Wiget, and G. Andersson. A unified analysis of security-constrained opf formulations considering uncertainty, risk, and controllability in single and multi-area systems. In *Bulk Power System Dynamics and Control - IX Optimization, Security and Control of the Emerging Power Grid (IREP), 2013 IREP Symposium*, pages 1–19, Aug 2013. 170, 171
- [107] S. Mishra, Y. Mishra, and S. Vignesh. Security constrained economic dispatch considering wind energy conversion systems. In *Power and Energy Society General Meeting, 2011 IEEE*, pages 1–8, July 2011. 174
- [108] Allen J Wood and Bruce F Wollenberg. Institution of Electrical Engineers, 2nd edition. 174
- [109] G. Jordan J. Zhu and S. Ihara. The market for spinning reserve and its impacts on energy prices. In *Proceedings of the IEEE Power Engineering Society Winter Meeting*, 2000. 174
- [110] Daniel Kirschen Yann Rebours. What is spinning reserve? *The University of Manchester*. 174, 175
- [111] Ifedi Kenneth Odinakaeze. Assessment of spinning reserve requirements in a deregulated system. 2010. 174, 175
- [112] F. Bouffard and F.D. Galiana. An electricity market with a probabilistic spinning reserve criterion. *Power Systems, IEEE Transactions on*, 19(1):300–307, Feb 2004. 174
- [113] Elia, Belgium electricity transmission system operator. <http://www.elia.be/en/grid-data/>, 2014. 180

Bibliography

- [114] K. Lindén, B. Jacobson, M. Bollen, and J. Lundquist. Reliability study methodology for hvdc grids. In *B4-108 CIGRÉ*, 2010. xix, 181, 182
- [115] UPWIND. *Survey of reliability of large offshore wind farms*. Work Package 9 Electrical grid, 2007. 181
- [116] C. Hudon, M. Levesque, D. Nguyen, C. Millet, and F. Truchon. Root cause analysis of generator failures. In *Electrical Insulation (ISEI), Conference Record of the 2012 IEEE International Symposium on*, pages 199–203, June 2012. xix, 182

Chapter 8

Publications

8.1 Journal articles

- Mònica Aragüés Peñalba, Agustí Egea-Àlvarez, Oriol Gomis-Bellmunt, Andreas Sumper. “Optimum voltage control for loss minimization in HVDC multi-terminal transmission systems for large offshore wind farms”, Electric Power Systems Research, Elsevier, Vol. 89 (August 2012), pp. 54-63, doi:10.1016/j.epsr.2012.02.006.
- Mònica Aragüés Peñalba, Agustí Egea-Àlvarez, Samuel Galceran Arelano, Oriol Gomis-Bellmunt. “Droop control for loss minimization in HVDC multi-terminal transmission systems for large offshore wind farms” Electric Power Systems Research, Elsevier, Vol. 112 (July 2014), pp. 48-55, doi:10.1016/j.epsr.2014.03.013.
- Mònica Aragüés Peñalba, Oriol Gomis-Bellmunt, Marcia Martins, “Co-ordinated Control for an Offshore Wind Power Plant to Provide Fault Ride Through Capability”, Sustainable Energy, IEEE Transactions on, vol.5, no.4, pp.1253,1261, Oct. 2014, doi: 10.1109/TSTE.2014.2344172.
- Mònica Aragüés Peñalba, Agustí Egea-Àlvarez, Samuel Galceran Arelano, Oriol Gomis-Bellmunt, “Optimal power flow tool for mixed hvac and hvdc systems for grid integration of large wind power plants”, IET Renewable Power Generation, 2015, doi:10.1049/iet-rpg.2015.0028.
- Mònica Aragüés, Johan Rimez, Jef Beerten, Dirk Van Hertem, Oriol Gomis-Bellmunt, “OPEX in hybrid DC/AC systems with large pene-

Chapter 8 Publications

tration of offshore wind taking into consideration spinning reserves”, *Under preparation.*

- Mònica Aragüés, Joan Sau, Eduardo Prieto, Agustí Egea, Oriol Gomis-Bellmunt, “Optimal power tool for HVDC/HVAC systems. Implementation in a HVDC scaled platform”, *Under preparation.*

8.2 Patents

- Inventors: Oriol Gomis Bellmunt, Mònica Aragüés Peñalba, patent *EP12382051 Method for avoiding voltage instability in an electrical grid of an offshore wind park*, filled in the European Patent Office 16/02/2012. The study corresponding to this patent has been presented in Chapter 4.
- Inventors: Oriol Gomis Bellmunt, José Luis Dominguez García, Mònica Aragüés Peñalba, patent *EP13382511.7 Multiphase generator-conversion systems*, filled in the European Patent Office 13/12/2013.

8.3 Book chapters

- Mònica Aragüés Peñalba, Oriol Gomis-Bellmunt, “Operation and control of offshore wind power plants”, in “HVDC Grids: for Offshore and the Supergrid of the Future”, to be published in John Wiley & Sons April 2016, ISBN: 978-1-118-85915-5.

8.4 Conference papers

- Mònica Aragüés Peñalba, Oriol Gomis-Bellmunt, “Optimal power flow tool for mixed HVAC and HVDC systems for grid integration of large wind power plants”, in EWEA, Barcelona, July 2014.
- Mònica Aragüés Peñalba, Oriol Gomis-Bellmunt, “Optimal power flow tool for mixed hvac and hvdc systems for grid integration of large wind power plants”, in IFORS, Barcelona, July 2014.

8.5 Other publications

- Mònica Aragüés, Jef Beerten, Johan Rimez, Dirk Van Hertem, Oriol Gomis-Bellmunt, “Optimal power flow tool for hybrid DC/AC systems”, in 11th IET International Conference on AC and DC Power Transmission, Birmingham, February 2015.
- Mònica Aragüés, Johan Rimez, Jef Beerten, Dirk Van Hertem, Oriol Gomis-Bellmunt, “Secure and optimal operation of hybrid AC/DC grids with large penetration of offshore wind”, in 11th IET International Conference on AC and DC Power Transmission, Birmingham, February 2015.
- Mònica Aragüés Peñalba, Oriol Gomis-Bellmunt, Marcia Martins, “Co-ordinated Control for an Offshore Wind Power Plant to Provide Fault Ride Through Capability”, in Powertech Conference, Eindhoven, June 2015. *Awarded as one of the four finalists in the Basil Papadias Award.*

8.5 Other publications

8.5.1 Other journals

- Mikel De Prada Gil, J.L. Domínguez-García, F. Díaz-González, M. Aragüés-Peñalba, Oriol Gomis-Bellmunt, “Feasibility analysis of offshore wind power plants with DC collection grid”, Renewable Energy, Volume 78, June 2015, Pages 467-477, 10.1016/j.renene.2015.01.042.
- Eduard Bullich Massagué, Ricard Farré, Mònica Aragüés Peñalba, Lluís Serrano, Carlos Pacheco, Oriol Gomis-Bellmunt, “Power Plant Control in Large Scale PV Plants. Design, implementation and validation in a 9.4 MW PV plant”, IET Renewable Power Generation, 2015.
- A. Egea-Àlvarez, M. Aragüés-Peñalba, O. Gomis Bellmunt, J. Rull-Duran, A. Sudrià Andreu, Sensorless control of a power converter for a cluster of small wind turbines, *Accepted for publication in IET Renewable Power Generation.*
- Ana Cabrera-Tobar, Eduard Bullich Massagué, Mònica Aragüés Peñalba, Oriol Gomis-Bellmunt, ”Topologies for Large Scale Photovoltaic Power

Chapter 8 Publications

Plants”, Accepted for publication in Renewable and Sustainable Energy Reviews, Elsevier.

- A. Egea-Àlvarez, M. Aragüés-Peñaiba, O. Gomis Bellmunt, ”Power reduction coordinated scheme for HVDC links”, *Submitted to IEEE, Transactions on Sustainable Energy*.
- Rodrigo Teixeira Pinto, Mònica Aragüés Peñalba, Oriol Gomis-Bellmunt, Andreas Sumper, ”Optimal Operation of DC Networks to Support Power System Outage Management”, *Submitted to IEEE Transactions on Smart Grid, Special Issue on Power Grid Resilience*.
- Ana Cabrera-Tobar, Eduard Bullich Massagué, Mònica Aragüés Peñalba, Oriol Gomis-Bellmunt, ”Review of advanced grid requirements for the integration of large scale photovoltaic power plants in the transmission system”, *Submitted to Elsevier, Renewable and Sustainable Energy Reviews*.

8.5.2 Other conference papers

- Mikel de Prada-Gil, José Luis Domínguez-García, Fco. Díaz-González, Mònica Aragüés Peñalba, Oriol Gomis-Bellmunt, David Berenguel, Marcia Martins, Gabriel Fullana “Analysis of DC collector grid for off-shore wind power plants”, in 12th International Workshop on Large-Scale Integration of Wind Power into Power Systems as well as on Transmission Networks for Offshore Wind Power Plants, London, October 2013.
- German Pérez, Joseba Lopez, Laura Val, Andreas Sumper, Frieder Schuon, Mikel De Prada, Mònica Aragüés Peñalba, Oriol Gomis Bellmunt, Helder Lopes Ferreira. “Deep offshore wind farm planning and cost calculation tools”, in EWEA offshore, Frankfurt, November 2013.
- E. Bullich-Massagué, M. Aragüés Peñalba, R. Ferrer-San-José, O. Gomis-Bellmunt, L. Serrano, C. Pacheco, “Power Plant Control Experience in Large scale PV Plant. Modelling, Control, Simulation and Implementation”, in 4th International Workshop on Integration of Solar Power into Power Systems, Berlin, November 2014.

8.5 Other publications

- Rodrigo Teixeira Pinto, Mònica Aragüés Peñalba, Oriol Gomis-Bellmunt, Andreas Sumper, Pavol Bauer, “Analysis of deviations on the OPF operation of MTDC networks: a comparison between droop control and the DVC Strategy”, in EPE Conference, Geneva, September 2015.

8.5.3 Magazines

- Mònica Aragüés Peñalba, Oriol Gomis Bellmunt, Toni Sudrià i Andreu, Agustí Egea-Àlvarez. “Offshore y repowering”, Enero 2013, Vol. 447, Automática e Instrumentación
- Mònica Aragüés Peñalba, Eduardo Prieto-Araujo, Agustí Egea-Àlvarez, Oriol Gomis Bellmunt. “Superredes, las redes elèctricas del futuro”, Mayo 2013, Buran (IEEE PES Studen Branch Barcelona Review)
- Agustí Egea-Àlvarez, Mònica Aragüés Peñalba, Toni Sudrià i Andreu, “Aerogeneradores: diseño y control”, Setiembre 2013, Vol. 454, Automática e Instrumentación
- Agustí Egea-Àlvarez, Mònica Aragüés Peñalba, “National Instruments en el sector eólico”, Abril 2014, Vol. 461, Automática e Instrumentación
- Francesc Girbau Llistuella, Mònica Aragüés Peñalba, Andreas Sumper, “Nuevos conceptos en microrredes para la distribución de energía eléctrica”, Enero 2015, Vol. 469, Automática e Instrumentación

8.5.4 Colloquiums

- Mònica Aragüés Peñalba presented “Modeling and simulation of HVDC transmission systems for offshore wind power plants, comparison of optimal power flow for losses reduction and droop control structure” in “2nd HVDC Doctoral Colloquium”, Barcelona, July 2011, organized by CITCEA-UPC.
<http://www.cerien.upc.edu/jornades/index.php?id=28>
- Mònica Aragüés Peñalba presented “Coordination of power reduction strategies in an offshore HVDC multi-terminal system” in “3rd HVDC

Chapter 8 Publications

Doctoral Colloquium”, Cardiff, July 2012, organized by Cardiff University.

<http://hvdc-colloquium.engineering.cf.ac.uk/agenda.html>

- Mònica Aragüés Peñalba and Agustí Egea-Àlvarez presented “Modeling and simulation of HVDC grids for offshore wind” in EES-UETP workshop “HVDC grids for offshore wind power”, Barcelona, December 2012, organized by Catalonia Institute for Energy Research (IREC).
<http://content.irec.cat/web/HVDC.pdf>.
- Mònica Aragüés Peñalba presented “Optimal Power Flow Analysis in HVDC Grids” in “4th HVDC Doctoral Colloquium”, Leuven, July 2013, organized by KU Leuven.
<https://www.esat.kuleuven.be/events/2013/4th-hvdc-doctoral-colloquium>
- Mònica Aragüés Peñalba presented “Optimal power flow tool for mixed HVAC and HVDC systems for grid integration of large wind power plants” in “5th HVDC Doctoral Colloquium”, London, July 2014, organized by Imperial College London.

Chapter 9

Appendix

Appendix: Interior Point Algorithm with barrier function

If the general constrained minimisation problem is expressed as:

$$[\text{MIN}] f(x) \quad (9.1)$$

subject to:

$$h(x) = 0 \quad (9.2)$$

$$g(x) \leq 0 \quad (9.3)$$

The Interior Point Algorithm solves the sequence of approximate minimization problems presented in equations (9.4) - (9.6), for each $\mu > 0$ (being μ a penalty parameter). They are equality constrained problems, easier than the original inequality constrained original problem.

$$[\text{MIN}] f(x, s) = [\text{MIN}] f(x) - \mu \sum_{i=1} \ln(s_i) \quad (9.4)$$

subject to:

$$h(x) = 0 \quad (9.5)$$

$$g(x) + s = 0 \quad (9.6)$$

There are as many slack variables, s_i as inequality constraints g . These slack variables must be positive in order to keep $\ln(s_i)$ bounded. As μ

Chapter 9 Appendix

decreases to zero, the minimum of $f(x, s)$ should approach the minimum of f . The added logarithmic term is called a barrier function. To solve the approximate problem, at each iteration, two main steps can be used: a direct step, also called a Newton step (it attempts to solve KKT equations for the approximate problem) or a conjugate gradient step (uses a trust region). By default, the algorithm takes direct step and if it can not, it attempts a conjugate gradient step.